National Library of Canada
Canadian Theses Service
Ottawa, Canada
K1A 0N4

Bibliothèque nationale du Canada
Services des thèses canadiennes

CANADIAN THESES

THÈSES CANADIENNES

NOTICE

The quality of this microfiche is heavily dependent upon the quality of the original thesis submitted for microfilming. Every effort has been made to ensure the highest quality of reproduction possible.

If pages are missing, contact the university which granted the degree.

Some pages may have indistinct print especially if the original pages were typed with a poor typewriter ribbon or if the university sent us an inferior photocopy.

Previously copyrighted materials (journal articles, published tests, etc.) are not filmed.

Reproduction in full or in part of this film is governed by the Canadian Copyright Act, R.S.C. 1970, c. C-30.

AVIS

La qualité de cette microfiche dépend grandement de la qualité de la thèse soumise au microfilmage. Nous avons tout fait pour assurer une qualité supérieure de reproduction.

S'il manque des pages, veuillez communiquer avec l'université qui a conféré le grade.

La qualité d'impression de certaines pages peut laisser à désirer, surtout si les pages originales ont été dactylographiées à l'aide d'un ruban usé ou si l'université nous a fait parvenir une photocopie de qualité inférieure.

Les documents qui font déjà l'objet d'un droit d'auteur (articles de revue, examens publiés, etc.) ne sont pas microfilmés.

La reproduction, même partielle, de ce microfilm est soumise à la Loi canadienne sur le droit d'auteur, SRC 1970, c. C-30.

THIS DISSERTATION HAS BEEN MICROFILMED EXACTLY AS RECEIVED

LA THÈSE A ÉTÉ MICROFILMÉE TELLE QUE NOUS L'AVONS REÇUE

THE UNIVERSITY OF ALBERTA

MEMBRANE IONIC CURRENTS AND ELECTRICAL EXCITABILITY IN BARNACLE NEURONS

by

© BRETT ANTHONY PREMACK

A THESIS

SUBMITTED TO THE FACULTY OF GRADUATE STUDIES AND RESEARCH

IN PARTIAL FULFILMENT OF THE REQUIREMENTS FOR THE DEGREE

OF DOCTOR OF PHILOSOPHY

DEPARTMENT OF ZOOLOGY

EDMONTON, ALBERTA

SPRING 1987

Permission has been granted to the National Library of Canada to microfilm this thesis and to lend or sell copies of the film.

The author (copyright owner) has reserved other publication rights, and neither the thesis nor extensive extracts from it may be printed or otherwise reproduced without his/her written permission.

L'autorisation a été accordée à la Bibliothèque nationale du Canada de microfilmer cette thèse et de prêter ou de vendre des exemplaires du film.

L'auteur (titulaire du droit d'auteur) se réserve les autres droits de publication; ni la thèse ni de longs extraits de celle-ci ne doivent être imprimés ou autrement reproduits sans son autorisation écrite.

ISBN 0-315-37650-3

THE UNIVERSITY OF ALBERTA

RELEASE FORM

NAME OF AUTHOR BRETT ANTHONY PREMACK

TITLE OF THESIS MEMBRANE IONIC CURRENTS AND ELECTRICAL EXCITABILITY IN BARNACLE NEURONS

DEGREE FOR WHICH THESIS WAS PRESENTED DOCTOR OF PHILOSOPHY

YEAR THIS DEGREE GRANTED SPRING 1987

Permission is hereby granted to THE UNIVERSITY OF ALBERTA LIBRARY to reproduce single copies of this thesis and to lend or sell such copies for private, scholarly or scientific research purposes only.

The author reserves other publication rights, and neither the thesis nor extensive extracts from it may be printed or otherwise reproduced without the author's written permission.

(SIGNED) B.A. Premack

PERMANENT ADDRESS:

11339 Loughren Drive,

Surrey, British Columbia,

Canada.

DATED December 2 19 86

THE UNIVERSITY OF ALBERTA

FACULTY OF GRADUATE STUDIES AND RESEARCH

The undersigned certify that they have read, and recommend to the Faculty of Graduate Studies and Research, for acceptance, a thesis entitled **MEMBRANE IONIC CURRENTS AND ELECTRICAL EXCITABILITY IN BARNACLE NEURONS** submitted by BRETT ANTHONY PREMACK in partial fulfilment of the requirements for the degree of DOCTOR OF PHILOSOPHY .

A.N. Spencer
.....
Supervisor

Harold J. Atwood
.....

K.G. Pearson
.....

Sh. Mallnia For A.S. French
.....

D.D. Beatty
.....

R.L. Mathias
.....

Date Dec 1 / 1986

DEDICATION

To my father, Fred; brother, Craig; and sister, Leah; who have supported me throughout this endeavor in all manner of ways; and especially to the memory of my mother, Mona.

ABSTRACT

Neurons in the ventral ganglion of the barnacle, *Balanus nubilus* were studied under either voltage or current clamp conditions in order to describe the membrane ionic currents and relate these to membrane excitability. Neurons were clamped at the soma using two microelectrodes and conventional voltage and current measuring circuitry. Five distinct ionic currents were identified, and the voltage dependence and kinetics of each described. These were: a fast Na^+ current, I_{Na}; a slow Ca^{2+} current, I_{Ca}; a transient K^+ current, I_A; a delayed K^+ current, I_K; and a slowly activating Ca^{2+}-dependent current, $I_{K(Ca)}$. This ensemble of ionic currents is quite typical of many neuronal somata, but barnacle neurons were found to differ in that much of the total outward current was Ca^{2+}-dependent.

A very rapidly activating fraction of I_A appeared to be Ca^{2+}-dependent, and was eliminated when Ca^{2+} influx was blocked by Co^{2+} or Mn^{2+}. The possibility that the reduction in I_A resulted from an alteration in the surface potential was examined, but found not to account for the observed Ca^{2+}-dependence. The major functions of both components of I_A were: regulation of the response time at the onset of a stimulus, repolarization of the action potential, and control of low frequency repetitive firing. A numerical simulation based on the voltage clamp data, using modified Hodgkin-Huxley formulations, indicates that the above physiological roles are consistent with the measured voltage dependence and kinetics of I_A. The adenylate cyclase activator forskolin accelerated the inactivation kinetics of I_A, and increased the excitability of neurons in current clamp. However, some of the evidence indicates that this effect may not be mediated by a rise in cAMP.

The other Ca^{2+}-dependent K^+ current, $I_{K(Ca)}$ appeared to be important in causing adaptation of the action potential frequency during maintained current stimuli. Elimination of Ca^{2+} influx reduced adaptation, as did intracellular iontophoresis of the Ca^{2+} chelator EGTA. Intracellular iontophoresis of Ca^{2+} augmented the rate of adaptation and, in voltage clamp, activated $I_{K(Ca)}$. When activated by Ca^{2+} iontophoresis $I_{K(Ca)}$ was weakly voltage dependent, showed no voltage threshold, and therefore could be activated at any physiological voltage. However, when activated by depolarization, the effective voltage

dependence of $I_{K(Ca)}$ was much steeper, and was almost identical to that of I_{Ca}, suggesting that voltage-dependent Ca^{2+} influx normally regulates $I_{K(Ca)}$.

ACKNOWLEDGEMENTS

A number of people contributed greatly to the material contained in this thesis. Stuart Thompson, Peter Ruben, and Jon Johnson were instrumental in getting all of the voltage clamp work started, and collaborated during aspects of the early experiments; for this I am very grateful. David Reye helped me to mold many of the rough ideas into stronger hypotheses during our late-night, beer-fueled discussions. Ian Gynther read rushed drafts of the chapters and helped me to get through the tough last months of writing.

My thesis supervisor, Andy Spencer provided me with direction, funding and especially friendship during my long and somewhat circuitous training process. Our research interests were dissimilar in many ways, and yet I was given the freedom to pursue my own interests. My supervisory committee; Dave Beatty, Andrew French and Keir Pearson gave me confidence and advice at many points along the way, and helped me to bypass the masters degree requirements and enter the doctoral program.

Gaels' support, friendship, and help throughout was invaluable. Also, I would like to thank Keir Pearson, Janet Yonida, and the members of Keirs' laboratory for making Edmonton feel a lot more like home.

Portions of the research were carried out at the Bamfield Marine Station, and at the Hopkins Biological Station of Stanford University. I was supported throughout my training by University of Alberta Graduate Teaching/Research Assistantships which I gratefully acknowledge. The research was funded by a Canadian NSERC grant to A. N. Spencer.

Table of Contents

Chapter — Page

DEDICATION iv

ABSTRACT v

ACKNOWLEDGEMENTS vii

I. GENERAL INTRODUCTION 1

II. IONIC BASIS OF THE ACTION POTENTIAL AND IDENTIFICATION OF MEMBRANE IONIC CURRENTS 4

INTRODUCTION 4

METHODS 6

Preparation 6

Solutions and perfusion apparatus 7

Separation of membrane currents 9

Electrical recording 11

Measuring membrane capacitance 14

Data storage and analysis 16

Suitability of barnacle neurons for the voltage clamp technique 17

RESULTS 18

Neuronal geometry and passive electrical properties 18

Ionic basis of the action potential in current clamped neurons 22

Membrane currents recorded in voltage clamped neurons 27

General observations 27

Capacitative and linear leakage currents 29

Inward sodium current 30

Inward calcium current 35

Delayed outward currents 38

Fast transient outward current 45

DISCUSSION 48

Passive electrical properties 49

Ionic basis of the action potential 50

Inward sodium current 53

Inward calcium current 53

Outward potassium currents 54

III. DESCRIPTION OF THE FAST TRANSIENT POTASSIUM CURRENT. 57

INTRODUCTION 57

METHODS 59

RESULTS 60

Separation of I_A 60

Voltage dependence and kinetics 65

Calcium sensitivity of I_A 73

Pharmacological sensitivity 91

DISCUSSION 98

Voltage dependence and kinetics 99

Calcium sensitivity 102

Pharmacological sensitivity 106

IV. REGULATION OF MEMBRANE EXCITABILITY BY THE FAST TRANSIENT POTASSIUM CURRENT 109

INTRODUCTION 109

METHODS 110

RESULTS 110

Effect of pre-stimulus voltage on membrane excitability 111

Effect of Ca^{2+}-free saline on membrane excitability 120

Effect of 4-aminopyridine on membrane excitability 124

Effect of forskolin on membrane excitability 128

Evaluation of the role of I_A in membrane excitability using a descriptive model 131

DISCUSSION 143

Response time 144

Action potential threshold 146

Action potential repolarization 147

Repetitive firing 148

Comparison with the previous literature 150

DESCRIPTION OF THE MATHEMATICAL MODEL 152

V. VOLTAGE AND CALCIUM DEPENDENCE OF THE SLOW MEMBRANE CURRENT RESPONSIBLE FOR SPIKE FREQUENCY ADAPTATION 155

INTRODUCTION 155

METHODS 156

RESULTS 157

Spike frequency adaptation and post-burst hyperpolarization 157

Activation of $I_{K(Ca)}$ by depolarizing voltage pulses 166

Activation of $I_{K(Ca)}$ by Ca^{2+} iontophoresis 170

Effect of Ca^{2+} injection on adapting spike trains 178

DISCUSSION 182

VI. GENERAL DISCUSSION 187

Representative crustacean neurons? 187

Voltage-dependent membrane currents 188

Ca^{2+}-dependent membrane currents 190

Repetitive action potential trains 192

Concluding remarks 193

VII. REFERENCES 195

List of Figures

Figure page

II-1 Ventral view of *Balanus nubilus* ventral ganglion external morphology. 8

II-2 Voltage clamp circuit, schematic diagram. 13

II-3 Voltage and current clamp fidelity. 15

II-4 Typical morphology of neurons used in current and voltage clamp studies. 19

II-5 Passive membrane response to a square hyperpolarizing current pulse. 21

II-6 Ionic basis of the action potential as determined by channel specific block. 23

II-7 Slow regenerative potentials observed in TTX, TEA saline. 25

II-8 Slow potentials are Ca^{2+} dependent. 26

II-9 Total membrane current elicited under voltage clamp in normal saline. 28

II-10 Activation characteristics of the early inward Na^{+} current. 31

II-11 Voltage dependence of I_{Na} system parameters. 34

II-12 I_{Ca} activation kinetics and voltage dependence. 36

II-13 Separation of voltage and calcium dependent components of slow outward current. 40

II-14 Instantaneous *I-V* curve for I_K. 41

II-15 Activation kinetics and voltage dependence of I_K system parameters. 43

II-16 Dose dependent blockade of I_K activation by TEA. 46

II-17 Hyperpolarizing prepulses activate a transient outward current, I_A. 47

III-1 Separation of I_A by voltage protocol. 62

III-2 Separation of I_A and I_K by sensitivity to external TEA. 63

III-3 Curve fit routines used to measure I_A parameters. 67

III-4 Dependence of I_A steady-state activation and inactivation on V_M. 69

III-5 Dependence of I_A activation time constant on V_M. 72

III-6 Dependence of I_A inactivation time constant on V_M. 74

III-7 Reduction of peak I_A in Ca^{2+}-free (Co^{2+}) saline. 77

III-8 Effect of Ca^{2+}-free (Co^{2+}) saline on the voltage dependence of b_∞ and $g_{A,peak}$. 80

III-9 Effect of Ca^{2+}-free (Co^{2+}) saline on the rate of I_A activation. 83

III-10 Effect of Ca^{2+}-free (Co^{2+}) saline on I_A time constants. 85

III-11 Comparison of experimental and calculated records describing the effect of Ca^{2+}-free (Co^{2+}) saline on I_A. 86

III-12 Effect of raising the external Ca^{2+} concentration on the voltage dependence of b_∞ and $g_{A,peak}$. 88

III-13 Effect of decreasing the external Ca^{2+} concentration on the voltage dependence of b_∞ and $g_{A,peak}$. 90

III-14 Effect of 1 mM 4-AP on I_A. 92

III-15 Effect of 100 μM verapamil on I_A. 94

III-16 Effect of 100 μM forskolin on I_A. 96

III-17 Effect of forskolin on the voltage dependence of τ_b and g_A. 97

IV-1 Effect of pre-stimulus voltage on action potential trains recorded in current clamp. 112

IV-2 Membrane conductance increase during the slow ramp depolarization. 114

IV-3 Outward current activated during the slow ramp depolarization. 116

IV-4 Dependence of the response time on the pre-stimulus membrane voltage. 117

IV-5 Effect of pre-pulse voltage on repolarization of the action potential. 119

IV-6 Effect of Ca^{2+}-free (Mn^{2+}) saline on the action potential frequency-current relation. 121

IV-7 Effect of Ca^{2+}-free (Mn^{2+}) saline on membrane excitability. 123

IV-8 Effect of Ca^{2+}-free (Mn^{2+}) saline on the slow ramp depolarization. 125

IV-9 Effect of 1 μM 4-AP on membrane excitability. 127

IV-10 Effect of 100 μM forskolin on membrane excitability. 129

IV-11 Effect of 100 μM forskolin on the neuronal response time. 130

IV-12 Simulation of the membrane action potential. 133

IV-13 Simulation of a repetitive action potential train following membrane pre-hyperpolarization. 135

IV-14 Simulation of the effect of pre-stimulus voltage on action potential repolarization. 137

IV-15 Simulation of the membrane currents underlying the slow ramp depolarization. 138

IV-16 Simulation of the membrane currents underlying slow repetitive firing. 140

IV-17 Simulation of the effect of Ca^{2+}-free (Co^{2+}) saline on membrane excitability. 141

IV-18 Simulation of the effect of forskolin on membrane excitability. 142

V-1 Effect of Ca^{2+}-free (Mn^{2+}) saline and EGTA injection on spike frequency adaptation and PSH. 158

V-2 Membrane current associated with spike frequency adaptation and PSH. 161

V-3 Reversal potential for the slow outward current. 163

V-4 Effect of Ca^{2+}-free (Mn^{2+}) saline on the slow outward current. 164

V-5 Voltage dependence of $I_{K(Ca)}$ activated by long depolarizing steps. 167

V-6 Voltage and Ca^{2+} dependence of $I_{K(Ca)}$ decay tails. 169

V-7 Voltage dependence of $I_{K(Ca)}$ tail current and peak I_{Ca}. 171

V-8 Sensitivity of $g_{K(Ca)}$ to injected Ca^{2+} and intrinsic voltage dependence of $g_{K(Ca)}$. 173

V-9 Effect of external TEA on $I_{K(Ca)}$ activated by Ca^{2+} injection. 175

V-10 Effect of prolonged high intensity Ca^{2+} injection on $I_{K(Ca)}$. 177

V-11 Effect of Ca^{2+} injection on frequency adaptation in current clamped spike trains. 179

V-12 Measurement of $I_{K(Ca)}$ activated by Ca^{2+} injection during an action potential train. 180

I. GENERAL INTRODUCTION

The voltage response of a nerve cell to synaptic or applied current is non-linear, and depolarizing stimuli can elicit complex, often regenerative voltage excursions. For this reason, the nerve membrane is said to be electrically excitable. Electrochemical excitability is the basis for most of the information transfer in nervous systems, and therefore this "chemical wave transmission" as it has been called (Hill, 1932) has long been of interest to physiologists. It was soon realized that signals are normally coded as the frequency of repetitive action potentials, and that these could be recorded from a wide variety of nervous (and non-nervous) tissues. The goal of many of the early studies was to understand the mechanism of excitation, and to elucidate the underlying physical processes which are fundamental to the operation of neurons as transmitters of frequency coded signals. Although this goal has been partially attained, and we now understand many of the principles governing excitation and the production of action potentials, there is still much to be learned. For example, we know relatively little about the way that subthreshold voltage trajectory and action potential encoding are regulated by membrane currents. This is the focus of much of the more recent work.

Experiments carried out over the past three decades have shown that transmembrane ionic currents, carried by ions flowing through membrane channels, are the basis for electrical excitability in nerve cells. Therefore, in order to understand the principles which govern signalling in the nervous system, we must first analyze the properties of membrane ionic currents and their respective channels. The initial development of the Na^+/K^+ hypothesis for excitation in the squid giant axon (Hodgkin and Huxley, 1952a, b, c, d) was followed later by similar investigations in other model preparations such as heart muscle (Noble, 1960), and myelinated axons (Frankenhaeuser, 1963). However, it was not until current measurement techniques were applied to the soma membrane of molluscan neurons that the variety in the types membrane currents became apparent. A number of new membrane current components were described, and these were found to have specialized roles in the generation and regulation of excitability (*e.g.* Geduldig and Gruener, 1971; Connor and Stevens, 1971b; Meech and Standen, 1975).

The original studies on molluscan neurons showed that soma membranes have a much more complex ensemble of ionic currents than do axonal membranes. This is probably a result of the functional differences between the soma and axon. The soma is often considered to be the 'integrating' part of a nerve cell, specialized for responding to various synaptic inputs and modulatory substances with the appropriate output. On the other hand, axons function primarily to transmit action potentials that have been coded at the soma over long distances and at rapid velocities. The true diversity of neuronal soma membrane current types is only now beginning to be fully appreciated as a larger number of species, and a larger range of neuronal types from each species are studied. The functional role of a number of these membrane currents has not been elucidated, and it is often assumed that functions proposed for molluscan neurons can be transferred freely to neurons from other groups.

In this thesis I examine the membrane ionic currents present in the soma membrane of barnacle neurons and analyze the functional role of two of the current components. The analysis was initiated primarily because the literature available at that time (early 1983) suggested that the ionic basis of excitability was not well understood for any neuronal soma other than molluscan neurons. This was particularly true for crustacean neuronal somata (see Atwood, 1982), although crustacean axons had been a favorite of physiologists for some time (*e.g.* Hodgkin, 1948). Thus, there was some value in studying crustacean neurons strictly from a comparative viewpoint, and because the axonal membrane systems were well understood made the soma properties of more interest. Perhaps more importantly, I wanted to test whether or not the hypotheses regarding the functional role of each of the current components, which had been proposed for molluscan neurons, were applicable in other types of neurons. I have concentrated on the role of ionic currents carried by K^+ and the mechanisms by which these currents regulate neuronal excitability. The emphasis on K^+ currents has developed for two reasons. First, the proliferation of K^+ currents in neuronal soma membrane is striking when compared to axons. This is true both for the relative magnitude of K^+ currents compared to other currents, which is large, and for the diversity of membrane current components carried by K^+. In some neuronal somata up to 5 different

components of membrane current are carried by K^+; however, the physiological role of each component is often not well understood, and may vary from one cell type to another. A second reason for concentrating on the role of K^+ currents was that I had the good fortune of receiving the technical and philosophical guidance of S. H. Thompson (Stanford University) and his co-workers during several visits to their laboratory. The emphasis there was on the physiological role of K^+ currents in molluscan neurons; therefore, my investigation of K^+ currents in barnacle neurons proved to be of mutual interest.

In Chapter II I present an overview of the major ionic currents in the somata of barnacle neurons. That chapter also serves as an introduction to the techniques and concepts involved in the description of membrane ionic currents. In the third chapter, I analyze the properties of a rapidly activating, transient K^+ current, and in the following chapter (IV) I examine its physiological role during single and repetitive action potentials. Chapter V investigates the mechanism of action potential frequency adaptation and describes the characteristics of a slowly developing, Ca^{2+}-dependent K^+ current which appears to be partly responsible for this phenomenon. Chapter VI consists of a general discussion and my concluding remarks.[1]

[1]This thesis is presented in 'paper format', which means that each chapter (except I and VI) represents a complete analysis including an introduction to the problem and discussion of the results. The citations for all chapters are combined in a single 'References' section which is located at the end of the thesis. At present, none of the chapters have been published or submitted for publication.

II. IONIC BASIS OF THE ACTION POTENTIAL AND IDENTIFICATION OF MEMBRANE IONIC CURRENTS

INTRODUCTION

Due in large part to the pioneering work of Hodgkin and Huxley (1952a, b, c, d) it is now accepted that specialized membrane currents, carried by ions passing through voltage-gated ionic channels, are the basis for excitability in nervous tissue. The approach used by Hodgkin and Huxley was to separate each of the ionic current components observed under voltage clamp, describe the time- and voltage-dependent behavior of the underlying conductances, and then to summarize this information in the form of a descriptive model. Although specific imperfections of the Hodgkin-Huxley (H-H) approach are now known to exist, descriptive empirical modelling of results obtained from tissue under voltage clamp conditions remains one of the most powerful tools for the investigation of excitability. Historically, application of H-H based models to tissues other than the squid axon has been driven by two general aims. First, there is the comparative approach, the goal of which has been to assess the general validity of the H-H kinetic model in preparations other than the squid axon. In most cases the standard H-H parameters have been modified slightly to provide reasonably good descriptions of excitability in a variety of cells. Second, the H-H philosophy has been used, with new formulations, to assess the role of conductance systems which are not present in the squid axon. These empirical models can then be used to provide a basis from which to evaluate the role of time- and voltage-dependent conductances besides I_{Na} and I_K in normal excitation.

Models based on the H-H squid axon formulations have been presented for other invertebrate axons (*Myxicola*, Goldman and Schauf, 1973; crab, Connor *et al.*, 1977), myelinated axons (Frankenhaeuser and Huxley, 1964), muscle cells (Noble, 1960; McAllister *et al.*, 1975, Beeler and Reuter, 1977), molluscan neuronal somata (Connor and Stevens, 1971c; Plant and Kim, 1976; Byrne, 1980a, b), and cat spinal motor neurons (Kernell and Sjoholm, 1973). In most of these cases the model could adequately describe experimental phenomena such as single action potentials, and even complex repetitive firing patterns,

from data based totally on voltage clamped membrane. Of these, only the work on *Myxicola* axon provides any strong evidence for specific shortcomings which may limit the utility of the H-H formulations. Goldman and Schauf (1972) found that the *Myxicola* axon Na^+ conductance was not well characterized by independent activation and inactivation terms as used in the H-H model.

The present study arose as an attempt to quantitatively describe the ionic conductances observed in a crustacean neuronal cell body. It is hoped that this type of analysis will provide a better understanding of processes underlying excitability in crustacean neurons. The membrane properties of crustacean ganglionic neurons are not well known, and description by the use of voltage clamp technique has been very limited and of a qualitative nature (Premack *et al.*, 1984; Tazaki and Cooke, 1984; Hartung, 1985; Shimahara, *et. al.*, 1985; Bruner *et. al.*, 1986). A few studies have investigated aspects of membrane ionic current in sensory receptors (barnacle photoreceptor, Brown *et al.*, 1969; Hudspeth and Stewart, 1979; stretch receptor soma and dendrites, Klie and Wellhoner, 1973; Chaplain, 1975; Mirolli, 1981, 1983). The lack of work on crustacean central neuronal somata arises for several reasons. The neuronal somata are not as large as those of many molluscan neurons, therefore they offer no real technical advantage. Perhaps more importantly, crustacean somata have been considered by many to be 'inactive' (not propagating an action potential) and thus serving little function in neuronal excitability or frequency coding (*e.g.* Hagiwara, 1961; Sandeman, 1969; Evoy, 1977; Tazaki and Cooke, 1983; Edwards and Mulloney, 1984). For the majority of crustacean neurons studied this may well be the case. In the larger, non-giant neurons of the ventral ganglion of the barnacle (*Balanus nubilus*) the situation differs. Action potentials are full-sized, and of short duration when recorded at the soma. Large electrotonic charging potentials do not contaminate records of soma-stimulated action potentials. In short, voltage recordings are often similar to those from neurons with active soma membranes, such as in many molluscan neurons.

The purpose of the present study is to describe the passive electrical properties, the ionic basis of the action potential, and to identify the membrane ionic conductances present in barnacle neuronal somata. Although it is possible to analyze ionic conductances without

reference to the parameters and measurement protocol used by Hodgkin and Huxley, in this analysis I follow a treatment similar to theirs. This was adopted because no other suitable simple, equivalently powerful alternative has yet been developed. Additionally, use of the 'standard' H-H treatment makes it somewhat easier to compare the results presented with those from other preparations. The descriptive equations derived by curve fitting will be used in a subsequent chapter (Chapter IV) where predictions from a H-H type model are analyzed.

METHODS

Preparation

All experiments were carried out using large (3 to 5 cm opercular diameter) specimens of the barnacle *Balanus nubilus*. Animals were collected from waters near the Bamfield Marine Station by SCUBA divers and maintained in either flowing natural seawater (Bamfield) or in recirculating artificial seawater (University of Alberta) at about 12 °C and fed frozen or live brine shrimp. Animals held in this way remained healthy for up to six months, but were seldom kept longer than two months.

Specimens were dissected in artificial seawater (Rila Mix, ASW) after cooling to 5 °C to produce anaesthesia. The ventral ganglion was removed as described by Gwilliam (1976) and stored in aerated artificial seawater at 5 °C until the experiment began. Usually this was within 30 minutes of dissection; however, in a few experiments, ganglia were kept for up to 8 hours prior to beginning an experiment. This treatment did not appear to have any ill effects on the tissue, and in some cases was advantageous because maintenance at 5 °C reduced unwanted synaptic currents.

The entire ventral ganglion, including 2 to 3 mm of all associated nerve trunks was transferred to a lucite perfusion/recording chamber lined with 'Sylgard' (Dow Corning). The ganglion was stabilized ventral side up, in the bottom of the chamber with cactus spines (*Opuntia* sp.) by pinning through each of the large nerve trunks. To aid in desheathing the ganglion a non-specific protease (Sigma type XIV) at 0.5 to 1 mg/ml was applied to the

ganglion for 3 minutes (12 °C) then washed off vigorously. After a one hour wash in ASW the sheath could be peeled away using fine forceps , exposing the surface 'rind' of numerous cell bodies.

Following the desheathing process the ganglion appeared much as it does in Figure II-1A. except that outlines of many cells could be seen. Individual neuronal somata appear circular in outline and range from about 10 to 60 μm in diameter. In each ganglion 5 to 10 of the largest surface cells were amenable to the voltage clamp technique used (see following). The larger cells could often be recognized on the basis of their position alone, but no specific attempt was made to limit experiments to identifiable neurons. Cell position was described by using a grid system for identifying the recording site. The *Balanus nubilus* grid system was based on the one used previously by Gwilliam (1976) for *Balanus cariosus*; however, there are differences in the shape and size of the ventral ganglia in the two species. The grid used, as well as a summary of the major nerve roots, is presented in Figure II-1B. Refer to Figure II-1 legend for details.

Of the results presented in this study only about 30% come from neurons which could be positively identified from ganglion to ganglion. The grid position and physiological characteristics of some of the larger, recognizable neurons were catalogued. Sometimes this was useful, when for example it was necessary to find a cell with "a large, fast I_A" to use in a particular experiment. Since only the largest cells were used in voltage and current clamp experiments, each grid location usually specified a single cell. Cells were not routinely labelled with marker dye, but were on occasion filled with Lucifer yellow (Sigma) in order to identify cells as motor or interneurons, and to determine the neuronal morphology.

Solutions and perfusion apparatus

Intact animals and stored ganglia were kept in the commercial artificial seawater preparation (ASW) whose ionic constituents were not known with certainty. The ASW was mixed to a total salt concentration of 30 parts per thousand (approximately 1000 m0s). For all experiments the external bathing medium was a simplified physiological saline that had been previously used for barnacles (Brown *et al.* 1971). This will be termed 'barnacle

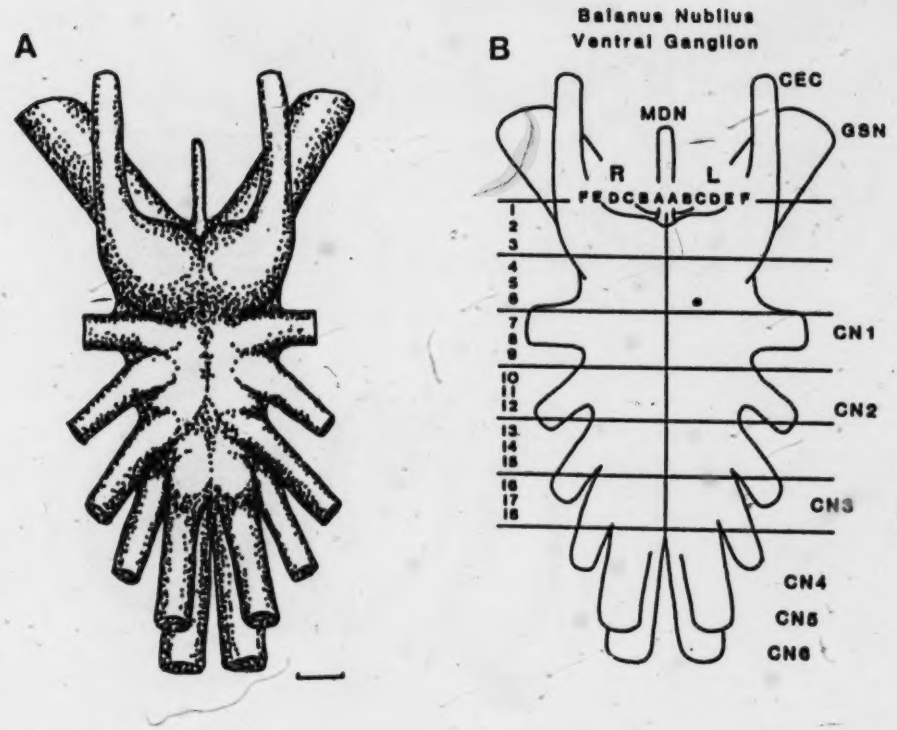

Figure II-1. A: Ventral view of *Balanus nubilus* ventral ganglion, showing the external morphology and major nerve roots. The drawing illustrates the ganglion much as it would appear viewed through a dissecting microscope prior to desheathing. B: Cell labelling grid system and nerve root identification. The grid system was used to identify recording points for intracellular recording, and to name identified neurons by their soma position. A cell at the position marked would be identified as C_L6. The major nerve roots are; circumesophageal connectives (CEC), great splanchnic nerves (GSN), middorsal nerve (MDN), cirral nerves 1 to 6 (CN1 to CN6). The scale bar is 100 μm and pertains to both A and B.

saline', or simply 'normal saline' throughout. The ionic composition of this saline is (in mM) 470 NaCl, 8 KCl, 20 $CaCl_2$, 5 $MgCl_2$. All salines contained 10 mM HEPES buffer (Sigma) and were maintained at a pH of 7.5 (± 0.05) by addition of 1 N HCl or NaOH. Experimental salines are discussed in detail in the 'Separation of membrane currents' section.

A gravity-fed perfusion system was used to produce near laminar flow through the 0.8 ml recording/perfusion chamber. Flow rate was adjusted to about 2 to 3 mls per minute by flow valves and waste perfusate was aspirated off. The preparation was not continually perfused; rather, 10 mls of fresh saline was added about every 15 minutes. This technique was adopted because the flowing perfusion system introduced noise into the current measuring amplifiers. The bath turnover time was estimated by using methylene blue dye added at low concentrations to the perfusion system. On addition of a known dye concentration to the header reservoir the bath reached 90% of the header concentration within 4 minutes, as measured with a Bausch and Lomb spectrophotometer (Spec 20). During experiments, test solutions were generally added to the perfusion reservoir in large enough volume to give a 10 to 15x bath volume change.

All experiments were conducted at 12 °C (± 0.5 °C). A telethermometer (Yellow Springs Instruments Model 73) was used to control current flow through four peltier blocks (Cambion) connected in series. Temperature was monitored by a linear thermistor (Yellow Springs Instruments), sealed and submerged within the external bathing medium. The perfusion chamber was mounted to a brass heat-sink with thermally conductive paste. The variability within the control system of ± 0.5 °C was initially considered somewhat excessive because of accompanying variation in measured rate and time constants during an experiment. However, calculations of rate constant variation (assuming a Q_{10} of 3.0) suggest that for events studied here the observed ±0.5 °C variation in temperature would lead to a maximum ± 6% error in measured rate constants. This was considered acceptable.

Separation of membrane currents

For many experiments it was necessary to observe individual membrane current components in relative isolation. In some cases this could be achieved by appropriate

manipulation of the holding or step potentials under voltage clamp. This 'voltage paradigm' separation of membrane current components is discussed in detail as the results are presented. During other experiments the components of membrane current were isolated by treatments which specifically blocked unwanted current components. The treatments fall roughly into two classes: 1) Separation by pharmacological block using channel specific drugs; 2) Separation by ion replacement or substitution.

Three pharmacological agents were routinely used alone, or in combination. Tetrodotoxin (Sigma, TTX) was used to block fast inward current carried by voltage dependent Na^+ channels. Since its first neurobiological application (Narahashi *et al.*, 1964) it has been proven reliable, and specific to voltage gated Na^+ channels in many preparations. TTX was prepared as a stock 100 μM solution in barnacle saline, stored frozen and (after thawing) added directly to the bath. Tetraethylammonium (as the chloride salt, Sigma, TEA) was used to block components of membrane current carried by delayed rectifier, I_K channels. Although different kinetic components are blocked in various tissues, TEA is thought to be a specific blocker of K^+ channels (Hagiwara and Saito, 1959). TEA was used in some experiments at concentrations of up to 100 mM. To preserve the tonicity of the bathing saline NaCl was omitted and replaced with the desired TEACl concentration. TEA salines were made up on a weekly basis from recently purchased TEACl. In some experiments, where it was desirable to eliminate Na^+ and K^+ currents, TEACl was used at a concentration of 470 mM, totally replacing NaCl. 4-aminopyridine (Sigma, 4-AP) was used in a few experiments as a blocker of fast K^+ channel activation (Pelhate and Pichon, 1974; Thompson, 1977). 4-AP saline was prepared fresh the day of the experiment, and pH adjusted using HCl.

Other pharmacological agents used at concentrations of less than 1 mM were prepared as stock solutions in 100% DMSO (dimethylsulphoxide, Sigma) and stored frozen until immediately prior to use. The stock solutions were then thawed and added to the bath directly to give the desired final concentration. Quinidine sulfate (Sigma), forskolin (Calbiochem), isobutylmethylxanthine (IBMX, Sigma), and verapamil (Sigma) were prepared in this way and stored at concentrations of 10 or 100 mM. Each was used at the

final concentrations noted where the results are presented.

In a number of experiments Ca^{2+} currents and obligatorily Ca^{2+} activated currents were eliminated by ionic substitution. $CaCl_2$ was omitted from normal saline and replaced with either $MnCl_2$ or $CoCl_2$ at an equimolar (20 mM) concentration. These salines are denoted Ca^{2+}-free in the text, with the replacing cation following in brackets. Both Mn^{2+} and Co^{2+} ions are thought to block Ca^{2+} channels by plugging the pore opening, as their hydrated radius is larger than that of Ca^{2+}. Addition of divalent cationic solutions directly to the bath was avoided because this was observed to produce measurable surface potential shifts sometimes called 'Frankenhaeuser-Hodgkin' shifts (Frankenhaeuser and Hodgkin, 1957).

Electrical recording

Cells were current or voltage clamped at the neuronal soma by the two microelectrode technique. Two glass (Heyer Corporation) micropipettes filled with 3 M KCl were brought above the target cell using sliding plate manipulators (Jena Instruments) and inserted individually into the soma. Brief oscillations induced by over compensating the electrode capacitance were used to facilitate microelectrode penetration. Current electrodes had resistances of about 10 MΩ and voltage electrodes 15 MΩ, after bevelling in a carborundum slurry, when measured in barnacle saline.

For the voltage monitor electrode a World Precision Instruments Model 701 microelectrode amplifier was used. This amplifier was chosen because the rise time was very fast (10-90% in 10 μs through a 20 MΩ source resistance) and the capacitance neutralization was well designed, and gave the voltage electrode a full DC to 30 KHZ bandwidth. The x1 output was filtered at 10 KHz and monitored as cell voltage. The unfiltered x5 output was used for input to the voltage control or 'voltage clamp' amplifier as discussed below.

The current electrode follower was a Getting Model 5 microelectrode amplifier, chosen because its constant current feature was used as the current clamp amplifier for driving spike trains. The current pump circuit monitored output current across a 100 MΩ

headstage resistor. The maximum current driveable was 120 nA through a 10 MΩ external resistance, although output current is only constant up to ± 30 nA. The standard headstage was modified by adding a low capacitance manually operated switch to bypass the Getting amplifier completely when in voltage clamp mode.

The voltage clamp amplifier was designed to produce a good clamp with barnacle neurons. The general circuit layout was of conventional design, but also incorporated modifications for DC boost (Dionne and Stevens, 1975), adjustable current feedback compensation (Katz and Schwartz, 1974) and high frequency gain control (Smith *et al.*, 1980). Details of the circuit are presented in Figure II-2. The open loop gain was high (usually 5,000 to 15,000 at 30 KHz) as result the voltage step rise time was less than 100 μsec and was accurate to within ±1 mV as measured with a second voltage electrode. In order to reduce electrode capacitative coupling, both electrodes were shielded with grounded aluminum foil wrapped to within 1 mm of the electrode tips. The bath level was kept low so that less than 200 μm of the electrode tips were submerged.

Membrane current was measured using a virtual ground circuit connected to the bath via a Ag/AgCl pellet and agar bridge (1% Agar in PE 50 tubing). The circuit converted current to voltage at either 1 mV/nA or 10 mV/nA depending on the feedback resistor used (either 1 MΩ or 10 MΩ, see Fig. II-2). Membrane currents were filtered at 1, 5, or 10 KHz using four pole Bessel type filters (damping factor, D=1.73) giving a -12 dB/octave roll-off (design as per Lancaster, 1975).

During voltage and current clamp experiments the desired step commands were produced by a rack mounted Rockwell AIM 65 microcomputer. The computer was programmed in BASIC (Microsoft Inc.) to automatically produce the desired step command and holding potentials. The AIM-65 was used to drive a Beckman 12-bit D-A converter with ±10 V output, rolled off at either 15 or 50 μs. The same computer was used to trigger oscilloscopes, and FM tape deck during data collection.

The speed, linearity and fidelity of the control ('clamp') systems were evaluated initially using a resistor-capacitor network which approximated the passive properties of a

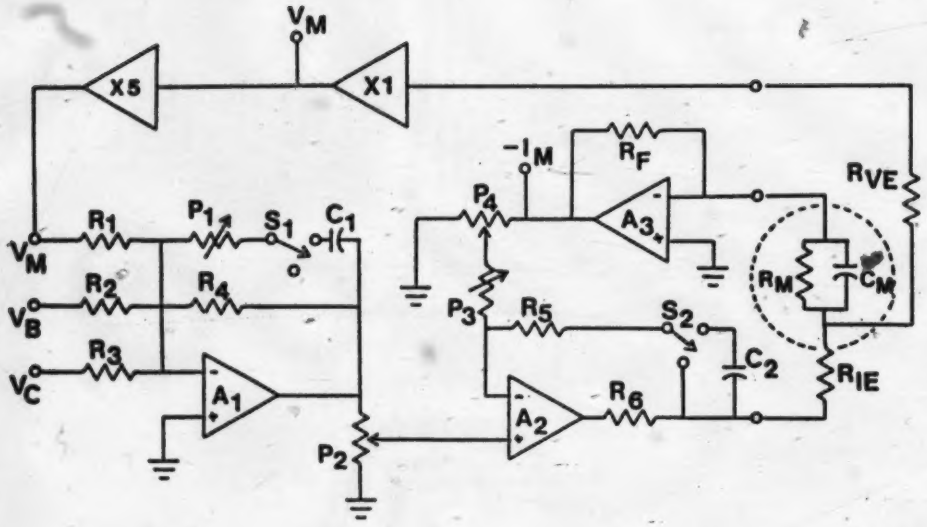

Figure II-2. Voltage-clamp circuit, schematic diagram. The voltage clamp amplifier consists of single operational amplifiers A_1 and A_2. A_1 is the first, fixed gain (-200x) stage that also acts as the summing point for cell voltage (V_M), bath voltage (V_B), and the voltage command (V_C). A_2 is a variable gain, non-inverting feedback amplifier set up to drive V_M to V_C by injecting current via the current passing electrode (R_{IE}) into the 'cell', represented here as the parallel resistance and capacitance (R_M, C_M). Amplifier A_3 is the virtual ground which monitors the current passed to the bath by A_2 ($-I_M$).

barnacle neuron (R_M = 10 MΩ, C_M = 1 nF). Fine tuning of the feedback system design produced a fast, linear system as shown in Figure II-3. Under current clamp (Figure II-3A) the current control system had a 90% rise time of about 200 μs over a ± 20 nA range. Actual current passed was always recorded using the virtual ground circuit and not the headstage resistor. The largest stimulating current used for most experiments was 10 nA and this was well within the linear current pumping limits of the amplifier. The current stimulus rise time is also much less than the 5 to 20 ms time constants encountered in barnacle neurons. In voltage clamp configuration, the system settled to the final command voltage with no damped oscillations or overshoot in 60 to 80 μs (Figure 11-3B). The current recording circuit did not saturate or ring during the capacitative transient even for 140 mV depolarizing steps. The settling of the current recording circuit had no slower components which might obscure early events or post-clamp 'tail' currents.

Measuring membrane capacitance

Displacement of the trans-membrane voltage in either a depolarizing or hyperpolarizing direction generates current flow across the membrane capacitance. If the voltage change is rapid the capacitative current is large and transient. The magnitude of this current, I_C, is dependent on; 1) the rate and the magnitude of the voltage step, 2) the amount of dielectric (membrane lipid) whose voltage is displaced. For a neuron in voltage clamp

$$I_C = C_M \cdot dV_M/dt \qquad \text{(II-1)}$$

Since the membrane capacitance, C_M, is constant, I_C peaks during the voltage step when dV_M/dt is maximal. The decay of I_C after an instantaneous voltage step is a single exponential.

With a triangle wave voltage stimulus dV_M/dt is constant magnitude, but reverses sign. Since dV_M/dt is constant under these conditions I_C is proportional to C_M alone. I use this relation to measure C_M under triangle voltage clamp. If the voltage changes instantaneously from a positive going to negative going wave, I_M is a square wave whose peak to peak amplitude is related to C_M by

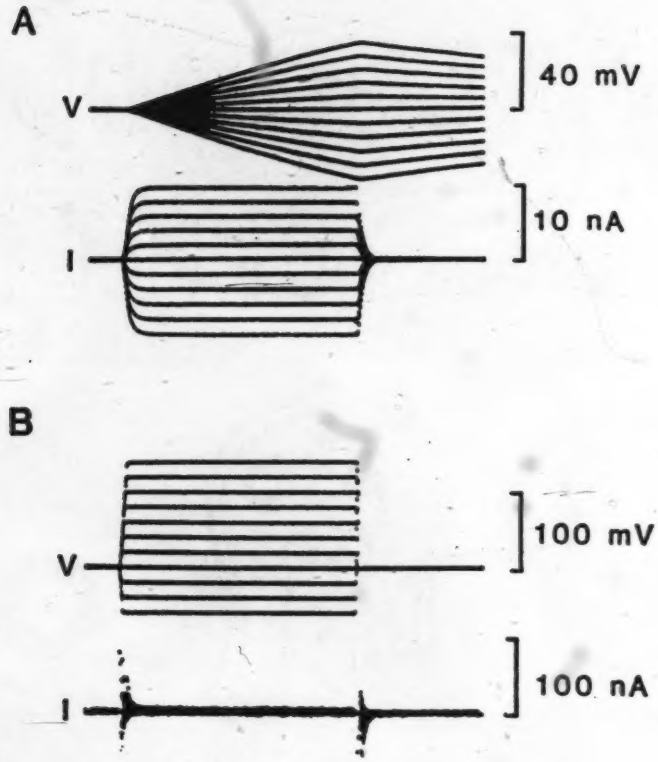

Figure II-3. Voltage and current clamp fidelity. A: Voltage response of a resistor-capacitor cell analogue under current clamp. The duration of the current pulse (lower trace) is 5 ms. Current clamps of -10 to +10 nA are shown. In each case the initial rise and fall of the current pulse is relatively fast compared to the much slower voltage time constant of the cell analogue (about 10 ms, top trace). Current and voltage traces filtered at 10 KHz. B: Response under voltage clamp conditions using maximal clamp gain (20,000x at 30 KHz.). The voltage steps are faithfully reproduced for commands of -100 mV to +140 mV. The duration of the voltage step is 5 ms.

$$C_M = I_M \bullet \lambda/4 \bullet dV_M \qquad \text{(II-2)}$$

where C_M is in nF, I_M is in nA, dV_M is the peak to peak triangle wave command in mV and λ is the period in ms (Palti, 1969).

In practice a 40 mV peak to peak triangle wave command with a 4 to 6 ms period gave the best results. The triangle wave was centered at -60 mV and thus oscillated between -80 and -40 mV. Of the membrane ionic currents, only a small I_{leak} is active in this voltage range. The capacitance measured in this way was independent of period over the range of 2 to 10 ms for both cell analogues and real neurons under voltage clamp.

Data storage and analysis

During experiments data were stored on one or more of 1) polaroid photographs of oscilloscope tracings 2) FM tape recordings 3) rectilinear chart recordings . The method of storage was usually determined by the relative speed of the event being studied. Very fast events were photographed directly from the oscilloscope screen because of the resolution and high frequency response (more than 10 MHz) of the display. Usually a Tektronix 511A analog oscilloscope or 5D10 waveform digitizer were used. Events in the slower range were stored on FM tape where the limited bandwidth (see below) would not influence measurements. These tapes were then analyzed using the laboratory minicomputer. Some very slow events that would take much tape and/or disc space were stored directly on a chart recorder (Gould Brush 220) with a DC to 60 Hz bandwidth. Data for computer analysis was stored on an FM tape deck (Hewlett Packard 3964A) at a carrier frequency of 13.5 KHz and tape speed of 15 cm/sec. The response was DC to 2.5 KHz (±1 dB) when used with a 3M type 888 tape and the internal flutter compensation on. The signal-to-noise ratio of the FM tape deck was quite poor and the taping process always introduced some noise. Occasionally data had to be re-filtered after storage on tape.

Measurements from some of the data already stored as polaroid photographs, or chart recordings, were digitized using a Grafbar GP-7 Sonic Digitizer (Science Associates Corp.). This system uses a high frequency emitting stylus under manual control, accurate in both x and y planes to ± 0.1 mm. The digitizer was run on-line in either 'stream' or

'single point' mode with the University of Alberta AMDAHL mainframe computer.

Much of the data analysis was performed on a LSI-11/03 based minicomputer system (Transduction Ltd.) equipped with Schmitt triggers and two channel 12 bit analog to digital conversion. All of the data sampling and analysis routines were run using the BOSS operating system and MOTLEY programming language (both courtesy of Dr. A. S. French, University of Alberta). Data (from the FM tape) were stored as serial files (512 data points/file) at sample intervals of 50 μs to 10 ms. Hard copies of computer analyzed data were produced using an Epson MX-100 dot matrix printer. Non-linear curve fitting was done by MOTLEY by transforming the data appropriately and then using simple linear regression as per Zar (1974). For complex functions where no transformation to linearity was available data were 'best-fit' by eye using iterative routines which varied equation parameters while simultaneously displaying data point and function plots. In the graphs vertical bars represent $\pm$ one standard error of the mean (SE).

Suitability of barnacle neurons for the voltage clamp technique

Over the course of preliminary experiments and those presented here, over 200 ventral ganglion neurons were studied with the two electrode technique. Most neurons appeared relatively healthy after dual electrode penetration, although these neurons never had as deep resting potentials or high input resistances as singly impaled neurons. This slight damage probably results from the need to use low resistance current electrodes (5 to 10 MΩ) with relatively small (40 to 60 μm) cells. However, the membrane current magnitudes that had to be controlled were in some cases up to 1 μA and large diameter electrodes could not be avoided.

During the course of an experiment the health of impaled cells generally declined slowly. This did not seem to be influenced by electrode filling solutions (diffusing into the cell) or membrane holding potential during the experiment. It appeared to result from a physical 'leak' in the neuron due to impalement damage, which was manifested as an increase in the measured ionic leakage component under voltage clamp. Usually cells would only remain viable under clamp for 30 to 60 minutes. Occasionally this limited the number

of test solutions that could be used during an experiment, or resulted in a lack of drug reversibility data for some treatments which were slow to take effect.

RESULTS

Neuronal geometry and passive electrical properties

Most of the cells used in these studies were chosen on the basis of their soma size. At the start of an experimental session the largest neurons in the ganglion were penetrated first (soma diameter 50 to 60μm), progressing to the smaller cells. In six ganglia a number of the largest, most visible somas were penetrated and filled with the fluorescent marker dye Lucifer yellow. Each of the twelve cells successfully filled had a single, relatively large diameter process coursing out of the ganglion via one of the motor nerve trunks. Therefore they are presumed to be motor neurons, although the possibility exists that some may be central sensory neurons. Interneurons in this ganglion usually had small diameter somas when filled with Lucifer Yellow. In a few earlier experiments in which some of the feeding appendages (cirri) were left innervated, stimulation of single large cells caused local muscle contraction. Larger soma size amongst motor neurons is consistent with findings in many preparations, and it seems likely that most of the neurons used were motor neurons.

Typically, the larger neurons were unipolar and the neuronal somata were essentially spherical. Figure II-4 shows drawings of two neurons from Lucifer Yellow fills. The paucity of dendritic fields is striking and, in general, most of the dendritic processes are very fine (less than 1 μm) and not heavily branched. For the cell pictured on the left the highest density of processes occurs where the 'neck' of the soma tapers into the major neurite. In a few cells, such as the one pictured on the left, fine dendrites project from the surface of the soma giving it a 'fuzzy' border when viewed at high magnification. This dendritic arborization was limited, though a few small processes extended out up to 4 times the soma diameter. Most had lengths of less than one soma diameter. The cells appeared to be morphologically compact and relatively uncomplicated.

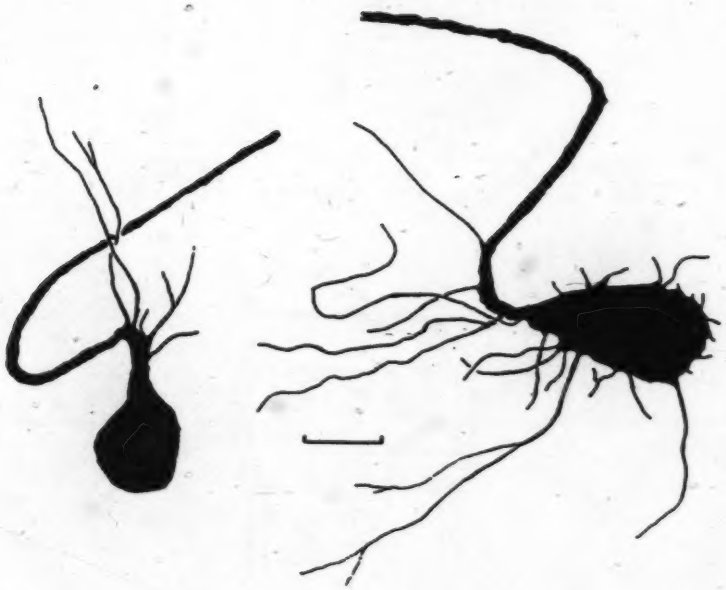

Figure II-4. Typical morphology of neurons used in current and voltage clamp studies. Two exemplar neurons are drawn from Lucifer yellow fills, after dehydration and clearing. Both neurons were unipolar, and the main process of the axon was unbranched throughout its course through the ganglion. The cell on the left has the more common morphology, with neuropilar branching limited to the initial segment. The cell drawn on the right has fine processes coming directly off the soma membrane. The drawings were traced by projection of photographic slides directly onto drawing paper. Scale bar 40μm. The scale bar refers to the soma dimensions prior to dehydration and clearing, and therefore the dimensions were not corrected for shrinkage.

Doubly penetrated neurons had resting potentials averaging -43 mV (range -35 to -60 mV) and input resistances averaging 6.2 MΩ (range 2 to 19 MΩ). In most neurons the voltage decline during a hyperpolarizing current step was well fitted by a single exponential regression ($r^2 >= 0.95$). In this way, the cell voltage response is similar to that of a single section parallel *RC* network (Figure II-5A). This suggests that these neurons are electrotonically compact. The electrical properties of the soma dominate the response of the cell and the cable properties of the attached axon and dendrites are relatively less important. This arrangement would be equivalent to the Rall model axon with the soma-axon coupling factor (α) set to a value close to zero (see Rall, 1969). Closer inspection of plots as in Figure II-5A revealed that small deviations from exponential response occur during the first few milliseconds of the pulse. This probably results from a small amount of current shunting to dendritic and axonal membrane. Membrane time constants, calculated by fitting regressions to the voltage decline for small hyperpolarizing current pulses, ranged from 5 ms to 20 ms.

In many neurons, sheathing cells in close proximity to the neuronal surface create a resistance in series with that of the neuronal input resistance. When membrane currents flow this can create a voltage drop across the series resistance (R_S), and thus an error in the measured value of V_M. The magnitude of the V_M error is $I_M R_S$. Several attempts to measure the effective R_S using the method of Moore and Cole (1963) suggested that R_S is very small in these neurons. Large (100 nA), brief hyperpolarizing current pulses (Figure II-5B) were used to test for series resistance, which would appear as a rapid downward deflection in the measured cell voltage. However, no instantaneous jump was measurable in these experiments. Assuming a jump was present, but of an amplitude less than would be observable above the electrode noise (0.5 mV), R_S could be at the largest 5 KΩ. 'Worst case' errors in the measurement of V_M arising from current flow through R_S would then be about 2 mV since the membrane currents studied were generally less than 400 nA. Therefore, no series resistance compensation was used during the following experiments.

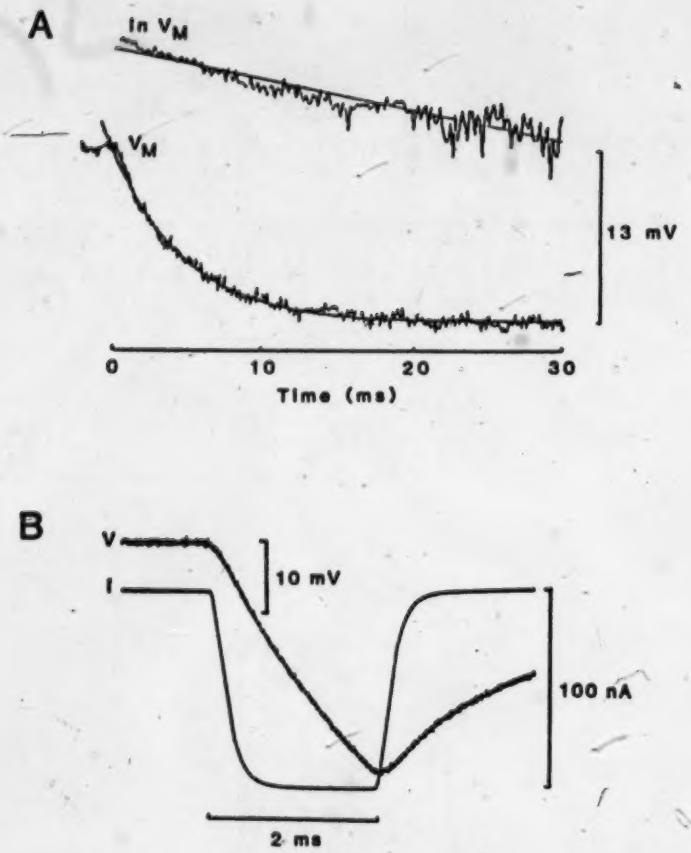

Figure II-5. Passive membrane voltage responses to square hyperpolarizing current pulses. A: A hyperpolarizing current pulse (-2 nA) was applied in current clamp at $t = 0$ to measure passive electrotonic properties. The steady-state voltage change was 13 mV, therefore the membrane input resistance was 6.5 MΩ. The neuronal voltage response is plotted after digitization (sample interval = 100μs). The upper trace is a plot of ln V_M, which linearizes the response. Bottom trace is the same data set for a linear V_M plot, the curve is the best fit single exponential (τ = 8 ms, amplitude = 13 mV) describing the data. Note that both fits deviate most during the first 2 to 3 ms. This deviation results from a small contribution by the passive cable properties of the dendrites and/or axon. B: Large hyperpolarizing pulse (-100 nA, 2 ms) used to assess the contribution of resistance in series with the cell input resistance. Upper trace, cell voltage (filtered at 10 KHz). Lower trace, transmembrane current recorded with a virtual ground (filtered at 10 KHz). No instantaneous voltage deflection was measurable at the onset of the current pulse. Such a deflection, if present would reflect current flow through a series resistance which has bypassed the membrane capacitance and thus rapidly shifts the measured V_M. The record in B was photographed directly from the oscilloscope screen.

Ionic basis of the action potential in current clamped neurons

For the larger ventral ganglionic neurons used in this study, short depolarizing current pulses elicited overshooting action potentials of 60 to 100 mV amplitude with durations at half maximum amplitude of 3 to 7 ms. The mean voltage reached at the peak of the action potential was +44 ±2 mV (± SE, n = 24 cells). There appeared to be a positive correlation between action potential amplitude and soma diameter, the largest cells usually having the greatest overshoot. Figure II-6A shows a typical action potential under current clamp. Spike threshold was 5 to 25 mV depolarized to the resting membrane potential (ranging about -35 to -25 mV) and the maximum dV/dt during the rising phase was 80 to 120 V/s. A large spike after-hyperpolarization was evident with a peak hyperpolarization in various cells of -45 to -60 mV. All cells studied were capable of firing repetitively to a maintained depolarizing stimulus. The characteristics of repetitive spike trains will be discussed in detail in subsequent chapters.

Action potentials were reversibly blocked in 4 to 6 min by low (10 to 100 nM) concentrations of the Na^+ channel blocker tetrodotoxin (TTX, Figure II-6B). Usually, however TTX was used at a standard bath concentration of 1 μM to assure saturation of binding sites. In most cases this treatment rendered the cells totally inexcitable to depolarizing stimuli under current clamp. Therefore, it appears that Na^+ is the major current carrier during the upstroke of the action potential. Bath application of TTX did not measurably alter the resting potentials or input resistances. With action potentials blocked (1 μM TTX) the V-I relationship under current clamp was linear for hyperpolarizing pulses (in the -90 to -40 mV range). Stimulation with depolarizing current pulses elicited voltage responses which showed an early 'hump' and prominent delayed rectification (resistance decrease) when V_M was driven above -20 mV. The small hump is probably due to current flowing through the membrane capacitance followed by the voltage-dependent opening of delayed rectifier K^+ channels which then decrease the membrane resistance.

Action potentials were prolonged bath application of the K^+ channel blocker tetraethylammonium (TEA). TEA concentrations of 5 mM or greater broadened the action potential in most cells by slowing the repolarization rate. In a few cells, concentrations as

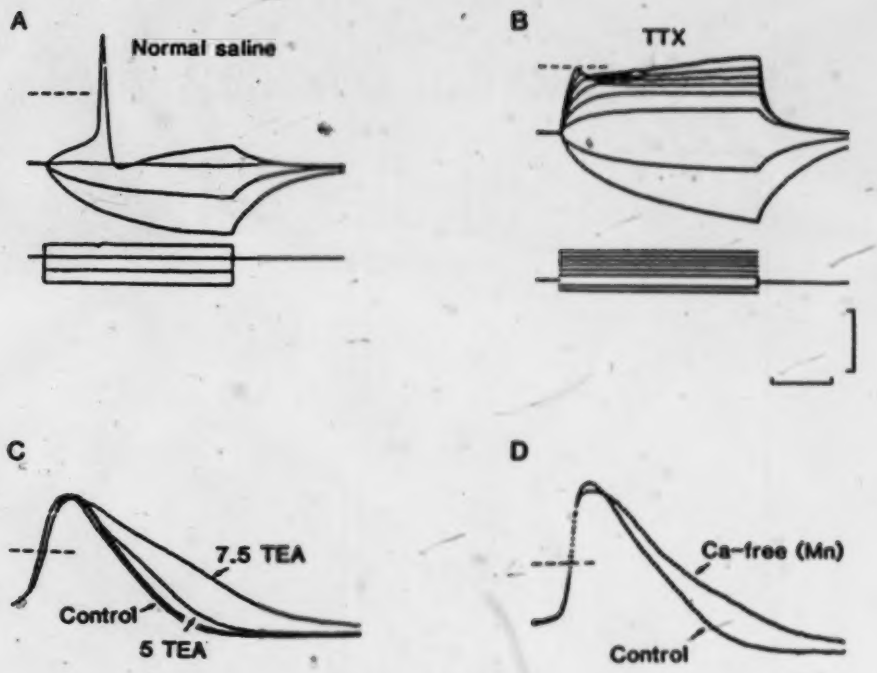

Figure II-6. Ionic basis of the action potential as determined by channel specific block. A: Action potential in normal saline elicited in current clamp. Membrane voltage responses to 120 ms duration current clamp pulses of -4 to +2 nA in 2 nA steps. In this cell, the input resistance to hyperpolarizing pulses was about 12 MΩ. The depolarizing pulse elicits a typical overshooting (to +30 mV) action potential, and following after-hyperpolarization. The initial cell resting potential was -44 mV, and the dotted line is 0 mV (bath potential). B: TTX (applied externally at 100 nM) completely blocks normal action potentials, presumably by blocking Na^+ depolarizing drive. The current stimuli used ranged from -4 to +12 nA. A and B are two different cells. C: Effect of low concentrations of TEA on repolarization of the action potential. The action potentials were elicited by a 2 nA, 20 ms current pulse. The superimposed traces were recorded for one cell in control, 2.5 mM, 5 mM, and 7.5 mM TEA external saline. The action potentials in the control and 2.5 mM TEA saline overlap, but the higher TEA concentrations cause a dose dependent increase in duration. D: Effect of Ca^{2+}-free (Mn^{2+}) saline on the action potential. The action potential threshold and rate of rise are unaltered, but the peak amplitude was decreased slightly in Mn^{2+}. The action potential duration was substantially increased, especially late in the repolarizing phase. The after hyperpolarization following the impulse was also reduced. The time scale bar is 40 ms in A and B, 4 ms in C and D. The voltage scale bar is 40 mV.

low as 2 mM altered the normal repolarization rate. For the cell shown in Figure II-6C 5 mM TEA resulted in a 17% increase in duration at half amplitude (4.8 ms to 5.6 ms), 7.5 mM TEA produced a 77% increase. The increase in duration was dose dependent and at high (50 mM) TEA concentrations action potentials up to 500 ms long were observed. TEA concentrations greater than 5 mM also reduce the after hyperpolarization following the action potential. At high TEA concentrations action potential broadening began within 30 s of bath application, suggesting that TEA acts at an external site, and not by permeating the membrane. Since TEA block is quite specific to K^+ channels, action potential repolarization must be dependent upon the opening of voltage activated K^+ channels and not strongly dependent on inactivation of Na^+ channels. Interestingly, TEA concentrations of up to 100 mM caused little decrease in the control resting potential (average in 100 mM TEA = -37 mV, 12 cells). This suggests that the K^+ channels responsible for maintenance of the negative rest potential are pharmacologically distinct from those which repolarize the action potential.

Replacement of the external Ca^{2+} in the bathing medium with Mn^{2+} or Co^{2+}, to block the contribution of inward Ca^{2+} current, had rather unexpected results on the action potential. Although the amplitude was often decreased slightly (5 to 10 mV), the predominant effect was a marked *increase* in action potential duration (Figure II-6D). This increase in duration was due to a pronounced shoulder during the repolarizing phase. This is not consistent with a decrease in depolarizing Ca^{2+} influx, which would be expected to decrease the action potential amplitude and duration.

In cells previously rendered inexcitable to current clamp stimulation by extracellular TTX (1 μM) the further addition of TEA (10 to 50 mM) to the bath often produced slowly activating, regenerative, potential changes when stimulated. These slow potentials had a higher threshold than Na^+ action potentials (-20 to -10 mV) and variable peak amplitudes, usually the maximum depolarization was +10 to +30 mV. The maximum dV/dt during the rising phase averaged about 5 V/s and durations at one half amplitude ranged from 60 to 460 ms (Figure II-7, A and B). Figure II-8 shows that replacement of all the external Ca^{2+} (20 mM) with impermeant Co^{2+} ions blocks the slow potential. Calcium replacement with

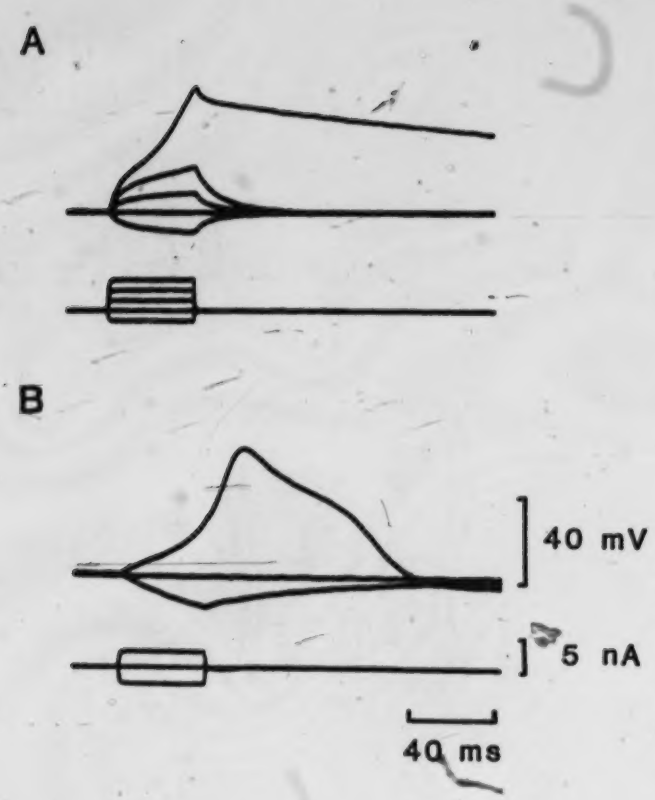

Figure II-7. Slow regenerative potentials elicited by depolarizing stimuli in TTX, TEA saline. A: Small hyperpolarizing and depolarizing pulses produce symmetrical passive changes in membrane voltage (top trace). The largest depolarizing pulse evoked a nonlinear regenerative plateau outlasting the stimulus by 450 ms (full decay not shown). The resting potential was -37 mV. B: Similar slow spike in another cell, but showing more rapid repolarization. This cell was hyperpolarized by a constant holding current of 1 nA. Without this bias the spikes occurred spontaneously and regularly at about 2 Hz. Both cells were bathed in 1 μM TTX, 50 mM TEA external saline.

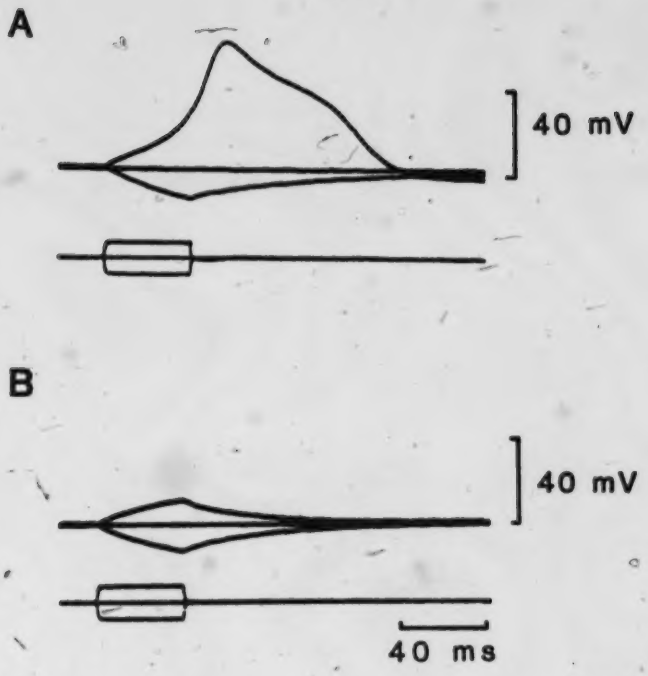

Figure II-8. Slow potentials are Ca^{2+} dependent. Replacing the normal saline with Ca^{2+}-free (Co^{2+}) saline blocked the active properties observed in 1 μM TTX, 50 mM TEA saline. A: Voltage response elicited by short depolarizing current pulse in TTX, TEA saline. B: The slow potential was eliminated after 10 min perfusion Ca^{2+}-free (Co^{2+}), TTX, TEA saline. A: is the same recording as shown in Figure II-7B.

equimolar Ba^{2+} increased the amplitude and duration of the slow potentials (data not shown). Taken together these results suggest that the slow potentials are similar to calcium spikes seen in other tissues (Hagiwara, 1971). In a few cells the slow potentials occurred spontaneously at low frequency (1 to 3 Hz.) and appeared similar to 'driver' potentials in crab cardiac ganglia (Benson and Cooke, 1985). Presumably, an inward Ca^{2+} current provides the necessary depolarizing drive during the upstroke, because Ca^{2+}-free saline also blocks the 'driver' potentials. Slow spikes as observed in TTX, TEA saline were never observed in normal saline.

Membrane currents recorded in voltage clamped neurons

General observations

Although there was some variability in the resting membrane potential of doubly penetrated neurons, all were voltage clamped at a standard holding voltage of -40 mV. This was chosen as the nearest decade value to the observed average rest potential (-43 mV). Consequently some cells when clamped were depolarized slightly to their rest value, while others were hyperpolarized by the voltage clamp feedback. Typically, this 'holding current', applied by the feedback amplifier, ranged from -2 to +2 nA at -40 mV.

Depolarizing voltage steps from the holding potential activated a complex mixture of voltage and time-dependent inward and outward membrane ionic currents. In addition, a large non-ionic displacement or capacitative current was present in all records. A small voltage and time invariant 'leakage' current was present at the holding voltage, and observable in isolation at potentials negative to -40 mV where it was the only membrane current active. Figure II-9 shows the membrane currents observed prior to any pharmacological separation, and illustrates the degree of current component separation which can be achieved by manipulation of the holding potential alone. Holding the membrane voltage at a value slightly depolarized to normal cell rest caused several components of the total membrane current to become inactivated, or nonconducting. In Figure II-9, V_M was clamped initially at -30 mV. The depolarizing step to 0 mV elicited an outward (plotted upward) going membrane current, which activated relatively slowly, and was maintained for

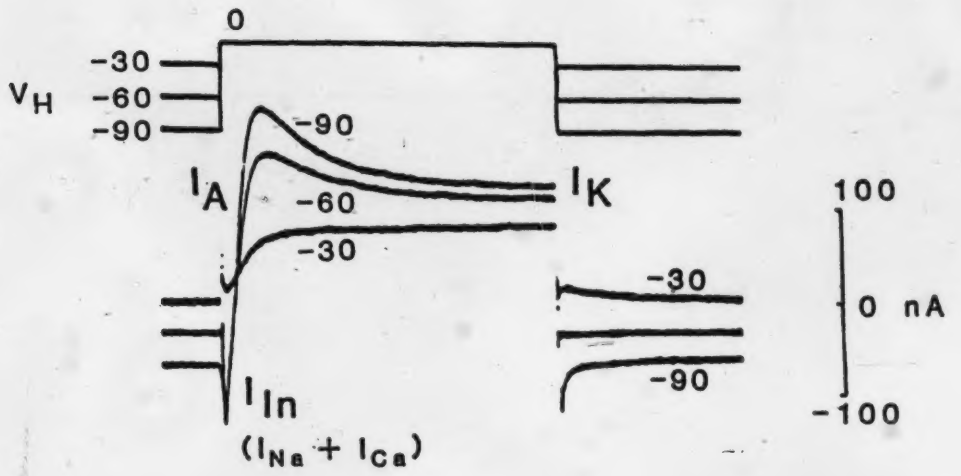

Figure II-9. Total membrane currents elicited under voltage clamp in normal saline. This figure illustrates the array of membrane currents observed in barnacle neurons prior to pharmacological separation, here shown partially isolated by voltage protocol. The top trace is membrane voltage (under clamp control), the lower trace is membrane current, three clamp steps were superimposed. Manipulation of the holding voltage (V_H) and command voltage (V_C) allows the components to be studied in partial isolation. Three holding voltages were used (-30, -60, -90 mV), with the depolarizing command to 0 mV, lasting 60 ms. The least complex current was recorded for the most depolarized (-30 mV) holding potential. The current was outward, monophasic, and relatively slowly developing, still increasing at the end of the clamp step. The kinetics, voltage dependence, and pharmacology (results to follow), suggest that this is a K^+ current analagous to I_K observed in other preparations. Membrane current generated from the -60 mV holding potential was triphasic. A rapid inward phase (peak 1 ms) was followed by an outward peak (peak 9 ms), and a later outward plateau. The measured current reflects the sum of an early transient inward component, a fast transient outward component, and the above mentioned slower outward component. The magnitude of both early components was increased by moderate hyperpolarization. The early inward and outward currents are therefore not readily separable by voltage protocol. The early inward current will be shown to be a mixed contribution of I_{Na} and I_{Ca}. The early outward current is a type of I_A. Further hyperpolarization of the holding potential (-90 mV) has little effect on the inward currents, but slightly increases the magnitude of the early outward current.

the length of the voltage step. This current is similar to the delayed rectifier or I_K, observed in squid axon. The same depolarizing voltage step from more hyperpolarized values (-60, -90 mV) evoke the full spectrum of inward and outward currents that would be associated with the production of an action potential. These are, the early transient inward currents, I_{Na} and I_{Ca}, and a transient outward current, I_A (see Figure II-9 legend). Each of these components of I_M is separable on the basis of pharmacological sensitivity and voltage dependence. In the following series of experiments the properties of each of the separate components of total membrane current are investigated under conditions which optimize their isolation and identification.

Capacitative and linear leakage currents

The capacitative transient after a step voltage command lasted 200 to 900 ms. Even in the best circumstances, this usually obscured the early part of both inward and outward ionic current onset. Computer subtraction of the transient by the addition of an equal, opposite polarity voltage command proved impractical because in many cases the transient was asymmetrical, and the subtraction left current artifacts. Measured using triangle wave voltage commands the whole cell capacitance averaged 1.4 nF (range 0.9 to 2.5 nF, n = 20). Assuming a spherical soma of 60 μm diameter, with no membrane infolding, and 1 μF/cm^2 membrane capacitance, the predicted soma membrane capacitance would be 113 pF. The measured average of 1.4 nF is about 12 times this value. Possibly the soma membrane is infolded, or dendritic and axonal membrane contribute to the capacitative currents measured under voltage clamp. The finding that these cells are relatively electrotonically compact, suggests that the extra capacitance comes in part from soma membrane infolding.

During experiments linear leakage currents were monitored by measuring the I-V relationship for voltage steps between -90 mV and -40 mV. In normal saline, healthy cells had leakage slope conductances of 0.1 to 0.9 nA/mV (equals μSiemens, abbreviated μS) averaging about 0.2 μS. The reversal potential, by definition, was considered to be the holding potential (-40 mV), since depolarizing steps generate an outward leakage, hyperpolarizing steps generate an inward leakage. The leakage current slowly increased in amplitude during an experiment as a part of the general 'run down' sometimes observed in

neurons which were doubly penetrated for long periods.

Inward sodium current

The voltage dependence and kinetic properties of the inward sodium current component could not be studied in detail because the very rapid onset kinetics were beyond the resolution of the clamp system. Preliminary observations are outlined here for completeness. A fast, steeply voltage dependent inward current persisted in Ca^{2+}-free (Co^{2+}) saline, but was abolished in Na^+-free (TEA) or 1 μM TTX saline, and therefore was probably carried by Na^+. In voltage clamp the inward Na^+ current reached maximal amplitude at -10 to 0 mV steps in 4 cells where it was studied. The magnitude of the current was quite variable, ranging in different cells from -30 nA to -290 nA at 0 mV (yielding approximate peak current densities of 35 to 150 $\mu A/cm^2$). The protocol used for studying I_{Na} is illustrated in Figure II-10A. The cell voltage was commanded from a value just hyperpolarized to cell rest (-50 mV) to voltages of -20 and -10 mV. The step to -20 mV generated the smaller, more slowly activating I_{Na}, the larger inward current was generated by the more depolarized step. The time to peak current decreased with depolarizing steps and usually could not be measured accurately for voltage steps above about +20 mV. In this range the current activation was so fast that the settling of the capacitative transient obscured much of I_{Na}. The bell shaped *I-V* relationship for I_{Na} in a cell bathed in Ca^{2+}-free (Co^{2+}), 50 mM TEA saline (to eliminate Ca^{2+} and K^+ currents) is shown in Figure II-10B. In this cell, the peak I_{Na} extrapolated to 0 nA reversed at about +40 mV.

The amplitude of measured I_{Na} in clamp was quite variable, and was correlated to the action potential amplitude recorded in current clamp. Usually cells with the largest action potentials (overshoot greater than +40 mV) had the most robust I_{Na}. In these cells the I_{Na} was under good spatial clamp (normal activation curves and current reversals), so it appeared that inward currents were expressed at the soma membrane. In other neurons, often those with smaller amplitude action potentials, the I_{Na} did not appear to be fully expressed at the soma membrane. Voltage clamps to study I_{Na} in these cells gave variable results due to problems associated with poor spatial clamp of I_{Na}. The inward current did

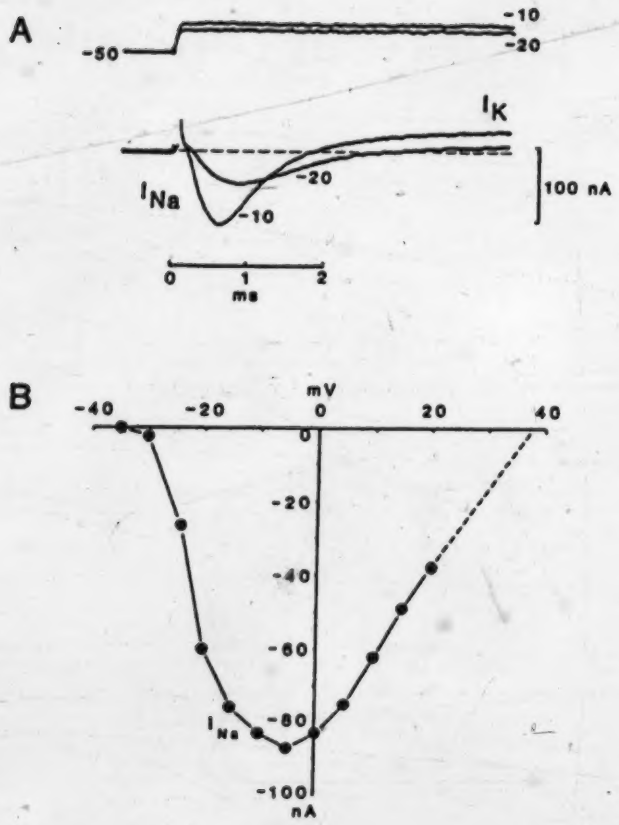

Figure II-10. Activation characteristics of the early inward Na^+ current. The cells were bathed in Ca^{2+}-free (replaced with Co^{2+}), 10 mM TEA saline, to block I_{Ca} and I_K from contaminating the records. Some residual outward currents remain unblocked. A: In this cell I_{Na} was first measurable as a small inward deflection following voltage steps to -25 mV. Voltage steps from V_H = -50 mV to -20 and -10 mV are shown. For both steps the current activates sigmoidally, followed by a slower inactivation phase. The time to peak and peak current are both steeply voltage dependent (see below). For this cell t_{peak} = 950 μs at -20 mV, and t_{peak} = 600 μs at -10 mV. The t_{peak} decreased with depolarization to 300 ms at +10 mV, above which it could not be measured accurately. The data were photographed from a dual trace digitizing oscilloscope screen. Voltage filtered at 10 KHz. Current filtered at 5 KHz. B: Voltage dependence of peak I_{Na} (different cell) in the same medium. The first measurable I_{Na} was activated at -30 mV. Maximum current (-87 nA) occurs at -5 mV, and the extrapolated reversal was about +40 mV.

not develop progressively with each increasingly depolarized step. Rather, at a given voltage step (about -30 mV) a large inward current 'notch' would appear in a threshold dependent manner. The notch did not increase in amplitude with increased depolarizing steps, but would merely activate earlier. These notches are probably caused by back propagation of action potentials initiated in poorly clamped, distal regions of the axon. Action potential currents would then be clamped out at the soma and show up as inward current notches. This situation arises because, as is common in neuronal voltage clamp experiments, the axon remains intact, and voltage clamp must fail at some point along the cable due to the voltage drop along the axoplasmic resistance.

The characteristics of I_{Na} appeared to be similar to the inward current of the squid axon as described by Hodgkin and Huxley (1952d). The barnacle I_{Na} could be adequately described by the same type of formalism, although several assumptions had to be made because of the limited time resolution and small number of cells with a large inward current. It was assumed that I_{Na} activates sigmoidally following m^3 kinetics, and that inactivation is controlled by a single variable. Thus,

$$I_{Na} = m^3 h \bar{g}_{Na}(V_M - E_{Na}) \qquad \text{(II-3)}$$

where: m is a variable describing Na^+ channel activation, which is dependent on V_M and varies between values of 0 and 1; h is a variable describing Na^+ channel inactivation, also voltage dependent and varying between 0 and 1; $\bar{g}_{Na}$ is the maximum Na^+ conductance with all channels open; $(V_M - E_{Na})$ is the electrochemical driving force acting on Na^+ ions. According to the H-H description, activation is maximal when $m = 1$, and inactivation is maximum when $h = 0$. Therefore, I_{Na} is greatest at membrane voltages at which there is maximal activation and minimal inactivation.

The voltage dependence of steady-state I_{Na} activation and inactivation, h_∞ were measured using two pulse tests similar to the H-H protocol. Steady-state activation, symbolized m_∞, was measured as the dependence of g_{Na} on the test activating test voltage used. The membrane voltage was first prepulsed to a large negative value (-80 mV) to remove steady-state I_{Na} inactivation (see below), followed by a test depolarizing step used to activate I_{Na}. The m_∞ plot was constructed by normalizing the value of g_{Na} at each test

voltage to the largest value obtained for that cell (assuming V_{rev} = +45 mV). The dependence of steady-state inactivation, h_∞, on V_M was evaluated by using a two pulse protocol in which the voltage of the conditioning pulse (first pulse) was varied. This was immediately followed by a second activating pulse to a fixed voltage, which maintained a constant amount of activation. In this way changes in I_{Na} measured during the second pulse could be attributed to the state of inactivation which had developed during the first pulse. Figure II-11A shows the steady state activation and inactivation curves for the barnacle data, using simple voltage shifts to obtain the best fit from the equations which describe the H-H squid axon data. The curves describe the barnacle data reasonably well. The steady state activation (m_∞) and inactivation (h_∞) curves were both shifted in a depolarized direction by 16 mV. The required shift probably results from the more depolarized resting potential of barnacle neurons which is, on average, 17 mV more depolarized than the H-H squid axon data.

In order to quantitatively describe the kinetics of I_{Na}, the voltage dependence of the inactivation time constant was investigated (no quantitative analysis of activation was possible due to the extremely rapid onset kinetics). The dependence of the inactivation time constant, τ_h, on V_M was measured in one of two ways. The method used depended on whether or not τ_h, was to be evaluated at a voltage where I_{Na} was activated. For membrane voltages greater than -30 mV, where substantial I_A was activated, τ_h, was simply measured as the I_{Na} decay following activation. This was usually a single exponential, and the time constant was measured simply by fitting a line to the *ln* transformed I_{Na} decay. At values of V_M where there was no significant I_{Na} activation τ_h cannot be measured as described above. In this case τ_h was measured by evaluating the relative refractoriness of I_{Na} in relation to V_M. The cell voltage was pulsed from a test voltage to a fixed activating voltage two times, the I_{Na} measured during the second pulse increased as a function of the duration of the interpulse interval. It was assumed that less I_{Na} was evoked by the second pulse due to inactivation remaining from the first. The period between activating pulses was varied until the amplitude of I_{Na} at the second pulse was 63% of the value of the first (one time constant). Measured in this way τ_h was a bell shaped function of V_M. The longest

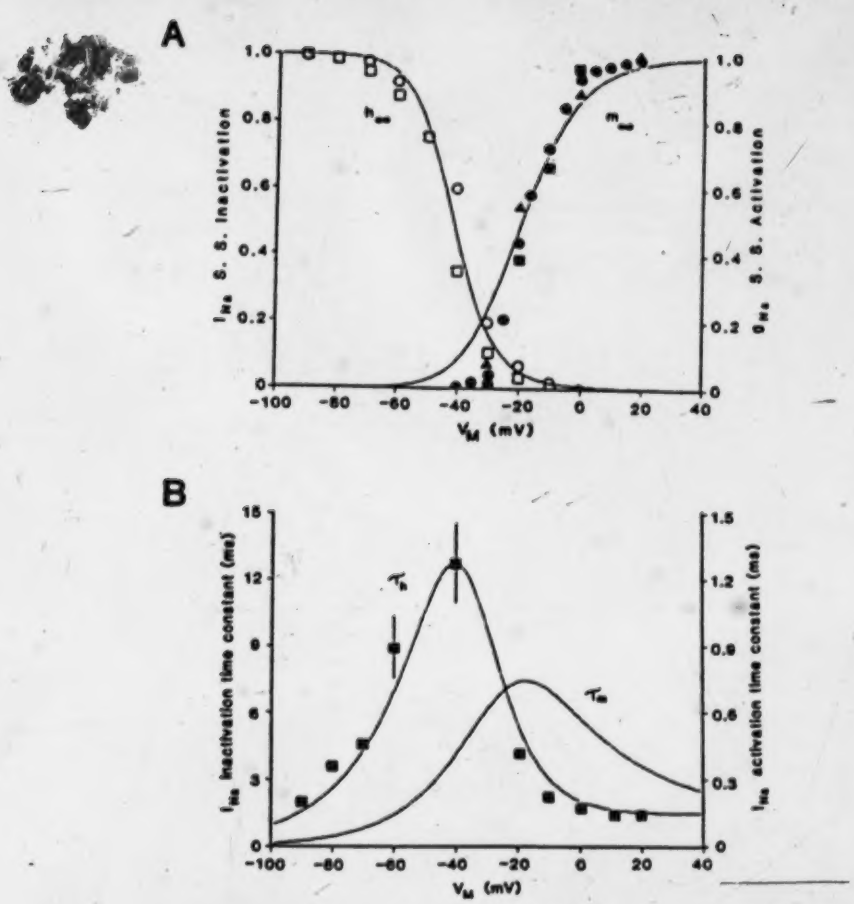

Figure II-11. Voltage dependence of I_{Na} system parameters. A: Steady-state activation and inactivation as measured by two pulse protocol. Activation (m_∞) was measured as peak inward conductance (using V_{rev} = +40 mV) in Ca^{2+}-free (Co^{2+}), TEA saline, the first pulse was to -80 mV, followed by a test pulse between -40 mV and +10 mV. The normalized conductance was then plotted against test voltage. Combined activation data from 3 cells are shown (filled circles, squares, and triangles). The curve was plotted according to the H-H formulation, but assuming a +17 mV shift to give the best fit to the data. Steady-state inactivation (h_∞) was measured using a variable test pulse (-90 to -10 mV) followed by a fixed (-10 or 0 mV) pulse to activate I_{Na}. The effect of the test prepulse was to increase I_{Na} activation as the prepulse was made more negative. Inactivation was plotted normalized to the current produced by the -90 mV prepulse (data from two cells, open circles and squares). The calculated curve is H-H h_∞ shifted by +22 mV. B: Voltage dependence of I_{Na} inactivation time constant, τ_h. The data for voltages greater than -30 mV were obtained by fitting the falling phase of I_{Na} isolated from subtraction recoreds before and after 1 μM TTX. Data at less than -30 mV were obtained by the two pulse method described in the text. The H-H τ_h curve was shifted +22 mV as suggested from by the steady-state inactivation data, and scaled vertically (in time) to fit the barnacle data by slowing the time constants to 2.8 times the 12 °C squid axon values. The curve peaking more to the right is the voltage dependence of the H-H activation time constant, τ_m, produced using a +17 mV shift (as for m_∞) and scaled in time as for τ_h. Activation was too fast in all cases to get sufficiently accurate barnacle data for comparison.

time constants were observed at -20 to -10 mV, as plotted in Figure II-11B. The curve was plotted by solving the the H-H τ_h descriptive equations, scaled to 12 °C and slowed 2.8x to better fit barnacle data (in addition to the same voltage shifts described above). I_{Na} onset was so rapid that it could not be accurately resolved from the fall of the membrane capacitative current following a voltage step. The τ_m curve that would result from applying the same scaling factors observed for inactivation parameters is plotted for comparison in Figure II-11B.

Inward calcium current

Experiments to detect the presence of an inward Ca^{2+} current were carried out in external saline containing 1 μM TTX, 100 mM TEA (replacing Na^+, and in some experiments 1 mM 4-aminopyridine (4-AP). This pharmacological combination blocks inward I_{Na} and most of the large voltage dependent outward currents in these neurons. Under these conditions and using electronic leakage subtraction, the Ca^{2+} current could be resolved (Figure II-12). The Ca^{2+} current turned on very rapidly at all voltages where it was activated, peaking in 3 to 6 ms prior to the onset of a slower exponential inactivation phase. Unlike the inward Na^+ current, the time to peak current of I_{Ca} was not strongly voltage dependent. The threshold voltage for activation was generally -20 to -15 mV. The voltage dependence of peak I_{Ca} was bell shaped with a maximum at +10 mV (5 cells). Reversal potentials ranged from +35 to +65 mV and were probably contaminated by residual, unblocked outward currents (see below). The peak inward Ca^{2+} current was much smaller than I_{Na} recorded in the same cells. In various cells the maximum peak I_{Ca} ranged from -10 nA to -63 nA (approximate current density, -11 to -40 $\mu A/cm^2$).

Ca^{2+} current onset kinetics were not investigated in detail. Activation appeared to have a sigmoidal onset, but this could not be evaluated accurately, because of slow settling of the capacitative transient. The activation time constant was less than 1 ms at all voltages where there was significant I_{Ca} activated. Inward Ca^{2+} tail currents recorded at the end of a depolarizing clamp step on return to hold potential (-40 mV) declined very rapidly ($\tau \simeq 0.2$ ms) and could not be measured accurately as the larger capacitative transient was also inward at this time.

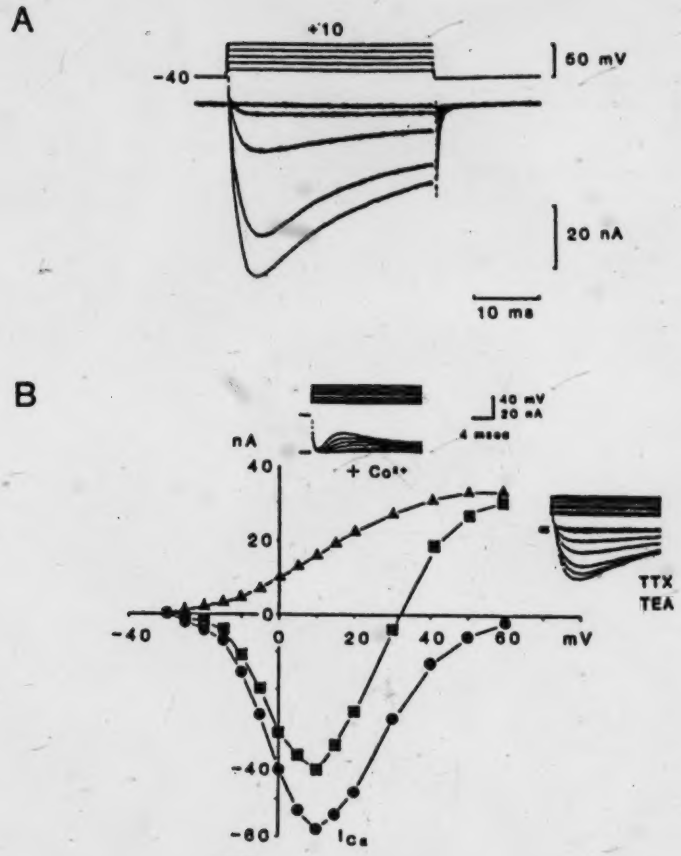

Figure II-12. I_{Ca} activation kinetics and voltage dependence. A: Separated I_{Ca} recorded in 1 μM TTX, 100 mM TEA saline to minimize the contribution of early Na^+ current and late K^+ current. Membrane current records are superimposed for voltage steps initiated from -40 mV, to potentials ranging from -30 to +10 mV (in 10 mV increments). Linear leakage currents have been subtracted electronically assuming ohmic behavior. The -30 mV step evoked no measurable inward or outward currents, suggesting that the subtraction is accurate. The Ca^{2+} current shows voltage dependent activation and apparent inactivation (see text). The time to peak was not strongly voltage dependent (about 5 ms at all voltages in this cell), although both the activation and inactivation time constants decrease with depolarization. The tail currents resulting from I_{Ca} deactivation on return to the holding voltage were extremely fast, and difficult to measure accurately ($\tau \approx .2$ ms). B: Bell shaped voltage dependence of peak I_{Ca} for a different cell (partial raw data in inset). The maximum current was evoked by steps to +10 mV, but the measures of I_{Ca} were contaminated by residual outward currents that persist through the pharmacological separation. The three curves illustrate subtraction method for obtaining I_{Ca} curve. The squares are peak inward currents measured in TTX, TEA saline after leakage subtraction (data inset at right). The triangles represent residual outward currents which remain after perfusion with Ca^{2+}-free (Co^{2+}), TTX, TEA saline (data in upper inset). Subtraction of the curves (circles) yields the more correct voltage dependence of I_{Ca}.

The Ca^{2+} currents were blocked by replacement of the external Ca^{2+} with Co^{2+} or Mn^{2+}. Co^{2+} replacement completely eliminated any net inward current, but a small inward current (< 5 nA) persists when using external Mn^{2+}. This inward current was probably carried by Mn^{2+} passing to a limited degree through Ca^{2+} channels. Perfusion with Ca^{2+}-free (Ba^{2+}) saline increases the peak amplitude of the inward currents by 30 to 50% suggesting that, as in other preparations, Ba^{2+} carries more current through Ca^{2+} channels than does Ca^{2+} (reviews, Hagiwara and Byerly, 1981; Tsien, 1983). Both I_{Ca} and I_{Ba} were weakly blocked by 10 to 100 μM concentrations of the organic Ca^{2+} channel antagonist verapamil. The block was slow to develop, and in some cells was not complete in 30 min. This contrasts with ionic block by Co^{2+} which develops fully within 5 min. Verapamil is membrane permeant (Hille, 1984) and may act from the inside of the Ca^{2+} channel. Verapamil was clearly non-specific for Ca^{2+} channels, altering the kinetics of outward current components at the same concentrations which were needed to block I_{Ca} (refer to Chapter III).

The Ca^{2+} currents appeared to inactivate completely within 60 to 200 ms. Occasionally the inward current would decline and net current would be slightly outward at the end of a depolarizing voltage step. This suggests that at least part of the observed inactivation results from simultaneous activation of unblocked outward current channels. Raising the external K^+ concentration to 10 times its normal value (to reduce the K^+ driving force) reduced the rate of apparent Ca^{2+} current inactivation and confirmed that the pharmacological block of K^+ channels was incomplete. When the Ca^{2+} current itself was blocked by addition of impermeant Co^{2+} to the bath a residual small slow outward current remained, but the magnitude of this residual current was too small to account for all of the inactivation of Ca^{2+} current observed. The inactivation process was weakly voltage dependent, the time constant decreasing with depolarization. This may have resulted not from a true voltage dependence, but rather from a Ca^{2+} mediated inactivation of Ca^{2+} channels (Brehm and Eckert, 1978). However, replacement of external Ca^{2+} with equimolar Ba^{2+} (n = 3) did not markedly alter the inactivation process. In other cell types, Ba^{2+} carries current through Ca^{2+} channels, but does not substitute for Ca^{2+} in the inactivation

process, thereby reducing the amount of inactivation (*e.g.* Eckert and Tillotson, 1981). In one experiment 50% of the external Ca^{2+} was replaced with relatively impermeant Mn^{2+} to reduce the peak Ca^{2+} influx. This treatment did not reduce the relative amount of inactivation. These experiments would seem to provide evidence for true voltage-dependent inactivation of Ca^{2+} channels, although voltage-dependent activation of a contaminating outward current cannot be ruled out. Further experiments were not carried out which might have enabled me to distinguish between these alternative inactivation mechanisms, and because of this no comprehensive description of I_{Ca} was attempted.

In most of the neurons studied I_{Ca} appeared to be under good spatial clamp, suggesting that this component of membrane current was somatic in origin. In two cells however, the Ca^{2+} currents were poorly controlled, and appeared as small notches, with the tail currents declining non-exponentially over many milliseconds. Although no further evidence was obtained, I believe that this type of behavior may represent Ca^{2+} spikes initiating in dendrites which are electrotonically distant from the soma and thus not at the point clamped area of membrane. Cells with this I_{Ca} pattern also had passive properties which suggested a high degree of dendritic coupling to the soma membrane.

Delayed outward currents

Delayed outward currents were studied in normal ionic saline containing 1 μM TTX to block large Na^+ currents. Using a holding voltage of -40 mV also helped to limit contamination by early transient outward current. The delayed outward currents, activated by membrane depolarization, made up the largest part of total membrane current in most cells. Steady-state values of up to 800 nA at +40 mV were observed, but usually the average was about 400 nA (approximate current densities up to 400 $\mu A/cm^2$). The reversal potential in normal saline, as measured by tail currents, averaged -60 mV (range -65 to -55 mV). The outward current was reduced by raising the K^+ concentration in the bathing medium to 10x normal (80 mM), to decrease the driving force for K^+ currents, or by the bath addition of K^+ channel blockers. The delayed currents are therefore carried mainly by K^+.

There was usually little delayed outward current for depolarizations to less than -10 mV; these steps generated mostly a linear leakage current. Increasing the magnitude of the step command evoked voltage dependent outward currents, activating sigmoidally, the time constant decreasing with depolarization (Figure II-13). Perfusion with Ca^{2+}-free (Co^{2+} or Mn^{2+}) saline demonstrated that a large fraction (10 to 50%) of the delayed outward current was dependent on Ca^{2+} ions for normal activation. The Ca^{2+} dependent fraction differs kinetically in that it activates more slowly, with a pronounced lag phase, and shows no voltage or time dependent inactivation. I designate these two components as I_K for the strictly voltage dependent component, and $I_{K(Ca)}$ for the component which is dependent on both Ca^{2+} and voltage. The nomenclature used follows Hodgkin and Huxley's (1952b) designation of I_K as a voltage-dependent K^+ current, and Meech and Standen's (1975) designation of $I_{K(Ca)}$ as a calcium-dependent slowly activating K^+ current. In barnacle neurons these two K^+ currents are not pharmacologically distinct for any of the agents tested (data to follow) other than those which directly effect Ca^{2+} influx. The properties of I_K can be studied in relative isolation in Ca^{2+}-free TTX saline. The properties of $I_{K(Ca)}$ must be inferred by computer subtraction from I_K (as per Figure II-13), or through experiments which specifically raise or lower the internal Ca^{2+} level. These types of experiments are discussed in detail in Chapter V.

The characteristics of the conductance change governing I_K were investigated initially using measurements made on deactivation tail currents. These tails were observed using a two pulse protocol. A first pulse steps V_M to a large positive value to activate substantial, constant I_K, and is immediately followed by a second pulse used to investigate the voltage dependent behavior of the tail current (refer to Figure II-14, inset). A plot of peak tail current amplitude verses V_M during the second pulse produces what has been termed the "instantaneous *I-V* relation" for I_K (Hodgkin and Huxley, 1952b). In barnacle neurons the instantaneous *I-V* plot (Figure II-14A) was fairly linear over the -80 to -10 mV range, with a current reversal at about -60 mV. The current reversal, V_{rev} is a measure of the driving electromotive force acting on K^+ moving through I_K channels. It is usually similar in value to the simple Nernstian equilibrium potential (E_K) for the current carrying ionic species

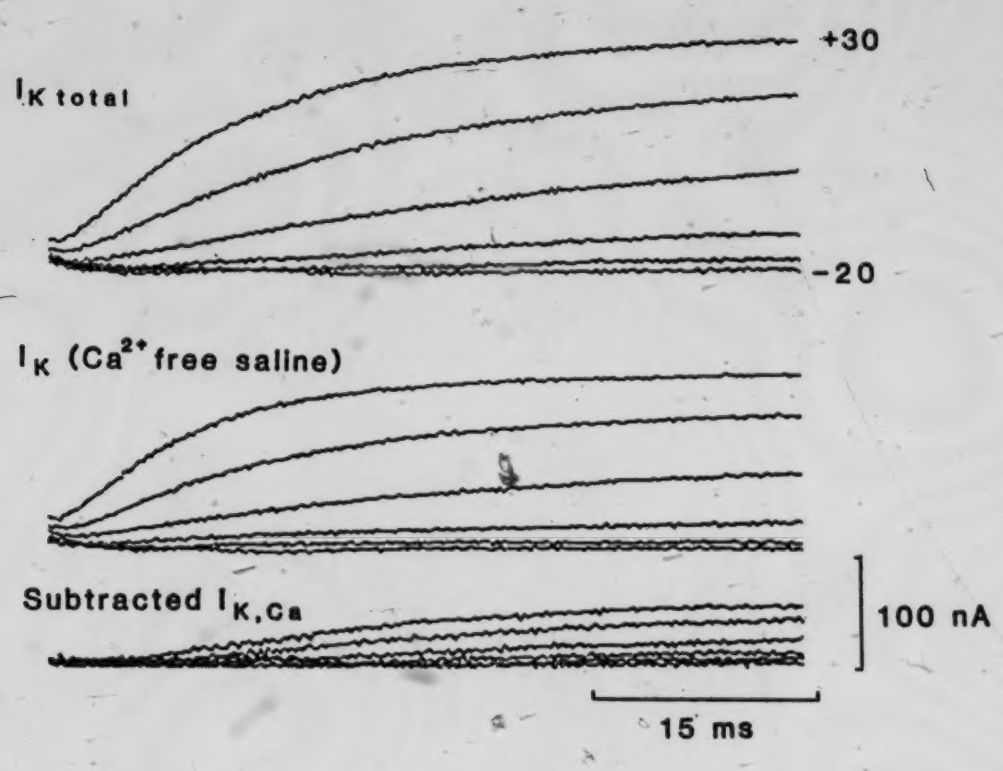

Figure II-13. Separation of voltage and calcium dependent components of slow outward current. Outward currents recorded in 1 μM TTX, normal saline are compared to those recorded in TTX, Ca^{2+}-free (Co^{2+}) saline for a family of voltage steps from -20 to +30 mV in 10 mV intervals. The upper current records ($I_{K,total}$) show slowly activating outward currents which result from the addition of the two components shown in the lower records. The I_K records (middle traces) are raw data for clamp steps in Ca^{2+}-free saline (replaced with Co^{2+}). The $I_{K(Ca)}$ records were obtained by computer subtraction of the normal and Ca^{2+}-free records. In this cell about 30% of the slow outward current was Ca^{2+} dependent. The kinetics of the two currents differ in that the $I_{K(Ca)}$ component activates more slowly, with a pronounced lag, and shows no apparent voltage or time dependent inactivation for long voltage clamps. The pure I_K component activates with sigmoidal onset and inactivates almost totally with long duration voltage steps (greater than 2-5 sec, data not shown). The plots were not corrected for leakage, and each omits the first 800 μs of data during the capacitative transient. Recordings were analog filtered at 5 KHz. The analog to digital sample interval was 400 μs.

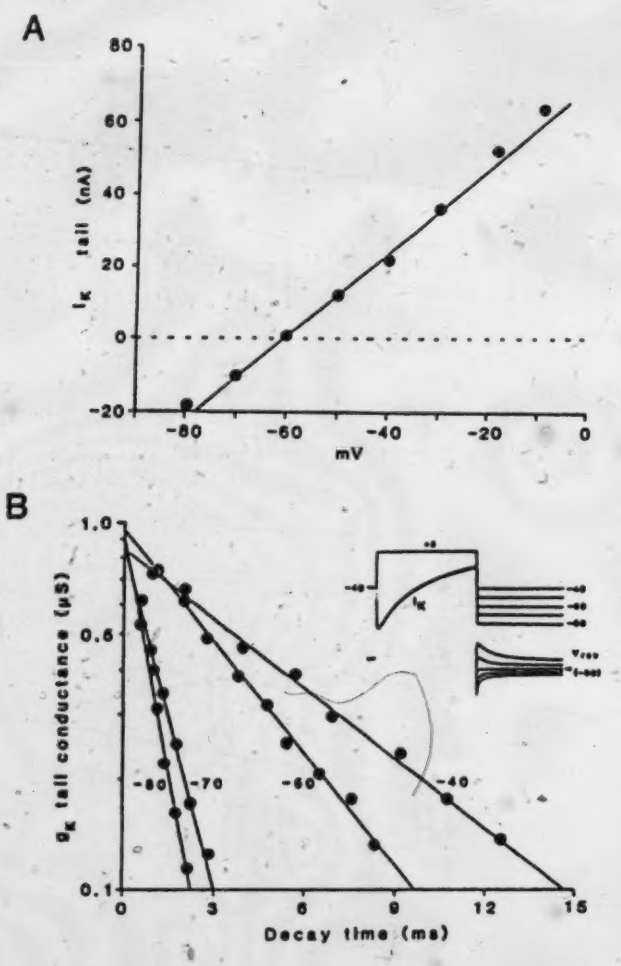

Figure II-14. Instantaneous *I-V* curve for I_K. Using a two pulse protocol, I_K was first activated at a depolarized voltage (+5 mV) to yield a constant conductance. The membrane voltage was then rapidly altered to a test voltage between -80 and -10 mV. Assuming that the rate of voltage change is 'instantaneous' in relation to the I_K time constants the second pulse measures the current flow through open channels at each test voltage. A: The straight line through the instantaneous I_K intersects 0 nA at -61 mV. This value is the reversal potential V_{rev}, which is near the expected E_K in these cells, and supports the hypothesis that I_K is carried by K^+ ions. The close fit to linearity (r^2 = .97) indicates that the membrane conductance was unchanged over this voltage range. Hence g_K acts as an ohmic conductance rather than as a voltage dependent permeability. B: Voltage dependence of deactivation tails. The voltage protocol was identical to part A. In this case measurements taken during the decaying I_K tails are plotted on a ln scale against time, and show simple exponential decay. The time constants for decay are voltage dependent, and are maximal at -40 mV (6.5 ms) decreasing to 0.9 ms at -80 mV. The inset illustrates partial raw data used to measure tail current decay and $I_K V_{rev}$.

(K^+), and is the most practical experimental measure of E_K. The close fit to linearity of the *I-V* plot shows that the conductance change underlying I_K is ohmic. Therefore, the relation between ionic conductance and ionic membrane current carried through I_K channels is

$$I_K = g_K(V_M - E_K) \qquad \text{(II-4)}$$

where g_K is the summed conductance through all I_K channels and $(V_M - E_K)$ is the electrical driving force acting on K^+ ions.

Using data from tail current experiments it can be shown that although the 'instantaneous' ionic conductance is independent of voltage of the second test pulse, the rates of change of the conductance at each test voltage do vary (Figure II-14B). Plots of *ln* g_K vs. time for tail currents are linear. This means that the tail conductances decay as a simple single exponential process at all voltages. However, the exponential rate of decay of the tail conductance increases as V_M was made more negative. The exponential rate of decay, or time constant, can be derived from the slope of a regression fitted to the decay of the tail current. For the cell illustrated, τ decreases from 6.5 ms at -40 mV to 0.9 ms at -80 mV. The behavior of the g_K time constant over a broader voltage range is described below.

The sigmoidal membrane current activation , followed by simple exponential deactivation tails, and the similarity to ohmic behavior suggest that the I_K in barnacle neurons can be described by a H-H type model. However, even when isolated in Ca^{2+}-free saline the I_K was not well described by H-H n^4 activation kinetics because the activation time course was poorly fit by the fourth power of a single activation term. This is clear in Figure II-15A where nonlinear curve fits are compared to digitized I_K activation curves. A second power (n^2) can approximate the initial lag, but only moderately describes the time course at later times (Figure II-15A) . To achieve the best description another voltage dependent parameter governing a slight initial delay could be introduced. Or alternatively, I_K could be described as a number of kinetically independent activation processes (see Connor and Stevens, 1971c; Dubois, 1981). Neither of these possibilities was pursued because there was not enough clear data to suggest which was the more correct description.

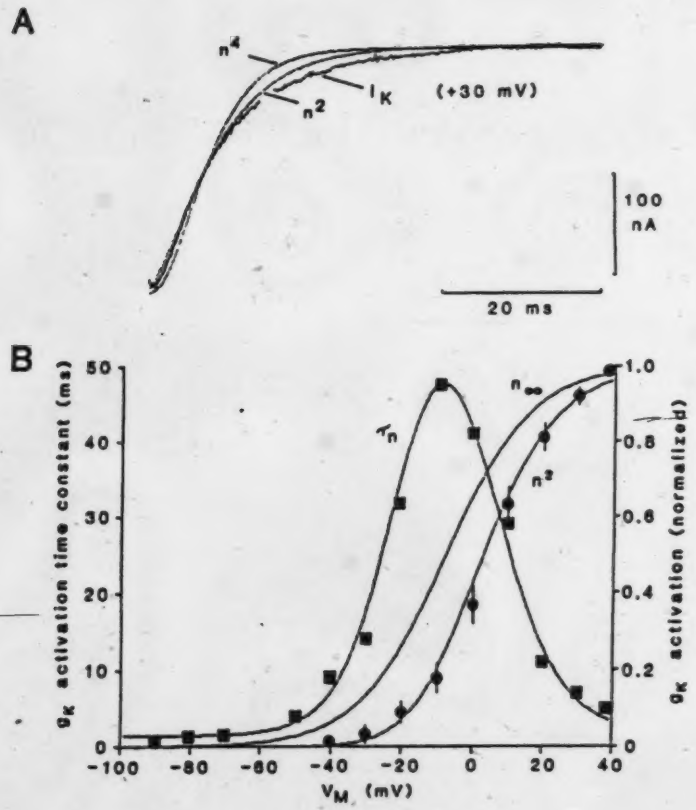

Figure II-15. Activation kinetics and voltage dependence of I_K system parameters. A: I_K activates with a sigmoidal onset, reaching a relatively long lived steady-state. Shown are curve fits to activation for n^2, and n^4 functions. The data record is the first 65 ms of a voltage step from -40 to +30 mV in Ca^{2+}-free (Mn^{2+}) saline. The data was best fitted by the n^2 curve, although the I_K curve rises to peak current more slowly. B: Voltage dependence of g_K steady-state activation, and the activation time constant. The voltage dependence of g_K activation was plotted as circles (mean ± SE, n = 7) assuming n^2 kinetics (normalized to +40 mV = 1.0). The associated curve is the best fit to a Boltzmann distribution, using an effective valence of 2.0, and assuming the conductance is one-half activated at +9 mV. The sigmoidal curve not associated with any data points is the voltage dependence of steady-state K^+ activation, n_∞, calculated as $\sqrt{g_K/g_{K,max}}$ The voltage dependence of the activation time constant, τ_n, is plotted as the squares and associated bell curve. Data are presented from a single cell only, as time constant values from different cells could vary as much as five fold, and no suitable way to normalize the data for comparison was discovered. In this cell τ_n was maximal at -10 mV and rapidly decreases as V_M is moved away from this value. At resting voltages (about -45 mV) τ_n is relatively fast. Refer to text for measurement protocol.

Additionally, the description of I_K was complicated by the presence of relatively rapid, near complete inactivation at voltages more positive than about +10 mV. This inactivation was approximately exponential with time constants of 200 to 400 ms at +40 mV.

I decided to pursue a kinetic description of I_K based on H-H n^2 kinetics, although this was not totally satisfactory for the reasons discussed above. It was assumed that the conductance could be modelled as

$$g_K = \bar{g}_K n^2 \qquad \text{(II-5)}$$

where $\bar{g}_K$ is the maximal conductance with all I_K channels fully activated and n is a voltage dependent activation term which varies between 0 and 1, describing the fraction of $\bar{g}_K$ which is activated. Depolarization increases the value of n, and thus increases the probability of opening of I_K channels.

The average voltage dependence of g_K activation over the range of -40 mV to +40 mV (n = 7) , is shown in Figure II-15B The values are normalized to the conductance at +40 mV, which was the most positive test potential used regularly (calculated using E_K = -60 mV). Voltage dependent ionic channel gating is a probability function which can be described by the Boltzmann distribution, if it is assumed that I_K channels have only two stable states (open or closed) and that the total conductance is the sum of the conductance of noninteracting identical channels. Under these conditions

$$g_K = \bar{g}_K [1+\exp(V_{1/2}-V_M)ze/kT]^{-1} \qquad \text{(II-6)}$$

where $\bar{g}_K$ is the maximal conductance, $V_{1/2}$ is the voltage at which the conductance is one half activated, z is the effective valency of the voltage sensing particle, and e/kT is the elementary charge divided by the product of Boltzmann's constant and the absolute temperature, which equals 0.041 at 12 °C. As can be seen by comparison with equation II-5, the terms within the square brackets represent the dependence of n on V_M. The curve in Figure II-15B is the best fit to the g_K activation data assuming $\bar{g}_K$ = 1 (normalized), $V_{1/2}$ = 9 mV, and z = 2.0. The values of g_K at +40 mV ($\simeq \bar{g}_K$) averaged 3.6 μS (range 1.9 to 9.6 μS, n = 7, approximate density 2 to 5 mS/cm^2). The variability in conductance density was not explained by variability in cell size because membrane surface area (as measured by whole cell capacitance) was already included in the measurement. Assuming

that all cells have a similar unitary I_K channel conductance, it seems that different cells must have widely varying I_K channel densities.

In order to describe changes in the kinetics of I_K with voltage, the time constant for activation, τ_n, was measured and the voltage dependence fitted with an arbitrary function chosen to produce the smallest deviations from the data (Figure II-15B). For voltages where substantial I_K was activated ($V_M > -10$ mV) the current onset was fitted directly with an n^2 function and the time constant derived. For more hyperpolarized voltages ($V_M < -10$ mV) the time constant was measured from deactivating tail currents, on the assumption that the same time constant governs both processes, these fits were made from plots such as those in Figure II-14B. τ_n, was greatest at -10 mV, averaging 26 ms (range 9 to 41 ms, $n = 7$) and decreased with both depolarization and hyperpolarization. At resting voltages (-45 to -40 mV) τ_n was relatively fast, averaging 9 ms (range 3 to 12 ms, $n = 3$). Most other kinetic descriptions have found that time constants are maximal at near resting voltage; the reason for this difference was not clear.

I_K was very sensitive to external TEA, the half blocking concentration, for I_K generated by large (+10 to +40 mV) depolarizations, occurs at 3.7 mM (Figure II-16). The block develops rapidly under voltage clamp and was generally complete in 5 minutes. The block by TEA was readily reversible following a 10 to 15 minute wash in normal saline. The rapid onset, and reversibility of the block suggest that TEA acts at an external site on I_K channels. Other blocking agents tested were not as specific for I_K and blocked other outward current components to varying degrees. These relatively non-specific K^+ channel blockers include 4-AP (tested at 1 to 5 mM), quinidine (tested at 0.1 to 2 mM), forskolin (100 μM), and verapamil (10 μM to 1 mM). Results for some of these pharmacological agents are presented in Chapter III.

Fast transient outward current

The fast transient outward current was almost completely inactivated at a holding potential of -40 mV and contributes little to depolarizing voltage steps initiated from this value. Short prepulses to more negative holding potentials rapidly remove inactivation,

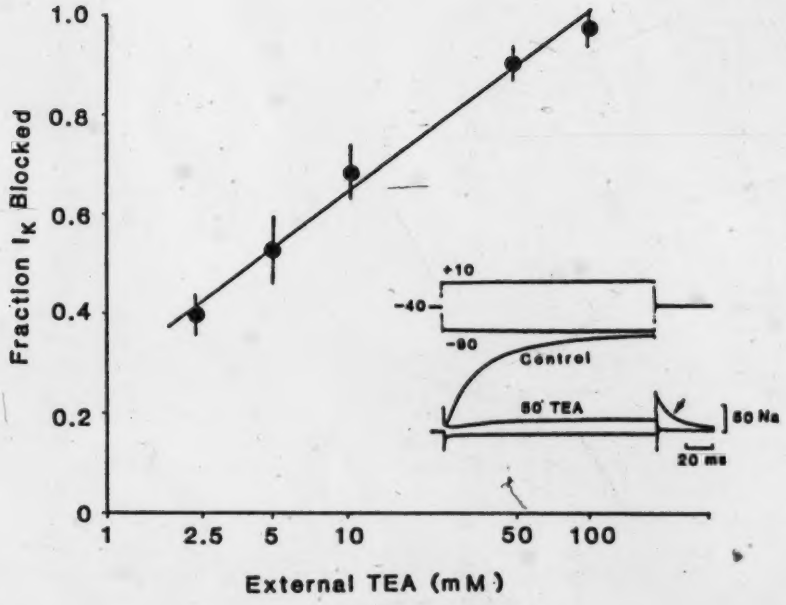

Figure II-16. Dose dependent blockade of I_K activation by TEA. The fraction of I_K blocked was plotted against external TEA concentration (log scale). The plot is linear (r^2 = 0.98) with a calculated KD_{50} of 3.7 mM TEA (combined data 12 cells). The measurements used were all taken at large positive voltages (+10 to +40 mV), and were pooled assuming that TEA block is voltage independent over this voltage range. The inset shows raw data for one TEA concentration (50 mM). TEA blocked 90% of the outward current activated by depolarization +10 mV and eliminated the deactivation tail at the offset of the voltage step (arrow). The superimposed control and TEA traces also show that the leakage component (symmetrical hyperpolarizing pulse) was unaffected by the treatment. The holding current at -40 mV was also unaffected by the treatment which means that the resting membrane potential has not changed. The external saline also contained 1 μM TTX.

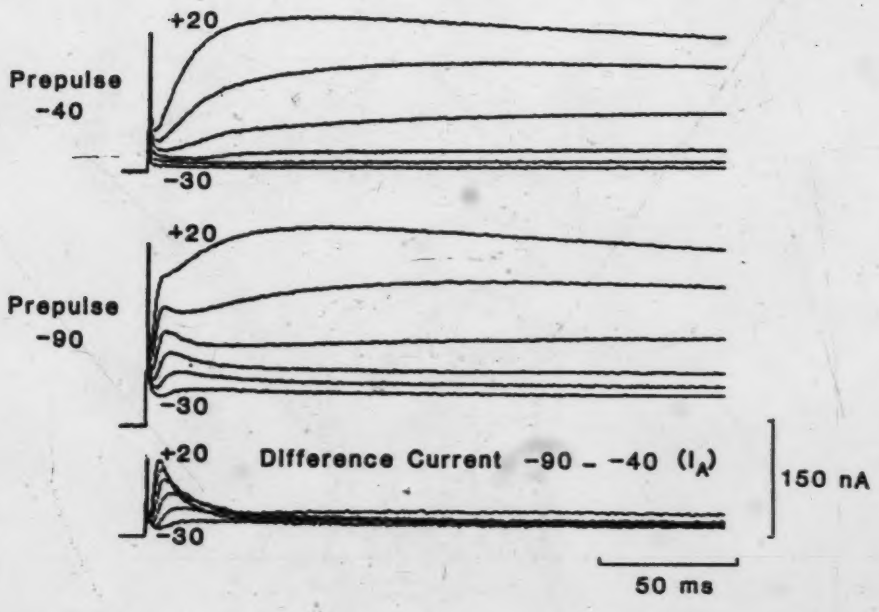

Figure II-17. Hyperpolarizing prepulses activate a transient outward current, I_A. Prepulses at the normal holding potential, -40 mV, followed by depolarizing commands yield typical I_K currents. The same depolarizing commands (-30 to +20 mV) after a short prepulse (500 ms) to -90 mV have little effect on I_K but additionally activate a smaller, faster, outward current, I_A. Computer subtraction of the two data sets yields the separated I_A, which peaks very early (4 to 10 ms) in a voltage dependent manner, and inactivates completely in 25 to 50 ms. Analog to digital sample interval = 1 ms.

which allows expression of the conductance if the pre-pulse is followed by a depolarizing stimulus to induce voltage dependent channel activation. The difference in outward currents activated with- and without a prepulse is shown in Figure II-17. The transient current, termed I_A was particularly prominent at voltages just depolarized to cell rest, near spike threshold. In this region the contribution of I_K and $I_{K(Ca)}$ was small, so that I_A was the most important of the outward currents. The difference current, which is the current affected by the hyperpolarizing prepulse, was almost pure I_A (Figure II-17). The isolated I_A was transient, rapidly rising to a peak, then completely inactivating. The time to peak was steeply voltage dependent, as are both the activation and inactivation time constants.

During the course of experiments to study the voltage dependence of $I_{K(Ca)}$ it was noted that conditions which decreased voltage dependent Ca^{2+} influx, through I_{Ca} channels, also reduced I_A. Up to 80% of I_A was blocked in some cells. This suggested that much of the early, transient I_A was activated by Ca^{2+} influx in addition to the intrinsic voltage dependence which is characteristic of I_A channels. Part of the transient outward current was still Ca^{2+}-dependent in cells bathed in a high concentration of extracellular TEA (50 mM), which eliminates the delayed outward currents, and provides a means of isolating I_A (refer to Chapter III). This also ruled out contamination by the more familiar $I_{K(Ca)}$ which is extremely TEA sensitive in these neurons (refer to Chapter V). Isolated in TEA, the early Ca^{2+}-activated I_A turned on rapidly, peaking in 4 to 6 ms at 0 mV. This situation is rather unusual. Ligand-activated channels are commonly thought to have a slow time course when compared to voltage-activated channels. A detailed kinetic analysis of both the strictly voltage dependent I_A, and the Ca^{2+}-dependent I_A will be presented in Chapter III.

DISCUSSION

The most important finding of this study is the identification of five ionic conductance systems present in the somata of barnacle neurons. There is little information available describing the membrane conductances of any arthropod neuron, and therefore this overview is particularly useful in that respect. In summary, two inward currents carried by

Na^+ and Ca^{2+}, and three outward currents, all most likely to be carried by K^+ (I_K, $I_{K(Ca)}$, I_A) and the Ca^{2+}-dependent fraction of I_A, have been described. This ensemble differs from the situation present in crustacean axons (I_{Na}, I_K, I_A; Connor, 1975; Quinta-Ferreira, 1982), and is most similar to that which has been reported for molluscan neurons (review, Adams *et al.*, 1980). An important *difference* from most molluscan neurons is the reduced current carrying capacity of the I_{Ca} system, and the more predominant, rapidly activated Ca^{2+} dependent outward currents. A Ca^{2+}-dependent transient K^+ current has been described in some muscle cell types (Mounier and Vassort, 1975; Siegelbaum and Tsien, 1980; Coraboeuf and Carmeliet, 1982; Salkoff, 1983). The Ca^{2+} dependent I_A in neurons has not been described in detail, although its existence has been reported (bullfrog neurons, MacDermott and Weight, 1982; barnacle neurons, Premack *et al.*, 1984; *Aplysia* neurons, Junge, 1985; rat hippocampal neurons, Zibcz and Weight, 1985).

Passive electrical properties

In general, the values measured for the passive electrical properties of barnacle neurons fall within the ranges of values reported for other crustacean neurons. The larger neurons used preferentially in this study ranged from about 50 to 60 μm in soma diameter. The input resistances averaged 6.2 MΩ and whole cell capacitances averaged 1.4 nF (yielding membrane time constants of 5 to 20 ms). Edwards and Mulloney (1984) report input resistances of 4.2 to 5.9 MΩ and time constants of 36 to 63 ms for the stomatogastric m.g. neuron of lobsters (soma diameter $\simeq$ 100 μm). For barnacle neurons, the specific membrane resistance can be calculated to average about 4400 Ωcm^2, which is 10 to 20x the values reported for other crustacean neuronal somata (see Atwood, 1982 for a summary table of earlier results). The reason for this is unclear, but the most likely reason for the difference is that at the resting potential there is little steady-state I_{Na} or I_K activation. Measures of cell input resistance by using hyperpolarizing current pulses tend to produce quite variable results, and depend on the quality of the impalement. At least part of the current applied is shunted past the microelectrodes and bypasses the actual membrane resistance. The membrane of these neurons may be quite infolded, since the specific membrane capacitance is about 12x that expected from the cell membrane area based on measurements of the soma

diameter. Takeda and Kennedy (1964) also found specific membrane capacitances of 10 to 12 $\mu F/cm^2$ in crayfish motor neurons, and concluded that the soma membrane was infolded. It is however, difficult to determine the contribution of dendritic and axonal membrane to these measurements.

Ionic basis of the action potential

The inward Na^+ current provides most of the depolarization during the upstroke of the action potential, as is evident from the lack of excitability in TTX treated neurons (Figure II-6B). These overshooting, short duration Na^+ action potentials observed in the larger barnacle neurons are unusual for crustacean neurons which generally exhibit only passive back propagation into the soma from the more excitable axonal spike initiating zone (Evoy, 1977). Most of the other smaller neurons in the ventral ganglion however *do* show the more typical, slow, variable amplitude spikes. Although not dealt with specifically, I have noticed that the major difference in membrane currents between 'active' and 'inactive' somas is the degree of expression of the inward Na^+ current. The other membrane current components are present at the same or higher density in neurons without overshooting action potentials. The reason for this is unclear, but has been discussed recently by Thomas (1984), for results on cockroach neurons, where a similar situation is seen. Thomas suggests that neurons with inactive somas may actually have larger K^+ currents than active somas. He terms this condition "actively inexcitable" because the inexcitability is derived from the stabilizing effect of voltage-dependent K^+ conductances. The terms active and inactive may be an oversimplification because intermediate conditions do exist. In barnacle neurons, it is the *ratio* of inward to outward membrane conductances which determines the degree of excitability (see below).

The inward Ca^{2+} current provides little depolarization during the normal Na^+ action potential (Figure II-6D). This may result from the slower activation kinetics ($\simeq$ 10x slower) compared to those of the I_{Na}, or as seems more likely, the current density may be too low (range -11 to -40 $\mu A/cm^2$) to provide enough inward current to break away from a large resting K^+ conductance. The major role of Ca^{2+} influx in excitation appears to be indirect,

occurring through the regulation of Ca^{2+}-dependent outward current channels. Single Na^+ action potentials are prolonged in Ca^{2+}-free saline (Figure II-6C), so clearly there must be enough Ca^{2+} influx during one action potential to activate substantial outward current. Mixed Na^+-Ca^{2+} spikes have been reported in many nerve cells (*e.g.* frog spinal ganglion cells: Koketsu *et al.*, 1959; molluscan giant neurons: Kerkut and Gardiner, 1967; Junge, 1967). In molluscan neurons (Geduldig and Junge, 1968), and several mammalian neurons (*e.g.* Hirst and Spence, 1973; Hirst *et al.*, 1985) TTX treated neurons can still produce Ca^{2+} action potentials. This could result from having either proportionately larger Ca^{2+}, or proportionately smaller K^+, current densities than the neurons studied here. Most other studies do not provide either current density measures or cell capacitances, making comparison difficult. Hirst *et. al.* (1985) do report I_{Ca} densities of up to 500 $\mu A/cm^2$ in mammalian myenteric neurons, which produce Ca^{2+} action potentials in TTX.

The neurons studied here do produce Ca^{2+} action potentials when treated with TEA at concentrations which block 50 to 90% of the delayed outward current (Figure II-7). This supports the hypothesis that in TTX saline, large outward currents limit the Ca^{2+} excitability expressed at the soma. Ross *et al.* (1985) have studied Ca^{2+} influx in barnacle circumesophageal ganglion neurons using Arsenazo III and current clamp. They find that while one neuron is inexcitable in TTX ('MG' cell), another cell in the same ganglion ('CC' cell) with particularly large absorbance signals (and presumably large Ca^{2+} currents), has Ca^{2+} action potentials in TTX. Therefore, Ross *et al.* conclude that the variation in excitability comes from variability in Ca^{2+} channel density and probably not K^+ channel density. My results do show a large variance in I_{Ca} density, but this is not as spectacular as the range of K^+ current densities. It is of interest that normally inactive insect neuronal somata can become excitable when injected with citrate ions, or treated with extracellular TEA (Pitman, 1979), both of which would reduce the large $I_{K(Ca)}$ present in these neurons (Thomas, 1984). Thomas has suggested that this occurs because a rapidly activating $g_{K(Ca)}$ conductance limits Ca^{2+} influx and at the same time reduces the membrane resistance, rendering the cells normally inexcitable.

A curious situation exists in the crayfish motor giant neuron (MoG), where it has been shown that spikes elicited from voltages depolarized to the normal resting potential generate slow Ca^{2+}-dependent spikes, while action potentials elicited from -90 mV are fast and Na^{+}-dependent (Shimahara *et. al.*, 1985). At normal resting potentials the cell is inexcitable. It is thought that hyperpolarization removes steady-state I_{Na} inactivation and allows expression of I_{Na}. I have never observed a similar situation in barnacle neurons, and usually cells were less excitable following hyperpolarizing prepulses because of removal of steady-state inactivation from K^{+} currents (see Chapter IV).

Driver and plateau potentials are slow, regenerative, endogenous depolarizations which serve to structure burst formation in crustacean cardiac and stomatogastric ganglia (these phenomena are qualitatively similar, although plateau potentials are often of longer duration). The similarity of Ca^{2+} spikes observed in TTX, TEA treated barnacle neurons to driver potentials or plateau potentials reported in other crustacean neurons is striking (Figure II-7B). Driver potentials are Ca^{2+}-dependent (blocked by Co^{2+} and Mn^{2+}), last 200 to 600 ms and are produced in the presence of TTX (Benson and Cooke, 1984). Extracellular TEA prolongs driver potentials; therefore, they are thought to be terminated by K^{+} channel activation. They are generated at the soma, because they are produced in isolated (ligatured) neuronal somata (Tazaki and Cooke, 1983), and can be initiated by short depolarizing current pulses at the soma. This set of characteristics is quite similar to the Ca^{2+}-dependent electrical responses of barnacle neurons in TTX, TEA saline (Figure II-7).

It may be possible that other crustacean neurons capable of this type of endogenous bursting merely have reduced I_{Na} and I_K current densities. The two cells shown as examples of slow Ca^{2+} potential activity (Figure II-7) were also analyzed under voltage clamp. In both cases the slow inward I_{Ca} was present, but the cell with a very long 'plateau' potential had no outward current other than leakage in 50 mM TEA. Presumably the plateau potential was terminated by I_{Ca} inactivation. The second cell which produced shorter duration, repetitive 'driver' potentials had only I_{Ca} and I_A under voltage clamp. The I_A may allow repetitive slow potentials by limiting the spike duration and hence Ca^{2+} influx. Similarly, Tazaki and Cooke (1984) have done preliminary voltage clamp experiments using

crustacean cardiac neurons, which produce driver potentials, and report the presence of predominately I_{Ca} and I_A. [A kinetic model based on barnacle neuron membrane properties (Chapter IV), reproduces driver potentials with only I_{Ca}, I_A, and capacitative branches activated, supporting the above hypothesis.]

Inward sodium current

The I_{Na} system is similar in voltage dependence to squid axon, when the differences in resting membrane potentials are considered (16 mV more depolarized in barnacle neurons). The shifted H-H m_∞ (+17 mV) and h_∞ (+22 mV) descriptive curves fit adequately to the barnacle data, although better fits could be achieved with other functions. It was considered more reasonable to use standard H-H parameters though, because the limited barnacle data did not warrant new formulations. The increased overlap of the m_∞ and h_∞ curves produced by the shifts used may be a common feature of the crustacean I_{Na} system, as a similar increased overlap was also reported by Connor *et. al.* (1977) for crab axons. The much slower inactivation time constants observed for barnacle cells (peak 12 ms at -40 mV, about 2.8x slower than 12 °C squid axon) are surprising, but are comparable with the general findings in other neuronal somata which often show time constants up to 10x slower than the corresponding axons (*e.g.* Adams *et al.*, 1982a). The equation fits to m_∞, h_∞, and τ_h data, and the approximate τ_m curve provide the basis needed to model the barnacle I_{Na} system.

Inward calcium current

The I_{Ca} observed under voltage clamp activates rapidly, and shows apparent complete inactivation at all voltages where it is activated (Figure II-12). The peak current occurs at 3 to 5 ms and is maximal at +10 mV which is similar to what has been reported for other cells (Akaike *et al.*, 1978; Adams and Gage, 1979; review, Hagiwara and Byerly, 1981). The observed inactivation is almost certainly contaminated by simultaneously activating outward current channels which are incompletely blocked by TEA and 4-AP. In the same way, reversal potentials (+35 to +65 mV) are more negative than would be expected for uncontaminated I_{Ca} (Hille, 1984; Bruner *et. al.*, 1986). Barnacle neuron Ca^{2+}

currents are unusual in that they show marked inactivation even in Ca^{2+}-free saline replaced with Ba^{2+}. This treatment removes fast I_{Ca} inactivation in most other neurons (review: Hagiwara and Byerly, 1981; Eckert and Tillotson, 1981; Kristal *et. al.*, 1981; Brown and Griffith, 1983; review: Tsien, 1983; Hirst *et al.* 1985), although true voltage dependent inactivation apparently occurs in *Helix* neurons (Brown *et al.*, 1981), and frog skeletal muscle (Fox, 1981). A recent report provides evidence for Ca^{2+}-dependent I_{Ca} inactivation in crayfish motor giant neurons, based on measures of intracellular Ca^{2+} levels with arsenazo III (Bruner *et. al.*, 1986). In that study large depolarizing prepulses (to +80 mV) , which elicit little Ca^{2+} influx did not cause inactivation of a I_{Ca} during a following test pulse. However, voltage prepulses that were associated with Ca^{2+} influx, as measured by arsenazo III, produced more I_{Ca} inactivation.

I_{Ca} probably can not be correctly described by a simple H-H formulation for several reasons. Firstly, plots of the current through open I_{Ca} channels against V_M are curved, and not linear through the calculated E_{Ca}. Therefore, open Ca^{2+} channels do not follow Ohm's law (Hille, 1984), and cannot be correctly described as a voltage-dependent conductance. Secondly, pure I_{Ca} tail currents do not deactivate as a single exponential, as H-H kinetics would predict (Tsien, 1983). Thirdly, activation and inactivation are probably not independent, because of the negative feedback loop created if there is Ca^{2+}-mediated inactivation of Ca^{2+} channels. Nevertheless, some authors have included I_{Ca} in H-H based models with a moderate degree of success (*e.g.* Byrne, 1980b).

Outward potassium currents

The four outward K^+ currents present in barnacle neurons under voltage clamp are separable on the basis of their kinetics, voltage dependence, Ca^{2+} requirements, and sensitivity to external TEA. The physiological role of each component is much less clear. In this study I have described only the voltage dependent delayed rectifier current, I_K in detail, even though up to 50% of the late outward current is Ca^{2+}-dependent. The major role of I_K is presumably the rapid repolarization of individual action potentials, since low TEA concentrations (5 mM) broaden the action potential by slowing the repolarization rate

(Figure II-6C). Under voltage clamp only the delayed outward currents (I_K and $I_{K(Ca)}$) are blocked by this treatment. It is also clear that Ca^{2+}-free saline alone (which reduces only $I_{K(Ca)}$ and a fraction of I_A) broadens action potentials but not as much as TEA. Action potentials up to 500 ms long were observed in 100 mM TEA saline, the longest durations in Ca^{2+}-free (Co^{2+} or Mn^{2+}) saline were 15 ms. Thus, by elimination, I_K must repolarize the action potential and the other outward currents contribute proportionately less to this process.

I_K activated sigmoidally, and with approximately second order (n^2) kinetics, when isolated in Ca^{2+}-free (Co^{2+} or Mn^{2+}) saline. A second power function also best describes I_K activation in *Xenopus* single Ranvier nodes (Frankenhaeuser, 1963), *Myxicola* axon (Goldman and Schauf, 1973) and bullfrog sympathetic neurons (Adams *et al.*, 1982a). The deactivation tails were less complex, and fell as single exponentials whose rates of decay were a bell shaped function of membrane potential peaking at -20 to -10 mV. In various cells the maximum activation time constant averaged 26 ms (range 9 to 45 ms). The instantaneous *I-V* relation, measured from deactivation tails, is linear, with a clear reversal at about -60 mV in normal (8 mM K^+) saline. The sigmoidal current onset, followed by simple exponential deactivation of a linear, ohmic conductance is in keeping with the predictions of a simple H-H model.

The voltage dependence of normalized g_K activation can be described as a simple Boltzmann distribution for a single gating particle with an effective valency (z) of 2.0. This implies that if the gating charge governing I_K channel opening moved across the full membrane potential drop, the equivalent of two charges would have to traverse the membrane. The greater the effective valency, the steeper the voltage dependence of channel conformational change (≃ gating). For the H-H squid axon I_K, $z = 4.5$, therefore the gating is more steeply voltage dependent than in barnacle neurons. In the limited number of studies for neuronal somata analyzed in this way, the steepness of gating of I_K appears to be more similar to the value I observe in barnacle neurons (*e.g.* rat sympathetic neurons, $z = 2.5$; Belluzi *et al.*, 1985) The conductance is one-half activated at a membrane potential of 9 mV, but little current actually flows for membrane potentials below about -10 mV

because of the proximity to the reversal potential. Measured at +40 mV, g_K averaged 3.6 μS (range 1.2 to 8.5 μS, approximate density 2 to 5 mS/cm^2). The above analysis provides the basis for a description of I_K using H-H kinetics, which will be used to investigate the characteristics of repetitive firing (Chapter IV).

Substantial voltage dependent inactivation of the delayed outward current is present at membrane voltages greater than about +10 mV. The time constants for inactivation are much more rapid than in most other tissues (200 to 400 ms at +40 mV). The description of I_K is incomplete without inclusion of these characteristics, but a full discussion of I_K inactivation is complex and beyond the scope of this chapter.

The results presented in this chapter provide an initial description of the passive electrical properties, and ionic basis of the action potential in a population of barnacle neurons. Additionally, it has been shown that 5 voltage- and Ca^{2+}-dependent membrane ionic currents can be recorded during voltage clamp of the soma membrane. The analysis is of limited detail, but serves to outline the membrane properties which contribute to the ionic basis of excitability in these neurons. The membrane ionic currents are not well known for crustacean neuronal somata, and this analysis demonstrates that the types of measurements which have become routine for other groups can be applied successfully to the smaller crustacean neurons. Although these neurons offer no technical advantage over the larger neurons found in molluscs, the different ensemble of membrane currents in barnacle neurons should prove interesting for comparative study.

III. DESCRIPTION OF THE FAST TRANSIENT POTASSIUM CURRENT.

INTRODUCTION

The fast transient potassium current was the third of the major voltage dependent ionic currents to be described using the voltage clamp technique. Following the description of I_{Na} and I_K by Hodgkin and Huxley (1952a, b, c, d), Hagiwara *et. al.* (1961) reported another type of potassium current, present in nerve cell bodies of the mollusc *Onchidium*, which showed rapid activation followed by slower complete inactivation. Today, the transient potassium current, termed I_A by Connor and Stevens (1971a), is sometimes considered to be a ubiquitous feature of excitable cells (see Rogawski, 1985, for recent review). It is worth noting that the squid giant axon is unusual as it is one of the few cells reported not to have a component of I_M attributable to I_A.

I_A differs from the more familiar I_K in voltage dependence, kinetics, pharmacological sensitivity, and in some cases, Ca^{2+} sensitivity. Thus, these two membrane current components are believed to be carried by distinct ionic channel types (see below). The difference in voltage dependence was first described, in molluscan neurons, by Connor and Stevens (1971b), and Neher (1971). Both studies showed that conditioning hyperpolarizing voltage clamps increased the magnitude of I_A during a following depolarization. This was interpreted as removal of steady-state inactivation in a manner analagous to removal of steady-state I_{Na} inactivation in squid axons (Hodgkin and Huxley, 1952c). The I_A waveform rises sigmoidally, with rapid onset kinetics, followed by a slower exponential decay phase, and thus resembles the I_{Na} waveform more than I_K. In fact, the similarity of I_A and I_{Na} voltage dependence and kinetics caused Neher and Lux (1972) to speculate that the current may be carried by K^+ moving through Na^+ channels. In the same study, this was shown not to be the case, because TTX selectively blocked I_{Na} but had no effect on I_A.

The first evidence for different pharmacological sensitivity of the early and late activating K^+ currents was provided by Nakajima (1966), who showed that, in puffer fish supramedullary neurons, TEA blocked the late outward current much more effectively than

the early activating outward current. Connor and Stevens (1971a), then Neher and Lux (1972) extended these observations in molluscan neurons, and found that I_K is about 10x more sensitive to TEA block than is I_A. In many neurons I_A is also pharmacologically distinct from I_K because it is blocked highly selectively by aminopyridine compounds (Thompson, 1977, 1982).

Direct recording of channel properties using the patch clamp technique has recently demonstrated that I_K and I_A are carried by distinct membrane channel types. I_A channel properties have been described by Cooper and Shrier (1985) and Kasai *et. al.* (1986). In both cases I_A channels are reported to have single channel conductances ($\simeq$ 20 pS), voltage dependences, and open time distributions which are unlike those of I_K channels.

There are mixed reports regarding the Ca^{2+}-sensitivity of I_A. In some cell types voltage-dependent Ca^{2+} influx appears to be coupled to I_A activation, while in others the process is strictly voltage mediated. Mounier and Vassort (1975) working on crab muscle, first suggested that there is a coupling between inward I_{Ca} and the following, rapid transient K^+ current, since they failed to observe transient outward current when there was no Ca^{2+} influx. More recently, Siegelbaum and Tsien (1980) and Coraboeuf and Carmeliet (1982) provide convincing evidence for Ca^{2+}-dependent I_A activation in cardiac Purkinje fibers. The literature for neurons is not as straightforward. In molluscan neurons, Thompson (1977) reported a 40% block of I_A when the bathing medium contained Co^{2+} to block Ca^{2+} channels, and hence voltage-dependent Ca^{2+} influx. He attributed this to "... an indirect effect (of Co^{2+}), involving translation of the steady-state activation and inactivation curves toward more positive voltages." MacDermott and Weight (1982) reported essentially the same blocking effect by divalent metal ions, in bullfrog sympathetic neurons, but concluded that since I_A was reduced, a component must be Ca^{2+}-sensitive. Several more recent studies reach the same conclusion; namely that replacement of Ca^{2+} with impermeant cations blocks I_A (Premack *et. al.*, 1984; Junge, 1985; Zibcz and Weight, 1985). However, none of these studies tests the 'voltage shift' mechanism suggested by Thompson. It is well known that shifts of voltage-dependent gating can be produced by altering the external Ca^{2+} concentration, or by addition of other divalent cations (*e.g.* Frankenhaeuser and Hodgkin,

1957; Hille *et. al.*, 1975).

Information regarding the physiological role of I_A has been obtained primarily from kinetic modelling studies based on Hodgkin-Huxley type analyses. These suggest that I_A is most important for the regulation of low frequency repetitive firing (Connor and Stevens, 1971c; Connor *et. al.*, 1977), and for the production of long delays in the response of *Aplysia* neurons to depolarization (Byrne, 1980a, b). However, there are relatively few experimental tests of these hypotheses under conditions which modify I_A activation or kinetics. The present study attempts to analyze the role(s) of I_A by quantitatively describing the kinetics, voltage- and Ca^{2+}-dependence, and pharmacological sensitivity of I_A in barnacle neurons. The results of this analysis will be applied in a companion paper (Chapter IV) which investigates the role of I_A in repetitive firing. That chapter will also compare the results obtained by alteration of I_A activation and kinetics during current clamp experiments, to the predictions of an empirical model based on the barnacle I_A data obtained from voltage clamp studies.

METHODS

Experiments were performed on barnacle ventral ganglionic neurons following pronase treatment and mechanical desheathing as previously described (Chapter II). The voltage clamp methods and data acquisition were also identical to those described previously.

All control salines used in this study consisted of normal barnacle saline plus 1 μM TTX to eliminate the inward Na^+ current which obscured the early outward currents being investigated. In some experimental salines the K^+ channel blocker TEACl (Sigma), replaced an appropriate fraction of the NaCl (50 or 100 mM) to maintain constant tonicity of the external medium. In Ca^{2+} replacement experiments either Co^{2+} or Mn^{2+} were substituted on a mole-for-mole basis. Normal barnacle saline contains 20 mM Ca^{2+}; high Ca^{2+} saline (30 mM) was prepared by addition of 10 mM $CaCl_2$. For low Ca^{2+} saline (5 mM) 80% of the $CaCl_2$ was omitted. The K^+ channel blocker 4-aminopyridine (Sigma) was prepared in normal saline immediately prior to use and adjusted to pH 7.5 using HCl. Verapamil hydrochloride (Sigma), forskolin (Sigma), and IBMX (isobutylmethylxanthine, Sigma) were

prepared as 10 or 100 mM stock solutions in 100% dimethylsulphoxide and stored at -5 °C. These solutions were warmed to 12 °C and added directly to the bath to give the desired final concentration (10 μM to 5 mM).

Best fit single exponential curves were derived for digitized raw data traces by simple linear regression after transformation to linearity (Zaf, 1976). Nonlinear 'best fits' were approximated by eye using an algorithm which varied equation parameters under partial manual control while simultaneously plotting the data traces and fit results. Usually these best fits appeared to describe the data quite well, although I did not attempt to evaluate this statistically. The curve fits which were used to describe the voltage dependence of membrane parameters, evaluated user specified equations at 1 mV increments along the X-axis (-100 mV to +40 mV) and linearly interpolated between these values.

RESULTS

Separation of I_A

In order to examine the characteristics of the fast transient K^+ current, I_A, it must be studied in relative isolation from other membrane current components which would normally be activated in the same time and/or voltage range. The fast inward Na^+ current, I_{Na}, is prominent in the same voltage range where I_A is most easily studied (-30 to 0 mV), but can be selectively blocked by 1 μM TTX, which was routinely added to the bath. I_{Na} peaks earlier than I_A, and contaminates measures of I_A activation because the inward current is inactivating at roughly the same time which I_A is activating. Thus, at early times following a depolarizing voltage step the total membrane current is biphasic, the sum of inward I_{Na} and outward I_A. The overlap in time and voltage dependence suggests that in unclamped membrane these competing early membrane currents may control excitability through their opposing effects on membrane voltage. Possible roles of fast I_A in spike threshold regulation, and spike frequency encoding will be analyzed in Chapter IV.

I_A can be isolated from the other major K^+ currents, I_K and $I_{K(Ca)}$ by taking advantage of the different voltage dependence and TEA sensitivity of the outward current

components. The membrane potential, V_M, influences the gating of I_A channels by affecting two kinetic processes, rapid activation (channel opening) and slower inactivation (channel closing). I_A channels are almost completely inactivated when V_M is held depolarized above the normal resting membrane potential. Brief hyperpolarization removes the 'steady-state' inactivation which has developed and increases the probability that I_A channels will open if presented with an appropriate depolarizing, or activating, voltage stimulus. Pronounced steady-state inactivation at voltages near resting membrane potential is not characteristic of I_K or $I_{K(Ca)}$ channels. Thus, recordings of whole cell outward current are composed of mostly the later activating I_K (and in some cells $I_{K(Ca)}$) when depolarizing voltage clamp steps are initiated from a holding potential -40 mV . Another difference in the voltage dependence of I_A and I_K is that I_A starts to be activated at less depolarized membrane potentials than I_K. Figure III-1 illustrates the differences in voltage dependence, and also shows a subtraction method for the isolation of I_A which takes advantage of the fact that I_A is mostly inactivated at -40 mV. Initially, depolarizing clamp steps were made from a -40 mV holding potential to -40 to -10 mV, in 10 mV increments. The voltage steps to -40, -30 and -20 mV generate only linear (ohmic) outward leakage current, I_L. The command to -10 mV elicited a slowly developing I_K in addition to I_L. The same depolarizing pulses from a -90 mV prepulse elicit biphasic, rapidly peaking outward currents that result from the additional activation of I_A. The subtraction record (-90 prepulse minus -40 prepulse) yields I_A added by the prepulse, which activated early after the onset of the voltage step, followed by slower, complete inactivation over the next 40 to 80 ms. The time to peak current was voltage dependent, decreasing from 29 ms at -40 mV to 8 ms at -10 mV. The transient outward current, measured in this way is the major component of I_M over the -40 to -10 mV range. An advantage of separation of I_A in this manner is that I_L is relatively unchanged by the prepulse, so the subtraction yields I_A uncontaminated by I_L or I_K.

The current components activated from -40 mV and those activated following a prepulse to -90 mV also differ in sensitivity to the K^+ channel blocker TEA. Figure III-2 (top left) shows the initial 100 ms of depolarizing clamp steps to -20, 0, +20, and +40 mV from a -40 mV holding potential. Little outward current develops at voltages less than 0

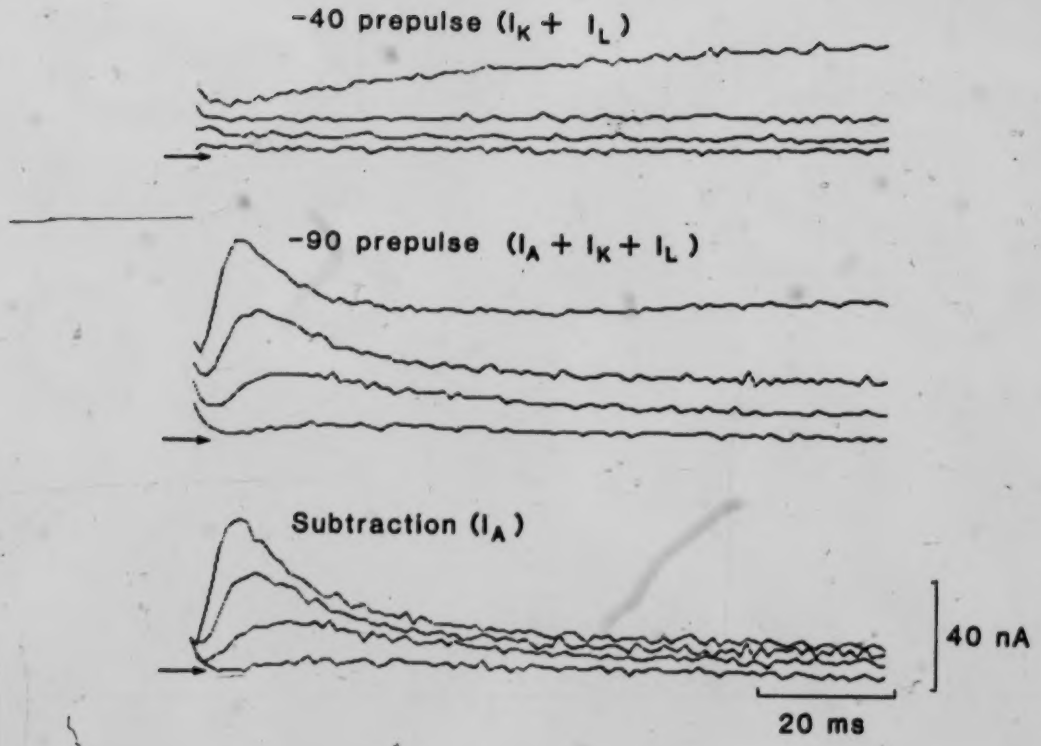

Figure III-1. Separation of I_A and I_K by voltage protocol. Initially, four depolarizing voltage clamp steps were made from a holding voltage of -40 mV, to final values of -40, -30, -20, and -10 mV. These pulses were given 10 s apart, and the records superimposed Only a linear leakage current, I_L was generated by the -40 to -20 mV steps, but with the step to -10 mV slowly developing I_K first becomes activated. The same clamp steps following a 500 ms prepulse to -90 mV yield a biphasic outward current, the sum of I_A, I_L, and I_K. Subtraction of the two records yields the current added by the prepulse, which is predominantly I_A. The arrows represent 0 nA for each record. In this, and all following figures in this chapter, 1 μM TTX was added to the bath to eliminate I_{Na}. The records omit the first 1 ms of data during the capacitative transient current. Data records were analog filtered at 2 KHz prior to storage on FM tape. The analog to digital sample interval used to load the data into the computer was 1 ms.

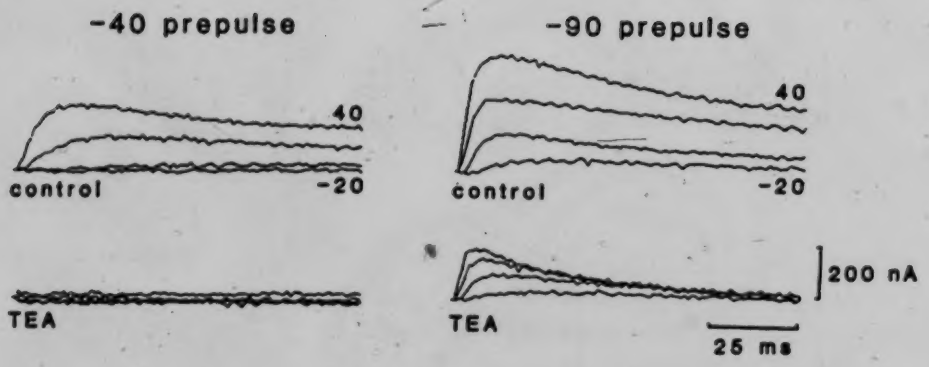

Figure III-2. Separation of I_A and I_K by sensitivity to external TEA. The outward currents activated following depolarizing steps to -20, 0, +20, +40 mV from -40 mV are abolished by 50 mM TEA (left panel, top is control, bottom is 50 TEA). These outward currents consist of mostly I_K (with a smaller contribution of $I_{K(Ca)}$). The peak outward current is 262 nA at +40 mV in control saline, and this is reduced to 35 nA in 50 TEA saline. The same depolarizing voltage steps following a prepulse to -90 mV yield larger, more rapidly activating outward currents which differ by the addition of I_A (right panel, top). The peak outward current in control saline is increased by the prepulse to 461 nA at +40 mV. Thus, the prepulse promotes a 201 nA increase in outward current. The I_A generated by the prepulse is TEA insensitive (right panel, bottom). Of the 201 nA increase generated by the -90 mV prepulse, 193 nA remains in 50 TEA saline. Therefore, 96% of the I_A activated by the prepulse is TEA insensitive. All traces have linear leakage current subtracted and omit the first 1 ms of data during the capacitative transient. Analog to digital sample interval = 1 ms.

mV, but larger, voltage dependent currents develop for pulses to membrane voltages above 0 mV. The ionic selectivity, voltage dependence, and kinetics suggest that these components are similar to I_K and $I_{K(Ca)}$ in other preparations (review, Adams *et. al.*, 1980). Extracellular TEA (100 mM) abolishes both large K^+ current components leaving only small non-specific outward currents or small inward currents (presumably I_{Ca}) following voltage clamp steps to -20 to +40 mV. In control saline, the same depolarizing clamp steps used above, but following prepulses to -90 mV, generate larger amplitude, faster activating outward currents (Figure III-2, top right). Note that the outward current also differs in the -20 to 0 mV range where the transient fraction is predominant, -40 mV prepulses activate almost no current in this voltage range. The membrane current activated following a -90 mV conditioning prepulse is relatively TEA insensitive (Figure III-2, bottom right). I identify this membrane current component as I_A by the combination of: selectivity for K^+ (see below); pronounced steady-state inactivation near resting membrane voltage; removal of inactivation by short -90 mV prepulses; and relative TEA insensitivity (see Thompson, 1977).

The simple experimental protocol described above does not actually provide evidence that the TEA sensitive and insensitive components are carried by separate membrane conductance systems. It is possible that the hyperpolarizing prepulse could remove TEA block of I_K, perhaps by altering the charge or structure of the blocked I_K channels. TEA molecules could then re-associate with open channels following depolarization, mimicking the rapid development of inactivation which is characteristic of I_A. Such complex behavior has not been described in the literature. Further evidence for separate early and late outward conductance systems can by summarized as follows. The membrane voltage at which the ionic tail current reverses in normal saline (V_{rev}) differs for the early and later currents. Using a standard two pulse protocol (refer to Chapter II) the I_A V_{rev} averages about -65 mV (range -70 to -62 mV), while that for I_K averages about -60 mV (range -65 to -55 mV). Compared in the same cell, the I_A V_{rev} is always more negative than the I_K V_{rev}. This suggests that the channel types differ in their ionic selectivity. Both are carried mainly by K^+ because raising the external K^+ concentration to 10 times the normal concentration

reversibly diminishes the voltage dependent outward current, and shifts the V_{rev} of both components by about +30 mV. The inactivation voltage dependence of the early and late outward components differ markedly, as described above. In addition the voltage at which the conductance is half activated is shifted significantly to more negative voltages for the I_A conductance (see below). Taken together these observations suggest that I_A and the slower I_K and $I_{K(Ca)}$ are carried by separate conductance systems. Evidence that I_K and $I_{K(Ca)}$ are carried by separate conductance systems is presented in other chapters (refer to Chapters II, V).

Voltage dependence and kinetics

The voltage dependence and kinetics of I_A were examined in detail in order to better assess its physiological role. I_A was analyzed assuming a modified H-H kinetic description, after separation either pharmacologically or by voltage protocol and subtraction. Each of the following assumptions is characteristic of the H-H description (although some are not stated specifically). The analysis presented assumes that channel activation is voltage dependent, and that opening is governed by a Markov process in which the opening channel moves from the closed to open state sequentially via a number of non-conducting intermediate states. The rate constants for the transitions between states are assumed to be unequal (decreasing with proximity to the open state), although uniformly voltage dependent. Thus, the whole cell ionic current flowing through the population of channels follows a sigmoidal onset, after an initial 'lag'. This type of activation can be described as a power function of a single activation term. Both lack of activation, and development of inactivation, can cause channels to close, but the processes are independent of one another. Inactivation is assumed to be a first order process, which is governed by a single exponential time constant. Therefore, I_A can be represented mathematically as,

$$I_A(V_M, t) = a^{\gamma} b \bar{g}_A (V_M - E_A) \qquad \text{(III-1)}$$

where, a describes I_A activation as a function of V_M and t (dimensionless, varying between 0 and 1), γ is an integer power describing the rise and fall of a, b describes I_A inactivation as a function of V_M and t, $\bar{g}_A$ is the maximal conductance with all I_A channels open, and $(V_M - E_A)$ is the net driving force on K^+ moving through I_A channels.

In order to empirically describe a single I_A waveform at a single test voltage, so that the voltage- and time-dependent parameters in Equation III-1 could be evaluated, voltage clamp I_A data were described as

$$I_A(V_{test}, t) = [1-\exp(-t/\tau_a)]^{\gamma} \cdot \exp(-t/\tau_b) \cdot AM \qquad \text{(III-2)}$$

where τ_a is the time constant for the activation process, γ is the exponent governing the sigmoidal activation onset, τ_b is the time constant for the inactivation process, AM is the amplitude of the function in units of nA, and t is time in ms. AM is easily converted to conductance, by dividing by $(V_{test}-E_K)$ to yield g_A at the test voltage. The time constants of activation and inactivation were derived by non-linear curve fitting to the above function. Leakage currents were first subtracted by linear extrapolation of the slope conductance measured over a a range of V_M (-85 to -45 mV) where other conductances are not activated.

The routine used for fitting the data is shown for a single I_A step in Figure III-3A. The I_A trace rises sigmoidally to a peak at 7.2 ms, followed by a slower, essentially complete, inactivation phase. Initially, the falling phase of I_A (inactivation) was fitted as a single exponential decay, $\exp(-t/\tau)$, by linear regression after *ln* transformation to linearize the data (curve 1, Figure III-3A). The decay curve gives the inactivation time constant, τ_b, and by extrapolation to $t = 0$ yields the 'zero time intercept' which gives the amplitude of the current, AM. The inactivation curve was then subtracted, or 'peeled off' the data to yield a prediction of activation in the absence of any inactivation. An iterative non-linear fitting routine was then used to evaluate the activation power (γ) and obtain the activation time constant. For all of the I_A data analyzed, raising the activation term to the 6th power consistently produced the best fit to both the initial lag phase and peak current. The second curve (curve 2, Figure III-3A) provides a description of the activation uncontaminated by inactivation. The final fit to I_A is obtained simply by multiplying the best fit activation and inactivation terms (unlabelled curve, Figure III-3A). Curves obtained by fitting to Equation III-2 for a wider voltage range are shown in Figure III-3B. In each case $\gamma = 6$ and the descriptive equation appears to fit to the data initial lag, peak current, and exponential decay quite well.

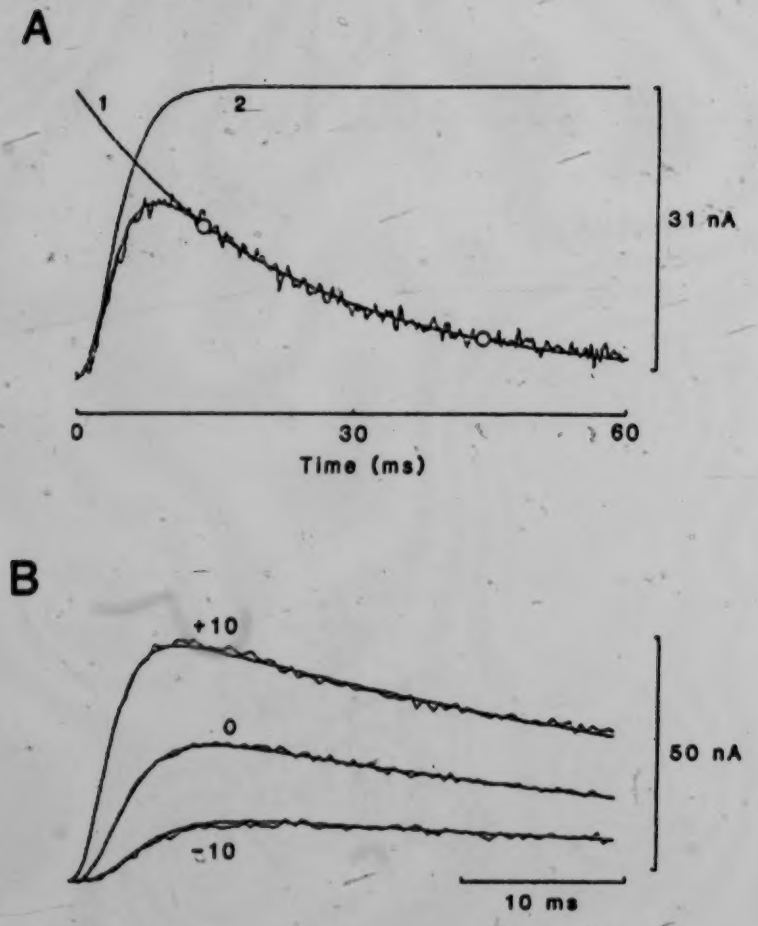

Figure III-3. Curve fit routines used to measure I_A parameters. A: Illustration of the curve fitting subroutines used to obtain the inactivation time constant, τ_b, activation time constant, τ_a, and current amplitude. First, curve 1 was fitted to the data by regression to the decay phase of I_A. This curve was then subtracted from the data to yield a theoretical plot of activation in the absence of any inactivation (curve 2). The time constant of curve 1 provides a measure of τ_b, and of curve 2 yields τ_a. The analysis used $\gamma = 6$ (see text). The raw data are from a single voltage step from -90 mV to -30 mV. B: The curves used to describe activation and inactivation, shown over a wider voltage range, provide an excellent fit to I_A records (in 50 mM TEA). The same fitting routine as above was used, but the curve plotted is only the product of curves 1 and 2 described above. This curve shows the description of I_A for each voltage step (refer to Equation III-2).

Steady-state activation, a_∞^4

The voltage dependence of steady-state activation, termed a_∞^4 (∞ = steady-state), was measured following a conditioning prepulse to remove steady-state inactivation, so that the peak g_A would be activated maximally. Preliminary experiments showed that $g_{A,peak}$ measured at depolarized voltages was maximal if preceded by conditioning prepulses to large negative voltages (*e.g.* -90 mV) for periods of 250 ms or greater (see below). I used a standard inactivation removal pulse of 500 ms at -90 mV in all experiments to measure a_∞^4. The cells were held slightly depolarized to resting membrane potential (*i.e.* at -40 mV) at all times and pulsed briefly to remove inactivation. Holding cells at -90 mV for longer periods was avoided because this caused an irreversible deterioration of cell health within a few minutes. The second pulse of the two-pulse protocol was used to activate g_A at membrane voltages ranging from -40 to +30 mV. Current values were converted to conductance using the measured average V_{rev} of -65 mV. Throughout this study, I use g_A as a general term to designate the conductance underlying I_A. When it is important to understand how g_A was determined I use the following more specific designations: $g_{A,peak}$ refers to the conductance value calculated from the measured peak I_A; $\dot{g}_A$ refers to the value of the theoretical conductance in the absence of inactivation, and is obtained by dividing by the best fit inactivation equation; $\bar{g}_A$ refers to the maximal value which $\dot{g}_A$ attains at large depolarizations, and is the best experimental measure of the conductance when all I_A channels are open.

The effect of membrane voltage on steady-state activation is shown in Figure III-4. Activation is measured as the normalized conductance, $\dot{g}_A$ (corrected for inactivation), and assuming 6th order kinetics (circles). The steady-state activation curve plotted in this way measures a_∞^4 as a function of V_M, which increased with depolarization towards a saturating value at about +30 mV. The data presented in Figure III-4 were normalized to allow pooling of data from different cells (n = 6, ±SE). The values of $\dot{g}_A$ for each cell were normalized to the maximum value obtained for that cell (at +30 mV), as $\dot{g}_A / \dot{g}_{A,max}$. The actual $\dot{g}_A$ values at +30 mV averaged 2.49 μS (range 1.03 to 4.51 μS, n = 6). Since $a_\infty^4 \simeq 1$ at +30 mV, these values of $\dot{g}_A$ approximate the maximal conductance, $\bar{g}_A$. The conductance

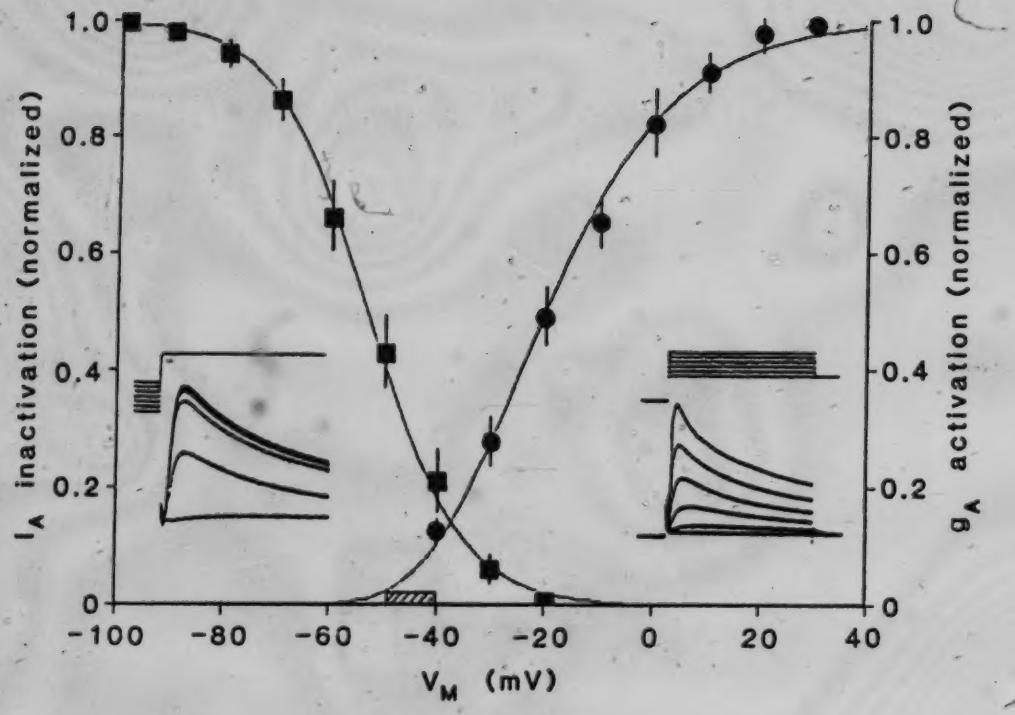

Figure III-4. Dependence of I_A steady-state activation and inactivation on V_M. Steady-state activation, a_∞^4 (circles), when plotted against membrane potential, V_M increases with depolarization towards a saturating value at +30 mV. Activation is measured as $\dot{g}_A$, corrected for inactivation by extrapolation to the onset of the clamp step. Each activating voltage step follows a 500 ms prepulse at -90 MV to remove steady-state inactivation. Pooled data are shown from 6 cells (±SE), normalized to the value of g_A at +30 mV. The curve is the best fit to the data, calculated from the Boltzmann distribution (Equation II-2) with an effective valency of 2.0 and $\dot{g}_A$ one-half activated at -19 mV. The steady-state inactivation data, b_∞ (squares), derived as explained in the text, are plotted against V_M during a 500 ms test prepulse. Inactivation is plotted as the ratio of $I_A/I_{A,max}$, measured at an activating voltage of -10 mV. Membrane pre-hyperpolarization causes an increase in the amplitude of I_A. The curve is plotted according to Equation III-3, where inactivation is one-half removed at -53 mV and the steepness of voltage dependence, k = 9 mV. The inactivation protocol shown in the inset (left) used prepulses of -100 mV to -40 mV, and the largest I_A corresponds to the -100 mV prepulse. The activation protocol (right inset) used voltage steps of -40 to +10 mV, the largest I_A corresponds to the +10 mV step. The cross-hatched rectangle represents the approximate range of resting V_M in the cells (-50 to -40 mV). Measurements were made on I_A separated in 50 or 100 mM TEA.

begins to be activated significantly at about -40 mV. The curve describing activation is the best fit to a simple Boltzmann probability distribution for two state voltage dependent gating (see Chapter II, Equation II-6), where the conductance is one-half activated at -19 mV and the effective valency of the voltage-sensing particle is 2.0.

Steady-state inactivation, b_∞

The voltage dependence of steady-state inactivation, b_∞, was evaluated by measuring the dependence of peak I_A on V_M during the conditioning prepulse. V_M during the conditioning prepulse was varied to test values between -100 and -30 mV, while the duration was maintained constant at 500 ms. This was immediately followed by a depolarizing activation pulse to a fixed value of -10 mV. In this way changes in the magnitude of I_A expressed at -10 mV could be attributed to changes in the value of b_∞ during the conditioning prepulse. The b_∞ data of Figure III-4 (squares) were also normalized to the maximal value obtained (at -100 mV) to put the data in a form similar to I_{Na} steady-state inactivation (h_∞; Hodgkin and Huxley, 1952c). Plotted in this way the data actually measure *removal* of inactivation, since a value of 1.0 means all steady-state inactivation is removed, and the effect of inactivation will be minimal. Hyperpolarized values of V_M remove steady-state inactivation, and this effect saturates at -80 to -90 mV. The curve describing inactivation gating, b_∞, as a function of V_M is calculated from

$$I_A/I_{A,max} = b_\infty(V_M) = 1/[1+\exp\{(V_M-V_{1/2})/k\}] \qquad \text{(III-3)}$$

where $V_{1/2}$ is the value of V_M where inactivation is one-half removed, and k, is a measure of the steepness of the curve. For the curve fit to the average inactivation data (n = 6) $V_{1/2}$ = -53 mV and k = 9 mV.

The above description of steady-state voltage dependence is important because it highlights several features of the I_A system which are of physiological interest. First, the voltage range where I_A is activated overlaps completely the range of voltages seen during a normal action potential. The peak after-hyperpolarization following an action potential usually reaches -55 to -50 mV, a voltage where up to 50% of steady-state inactivation could be removed. At the peak of an action potential the membrane voltage is usually +30 to

+50 mV and thus could produce near maximal I_A activation. Secondly, the curves describing activation and inactivation show considerable overlap, intersecting at value of 0.14 at -38 mV. The overlap means that there is a range of voltages where I_A is expressed tonically because the underlying conductance has some of the inactivation removed and is also activated at the same voltage. This region of the curve encompasses the normal rest potential (-50 to -40 mV) and action potential threshold (-38 to -25 mV).

The voltage dependence of steady-state activation and inactivation can only hint at the possible physiological role of I_A. This is because the kinetics, *i.e.* the rates of change of the conductance at each voltage, will also determine what effect I_A will have on membrane voltage during an unclamped action potential.

Activation and inactivation kinetics

The bell-shaped dependence of the I_A time constant of activation, τ_a on the membrane potential is shown in Figure III-5. Over the voltage range where I_A is substantially activated (-40 to +30 mV) τ_a was measured directly by curve fits to the membrane currents as described above. Values for τ_a at membrane potentials less than -40 mV were obtained by fitting time constants to the deactivation tails elicited by repolarization to various test potentials following the I_A peak. These tail currents decayed as single exponentials whose time constant decreased as V_M was made more negative. Assuming a sequential model of channel activation, the time constant governing activation should be the same as the time constant governing deactivation at the offset of a depolarizing voltage step. Values of τ_a measured in this way were maximal at -40 mV, and averaged 6.4 ms (range 4.8 to 10.8 ms, $n = 6$). τ_a is steeply voltage-dependent, decreasing to an average of 1.7 ms at -10 mV (range 1.0 to 2.1 ms, $n = 11$). τ_a is decreased by about 4 fold over a 30 mV range of depolarization. The plots in Figure III-5 were normalized by dividing the measured time constants for each cell by the maximum value for that cell. This allows a better fit when pooling data from a number of cells. Therefore, the data points are all plotted as normalized mean ±SE, except at -40 mV which is arbitrarily 1.0 with no corresponding SE. The points derived in this way were then fitted with a function of the form,

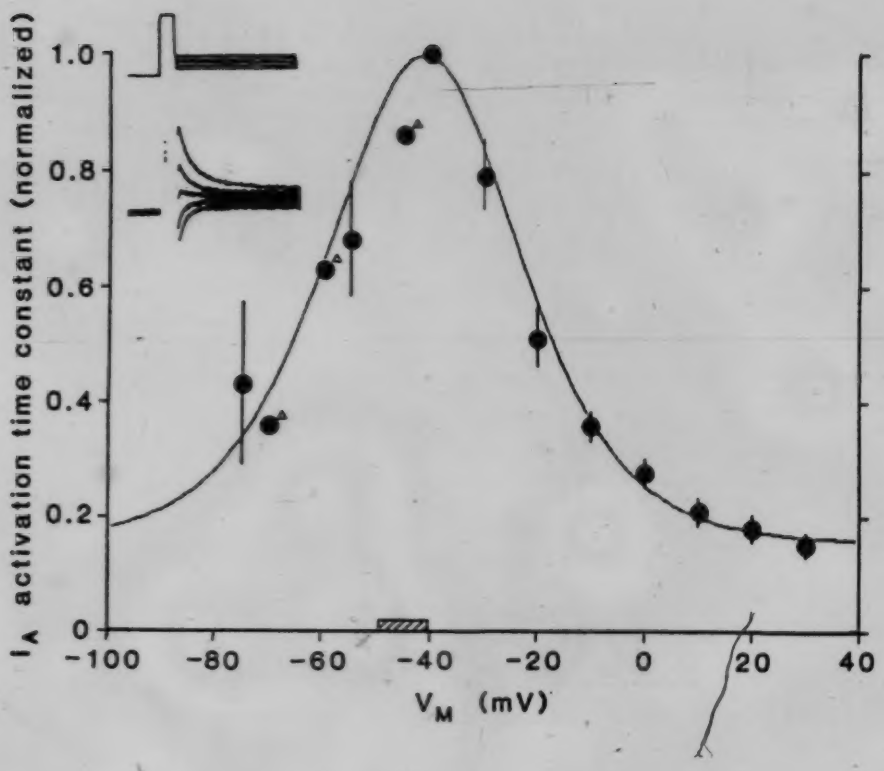

Figure III-5. Dependence of I_A activation time constant on V_M. The activation time constant, τ_a, is a bell-shaped function of V_M. τ_a is maximal at -40 mV (near resting potential) and decreases sharply with depolarization or hyperpolarization of V_M. Normalized data (τ_a at -40 = 1.0) obtained from 6 cells (±SE), except the data points marked with an open triangle, which are single measures for a single cell. The actual values of τ_a at -40 mV averaged 6.4 ms (range 4.8 to 10.8 ms). The inset shows deactivation tail currents recorded for commands from -50 to -75 mV (5 mV steps). The tail current reverses at about -65 mV, and τ_a decreases as the test step becomes more negative. The cross-hatched rectangle represents the approximate range of resting V_M in these cells (-50 to -40 mV).

$$\tau_a(V_M) = c*[d/\{1+\exp((a-V_M)/b)\}*\{1+\exp((V_M+a2)/b2)\}+e] \qquad \text{(III-4)}$$

The best fit values for the variables a, b, c, d, e, a2, and b2, derived from the average data, can be found in the Appendix to Chapter IV.

Inactivation time constants were also maximal at -40 mV, decreasing as V_M is moved from this value. Average, normalized inactivation time constants are plotted along with the best fit curve, as was done for the activation data (Figure III-6). Inactivation time constants were measured for V_M of -40 mV or greater simply by obtaining the decay τ_b as I_A inactivated at each test voltage following a conditioning prepulse to -90 mV. τ_b was quite variable from cell to cell in the ganglion. At -40 mV τ_b averaged 311 ms (range 170 to 625 ms, n = 6). This decreased sharply to an average value of 24.2 ms at -10 mV (range 8.3 to 57.7 ms, n = 11). The decrease in τ_b is therefore about 13 fold for a 30 mV depolarization. To measure τ_b at more negative potentials where little I_A is activated a two step protocol was used. From the holding potential, a variable duration conditioning pulse was initiated, followed by a fixed activating pulse to -10 mV. At each test voltage peak I_A was plotted against the duration of the conditioning pulse. The I_A measured at -10 mV increases as a function of time at the conditioning voltage, until a steady value is reached at longer times (Figure III-6 inset). The time course of removal of inactivation measured in this way is a single exponential which yields τ_b at the voltage used for the conditioning pulse. The time involved in measuring τ_b by this method is long in relation to the period of time that cells remain viable. Because of this, τ_b was usually measured at only at -90 mV using the double pulse protocol, and few data points were available in the -80 to -50 mV range. Therefore the part of the curve describing τ_b in this voltage range should be considered approximate. At -90 mV τ_b averages 61 ms (range 35 to 100 ms, n = 5).

Calcium sensitivity of I_A

In many neurons, the rise in intracellular Ca^{2+} which follows depolarizing voltage clamp steps or action potentials, results from Ca^{2+} influx through voltage dependent Ca^{2+} channels and not through release from intracellular stores (Hagiwara and Byerly, 1981; Tsien, 1983). Therefore one can experimentally limit the rise in internal Ca^{2+} by blocking

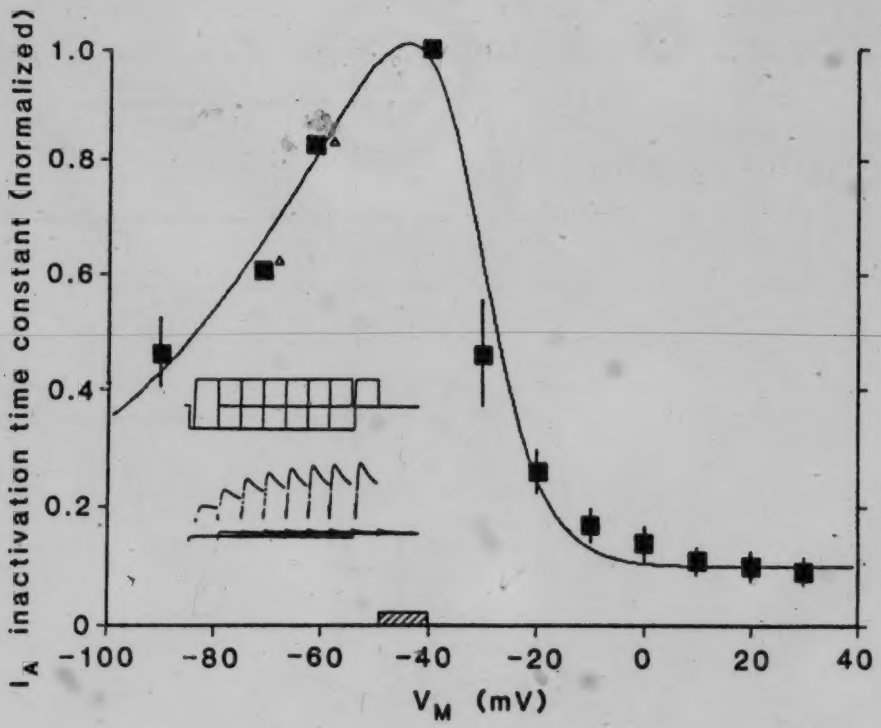

Figure III-6. Dependence of I_A inactivation time constant on V_M. The inactivation time constant, τ_b, is a skewed bell-shaped function of V_M which is maximal at -40 mV. The figure shows normalized data obtained from 6 cells. The actual values of τ_b at -40 mV averaged 311 ms (range 170 to 625 ms). The inset illustrates the protocol for measuring τ_b by the removal of inactivation at a test voltage of -90 mV. Refer to the text for a description of the methods used to measure τ_b. The cross-hatched rectangle represents the approximate range of resting V_M in these cells (-50 to -40 mV).

Ca^{2+} influx. The Ca^{2+}-dependence of I_A was evaluated by comparing currents before and following treatments which block the Ca^{2+} influx through Ca^{2+} channels. Ca^{2+} influx can be blocked by three methods. The most common is to physically block the entrance to the Ca^{2+} channel with divalent cations whose hydrated ionic radius is larger than that of Ca^{2+} (Hille, 1984). Divalent cations such as Co^{2+}, Mn^{2+}, and Cd^{2+} are the most suitable, as other heavy metal ions (*e.g.* Hg^{2+}, Cu^{2+}) are toxic to nerve tissue. For such experiments, Ca^{2+} is omitted from the bathing medium, and replaced by equimolar concentrations of another divalent cation. Simple addition of divalent cations to the bath, while technically simpler, is not adequate, since the ensuing increase in bath osmolality and total divalent cation charge will shift membrane conductance parameters along the voltage axis (Frankenhaeuser and Hodgkin, 1957). A second way to eliminate Ca^{2+} influx is simply to omit Ca^{2+} from the bathing medium, but this was considered unsatisfactory for the same reasons. Thirdly, several organic 'Ca^{2+} channel antagonists' are available which are reported to block Ca^{2+} channels at micromolar concentrations (Hagiwara and Byerly, 1981). Unfortunately, in barnacle neurons, the organic Ca^{2+} blockers tested (verapamil and nifedipine) only weakly blocked I_{Ca}, and also non-specifically altered the kinetics of K^+ currents (see below) and therefore were not useful in the present analysis. Thus, for the experiments reported here, the first method (ionic substitution) was used, with the replacing cation either Co^{2+} or Mn^{2+}. The term Ca^{2+}-free ( ) is used to describe the external medium, with the replacing cation noted in the brackets.

The effect of Ca^{2+}-free (Co^{2+} or Mn^{2+}) saline on I_A was studied in 22 cells. Of these, 19 cells showed a reduction in the peak I_A after elimination of the Ca^{2+} influx. The peak I_A measured in Ca^{2+}-free saline was reduced by 20 to 80% when compared to the control values at the same voltage. In some of these experiments I_A was isolated in 50 or 100 mM TEA saline to reduce contamination of the I_A records by I_K and $I_{K(Ca)}$. This did not materially affect the results. The quantitative results presented are mostly from experiments done using Ca^{2+}-free (Co^{2+}) saline, because those experiments happened to produce the most complete data sets for analysis. However, qualitatively similar results were also obtained for cells bathed in Ca^{2+}-free (Mn^{2+}) saline. The results presented in Figures

III-7 to III-11 are from a single exemplar cell which showed a typical reduction of I_A in Ca^{2+}-free (Co^{2+}) saline. Mean values for other experiments are presented where relevant.

Figure III-7 shows the membrane currents recorded from an experiment which demonstrates that a substantial fraction of I_A is blocked in Ca^{2+}-free (Co^{2+}) saline. I_A was first isolated in saline containing 1 μM TTX, and 50 mM TEA. For each data set the membrane voltage was stepped from -30 mV to +20 mV in 10 mV increments. All clamp steps follow a conditioning prepulse to -90 mV (for 500 ms). Linear leakage currents have been mathematically subtracted. The control traces are typical of I_A in barnacle neurons. Rapid activation is followed by a slower voltage dependent inactivation phase, producing a time to peak which is voltage-dependent. For the -30 mV step, the peak current of 6.8 nA occurred at 14.4 ms, the amplitude increased to 117.2 nA at 3.6 ms for the +20 mV step. Co^{2+} replacement reduced the peak current at all voltages and slowed the current onset, increasing the time to peak current. For the -30 mV step the peak current was reduced to 1.7 nA at 20.2 ms, and for +20 mV the peak was 77.8 nA at 7.6 ms. Therefore, about 75 % of the peak I_A is blocked in Co^{2+} saline for the -30 mV step and 34% is blocked for the +20 mV step.

Digital subtraction of the I_A records for control, and Ca^{2+}-free (Co^{2+}) saline at each test voltage, yields the Ca^{2+}-dependent membrane current components. The current is outward for all voltages tested, and shows very rapid activation and inactivation (Figure III-7, bottom). The membrane current record obtained by subtraction is a combination of I_A and I_{Ca}, but the record shows only net outward current because the contribution of I_{Ca} is small. No separation protocol can be used to eliminate contamination of the subtraction record by I_{Ca} because any procedure which limits I_{Ca} would obligatorily block the activation of the Ca^{2+}-dependent fraction of I_A. Therefore, all of the experiments in which the peak conductance or kinetics of I_A were studied are contaminated to a small degree by simultaneous changes in I_{Ca}. In a few experiments I_A was eliminated by 4-AP (see below), showing that the net inward I_{Ca} was maximal at about +10 mV, and small compared to I_A at +10 mV. I_{Ca} contamination was also lessened by choosing cells with a large contribution of I_A relative to other membrane current components. In any case, elimination of I_{Ca}

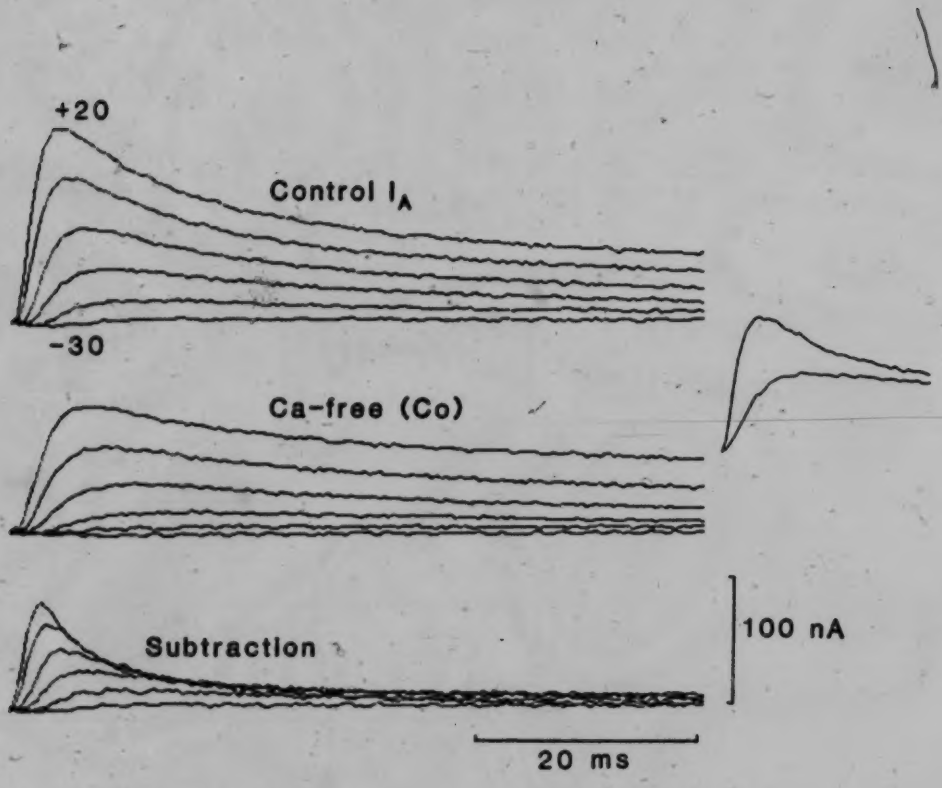

Figure III-7. Reduction of peak I_A in Ca^{2+}-free (Co^{2+}) saline. The upper records show I_A recorded in 1 μM TTX, 50 mM TEA saline, for command steps from -30 mV to +20 mV in 10 mV increments (data superimposed). Perfusion with Ca^{2+}-free (Co^{2+}) saline reduces the peak I_A at all voltages and slows the rate of activation and inactivation. The reduction in peak I_A ranges from 34% (at +20 mV) to 75% (at -30 mV). The current eliminated in Ca^{2+}-free (Co^{2+}) saline can be visualized by subtracting the control and Co^{2+} records (bottom records). The current remaining after subtraction is outward for all voltages, and appears to activate and inactivate much more rapidly than the control I_A. The inset compares the records taken in 20 mM Ca^{2+} and 20 mM Co^{2+} at 0 mV. Refer to the text for a more complete analysis of the data records. The raw data for the control and, Ca^{2+}-free (Co^{2+}) are plotted following leakage correction. The subtraction was carried out on the raw data files prior to leakage correction. The plot omits the first 800 μs of data during the capacitative transient. Analog to digital sample interval = 400 μs.

would tend to increase the amplitude of I_A, giving an underestimate of the Ca^{2+}-dependent I_A fraction.

The reduction in peak I_A does not occur through a reduction of the K^+ driving force, or alteration of the ionic selectivity of I_A. Replacement of external Ca^{2+} with Mn^{2+} or Co^{2+} does not alter the post-pulse tail current reversal by more than 1-2 mV. In most cases the measured V_{rev} was slightly more negative after Ca^{2+} replacement, which would tend to increase I_A measured at depolarized voltages. Thus, the peak conductance associated with I_A, and not the driving force, appears to be reduced.

In the following analysis of I_A Ca^{2+}-dependence, I will argue that: 1) A significant fraction of the reduction in $g_{A,peak}$ in Ca^{2+}-free (Co^{2+}) saline is produced by shifts in voltage dependence, though the shifts observed are not consistent with a simple, uniform surface screening effect; 2) Alterations in I_A kinetics do not account for the reduced peak conductance, although they may explain in part the increased excitability observed in current clamped neurons in Ca^{2+} replaced saline; 3) Experiments in which the external Ca^{2+} level was altered are consistent with both a surface charge screening effect, and the hypothesis that a fraction of I_A is Ca^{2+}-dependent.

The effects of Ca^{2+}-free (Co^{2+} or Mn^{2+}) saline on the voltage dependence of the I_A system parameters must be distinguished from simple surface charge screening effects on the membrane surface potential. Previous studies have shown that replacement of Ca^{2+} by other period 4 divalent cations can alter the voltage dependence of ionic conductances simply by altering the membrane surface potential (Dodge, 1961; Goldman and Blaustien, 1969; Ehrenstien and Gilbert, 1969; Hille *et. al.*, 1975; Brismar, 1980; Hille, 1984). The transmembrane electric field, as sensed by a voltage dependent channel, would then be shifted as though a potential bias was added to the membrane potential. According to this theory, the direction of the voltage shift depends on the relative ability of the replacing cation to titrate fixed negative surface charges at surface of the membrane (Mozhayeva and Naumov, 1970). This is thought to alter the steepness of the effective potential gradient across the membrane.

The effects of a change in surface potential cannot be evaluated by measuring changes in V_M. Measured with microelectrodes as the difference between intracellular voltage and extracellular voltage, V_M is only a spatial average of the potential gradient across the cell membrane. The potential gradient at the membrane itself could be somewhat different, due to ion accumulation at the membrane surface. The effect of surface potential on the voltage sensor of I_A channels, and hence on the whole cell I_A magnitude can be described as

$$I_A = a^6 b^3 g_A (V_{Ch} - E_A) \qquad \text{(III-5)}$$

where V_{Ch} is the voltage difference sensed by a transmembrane I_A channel, and

$$V_{Ch} = V_M - (\phi_O + \phi_I)$$

Thus, the voltage sensed by I_A channels differs from V_M by the subtraction of the net surface potential, which is the sum of the membrane outer surface potential, ϕ_O, and inner surface potential, ϕ_I.

An increase in extracellular Ca^{2+} or Ca^{2+} replacement by other divalent cations, usually shifts voltage dependent parameters in a depolarizing direction by a few to tens of millivolts (Frankenhaeuser and Hodgkin, 1957). This can be interpreted as an increase in the net surface potential, due to an increase in positive charge at the membrane outer surface. This would make the effective voltage drop sensed by the channel more negative than measures of V_M alone would predict.

The reduction of I_A observed in Ca^{2+} replaced saline is not consistent with a simple surface potential effect on voltage dependent parameters. A surface charge screening model would predict that all voltage dependent parameters be shifted uniformly along the voltage axis, because only ϕ_O should be effected. This is not what was observed for I_A system parameters. Figure III-8 shows $g_{A,peak}$-V and steady-state inactivation curves measured as described previously. The effect of 20 Co^{2+} saline on the net surface potential was evaluated using the following logic. It was assumed that the steady-state inactivation curve, b_∞, was a more useful measure of a potential shift (*i.e.*, changes in net surface potential) than the $g_{A,peak}$-V curve. This was considered to be true because the shape and voltage dependence of steady-state inactivation curve are independent of the magnitude of the conductance

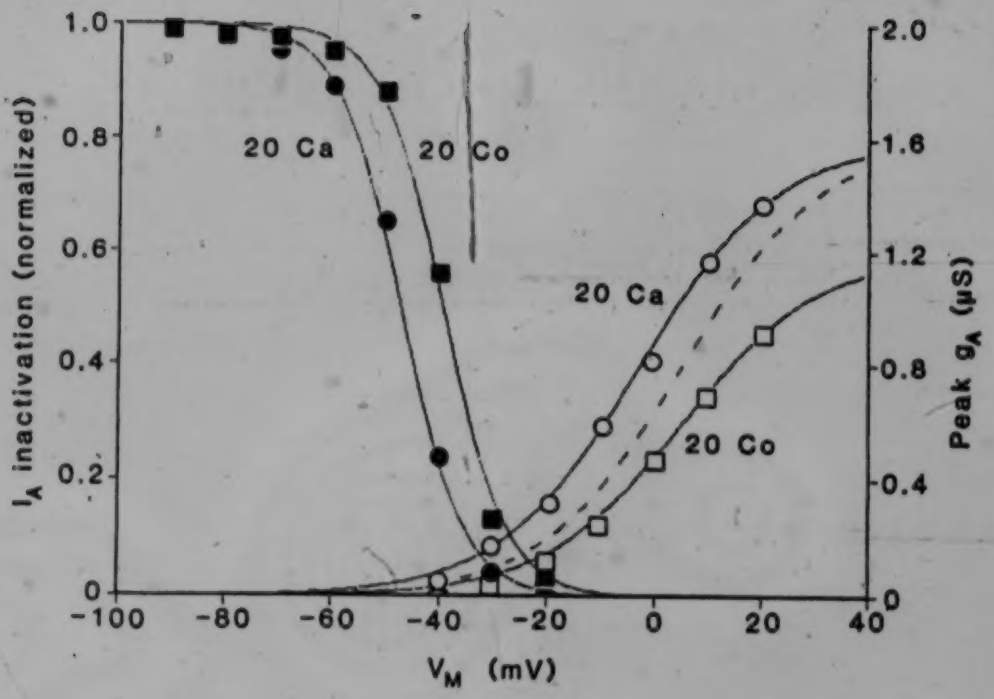

Figure III-8. Effect of Ca^{2+}-free (Co^{2+}) saline on the voltage dependence of b_∞ and $g_{A,peak}$. Normalized inactivation, b_∞, and $g_{A,peak}$ were measured as a function of V_M, at 10 mV increments, in 20 Ca^{2+} (circles) and 20 Co^{2+} saline (squares). The major effects of Co^{2+} replacement are a +8 mV shift in b_∞ and a large voltage-dependent reduction in $g_{A,peak}$. The dashed curve shows the expected $g_{A,peak}$, calculated assuming that the shift in voltage dependence was equal to the shift observed for b_∞. The measured $g_{A,peak}$ deviates from the the prediction based on an equal surface potential shift, and this is most prominent at more depolarized test voltages. I_A was isolated in saline containing 1 μM TTX, and 50 mM TEA.

activated (this assumption was tested using other K^+ channel blockers; see also Thompson, 1977). In addition, steady-state inactivation readily saturates at potentials less than about -80 mV, and thus, the control and experimental curves are easily normalized for comparison.

The 20 Ca^{2+} inactivation data (Figure III-8) were fitted with equation III-3 to yield the steepness (k = 6), and membrane potential at which inactivation is 50% removed ($V_{1/2}$ = -46 mV), and plotted as the curve through the filled squares. The 20 Co^{2+} data were then fitted by shifting the same curve along the voltage axis, maintaining all other parameters the same. Measured in this way, the effect of Ca^{2+}-free (Co^{2+}) saline is equivalent to a +8 mV shift of b_∞ along the voltage axis (mean shift = +9 mV, for this and two other cells in Co^{2+}). The shape of the inactivation curve appears to be otherwise unaltered. If the only effect of Ca^{2+}-free (Co^{2+}) saline on g_A was a surface potential change then the $g_{A,peak}$-V curve should also be shifted +8 mV, the same as was seen for inactivation. Figure III-8 shows that this is not the case. The $g_{A,peak}$ data (open circles) were best fitted and the curve describing the voltage dependence shifted by +8 mV (dashed curve), to approximate the effect of a simple voltage shift on $g_{A,peak}$. Clearly, a surface potential shift would predict a reduction in peak g_A over the voltage range studied. However, the peak g_A in Co^{2+} saline (open squares) is reduced even more than predicted by the dashed curve derived from the inactivation shift, and therefore the decreased $g_{A,peak}$ cannot be fully explained by potential shift hypothesis. The reduction in $g_{A,peak}$ did not appear to result from a disproportionately large shift in steady-state activation, a_∞^4, because plots of normalized g_A were shifted approximately the same amount as b_∞. This was difficult to assess with certainty though, because the g_A curves in Co^{2+} did not reach a saturating value over the voltage range studied.

In 3 cells where the effect of Co^{2+} on g_K was studied, the average shift was only +5 mV, and the reduction in peak g_K was much less pronounced than for peak g_A in the same cells. In these experiments on I_K, cells were chosen which had a small contribution of the slow Ca^{2+}-dependent K^+ current, $I_{K(Ca)}$. This was done by analyzing the records and using only cells which had had a minimal slow Ca^{2+}-dependent tail current component (refer to Chapter V). These results suggest that Co^{2+} replacement has specific effects on peak g_A and

that these are not seen to the same degree for g_K, further ruling out a surface potential effect as being causal to the reduction of $g_{A,peak}$.

Given that a simple surface potential shift effect does not account for all of the reduction of $g_{A,peak}$, I investigated the possibility that alterations in kinetics produce the reduction in $g_{A,peak}$. It was apparent that activation was slower, and the time to peak I_A was increased when Co^{2+} replaced Ca^{2+}. Therefore an alteration of kinetics does occur (Figure III-7). This result could be interpreted in either of two ways. The first would be to assume that I_A is made up of two subpopulations of channels: one producing a rapid Ca^{2+}-activated I_A which is also intrinsically voltage dependent; the other producing a slower, strictly voltage dependent I_A. Eliminating Ca^{2+} influx would then remove activation from the faster I_A population, yielding a smaller, more slowly activating current reflecting only activation of the slower voltage dependent channels. This was the conclusion reached for rat hippocampal neurons (Zibcz and Weight, 1985). An alternative hypothesis would be that Co^{2+} (or Mn^{2+}), used to replace Ca^{2+}, have specific effects on the activation kinetics of I_A channels. The observed slowing of activation could then be the result of a single population of I_A channels which are modified kinetically in the presence of heavy metal cations. This type of mechanism has been suggested for the slowing of I_K activation gating in squid axons treated with Zn^{2+} (C[illegible] and Armstrong, 1982).

The kinetics of I_A activation in Ca^{2+} and Co^{2+} saline were compared visually by superimposing the activation phase recorded in the two salines. All of the current traces were scaled to yield the same peak current amplitude. The current activates much more slowly in Co^{2+} (and would be reduced in amplitude, refer to Figure III-9 legend for scaling factors). The record for activation onset during a depolarization to +10 mV in Co^{2+} essentially overlaps the 20 Ca^{2+} record for a depolarization to -10 mV. The two records activate with similar lag time, and have almost identical time constants. This means that Co^{2+} replacement slows activation in a manner which appears to be the equivalent of a +20 mV shift (at -10 mV) of the activation time constant voltage dependence. Similar results over a wider range of voltages are discussed below.

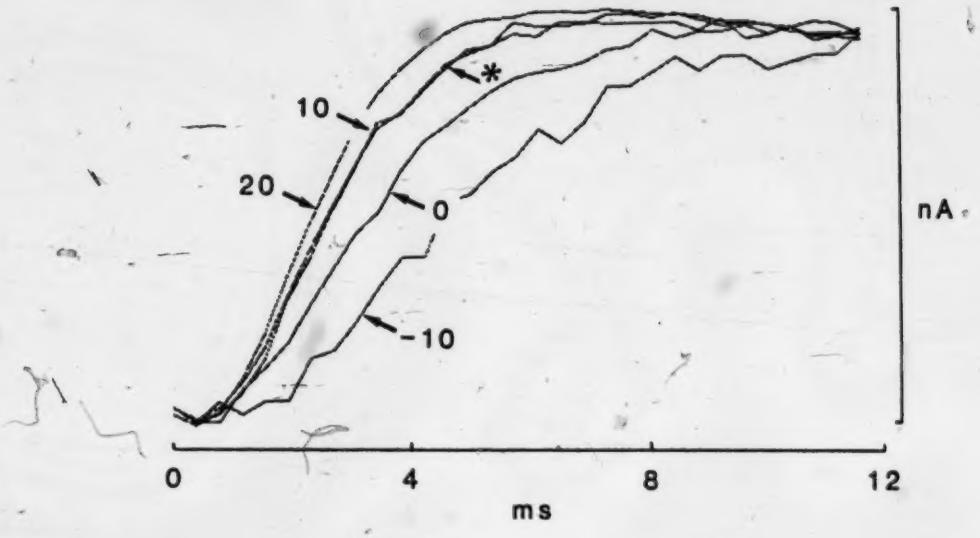

Figure III-9. Effect of Ca^{2+}-free (Co^{2+}) saline on the rate of I_A activation. The rising phase for I_A recorded in 20 Ca^{2+} saline (trace marked *) is compared to the rising phase for I_A recorded in 20 Co^{2+} saline. The voltage steps in Co^{2+} are labelled by the value of the depolarization. All records have been scaled to yield approximately equal peak I_A so that the rising phase could be examined more closely. The trace labelled -10 was recorded in Co^{2+} at the same voltage as the control. Clearly the current rise was slowed in Co^{2+}, and the amplitude would be reduced (see below). The record for a command to +10 mV in Co^{2+} essentially overlaps the record for 20 Ca^{2+} at -10 mV. Thus, the rising phase of I_A is slowed in a manner equivalent to a 20 mV reduction in the voltage used to activate I_A. The actual peak I_A values prior to scaling were; 20 Ca^{2+}, -10 mV = 33.4 nA; 20 Co^{2+}, -10 mV = 13.7 nA, 0 mV = 30.7 nA, 10 mV = 52.8 nA, 20 mV = 77.5 nA. I_A was isolated in saline containing 1 μM TTX, and 50 mM TEA. The data records omit the first 800 μs of data during the capacitative transient. Analog to digital sample interval = 400 μs.

The effect of Ca^{2+}-free (Co^{2+}) saline on the voltage dependence of I_A activation and inactivation time constants is summarized in Figure III-10. In this experiment the time constants were derived from curve fits to the membrane current records. The left panel are results for fits to activation. The activation time constant, τ_a, is increased at all voltages where it was measured in Ca^{2+}-free (Co^{2+}) saline. The exponential curve fitted to the 20 Ca^{2+} data points (filled circles, left panel) is derived from Eqn. III-4. The 20 Co^{2+} data points were fitted reasonably well by shifting the curve describing τ_a by +17 mV (rightward) on the voltage axis. It appeared that the slowing of τ_a was voltage-independent and, over the -20 to +20 mV range, roughly equivalent to a 17 mV reduction in the depolarizing voltage step used to activate I_A.

When measured in Ca^{2+}-free (Co^{2+}) saline the I_A inactivation time constant, τ_b, was also increased at all voltages studied (Figure III-10, right panel). This effect was very pronounced, and the increase was voltage dependent. τ_b was slowed 1.4x at -20 mV and 2.0x at +20 mV. Unlike the change in τ_a, no simple voltage shift of the 20 Ca^{2+} τ_b curve could produce a reasonable fit to the 20 Co^{2+} data. The amplitude and steepness of the curve also had to be altered to fit the Co^{2+} data. The dotted line shows the predicted values for τ_b if the shift was equal to the shift (+8 mV) measured for b_∞. Clearly the two parameters of the same gating function are 'shifted' unequally.

Do the changes in kinetics observed in Ca^{2+}-free (Co^{2+}) saline explain the reduced $g_{A,peak}$? Probably not; both activation and inactivation are slower in Ca^{2+}-free (Co^{2+}) saline, but inactivation is slowed proportionately more. For this reason, the $g_{A,peak}$ should be larger in Ca^{2+}-free (Co^{2+}) saline, the opposite of what is observed. It is difficult to determine exactly how much of a reduction of $\bar{g}_A$ occurs in Ca^{2+}-free (Co^{2+}) saline, because the accompanying changes in time constants alter the measured $g_{A,peak}$. In order to examine this, the descriptive formulation for I_A (Eqn. III-2) was used to produce predicted current waveforms which could be compared to data records. Plots of this type of comparison are shown in Figure III-11. The experimental I_A records were obtained in 20 Ca^{2+} and 20 Co^{2+} saline for a voltage step from -90 mV to 0 mV. The upper calculated record is a plot of I_A vs. time, calculated from Eqn. III-2, using the values of τ_a, τ_b and g_A obtained from the

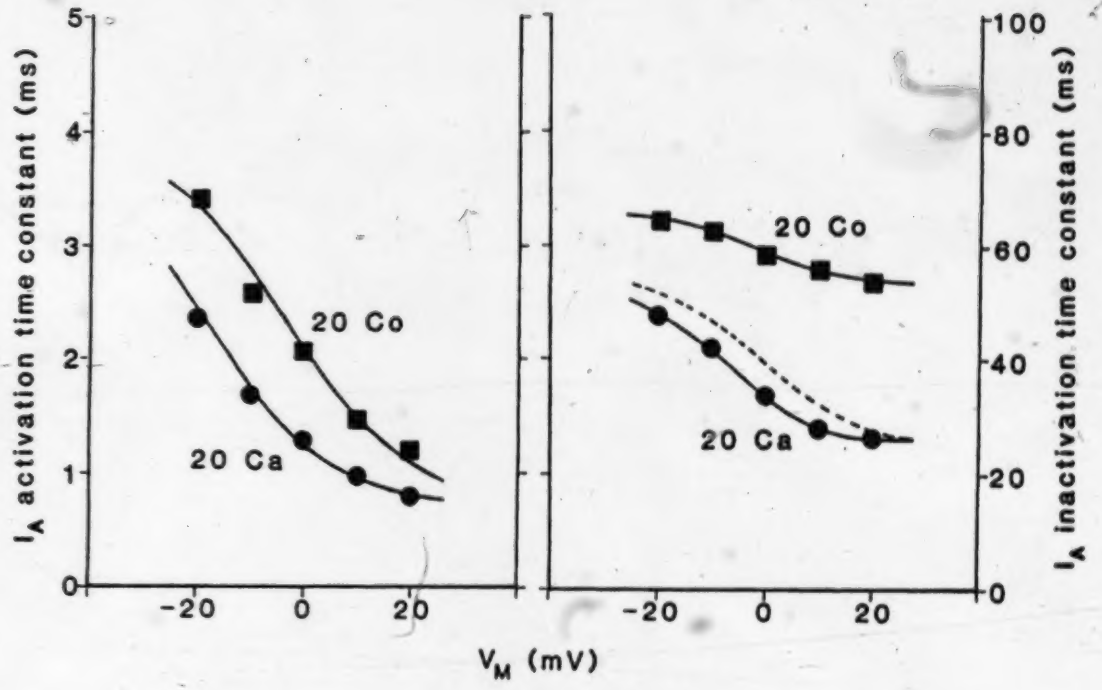

Figure III-10. Effect of Ca^{2+}-free (Co^{2+}) saline on I_A time constants. Activation, τ_a and inactivation, τ_b were measured as a function of V_M in 20 Ca^{2+} (circles) and 20 Co^{2+} (squares) saline. Over the range of V_M studied (-20 to +20 mV) both τ_a and τ_b decrease as V_M increases. Replacement of Ca^{2+} with 20 Co^{2+} increased τ_a and τ_b over the entire voltage range. The effect on τ_a (left) was the equivalent of a +17 mV shift of the curve used to describe the 20 Ca^{2+} data points. The effect of Co^{2+} replacement on τ_b was not equivalent to a simple shift in voltage dependence because no simple shift of the curve fitted to the 20 Ca^{2+} points could adequately describe the 20 Co^{2+} data. The dashed line shows the predicted values of τ_b if τ_b were shifted by the same amount as b_∞ (+8 mV) in the same cell (Figure III-8). The two parameters of the same gating function (b) were therefore not affected in the same way by Co^{2+} replacement.

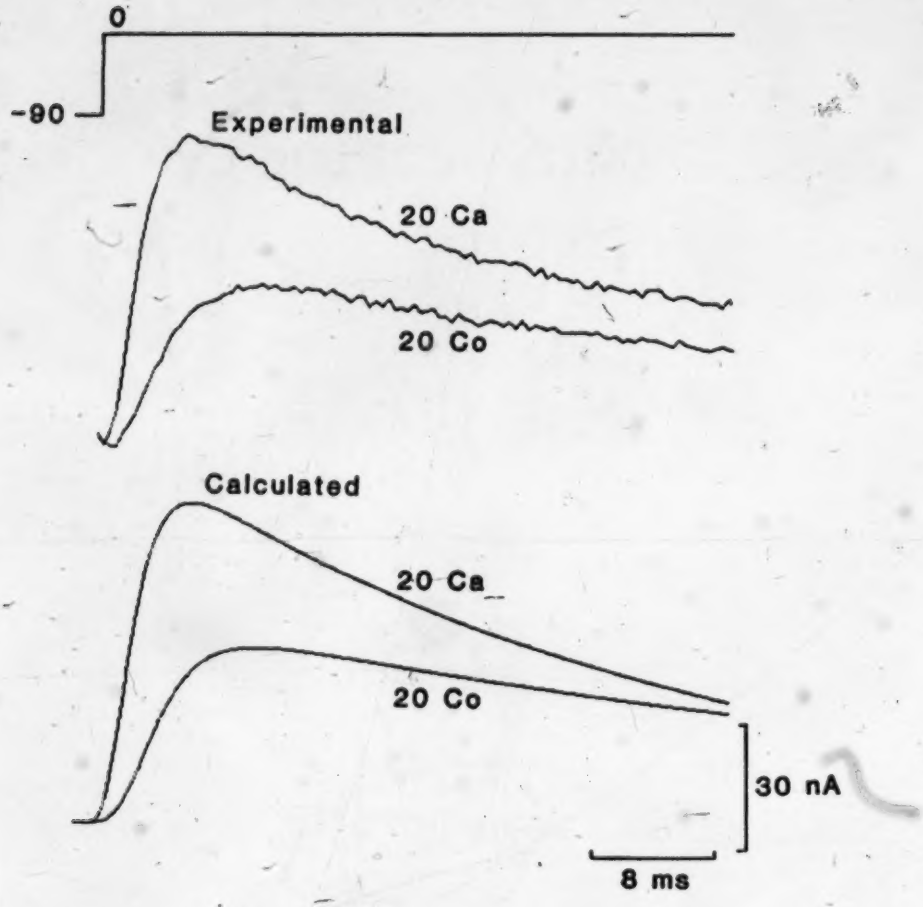

Figure III-11. Comparison of experimental and calculated records describing the effect of Ca^{2+}-free (Co^{2+}) saline on I_A. The experimental traces were recorded for a depolarization to 0 mV in 20 mM Ca^{2+} and 20 mM Co^{2+} saline (same neuron as previous figures). The upper calculated record was derived from Equation III-2, using the experimentally obtained values of τ_a, and τ_b recorded in 20 Ca^{2+} saline, and fitting to obtain the appropriate g_A. Altering τ_a and τ_b to the values measured in 20 mM Co^{2+} saline produced a calculated peak I_A which was 1% larger than the control (20 mM Ca^{2+}) I_A (not shown). Therefore, g_A had to be reduced to produce a calculated record similar to the 20 mM Co^{2+} data. Assuming that g_A was reduced by 47% yielded a calculated trace very similar to the experimental result in 20 mM Co^{2+}. This analysis demonstrates that the conductance underlying g_A has to be reduced by Co^{2+} replacement. An important point to note is that this differs from the previously mentioned reduction of *peak* g_A because $g_{A,peak}$ could be reduced without a reduction in the underlying g_A if the time constants were altered by the treatment.

20 Ca^{2+} data in part A (τ_a = 1.3 ms, τ_b = 33.7 ms, g_A = 1.42 μS, calculated peak I_A = 58.2 nA). The time constants used in the calculation were then altered to the values measured from the data taken in Co^{2+} saline (τ_a = 2.1 ms, τ_b = 58.6 ms). Without changing g_A this yielded a predicted peak I_A which was about 1% *larger* than that calculated using the 20 Ca^{2+} time constants (peak I_A = 59.0 nA, curve not shown). The peak g_A used in the calculation was then progressively reduced until the predicted peak I_A was equal to that measured from the data taken in 20 Co^{2+} (30.7 nA). A value of g_A = 0.76 μS produced the closest fit to the data (20 Co^{2+} trace in Figure III-11). This suggests that, at 0 mV, g_A was reduced by 47% in Co^{2+} saline once the changes in time constants are taken into account. Similar calculations over a wider range of voltages showed that for this cell g_A was reduced by 75% at -30 mV, and 36% at +20 mV, independent of the changes in time constants.

One of the effects of replacing external Ca^{2+} with Co^{2+} is the shift in voltage dependent parameters, another is the reduced $g_{A,peak}$. The following experiments were undertaken to determine whether these two effects can occur independently, or whether they are coupled. The approach used was to intentionally create a large depolarizing shift in I_A voltage dependence by increasing the external Ca^{2+} concentration. Figure III-12 shows the b_∞ and $g_{A,peak}$ curves for a cell in 20 Ca^{2+} and 30 Ca^{2+} saline. In this experiment, a 50% increase in Ca^{2+} shifted the b_∞ curve by +12 mV in the depolarizing direction, as measured by fitting to Eqn. III-3. Therefore, increasing the Ca^{2+} concentration by 10 mM had a similar effect on inactivation voltage dependence as replacing Ca^{2+} with Co^{2+}, except that the shift is +4 mV larger for 30 Ca^{2+} saline (compare to Figure III-8). The peak g_A data recorded in 20 Ca^{2+} saline were fitted with an arbitrary exponential function, and this same function shifted by +12 mV. When the 30 Ca^{2+} data points are compared to the shifted activation curve the $g_{A,peak}$ is larger than the shifted activation curve would predict. Thus, although the shift in inactivation voltage dependence (and presumably surface potential) is in a similar direction to that observed in Ca^{2+}-free (Co^{2+}) saline the effect on $g_{A,peak}$ is opposite that seen in Co^{2+}. In other words, the 30 Ca^{2+} $g_{A,peak}$ data are actually reduced from the 20 Ca^{2+} data, but the reduction is less than would be expected if all parameters

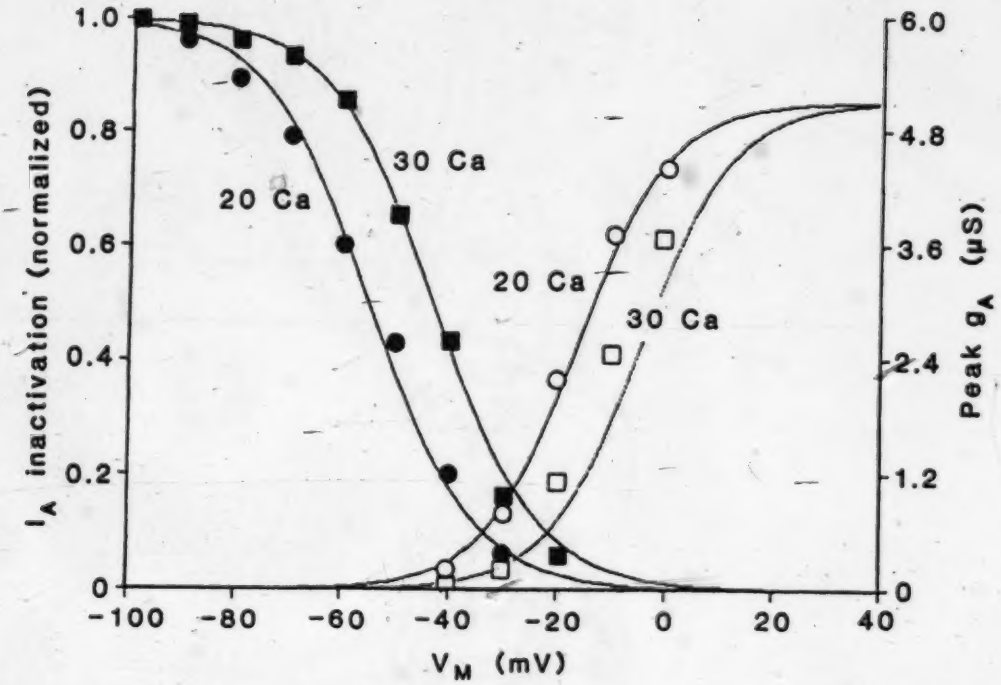

Figure III-12. Effect of raising the external Ca^{2+} concentration on the voltage dependence of b_∞ and $g_{A,peak}$. Normalized inactivation, b_∞ and $g_{A,peak}$ were measured as a function of V_M in 20 mM Ca^{2+} (circles) and 30 mM Ca^{2+} saline (squares). Increasing the external Ca^{2+} by 10 mM shifted b_∞ by +12 mV, with little change in steepness of the voltage dependence. The $g_{A,peak}$ was reduced in 30 mM Ca^{2+} saline, but not as much as if b_∞ and $g_{A,peak}$ were shifted equally. Therefore, raising the external Ca^{2+} concentration mimics the depolarizing shift of b_∞ observed in 20 mM Co^{2+} saline, but does not mimic the marked reduction in $g_{A,peak}$ (compare to Figure III-8).

were shifted equally. Only part of the $g_{A,peak}$ reduction observed when Co^{2+} is substituted for Ca^{2+} is observed when a similar depolarizing surface potential shift is elicited by increasing the external Ca^{2+} concentration. Therefore, the markedly reduced $g_{A,peak}$ in Ca^{2+}-free (Co^{2+}) is caused by either Co^{2+} itself reducing g_A, or by the accompanying reduction of Ca^{2+} influx produced by the blocking effect of Co^{2+} on I_{Ca} channels.

Reducing the external Ca^{2+} concentration to 5 mM shifts the b_∞ curve in a hyperpolarizing direction and also reduces $g_{A,peak}$ (Figure III-13). The measured shift in b_∞ is -10 mV. An equivalent shift of the curve describing peak g_A suggests that the major effect of such a voltage shift should be an increase in the conductance measured during the activating steps. Curiously, $g_{A,peak}$ was increased at more negative test voltages, but decreased at voltages greater than -30 mV. At the more negative test voltages $g_{A,peak}$ comes closest to following the potential shift measured for b_∞. A possible explanation for this result is related to the fact that voltage dependent Ca^{2+} influx carried by I_{Ca} is activated starting at about -20 mV in these cells (Chapter II). The voltage range over which $g_{A,peak}$ was more reduced corresponds to voltages where I_{Ca} would be activating substantially. At 0 mV $g_{A,peak}$ is reduced to 65% of the control (20 Ca^{2+}) value. This type of experiment is important because it demonstrates a Ca^{2+}-dependent reduction in $g_{A,peak}$ which is clearly opposite to the result expected from an effect on the surface potential. In addition, the reduction of $g_{A,peak}$ in the absence of any replacing metal cation rules out an effect of these ions on g_A as being causal to the reduced conductance.

In summary, the results presented support the hypothesis that part of the I_A in barnacle neurons is Ca^{2+}-dependent. Replacing the external 20 mM Ca^{2+} with Co^{2+} shifts I_A voltage dependent parameters unequally in a depolarizing direction along the voltage axis. This reduces $g_{A,peak}$, and increases τ_a, τ_b, and the time to peak current. The apparent shifts are about +8 mV for b_∞ and a_∞, and +17 to +20 mV for τ_a. The effects on $g_{A,peak}$ and τ_b are not well described by a simple voltage shift. Peak g_A is also reduced when the external Ca^{2+} is either increased or decreased with no replacing cation. In high Ca^{2+} (30 mM) the reduction in $g_{A,peak}$ is explained simply as a depolarizing surface potential shift. The reduction of $g_{A,peak}$ in low Ca^{2+} (5 mM) saline is the opposite of what would be

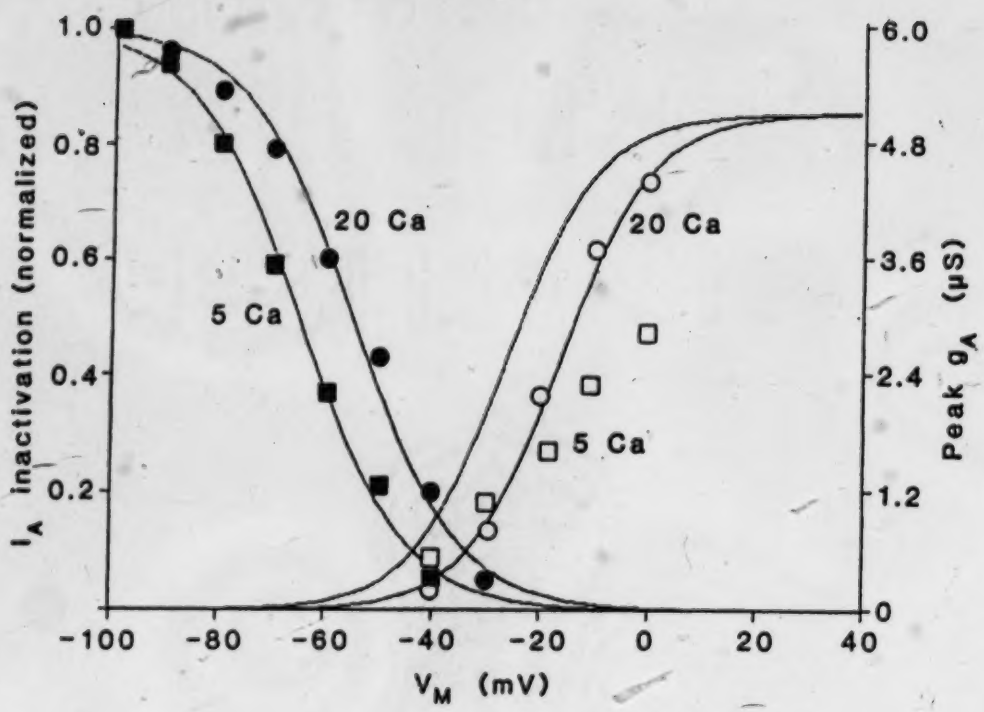

Figure III-13. Effect of decreasing the external Ca^{2+} concentration on the voltage dependence of b_∞ and $g_{A,peak}$. Normalized inactivation, b_∞ is plotted as a function of V_M in 20 mM Ca^{2+} (filled circles) and 5 mM Ca^{2+} saline (filled squares). In 5 mM Ca^{2+} saline b_∞ was shifted to more hyperpolarized voltages by -10 mV. In 5 mM Ca^{2+} the $g_{A,peak}$ (open squares) was reduced at the more positive test voltages (>-30 mV), but increased at the lower test voltages when compared to the control (open circles). An equivalent shift of the $g_{A,peak}$ curve suggests that $g_{A,peak}$ should be increased at all test voltages if the decrease in external Ca^{2+} concentration acted simply as a potential shift.

expected from a surface potential shift, and suggests that a reduction in Ca^{2+} influx obligatorily reduces g_A.

Pharmacological sensitivity

4-Aminopyridine

The I_A in barnacle neurons is sensitive to the K^+ channel blocker 4-aminopyridine (4-AP) at relatively low external concentrations. One mM 4-AP blocks 60 to 90% of the peak I_A measured 30 min after application (n = 5). The effect develops in two phases. Initially (during the first 3 to 10 minutes) bath application of 4-AP blocks I_A quite selectively; however, later the 4-AP begins to act more nonspecifically and affects the other outward currents as well. Figure III-14 shows the development of 4-AP blockade of I_A. The membrane currents shown were recorded in saline containing 1 μM TTX, but no TEA. The membrane voltage was stepped from a prepulse value of -90 mV to -10 mV to activate I_A. In this saline, most of the early outward current is I_A, while the small, later 'plateau' is a combination of I_K, $I_{K(Ca)}$, and leakage. In the experiment shown, during the first 3 minutes 4-AP blocked mostly the early outward I_A, but during the next 12 to 15 minutes most of the late outward plateau was also blocked. Twenty minutes after 1 mM 4-AP application 72% of the control I_A and 64% of the later outward currents measured at -10 mV are blocked. The outward current which remains is rapidly activating, and transient. Part of the 4-AP effect on I_A could be reversed relatively rapidly (within 5 to 10 minutes) by washing with normal saline, but full drug reversal was never observed.

Usually 4-AP is considered to be a relatively specific blocker of I_A (*e.g.* Thompson, 1977; Adams *et. al.*, 1980). The time course of block suggested that 4-AP may act either externally, or at a lower internal concentration to block I_A, and that as it permeates the membrane and its internal concentration increases, other current components are affected. 4-AP is lipid soluble and hence membrane permeant (Hille, 1984). In some cells 1 mM 4-AP was observed to inhibit inward currents, and alter their voltage dependence, but this effect took more than 15 minutes to develop. It is possible that the non-specific 4-AP effects result from an action on the inner side of the membrane, because the external

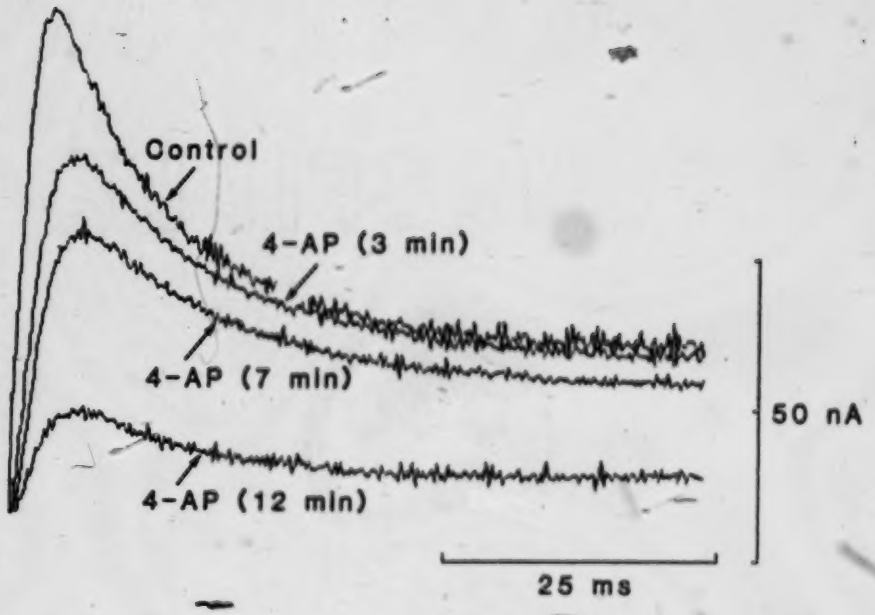

Figure III-14. Effect of 1 mM 4-AP on I_A. The control record was obtained in normal saline containing 1 μM TTX, for a voltage step from -90 mV to -10 mV. In this saline, the peak outward current is predominantly I_A, while the later outward plateau is I_K. The same voltage step was used repetitively to follow the time course of block by 1 mM 4-AP. The test steps are shown for 3, 7, and 12 min after bath application of the 4-AP. During the first 3 min I_A was blocked fairly selectively, but at later times the outward current plateau of I_K was also blocked. A transient current remains at 12 min, by which time the effect had stabilized, which is presumably unblocked I_A.

concentration would be expected to stabilize rapidly after 4-AP bath application (in less than 1 minute).

The fraction of I_A blocked by 4-AP and that blocked by Ca^{2+} replacement (Mn^{2+}) may be distinct, although this was only tested directly in one cell. In that experiment, the stabilized effect (20 minutes) of 1 mM 4-AP was a 69% reduction in I_A measured at -10 mV. Perfusion with saline containing 1 mM 4-AP and Mn^{2+} replacing Ca^{2+} further reduced the peak I_A so that 88% of the control I_A was blocked. This provides some evidence that the Ca^{2+}-dependent I_A fraction may be less 4-AP sensitive than the strictly voltage-dependent fraction. The effects of 4-AP on other I_A parameters were not investigated in detail, but 4-AP did not appear to significantly alter b_∞, τ_a or τ_b.

Verapamil

In a few earlier experiments designed to study the Ca^{2+}-dependence of I_A the organic Ca^{2+} antagonist verapamil was used to eliminate voltage dependent Ca^{2+} influx. The results of these experiments were very intriguing. In all cases (n = 7) verapamil blocked I_A, and at increased concentrations, I_K also. The same effect was also observed in Ca^{2+}-free (Co^{2+}) saline, ruling out the possibility of an indirect response through a block of I_{Ca}. Applied externally, at 100 μM verapamil blocked up to 50% of the outward current. This is the same verapamil concentration as is commonly used to block I_{Ca} in other studies (*e.g.* Junge, 1985; Feldova *et. al.*, 1985). In two cells where higher concentrations (500 μM) were tested, the peak I_A was reduced within 1 min, and both I_A and I_K were almost totally eliminated.

The main effect of verapamil on I_A appeared to be a substantial decrease (about 5 to 15 fold) in τ_b. As the block develops the inactivation becomes so rapid that the peak current is reduced. The verapamil block of I_A, which was previously isolated in 1 μM TTX and 50 mM TEA, is shown in Figure III-15 . In this experiment, verapamil was used at 100 μM. The left panel shows superimposed clamp steps for -40 to +10 mV in 10 mV increments, from -90 mV. I_A is quite large and relatively slow in the control (1 μM TTX, 50 mM TEA) saline. The right panel shows the same cell 9 minutes after the application of

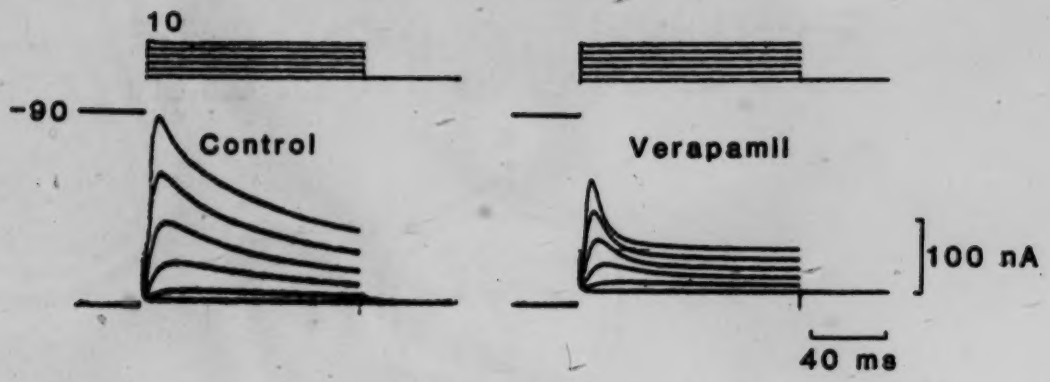

Figure III-15. Effect of 100 μM verapamil on I_A. In the control saline, containing 1 μM TTX and 50 mM TEA, the I_A is very large and slow in this cell. Bath application of 100 μM verapamil markedly reduced the peak I_A, and modified the rate of inactivation. The effect is voltage dependent, and is more prominent at depolarized test voltages. The verapamil record was taken at 9 min after application, and the effect appeared to have stabilized at this time. The rapidly decaying I_A which remained after verapamil treatment was reversibly blocked by 1 mM 4-AP (data not shown), suggesting that these two pharmacological agents act at distinct sites on the I_A channel.

verapamil. At +10 mV the peak I_A is reduced from 295 nA to 195 nA, a 34% reduction. Most striking though is the pronounced effect of verapamil on the rate of inactivation, τ_b is markedly reduced, particularly at more depolarized clamp steps. There did not seem to be any effect on τ_a, g_A, or $I_A V_{rev}$. Thus, verapamil acts as a powerful, relatively specific modulator of inactivation. Quantitative data describing the effects of verapamil are still being analyzed.

Forskolin

Forskolin, a diterpine activator of the adenylate cyclase system (Seamon *et. al.*, 1981) has recently been reported to alter inactivation kinetics of I_A in *Aplysia* bag cells (Strong, 1984). I also found that bath applied forskolin (100 μM) markedly accelerated the inactivation kinetics of I_A in barnacle neurons. In four cells tested, τ_b was decreased measurably within 5 minutes of forskolin application, although the effect continued to develop more fully over the following 15 to 20 minutes. In the example shown in Figure III-16 three records are superimposed for control I_A (in 50 mM TEA) and 100 μM forskolin (5 and 12 minutes). The depolarizing voltage step was to 0 mV from a -90 mV prepulse in both cases. The peak control I_A of was reduced by 55% after 12 min in the presence of 100 μM forskolin. In forskolin the rate of activation was not markedly altered (control τ_a = 1.6 ms, forskolin τ_a = 1.7 ms), but inactivation was much faster (control τ_b = 24.4 ms, forskolin τ_b = 9.8 ms), so that the peak I_A occurred earlier (control = 6.5 ms, forskolin = 5.5 ms). The record for 5 min in forskolin shows a component of both the initial control τ_b and the faster modified τ_b produced by forskolin. Once the forskolin effect had reached a steady-state the falling phase of I_A was fairly well described as a single exponential using just the faster time constant.

The modification of inactivation kinetics by forskolin is quite specific, and only reduces $\bar{g}_A$ by 8% (Figure III-17). The modification of τ_b kinetics appears to be voltage independent because τ_b is reduced from the control by a similar amount at all voltages. Activation kinetics, measured as τ_a were unaffected over the range of V_M examined, τ_a never varied by more than 10% between the control and forskolin data (results not shown).

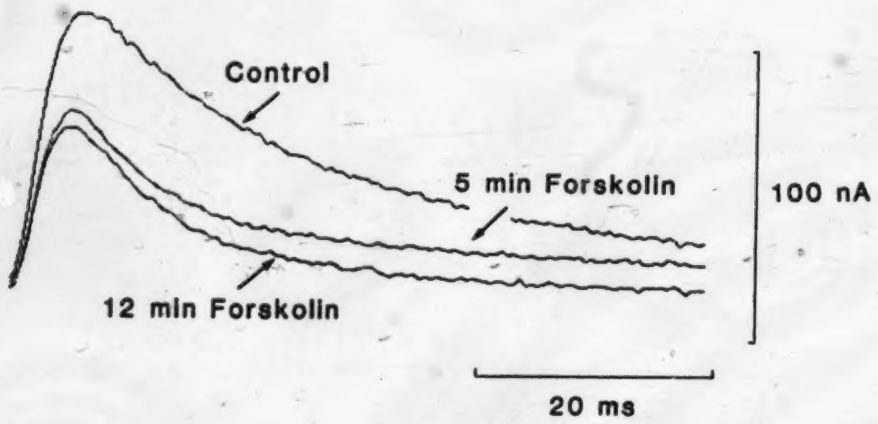

Figure III-16. Effect of 100 μM forskolin on I_A. Bath applied forskolin partially blocks I_A and modifies inactivation kinetics. The control I_A record was obtained for a -90 to 0 mV step in 1 μM TTX, 50 mM TEA saline. Forskolin rapidly reduced the peak I_A during the first 5 min following application, and the effect had stabilized at 12 min. The major effect of forskolin was to reduce the peak I_A from 98.6 nA (at 6.5 ms) to 56.0 nA (at 5.5 ms), and this appeared to be a direct effect of an acceleration of the inactivation kinetics. In the control, τ_a = 1.6 ms, τ_b = 24.4 ms, and at 12 min in forskolin, τ_a = 1.7 ms, τ_b = 9.8 ms. Kinetically, the modification of inactivation appears to be fairly specific, and activation is relatively unaffected. I_A was first isolated in 1 μM TTX, 50 mM TEA saline. Refer to Figure III-17 for further effects of forskolin. The records omitted the first 1 ms of data during the capacitative transient. Analog to digital sample interval = 500 ms.

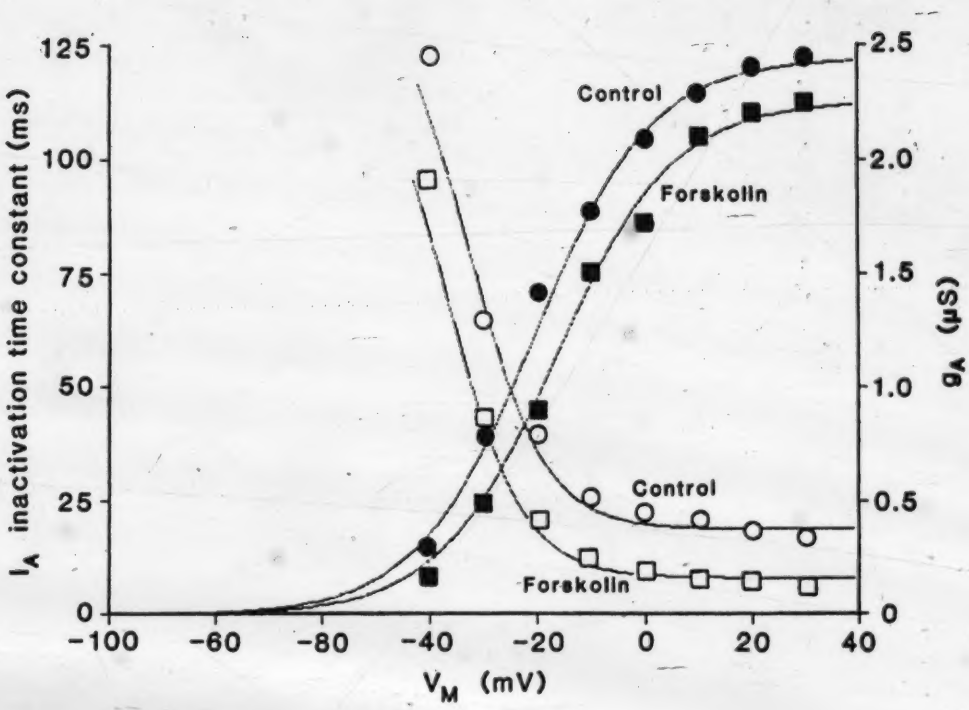

Figure III-17. Effect of forskolin on the voltage dependence of τ_b and $\hat{g}_A$. τ_b (open symbols) and g_A (filled symbols) were measured as a function of V_M for for a cell bathed in control and 100 μM forskolin saline. Over the -40 to +30 mV range forskolin reduces τ_b (open squares) in a manner which appears to be voltage independent. The curve fitted to the control τ_b measures (open circles) also fits the forskolin data reasonably well by assuming a voltage independent 12 ms decrease in τ_b and a -4 mV shift in the τ_b voltage dependence. Forskolin has relatively little effect on g_A compared to the reduction in peak I_A. The control curve (filled circles) is the best fit to the Boltzmann distribution, assuming $V_{1/2}$ = -20 mV, z = 2.2 and $\hat{g}_A$ = 2.44 μS. The fit to the forskolin data was obtained by constraining z to equal 2.2, the other parameters are then $V_{1/2}$ = -16 and $\hat{g}_A$ = 2.25 μS. Thus, $\hat{g}_A$ is only reduced by 8% even though τ_b is reduced by up to 65% (at +30 mV). Note that $g_{A,peak}$ would be reduced much more than $\hat{g}_A$ at any voltage because of the decrease in τ_b.

Similarly, in one cell where it was approximately evaluated there did not appear to be any change in b_∞. Therefore, it seems likely that the major effect of forskolin on I_A is a simple voltage-independent reduction of τ_b.

At the outset of the experiments using forskolin, I assumed that forskolin modified I_A by a specific action associated with increased levels of intracellular cAMP (*i.e.* protein phosphorylation). However, I observed that the forskolin effect was not potentiated by the bath addition of IBMX, a specific phosphodiesterase inhibitor. Nor could IBMX alone produce a similar action on τ_b as was seen with forskolin. This phenomenon needs to be examined further to determine if the actions of forskolin are partially independent of intracellular cAMP. The use of membrane permeable cAMP analogs, or the injection of cAMP itself may answer this question.

The effects of forskolin and verapamil were quite similar in terms of time course and in that both produced a reduction of τ_b. It was of interest to know if the effects were cumulative, or if once modified to the faster time constant no further modification could occur. This was analyzed in one cell, which was initially treated with 100 μM forskolin, and showed a large reduction in τ_b and peak I_A (from 129 to 71 nA) . After 15 minutes the forskolin effect had fully stabilized, and 100 μM verapamil was added. This further decreased τ_b and peak I_A very rapidly, so that 4 min after the addition of verapamil the peak I_A was only 20 nA. The effect of verapamil differed from the action of forskolin in that the modification of τ_b was not as specific; g_A was also reduced. This result suggests that these two agents act at independently to alter inactivation, by different mechanisms, although the result is quite similar. The rapid onset of the verapamil effect suggests an external site of action, although this can not be determined with certainty in these experiments.

DISCUSSION

The present study has provided a description of the transient K^+ current, I_A in barnacle neurons. The major new findings are: 1) The voltage dependence of steady-state activation and inactivation show considerable overlap; therefore, there is a range of V_M

where I_A is activated tonically. 2) About 20 to 40% of I_A channels are available for activation at the resting membrane potential. 3) The activation and inactivation time constants are steep, bell-shaped functions of V_M, with maxima at -40 mV. 4) A fraction of I_A is significantly reduced by treatments which decrease Ca^{2+} influx. This was observed for replacement of Ca^{2+} with Co^{2+}, and for a decrease of the external Ca^{2+} concentration. 5) Two pharmacological agents, verapamil and forskolin, alter the inactivation kinetics of I_A in a relatively specific manner. Each of these findings is discussed in detail below.

Voltage dependence and kinetics

Following hyperpolarizing prepulses to remove steady-state inactivation, I_A in barnacle neurons reaches a transient peak, prior to a complete exponential decay phase. I_A begins to be activated significantly by depolarizing pulses to membrane voltages of -40 mV or greater. Over the -40 to -10 mV range, I_A is the predominant outward current because little I_K is activated below about -10 mV. Even in the absence of hyperpolarizing voltage commands, I_A can contribute to the membrane current recorded in this voltage range because some inactivation is removed at resting membrane voltages. For voltage commands to -40 mV, following a conditioning prepulse to -90 mV, the peak I_A averages about 10 nA (at 29 ms), and this increases to an average of 76 nA (at 7 ms) for steps to -10 mV.

The conductance underlying I_A is on average, one-half activated at -19 mV, and inactivation is one-half removed at -53 mV. The conductance tends toward saturation at about +30 mV, and the probability of activation is well fitted by a Boltzmann distribution for voltage dependent gating, assuming an effective valence of 2.0 for the voltage sensing particle (*e.g.* Ehrenstien *et. al.*, 1974). I_A activation was best described as an exponential function raised to the 6th power. Using a^4 produced the best fit to the initial current lag and peak current for values tested between 2 and 6. Most kinetic studies of I_A have simply used a value of a^3 to approximate activation, based on the similarity to squid axon m^3h kinetics (Neher, 1971; Connor *et. al.*, 1977; Byrne, 1980b; Quinta-Ferreira, 1982), although Connor and Stevens (1971c) used a^4 to describe activation in nudibranch neurons.

At normal resting membrane potentials (-50 to -40 mV) $b_\infty \simeq 0.2$ to 0.4, thus between 20 and 40% of I_A channels would be available for activation by a depolarizing stimulus. At the same range of V_M $a_\infty^4 \simeq 0.02$ to 0.1, and about 2 to 10% of channels available would be activated. Therefore, some 1 to 2% of I_A channels will be in a conducting state at the resting potential. Assuming the observed mean maximal conductance for I_A ($\bar{g}_A = 2.49$ μS) the resting g_A would be about 0.03 to 0.05 μS. The input resistance of these neurons at the resting potential averages about 6 MΩ, or equivalently, the input conductance is about 0.17 μS. Thus, the resting conductance for I_A can be calculated to be roughly 20 to 30% of the resting membrane conductance.

The presence of a standing g_A at resting potential is likely to have several effects on excitability. Firstly, the high resting K^+ conductance would move the resting potential to a value closer to E_K. Also, the standing g_A may stabilize small perturbations of the membrane voltage (*i.e.* synaptic potentials). Excitatory potentials would tend to be shunted because of the accompanying resistance decrease that will follow any depolarization, coupled with the hyperpolarizing effect of a potentiated g_A. Inhibitory potentials would smoothed out because the resulting hyperpolarization would reduce the activation of g_A which would result in membrane depolarization.

A similar situation exists in crab walking leg axons, where there is a large overlap of a_∞ and b_∞ curves, and b_∞ is about 0.3 at rest (Connor, 1975; Connor *et. al.*, 1977). The resting potential lies in the region of a_∞-b_∞ overlap, and it has been suggested that a steady I_A contributes to the resting potential in these axons. Interestingly, only the axons capable of sustained repetitive firing show the predominance of I_A. Other crab axons, which do not exhibit sustained repetitive firing, show proportionately much less I_A (Connor, 1975).

In other studies of neuronal somata there is less standing I_A at resting potentials. In most molluscan neurons the value of b_∞ is very small at rest (<0.05), although a_∞ can be quite large (Connor and Stevens, 1971b; Neher, 1971; Thompson, 1977). Thus, very little I_A would be activated at resting potentials. The motor neurons responsible for controlling inking in *Aplysia* seem to be an exception. Because of their very deep resting potentials (≃

-70 mV) b_∞ is close to 1. However, I_A is not activated at this voltage and only contributes if the membrane is depolarized from rest (Byrne, 1980a, b). Those vertebrate neurons which have been investigated have relatively large values of b_∞ at resting potential ($\simeq$ 0.2 in mouse spinal neurons, Segal *et. al.*, 1984; $\simeq$ 0.5 in rat sympathetic neurons, Belluzi *et. al.*, 1985; $\simeq$ 0.5 in guinea pig hippocampal neurons, Zibcz and Weight, 1985). None of these studies puts their activation data in a form suitable for comparison, but it appears that little g_A is activated at rest in these neurons. A recent patch clamp study on rat nodose ganglion neurons (Cooper and Shrier, 1985) states that I_A was "largely inactivated" at the resting potential, making it difficult to establish whether there were openings at rest or not.

In barnacle neurons τ_a and τ_b are steep, bell shaped functions of V_M. Similar voltage-dependent time constants have been reported for several other preparations (Neher, 1971; τ_b only Connor *et. al.*, 1977; Byrne, 1980b; Belluzi *et. al.*, 1985). However, for some molluscan neurons (Connor and Stevens, 1971c; Thompson, 1977) and cultured mouse hippocampal and spinal neurons (Segal *et. al.*, 1984) the time constants are independent of voltage. Thus, there appears to be two distinct kinetic profiles for the systems that have been studied. The modelling study of Connor and Stevens (1971c) is based on I_A time constants which are both very slow, and voltage independent (τ_a = 12 ms, τ_b = 235 ms, study at 5 °C). This differs radically from the situation observed in barnacle neurons (τ_a = 6.4 ms at -40 mV to 1.7 ms at -10 mV, τ_b = 311 ms at -40 mV to 24.2 ms at -10 mV). In retrospect, it seems likely that Connor and Stevens' finding that I_A is most important during slower membrane phenomena, such as the interspike interval, is a function of the type of I_A studied, and not necessarily a general property of I_A. Presence of voltage-dependent time constants, as described in this study could mean that I_A can respond slowly at sub-threshold voltages, but also respond very rapidly at more depolarized voltages. This behavior could significantly alter the functional role of I_A.

In relative terms, τ_a in barnacle neurons decreases four-fold over a 30 mV depolarization where the voltage-dependence is the steepest (-40 to -10 mV). This is very similar to the relative change of τ_a, for *Helix* neurons, of about four-fold over 30 mV (Neher, 1971, Figure 8). In *Aplysia* neurons, τ_a changes about three-fold over the same

voltage range (Byrne, 1980b, Figure 5B). It is however, τ_b which is most steeply voltage-dependent in barnacle neurons, decreasing about thirteen-fold over the -40 to -10 mV range. The relative change is much greater than for *Helix* neurons (four-fold) or *Aplysia* neurons (three-fold). The curve for the voltage-dependence of τ_b in rat sympathetic neurons is more comparable to barnacle values (τ_b decreases ten-fold over -70 to -40 mV; Belluzi *et. al.*, 1985). The functional importance of τ_a and τ_b voltage-dependence can probably be evaluated by description in a kinetic model. Intuitively, it seems that the speeding up of I_A kinetics with depolarization may give rise to a situation where I_A activation contributes to action potential repolarization. Since τ_b is quite rapid when V_M is depolarized this may allow rapid recovery from inactivation, and I_A could contribute to spike repolarization, even at relatively high frequencies of repetitive firing.

Calcium sensitivity

In many barnacle neurons, replacement of the external Ca^{2+} by Co^{2+} or Mn^{2+}, or alteration of the Ca^{2+} concentration, reduces the peak and I_A, and correspondingly, the $g_{A,peak}$ elicited by depolarizing voltage commands. There are at least three mechanisms by which this reduction could occur. The first two could be considered indirect effects of the experimental protocol; shifts in the membrane outer surface potential may alter the voltage dependence, or divalent cations could bind non-specifically in some manner to the I_A gating system, altering the voltage dependence of gating. Alternatively, a rapidly activating fraction of the conductance underlying I_A may require Ca^{2+} as a ligand during activation, and removal of the ligand leaves only a slower voltage dependent fraction. Initially, I will assume that these mechanisms are independent and separable.

Frankenhaeuser and Hodgkin (1957) initially suggested that Ca^{2+} may accumulate at the membrane outer surface, drawn to fixed negative charges (possibly phospholipid head groups). The hypothesis was formulated to explain their observations that a five-fold reduction in external Ca^{2+} was roughly equivalent to a depolarizing bias of 10 to 15 mV added to V_M. It was postulated the Ca^{2+} was adsorbed to the outer surface of the membrane, and could add to the electric field provided by V_M. Experimental manipulation

of the external Ca^{2+} level could then be expected to alter the net surface charge sensed by the gating apparatus of a voltage-dependent transmembrane channel. There seems to be little question that fixed negative surface charges do exist, and that ionizable surface groups contribute to the total charge (see discussion by Hille, 1984). The data presented here show that Co^{2+} and Mn^{2+} shift the b_∞ curve (and probably the surface potential) by differing amounts (mean = +9 mV for Co^{2+}, +5 mV for Mn^{2+}). For a surface charge model with no binding, just simple screening by charge proximity, all divalents should produce equivalent shifts (assuming they get equally close to the membrane). Therefore, it is probable that Co^{2+} and Mn^{2+} bind to sites at the membrane surface, and that the binding affinity for Co^{2+} is larger. Whether one considers a surface screening or surface binding model of fixed surface charge, the prediction would be similar; alteration of the net surface potential should be indistinguishable from pure shifts of V_M.

The data presented for barnacle neurons bathed in Ca^{2+}-free (Co^{2+}) saline show that $g_{A,peak}$, τ_a, b_∞, and τ_b are all 'shifted' unequally and in a complex manner. In addition, I_A parameters are shifted more than I_K parameters. Thus, the data rule out any simple surface potential effect as underlying the parameter alterations. However, it is well documented that heavy metal ions can affect channel gating in this type of complex manner. Ni^{2+}, Cu^{2+}, and Zn^{2+} have been shown to slow activation and inactivation kinetics in addition to a voltage shift effect (Dodge, 1961; Hille, 1968; Arhem, 1980). In lobster axons, Blaustien and Goldman (1968) have shown that replacement of Ca^{2+} with Co^{2+} shifts g_{Na} +9 mV, while g_K is shifted +17 mV in the same medium. Some heavy metal ions (*e.g.* Ln^{3+}, Zn^{2+}) are known to reduce g_{Na} in addition to producing a positive shift along the voltage axis (Takata *et. al.*, 1966; Blaustien and Goldman, 1968; Brismar, 1980). Gilly and Armstrong (1982a) have shown that in squid axons, Na^+ channel activation (and on gating current) is slowed in the presence of external Zn^{2+}, but that channel deactivation (and off gating current) is unaffected. As originally shown by Frankenhaeuser and Hodgkin (1957), Ca^{2+} itself can have a number of similar effects on gating parameters if the external concentration is changed. Recently, Armstrong and Matheson (1986) have demonstrated that increasing the external Ca^{2+} concentration alters I_K on gating kinetics more than off gating kinetics in

squid axons. The most plausible hypothesis which explains many of the observations is that divalent cations are bound to a negatively charged part of the gating apparatus, at a point near the channel opening. The binding probably occurs while the channel is closed (for a detailed discussion see Gilly and Armstrong, 1982a; Armstrong and Matheson, 1986). In this type of model, the kinetics of one channel type (or one gating parameter) are open to modification without the assumption of a uniform effect on all channel types (or all gating functions).

The implication of the above discussion is that divalent cations, and in particular metal cations, influence channel gating and slow activation kinetics in most preparations examined. Therefore, one cannot justifiably reach the conclusion that the barnacle I_A is Ca^{2+}-dependent on the basis of the reduced conductance or slowed kinetics in Ca^{2+}-free (Co^{2+}or Mn^{2+}) saline alone. Other factors could produce this effect. I ruled out the possibility that alterations of kinetics *per se* give rise to the reduced $g_{A,peak}$ (Figure III-11). In addition, raising the external Ca^{2+} concentration by 50% produced voltage shifts which were similar to those produced by replacing Ca^{2+} with Co^{2+}, but this treatment did not markedly reduce $g_{A,peak}$ (Figure III-12). A number of studies have found that equimolar replacement of Ca^{2+} with other divalent cations has the same effect on gating parameters as raising the external Ca^{2+} concentration (*e.g.* Arhem, 1980). The fact that barnacle I_A is more reduced under conditions which produce depolarizing voltage shifts *and* block voltage dependent Ca^{2+} influx (*i.e.* Co^{2+} replacement) suggests a true Ca^{2+}-dependent component to I_A.. In line with this hypothesis, experiments in which the external Ca^{2+} concentration was reduced, shifted voltage dependent parameters towards more negative values of V_M, and yet these treatments still reduce the peak g_A. These conditions would be expected to increase the conductance measured at non-maximally activating voltage steps for Ca^{2+}-independent gating parameters (*e.g.* Frankenhaeuser and Hodgkin, 1957). The reduction of I_A is most prominent over the voltage range where I_{Ca} could be expected to be significantly activated. Therefore, I conclude that the I_A in these neurons is, in part, dependent on Ca^{2+} influx from the external medium for activation.

In this study no marked pharmacological difference, other than the Ca^{2+}-dependency, allowed separation of the early transient components. Both components are insensitive to 50 mM TEA, and are partially blocked by 1 mM 4-AP (the Ca^{2+}-dependent fraction may be slightly less 4-AP sensitive). The Ca^{2+}-dependent I_A present in vertebrate neurons is said to be TEA sensitive, and unaffected by 4-AP (MacDermott and Weight, 1982; Zibcz and Weight, 1985). Similarly, the Ca^{2+}-dependent I_A seen in sheep Purkinje fibres (Corabeouf and Carmeliet, 1982) and *Drosophila* muscle (Salkoff, 1983) also appears to be insensitive to 4-AP. It is possible that at a lower concentration of 4-AP than was used here (< 1 mM), a difference in 4-AP sensitivity exists for the two I_A fractions in barnacle neurons.

It is difficult to accurately measure the kinetics of the Ca^{2+}-dependent fraction of I_A. Digital subtraction of control and Ca^{2+}-free (Co^{2+}) records (Figure III-7) probably provides incorrect measures of the amplitude and time course because the subtraction records are contaminated in two ways. First, a small inward I_{Ca} is blocked whenever Ca^{2+} influx is eliminated, and this will tend to cause an underestimate of the amplitude of the Ca^{2+}-dependent outward current. Second, alterations in the kinetics of any remaining I_A must occur when the divalent cation level is altered, and this could lead to an incorrect kinetic picture of the current obtained by subtraction. For example, a slowing of activation kinetics, produced by the experimental protocol, would appear as a rapid transient outward current in the subtraction record. Curiously, studies which report a Ca^{2+}-dependent I_A using subtraction, also find that the Ca^{2+}-dependent fraction is very rapid and transient, activating faster than the Ca^{2+}-independent fraction (MacDermott and Weight, 1982; Zibcz and Weight, 1985).

It may be possible to obtain more detailed kinetic measurements of the Ca^{2+}-dependent and independent components by pursuing a detailed study of the deactivation tail current kinetics. I_A tail currents could not be measured accurately because they were too rapid and small at the temperature (12 °C) and external K^+ concentration (8 mM) used in this study. Cooling the preparation, and raising the K^+ concentration may be a practical way to study 'inverted' tail currents. Even under those conditions it would be difficult to make accurate kinetic statements because the same external surface potential effects would

be present. Single channel recording from inside-out I_A patches would allow control of the intracellular Ca^{2+} level directly, and may be a more practical alternative for the study of I_A Ca^{2+}-dependence. In one study where this has been done (Kasai *et. al.*, 1986), I_A channel opening was found to be independent of the cytoplasmic Ca^{2+} concentration.

In summary, replacement of the external Ca^{2+} with Co^{2+} or Mn^{2+} has pronounced effects on the voltage dependence, kinetics, and conductance underlying I_A. These effects are not seen to the same degree for I_K, although a small shift in voltage dependence and slowing of kinetics has been observed. Therefore, of the major outward currents present in these neurons, Ca^{2+} replacement can be expected alter only the early I_A and the later activating $I_{K(Ca)}$. The effects of external Ca^{2+} replacement, studied under current clamp conditions should help to elucidate the physiological role of both I_A and $I_{K(Ca)}$ in these neurons.

Pharmacologieal sensitivity

The pharmacological block of I_A by 4-AP is unusual in that membrane currents other than I_A are also reduced. During the initial few minutes following 1 mM 4-AP application I_A seems to be blocked selectively, but later the effect is less specific. In several axons 4-AP blocks the delayed rectifier, I_K (*e.g.* Pelhate and Pichon, 1974; Quinta-Ferreira *et. al.*, 1982), and it may be that the barnacle I_K channels bear some structural similarity to axonal channels, since I_K is also partially blocked by 4-AP. In the majority of neurons 4-AP blocks I_A highly specifically (Thompson, 1977; Rogawski, 1985; but see also Hermann and Gorman, 1981). However, Mirolli (1981) has shown that 4-AP blocks early and late outward currents with equal sensitivity in crustacean stretch receptor dendrites, suggesting a similarity amongst crustacean neurons. Recently, Belluzi *et. al.* (1985) report that I_A in rat sympathetic neurons is only weakly inhibited by 4-AP, although in several other closely related mammals 4-AP does block I_A (Segal *et. al.*, 1984; Zibcz and Weight, 1985). Thus, for mammals there appear to be inter-species differences in I_A pharmacological sensitivity. Therefore, 4-AP should be used cautiously until the appropriate voltage-clamp studies have been carried out.

The large acceleration of inactivation kinetics produced by verapamil and forskolin are intriguing. The effect by verapamil is interesting because it is usually considered to be a relatively specific inhibitor of I_{Ca} channels. A previous report does briefly mention an acceleration of outward current kinetics, in a discussion of the pharmacology of I_K in *Helix* neurons (Kostyuk *et. al.*, 1976). There are numerous studies which show that "Ca^{2+} channel" functions are altered by external verapamil application. These range from simple block of isolated I_{Ca} at 100 μM (*e.g.* Akaike *et. al.*, 1981; Brown and Griffith, 1983) to clinical cancer chemotherapy studies where verapamil is applied intravenously and assumed to limit Ca^{2+} influx to tumors (Simpson, 1985). Only the kinetic results obtained for forskolin will be discussed because the verapamil results are preliminary.

Forskolin is thought to be a fairly specific activator of the adenylate cyclase system (Seamon *et. al.*, 1981), resulting in an increase of intracellular adenosine 3':5'-monophosphate (cAMP). Recently, Strong (1984) showed that externally applied forskolin reversibly speeds up I_A inactivation kinetics in *Aplysia* bag cells. In that study the effect of I_A was primarily a reduction of the I_A decay time constant with a reduction of τ_b of up to 5 fold. There was no effect on b_∞ or time to 1/2 peak ($\simeq \tau_a$), and in these respects the results were similar to my findings. Strong found evidence that a fraction of I_A channels (19 to 34%) did not have their time constant modified by forskolin, and retained the control τ_b. I have not studied this aspect of the influence of forskolin, but the stabilized forskolin τ_b data were well fitted as a single exponential in most cases. The time course of development is rather different in barnacle neurons, with most of the modification occurring during the first 5 minutes (Figure III-16). In *Aplysia* bag cells there is a distinct delay (lasting 5 to 10 minutes) before the modification begins. Since both studies were done at similar temperatures, and forskolin has to permeate the membrane to modify I_A channels, as seems likely, then it would appear that barnacle neurons are more permeable than *Aplysia* neurons.

It is important to know whether the effect of forskolin results from a rise in intracellular cAMP levels, or is some direct effect by forskolin. Strong (1984) found that forskolin, theophylline, and R020-1274, all of which are known to elevate cAMP levels, had

similar effects on I_A. In the same neurons, Kaczmarek and Strumwasser (1984) have shown that membrane permeant cAMP analogs cause an increase in the rate of decay of I_A. This provides strong evidence that in *Aplysia* bag cells cAMP is likely to be involved in the process leading to channel modification, and possibly in *in vivo* regulation of I_A. In preliminary experiments, I found that IBMX (applied at 500 μM to 5mM), a phosphodiesterase inhibitor, could not mimic the actions of forskolin. IBMX at these concentrations should elevate cAMP levels by limiting phosphodiesterase catalyzed conversion of cAMP to AMP. These results seem to be at odds with the findings of Strong (1984) and suggest that forskolin itself may act as a modulator of I_A channels. In dorid nudibranch neurons, external application of membrane permeable cAMP analogues or phosphodiesterase inhibitors, and intracellular injection of cAMP do not mimic the effect of forskolin (J. Coombs and S. H. Thompson, personal communication). The rapid appearance of modified I_A inactivation waveforms observed here, could mean that forskolin interacts directly with I_A channels, perhaps while permeating the membrane, rather than through a second messenger system. Thus, although it is apparent that forskolin modifies inactivation kinetics quite specifically in barnacle neurons, it is not clear whether this modification is cAMP dependent.

I was most interested in the modification of I_A by forskolin, not primarily because of an interest in second messenger systems, but rather for use as an experimental tool for studying I_A during repetitive action potential trains. With respect to I_A, the effect on τ_b is quite specific, and therefore, forskolin could be used to study the role of I_A inactivation during action potentials. The decay of I_A has been suggested to produce acceleration of the action potential frequency during long trains in crab axons (Connor *et. al.*, 1977), and to create long delays to the first action potential in *Aplysia* neurons (Byrne, 1980b). Forskolin application may provide a means to test these hypotheses, since, under certain conditions, barnacle neurons display both frequency acceleration, and long delays to the first action potential following the onset of depolarizing stimuli.

IV. REGULATION OF MEMBRANE EXCITABILITY BY THE FAST TRANSIENT POTASSIUM CURRENT

INTRODUCTION

The physiological roles of I_{Na} and I_K are understood to be simply the rapid depolarization and slower repolarization of individual action potentials. The physiological role of I_A is less well understood. Two approaches have been used to determine the role of I_A in excitability. The earlier studies evaluated the function of I_A by incorporating a description of I_A into a kinetic model similar to the Hodgkin-Huxley formulations (Connor and Stevens, 1971c; Connor *et. al.*, 1977; Byrne, 1980b). More recently attempts have been made to pharmacologically block I_A and evaluate the effect on current clamped action potentials (MacDermott and Weight, 1982; Segal *et. al.*, 1984).

Based on Hodgkin-Huxley type kinetic modelling it has become generally accepted that I_A has two major roles in repetitive firing. Connor and Stevens (1971c), and later Connor *et. al.* (1977) have shown that I_A serves to enable low frequency repetitive firing of action potentials by slowing depolarization during the interspike interval. Removal of I_A inactivation during the spike after-hyperpolarization is thought to increase I_A activation during the following interspike interval, adding a hyperpolarizing bias to the membrane potential at this time. In an extension of the kinetic model proposed by Connor and Stevens, Byrne (1980b) showed that I_A could create long delays in the response of *Aplysia* neurons to depolarizing input. For this to occur, the cell resting potential has to be deep enough to remove I_A inactivation. Depolarizing input would then be 'shunted' because extra time is needed to drive the cell to spike threshold against the hyperpolarizing effect of I_A.

Few studies have attempted to evaluate the role of I_A experimentally. The approach that must be used is to determine which pharmacological agents block I_A, as specifically as possible, under voltage clamp, and then analyze spike trains under current clamp using similar pharmacological manipulation. MacDermott and Weight (1982) reported that removal of Ca^{2+} from the bathing medium, or replacement with Mn^{2+}, blocks much of I_A

and slows repolarization of individual action potentials recorded in current clamp. However, Segal *et. al.* (1984) have shown that in hippocampal neurons, 4-aminopyridine blocks I_A in voltage clamp, and also alters excitability under current clamp, but by a different mechanism. They find that block of I_A reduces the threshold for single and repetitive action potentials, with no effect on the amplitude or duration of action potentials. Thus, the only two experimental studies to investigate the role of I_A appear to reach opposing conclusions.

This chapter examines the functional role of I_A in barnacle neurons. Experimentally, this is easiest to evaluate under conditions which either maximize or minimize the relative contribution of I_A during current clamped action potential trains. Changes in membrane excitability can then be ascribed to changes in I_A produced by the experimental protocol. In the previous chapter it was shown that I_A is increased following hyperpolarizing pre-pulses to remove inactivation, and decreased in Ca^{2+}-free saline, or in saline containing 4-AP or forskolin. These results will be used in this analysis of excitability in current clamped neurons.

METHODS

The methods used for two electrode current and voltage clamp of barnacle ventral ganglionic neurons were described previously (Chapter II), as was the preparation of control and experimental salines (Chapter III).

RESULTS

At resting membrane potentials (generally -50 to -40 mV) most barnacle ventral ganglionic neurons do not spontaneously produce action potentials. Action potential threshold is usually -35 to -25 mV and therefore a stimulus must be used to depolarize the membrane by about 5 to 25 mV to initiate an action potential. In the following experiments constant current stimuli (current clamp) were delivered as square pulses in order to elicit single action potentials or repetitive trains.

I generally use the following properties of the response of a neuron under current clamp to operationally define the membrane excitability. 1) Action potential threshold - the

membrane voltage at which a rapid increase in the slope trajectory indicates the onset of an all-or-none depolarizing action potential. This differs from threshold as measured by incrementally increasing depolarizing current steps, in that it is not as accurate, but can be obtained from a single current step. 2) Response time - the time from onset of a depolarizing stimulus to the threshold of the first action potential. This term is synonymous with 'utilization time', which appears in some of the older literature (*e.g.* Hodgkin, 1948). 3) Rate of rise of the action potential - the maximum slope obtained during the depolarization phase. This was usually in relative terms, *i.e.* compared between a control and treatment, rather than measured in absolute terms. 4) Action potential duration - measured at one-half maximum amplitude. 5) Magnitude of the after-hyperpolarization (AHP) - the hyperpolarization following the action potential, measured as the peak (negative) value attained. 6) Repetitive firing frequency - measured as 'instantaneous' frequency (reciprocal of the interspike interval). Not all types of measurements were made in any given experiment.

Effect of pre-stimulus voltage on membrane excitability

The previous chapters have provided evidence that membrane pre-hyperpolarization removes inactivation, and maximizes the expression of I_A. The equivalent experiment done under current clamp is to initiate action potential trains from various pre-stimulus values of V_M. The results from this type of experiment are shown in Figure IV-1. The resting potential of this cell was -50 mV after dual electrode penetration. A depolarizing or hyperpolarizing bias was added to the membrane in order to obtain membrane voltages of -40 and -60 mV for comparison to spike trains initiated from resting potential. A depolarizing current step to +4 nA for 5 seconds was given from each test voltage. The spike train initiated from -40 mV began rapidly with a very short response time (20 ms). The spike frequency was maximal between the first two spikes, and this decreased, or adapted to a lower frequency over the duration of the stimulus. The same depolarizing stimulus initiated from -50 or -60 mV elicited spike trains with a much increased response time. The increase in the response time was associated with a decrease in the early frequency of the spike train, so that the train accelerated during the maintained stimulus.

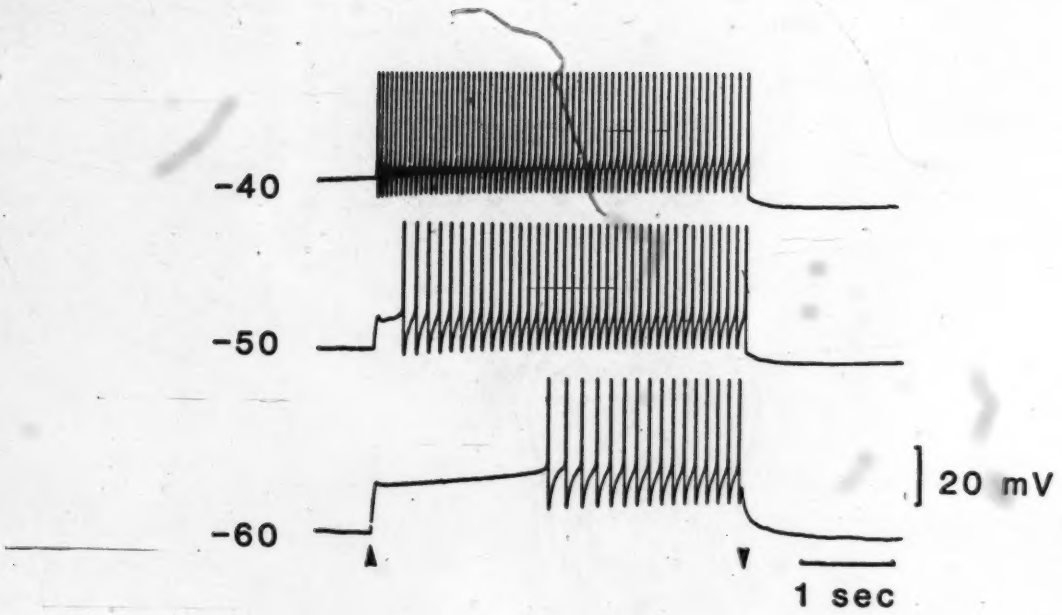

Figure IV-1. Effect of pre-stimulus voltage on action potential trains recorded in current clamp. The trains were elicited by a +4 nA (net value) , 5 second current pulse (on at up arrow), from pre-stimulus voltages of -40, -50 or -60 mV. The resting potential of this cell was -50 mV, the -40 and -60 mV pre-stimulus voltages were obtained by adding a depolarizing or hyperpolarizing current bias. From -40 mV, the first action potential was initiated rapidly, with a response time of 20 ms, and the frequency decelerated, or adapted during the stimulus. The same depolarizing stimulus, initiated from the resting potential, or -60 mV elicited a train which began after a longer delay, and accelerated during the stimulus. The longer response times (360 ms from -50 mV, 1.7 sec from -60 mV) were associated with a slow ramp depolarization prior to the initiation of the first action potential. The action potentials were attenuated by the pen recorder (frequency response DC to 60 Hz).

When the stimulus was initiated from more hyperpolarized membrane potentials, the early depolarization occurs in three phases. Initially, V_M rose rapidly to about -40 mV; at this voltage the rising trajectory was reversed, and V_M became slightly more negative, producing a small overshoot (most apparent for the -50 mV, pre-stimulus). Following this, a slow ramp depolarization, lasting up to several seconds, brings the cell to spike threshold. For the cell shown, this type of spike train was elicited from the resting potential of -50 mV. Therefore, this was probably a typical response of this cell to depolarizing input.

Modelling studies by Connor and Stevens (1971c) and Byrne (1980b) have shown that this type of slow ramp trajectory is associated with the activation and following inactivation of I_A. The experimental data from barnacle neurons are quite similar to those obtained in *Aplysia* ink motor neurons by Byrne, although two differences are also apparent. First, in barnacle neurons the AHP following the early spikes of a train was increased by prior hyperpolarization (refer to figure IV-1). Second, the action potential frequency accelerated during the train which follows the long ramp delay. Although not present in *Aplysia* neurons, this type of acceleration, or 'warming up' of spike trains has been reported in crustacean axons (Hodgkin, 1948; Chapman, 1966; Connor *et. al.*, 1977). The following experiments examined the hypothesis that the long response times and following spike train acceleration are due to changes in I_A.

The slow ramp depolarization was associated with a membrane conductance increase. For the cell shown in Figure IV-2, a hyperpolarizing pre-pulse to -68 mV, followed by a depolarizing stimulus produced a slow ramp depolarization lasting 1.4 seconds. The membrane conductance during the slow depolarizing phase was measured by small hyperpolarizing 'conductance testing' pulses. The resting membrane conductance of 0.14 μS was increased to 0.33 μS following the hyperpolarizing pre-pulse. The conductance increase appeared to be fully activated by the first test pulse during the slow ramp phase (at about 150 ms), and was activated at a membrane voltage of -45 to -40 mV. The conductance fell to near resting value by the time spike threshold was reached. Therefore, it appears that a rapidly activated conductance, followed by a slower decline, produces the long response time. When this conductance has fallen to a sufficiently low value, the increase in membrane

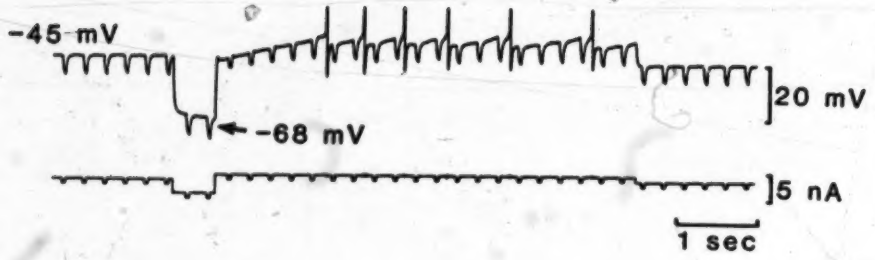

Figure IV-2. Membrane conductance increase during the slow ramp depolarization. The membrane conductance was measured by -1 nA, 50 ms current pulses. Following a hyperpolarizing pre-pulse to -68 mV (-2.5 nA, 500 ms) a depolarizing stimulus (+1 nA, 5 sec) was used to elicit a slow ramp depolarization and an action potential train. The resting membrane conductance of 0.14 μS was slightly decreased (to 0.12 μS) during the pre-pulse, and markedly increased during the early part of the ramp depolarization (to 0.33 μS). The membrane conductance fell slowly, to a value close to that observed at rest, just prior to the first action potential. The conductance increase was complete by the first test pulse after the depolarizing current step. The action potentials are clipped at about -25 mV, the full deflection was off scale at this voltage gain. Chart recording, frequency response DC to 60 Hz.

resistance enables the membrane potential to be driven to spike threshold by the depolarizing current stimulus.

A small, slowly declining net outward current was observed in experiments where voltage clamp was initiated during the slow ramp depolarization (Figure IV-3). Part A of Figure IV-3 shows the membrane voltage response to a depolarizing current stimulus (on at arrow) initiated from -70 mV. After 2 to 3 seconds the first action potential was elicited, and this was followed by an accelerating train. In part B, the electronic feedback was switched from current to voltage clamp, with the holding voltage preset to -40 mV. The switching process generated a rapid, transient artifact and this was followed by a slowly decaying outward current with a net amplitude of +2 to +3 nA. The same clamp protocol, but using a holding voltage of -65 mV, generated no measurable outward current (part C), suggesting that the driving force acting on the current was very small at this voltage. This value is near the experimentally measured current reversal potential for I_A in these cells (about -65 mV), and therefore, the small outward current is likely to be carried by I_A. Part D shows that the outward current recorded in voltage clamp during the slow ramp phase declined, and became negligible by the time of the onset of the first action potential. In part D the holding potential in voltage clamp was -45 mV, and this corresponded very closely to the value of V_M during the slow ramp. The outward current measured at this voltage had an amplitude of only +1.5 to +2 nA. It should be noted that the currents underlying the slow rise to spike threshold are very small in relation to the magnitude of ionic currents normally measured under voltage clamp with large instantaneous voltage steps. However, because the membrane conductance is normally quite low in this voltage range, even small membrane currents have pronounced effects on membrane voltage. These experiments do not rule out the possibility of inward current coactivation during the slow ramp depolarization, but do suggest that the magnitude of inward currents would be small since the net current was outward.

The response time of these neurons is dependent on the pre-stimulus voltage (as was shown in Figure IV-1). The voltage dependence of the response time is shown in Figure IV-4 (plotted as squares). The results from 6 cells (±SE) are pooled and normalized to the

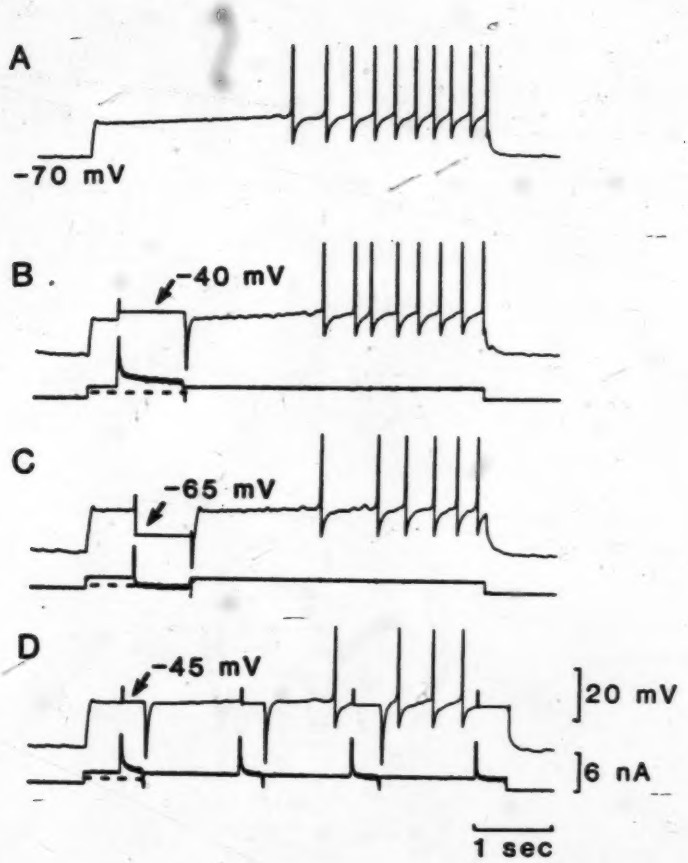

Figure IV-3. Outward current activated during the slow ramp depolarization. In this experiment, the feedback amplifiers were switched from current clamp to voltage clamp during the slow ramp depolarization. A: Control action potential train initiated by a +1.5 nA, 5 sec current pulse. A -1 nA current bias was added to produce the -70 mV pre-stimulus voltage. B: The feedback was switched to voltage clamp (preset at -40 mV) early in the ramp depolarization. The upper trace is membrane voltage, the lower stimulating current, or in voltage clamp, membrane current. The rapid peak in the current trace is a switching artifact, but was followed by a slowly declining outward current of +2 to +3 nA amplitude. C: The same protocol, but voltage clamping to -65 mV, elicited no outward current. The dashed line is 0 nA. D: The small transient outward current declined while the depolarizing stimulus was maintained. After the first action potential the current had declined to a value near that used to stimulate the action potential train (+1.5 nA). The action potentials were attenuated by the pen recorder (*frequency response DC to 60* Hz).

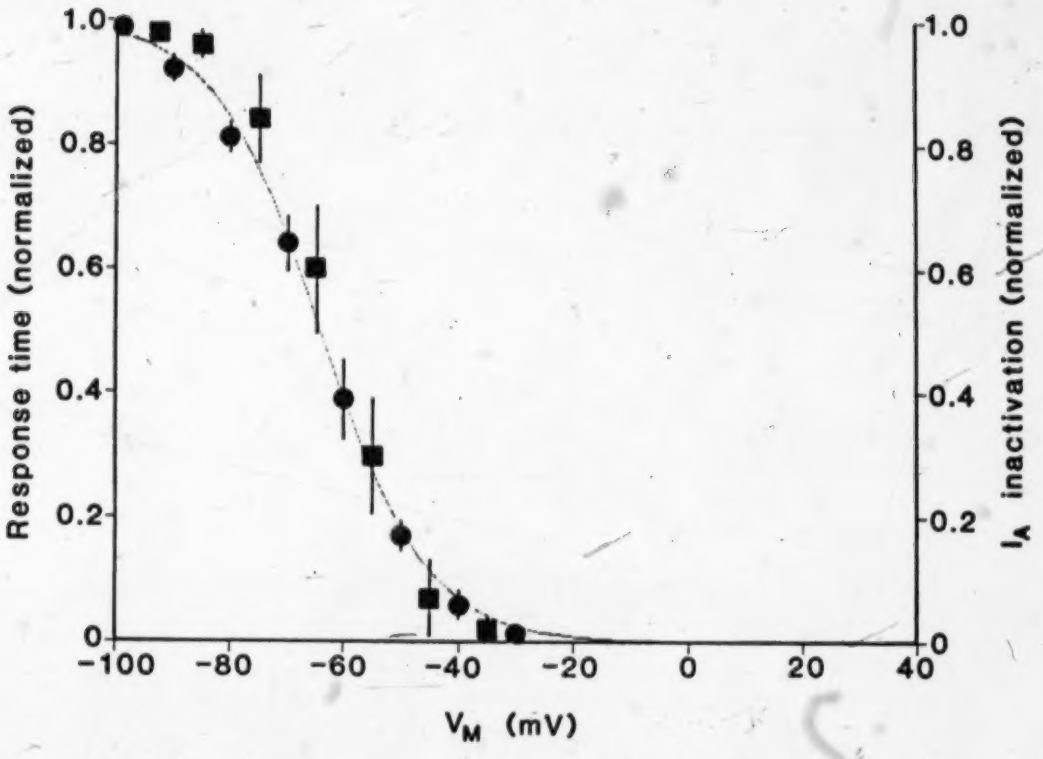

Figure IV-4. Dependence of the response time on the pre-stimulus membrane voltage. The neuronal response time measured under current clamp (squares) was plotted against the pre-stimulus value of V_M. The response time increased with prior hyperpolarization. The data are plotted for 6 cells, normalized to the longest response time (at -95 mV). In these experiments it was difficult to obtain the desired value of V_M since current was under control, and not voltage. For this reason, the data were pooled and plotted in 10 mV bins. For example, all results from cells at pre-pulse voltages of -90 to -100 mV were pooled and plotted at -95 mV. The actual response times at -90 to -100 mV ranged from 2.2 to 4.2 seconds. The circles and best fit curve show the removal of inactivation from I_A, for 7 cells in voltage clamp, using an activating voltage of -20 mV. The similar voltage dependence suggests that I_A controls the response time in these neurons.

maximal response time observed with large pre-hyperpolarizations. The increase in response time produced by prior membrane hyperpolarization saturates at -90 to -100 mV, and is one-half maximal at about -50 mV. Also plotted for comparison in the same figure are data describing the voltage dependence of I_A removal of inactivation (b_∞, plotted as circles) for 7 cells (±SE). The similar voltage dependence for the two phenomena strongly suggests that removal of steady-state inactivation from I_A underlies the slow ramp depolarization and long response times observed in many barnacle neurons.

The above results all support the hypothesis that I_A activation, following hyperpolarizing pre-pulses, produces the long response times observed in current clamp. The conductance increase has a threshold of about -45 mV, activates rapidly and declines slowly over several seconds. The current measured during the ramp phase of depolarization is outward, and is small at voltages near the reversal potential for I_A. In addition, the voltage dependence of removal of I_A inactivation essentially overlaps the voltage dependence of the response time recorded in current clamp.

The pre-stimulus voltage also had marked effects on the duration of action potentials produced during depolarizing current steps. Figure IV-5 shows action potentials generated from pre-stimulus voltages of -40 mV and -60 mV. For the train generated following a -40 mV (200 ms) pre-pulse, the first action potential was slightly larger in amplitude and longer in duration than the later action potentials. The same depolarizing stimulus following a -60 mV pre-pulse generated a train in which the first action potential was short, and the later action potentials progressively increased in duration. The AHP following the first action potential also reached a more negative voltage than those later in the train. After about the 6th action potential the duration had stabilized.

The decrease in action potential duration following pre-pulses to -60 mV could arise by several mechanisms. It is possible that an increase in I_{Na} inactivation rate causes more rapid repolarization. This seems unlikely because the largest change in duration occurs late in the repolarization phase, and would not be affected by I_{Na} inactivation. A second possibility would be that the -60 mV pre-pulse causes inactivation of I_{Ca}, decreasing the

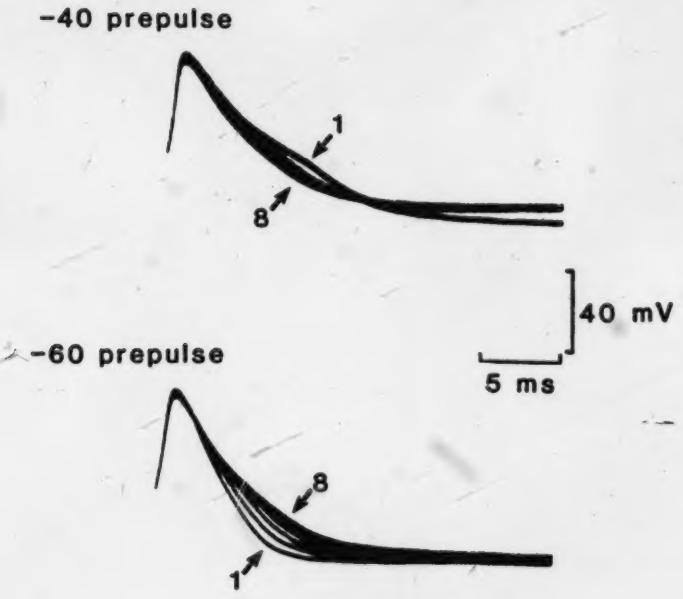

Figure IV-5. Effect of pre-pulse voltage on repolarization of the action potential. The first 8 action potentials generated by a +2 nA, 5 sec current pulse are superimposed. The upper record shows the action potentials which followed a 200 ms depolarizing current step, which yielded a pre-stimulus voltage of -40 mV. The first action potential of the train had the slowest repolarization (labelled 1). The following action potentials repolarized more rapidly. Following a 200 ms pre-pulse to -60 mV the first action potential repolarized most rapidly. The following action potentials repolarized more slowly than the first. Data photographed from a storage oscilloscope screen.

action potential duration. This also seems unlikely because in most neurons I_{Ca} is increased by prior hyperpolarization (*e.g.* Bruner *et. al.*, 1986). Thus it is most likely that an increase in I_K or I_A produces the change in duration, and this hypothesis is more consistent with an increase in the AHP following hyperpolarizing pre-pulses. In molluscan neurons, membrane pre-hyperpolarization is said to reduce action potential duration by removing inactivation from I_K (Ruben and Thompson, 1984). This mechanism seems unlikely for barnacle neurons for two reasons. Firstly, I_K amplitude is altered relatively little by pre-pulses to -60 mV. Secondly, short pre-pulses (50 to 200 ms) can produce near maximal narrowing of the following action potentials. The I_K inactivation time constant is usually greater than 1000 ms at -60 mV. However, the time constant for removal of I_A inactivation averages 61 ms at -90 mV and 311 ms at -40 mV, suggesting that substantial inactivation could be removed, even for relatively short hyperpolarizing pulses. In addition, the voltage dependence of I_A removal of inactivation is quite steep over the -40 to -60 mV range and this would tend to maximize the increase in I_A over this voltage range. So it appears that, under conditions where I_A would be expected to be augmented, action potential duration is reduced. These results suggest that, in barnacle neurons, I_A can contribute to action potential repolarization.

Effect of Ca^{2+}-free saline on membrane excitability

For neurons under current clamp the major effect of replacing the external Ca^{2+} with Co^{2+} or Mn^{2+} is an increase in excitability, particularly at low repetitive firing frequencies. Figure IV-6 shows the relationship between spike frequency, measured during the first interspike interval of a train, and the stimulus current intensity used to elicit the repetitive train. The spike frequency increases with stimulus intensity over the range studied. Replacement of the external Ca^{2+} with Mn^{2+} increased the spike frequency by up to 260% at the lower stimulus intensities. In this experiment, at higher stimulus intensities the control spike frequency appeared to be reduced slightly in Mn^{2+} saline. However, the crossing of the curves may be partly an artifact. The control data were obtained earlier in the recording session, at a time when the input resistance was slightly higher and this would tend to

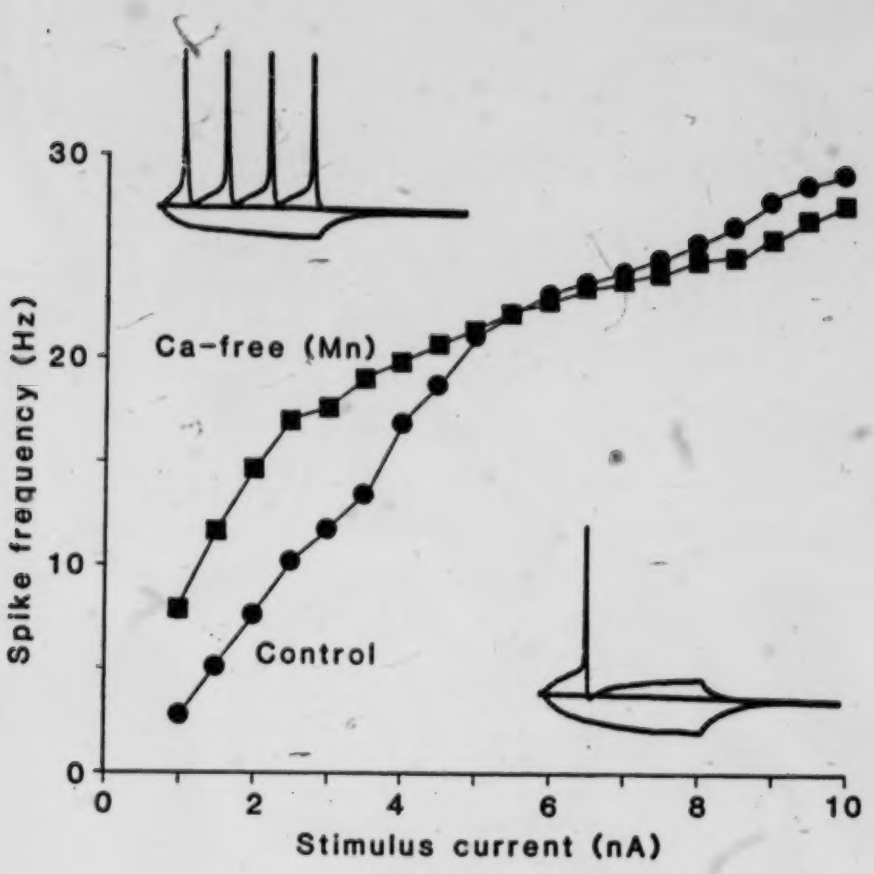

Figure IV-6. Effect of Ca^{2+}-free (Mn^{2+}) saline on the spike frequency-current relationship . Spike frequency for the first interspike interval of a train is plotted as a function of stimulus current, to produce the *f-I* relationship. The frequency measured in Ca^{2+}-free (Mn^{2+}) saline (circles) is increased (over the lower frequency range, 2 to 20 Hz) when compared to the control (squares). Over this range, the *f-I* relationship is quite linear for the control, but more non-linear for the Ca^{2+}-free (Mn^{2+}) data. The Ca^{2+}-free (Mn^{2+}) data could be fitted reasonably well assuming a logarithmic relation between frequency and stimulus current ($f \propto ln\ I$, plot not shown). The crossing of the control and Ca^{2+}-free (Mn^{2+}) curves was not a consistent finding, and the reason for this is discussed in the text. The insets show raw data records for current steps of -1, 0, +1 nA (500 ms) recorded in control (bottom) and Ca^{2+}-free (Mn^{2+}) saline (top). The Ca^{2+}-free (Mn^{2+}) curve was taken 15 minutes after perfusion with Ca^{2+}-free (Mn^{2+}) saline, and about 20 minutes after the control curve.

decrease the frequency response to an applied stimulus (control R_M = 18 mΩ, Mn^{2+} R_M = 16 mΩ). In other experiments the curves were observed either to cross (n = 4) or simply run parallel (n = 3) at high stimulus intensities. Nevertheless, all experiments were similar in that the most marked effect of Ca^{2+}-free (Co^{2+} or Mn^{2+}) saline was at low stimulus intensities, and correspondingly, at low spike frequencies. In these experiments frequency was measured only during the first interspike interval (as 'instantaneous' frequency) because later in the train the slower Ca^{2+}-dependent $I_{K(Ca)}$ becomes more prominent and is important in spike frequency regulation. Therefore, the first interspike interval was chosen to assess the effects of I_A, because at that time the repetitive train should be relatively uncontaminated by effects of $I_{K(Ca)}$ (discussed further in Chapter V).

The previous chapter has demonstrated that replacement of Ca^{2+} with Mn^{2+} or Co^{2+} reduces and slows I_A activation. The above results show that the same treatment under current clamp increases the spike frequency response to small depolarizing current steps. Therefore, it is tempting to suggest that I_A regulates low frequency repetitive firing in these neurons as in molluscan neurons (Connor and Stevens, 1971c), and crustacean axons (Connor *et. al.*, 1977). However, as discussed previously (Chapter III), replacement of Ca^{2+} with other divalent cations can alter the voltage dependence and kinetics of conductances which are not traditionally considered to be Ca^{2+}-dependent. Surprisingly though, Mn^{2+} and Co^{2+} have very little effect on the action potential threshold or slope of the depolarizing phase in these neurons (Figure IV-7A). In this cell the voltage threshold was unchanged within the resolution of the measurement (±1 mV) even when analyzed at large voltage gains. In other cells the voltage threshold was observed to shift by only +1 to +2 mV in a depolarized direction from the control. These changes would tend to make cells slightly less excitable. The rate of rise of the action potential was unaltered in Ca^{2+}-free (Mn^{2+}) saline (although the peak amplitude was reduced slightly, probably due to elimination of I_{Ca}). This suggests that there was no major effect on the activation of I_{Na}. These results are in contrast to the effects of divalent cations on crustacean axons, where I_{Na} parameters are shifted rightward along the voltage axis, increasing the threshold and slowing the rate of rise of the action potential (Takata *et. al.*, 1966; Blaustien and Goldman, 1968).

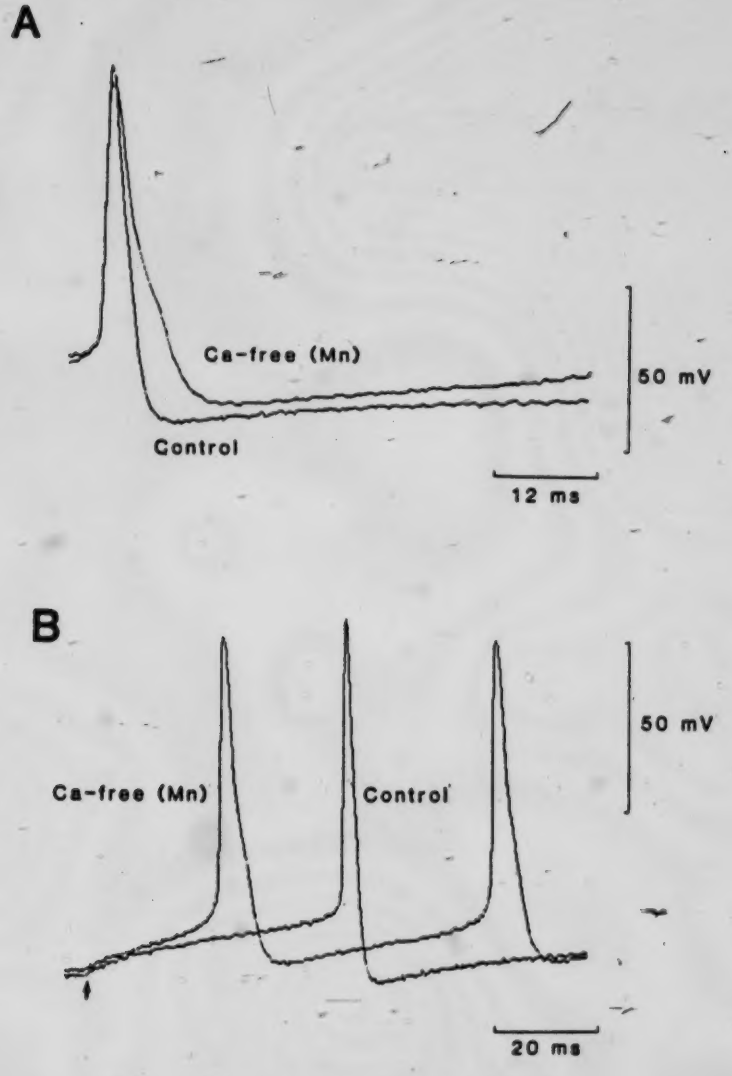

Figure IV-7. Effect of Ca^{2+}-free (Mn^{2+}) saline on membrane excitability. A: The threshold potential, and rate of rise of the action potential were not markedly affected by perfusion with Ca^{2+}-free (Mn^{2+}) saline (15 minutes). However, the repolarization rate was much slower, and the AHP reduced by 6 mV. B: The increased action potential frequency in Ca^{2+}-free (Mn^{2+}) saline resulted primarily from reduced hyperpolarization during the interspike interval. In this cell the resting potential was reduced from -50 to -48 mV after perfusion with Ca^{2+}-free (Mn^{2+}) saline. Analog to digital sample interval = 500 μs.

Replacement of the external Ca^{2+} with Mn^{2+} or Co^{2+} did have marked effects on the repolarizing phase of the action potential, and the changes appeared to be voltage-dependent. Above 0 mV, the repolarization rate was only slightly slower than normal, for the experiment shown in Figure IV-7, the action potential duration measured at +10 mV increased from 3 to 4 ms. However, below 0 mV there was a pronounced slowing of repolarization, which led to an increase in duration from 4 to 8 ms measured at -30 mV. The AHP was reduced in Ca^{2+}-free (Mn^{2+}) saline and this was probably the major cause of the increased repetitive firing frequency observed in the *f-I* curves of the type shown earlier (Figure IV-6).

In some experiments the resting membrane potential was reduced by a few millivolts (from -45 mV to -42 mV for the cell shown in Figure IV-7B) after perfusion with Ca^{2+}-free (Mn^{2+}) saline. In addition, the response time was often reduced as was the case for the cell in Figure IV-7B. However, this change in response time could be a by-product of the more depolarized resting potential; for cells that were held at the control membrane voltage using a hyperpolarizing current bias, the response time was changed less in Ca^{2+}-free saline. Ca^{2+}-free (Mn^{2+}) saline does not eliminate the long response times which follow membrane hyperpolarization. Figure IV-8 shows the membrane voltage response following a hyperpolarizing pre-pulse, for a cell bathed in control and Ca^{2+}-free (Mn^{2+}) saline. In the control saline the response time was 1200 ms; this was reduced only slightly, to 1050 ms, in Mn^{2+} saline. Note that the slow adaptation of the spike train present in the control was eliminated in Mn^{2+} saline, suggesting that the membrane currents which underlie spike frequency adaptation, and those underlying the slow ramp depolarization differ in Ca^{2+}-sensitivity.

Effect of 4-aminopyridine on membrane excitability

I was hesitant to use 4-AP in current clamp experiments because it did not appear to specifically block I_A in barnacle neurons (Chapter III). However, I decided that experiments using 1 mM 4-AP could be interpreted as blocking predominantly I_A if recordings were limited to less than 5 minutes following application of 4-AP. That is, during the early

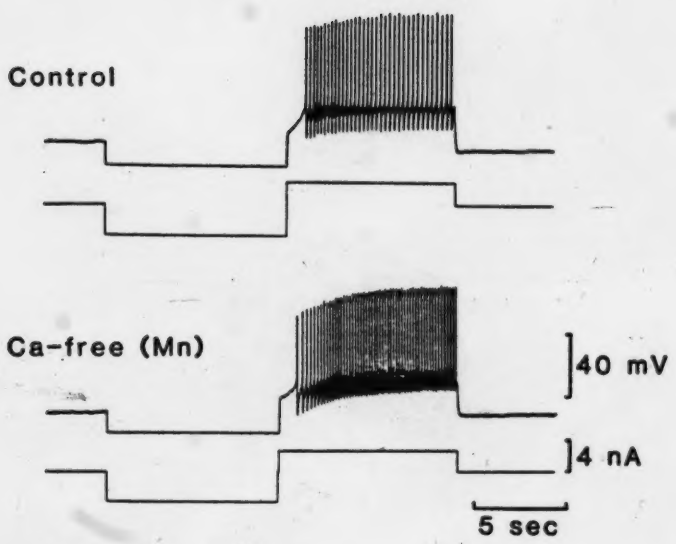

Figure IV-8. Effect of Ca^{2+}-free (Mn^{2+}) saline on the slow ramp depolarization. Perfusion with Ca^{2+}-free (Mn^{2+}) saline for 20 minutes did not eliminate the ramp depolarization and long response time (response time = 1200 ms for the control, and 1050 ms Ca^{2+}-free). The action potential train was elicited by a +3 nA stimulus, which followed a -4 nA pre-pulse, yielding a pre-stimulus voltage of about -65 mV (off scale in both traces). The resting potential was -48 mV in both control and Ca^{2+}-free (Mn^{2+}) saline. The action potentials were attenuated by the pen recorder, response DC to 60 Hz.

period when the block was relatively specific to I_A. Also, 4-AP has the disadvantage when used in current clamp studies, that the block is extremely use- and voltage-dependent (see Thompson, 1982). For the present, I will ignore these complications, the purpose of these experiments being primarily to obtain data for comparison with the results of Segal *et. al.* (1984) who did use 4-AP in a current clamp study to evaluate the role of I_A in regulation of excitability of mammalian hippocampal neurons.

Records for the early parts of action potential trains in control and 1 mM 4-AP saline (4 min after bath application) are shown in Figure IV-9. Both parts, A and B are from the same data record, but A shows the initiation of the train, and B shows the first interspike interval. In A, the response time was reduced, and this appeared to result primarily from a shift of the action potential threshold, with no reduction in the resting potential. The threshold was shifted by -3 mV, which caused the first action potential to occur 13 ms earlier than when the same stimulus was applied in the control saline. The action potential duration was only slightly increased in 1 mM 4-AP (inset).

The threshold potential for the second spike of the train was unaltered from the control, even when plotted at increased gain (Figure IV-9B). This was observed throughout the remainder of the train, only the threshold for the first spike was more hyperpolarized in 4-AP. This result suggests that there is a use-dependent component to the 4-AP effect on spike threshold.

The first interspike interval was reduced in the presence of 4-AP (Figure IV-9B). This appeared to result from two kinds of changes during the interspike interval. Firstly, the AHP was slightly reduced, and secondly, the interspike voltage trajectory was altered. In 4-AP the cell was less hyperpolarized throughout the interspike interval, and this decreased the interspike interval. This result suggests that 4-AP blocks a K^+ current which is normally activated during the interspike interval. Similar results were observed in other cells, but the results were usually less clear cut. 4-AP application (1 mM) was often associated with a general deterioration of repetitive firing ability, and a decrease in cell health (*e.g.* decreased resting potential, and reduced potential amplitude).

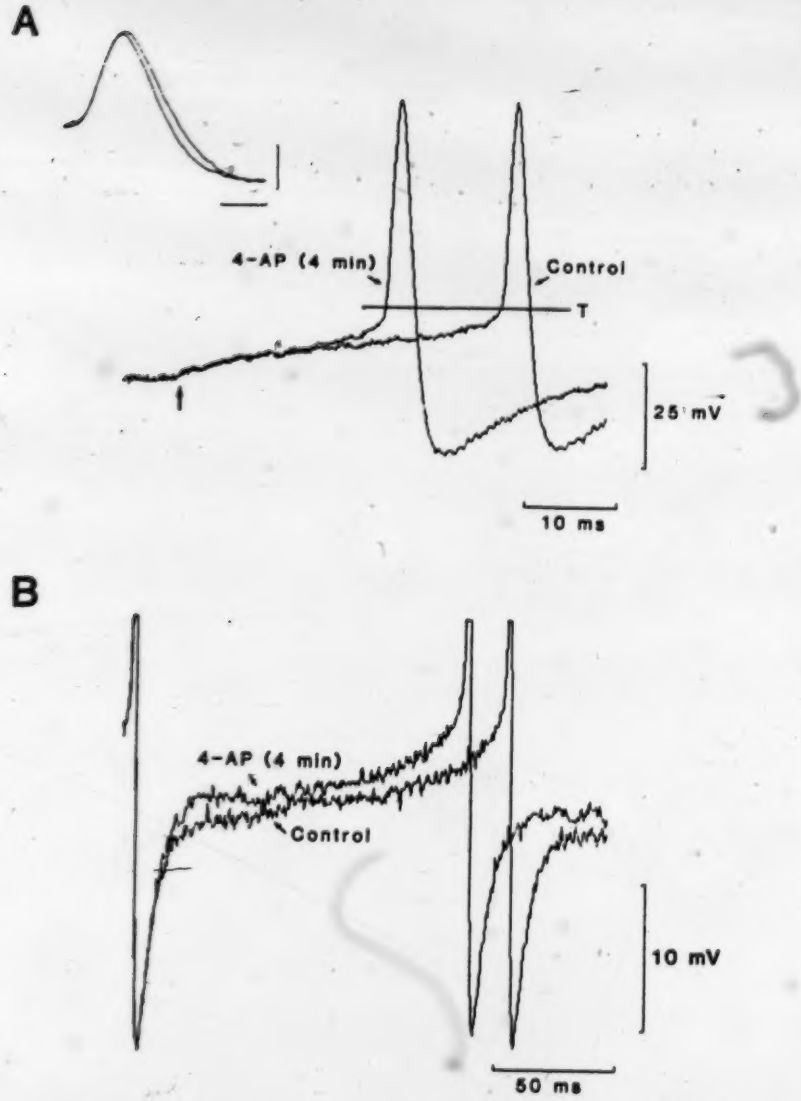

Figure IV-9. Effect of 1 μM 4-AP on membrane excitability. A: Measured at 4 minutes after bath application, 4-AP decreased the action potential threshold by -3 mV and reduced the response time. The line marked 'T' shows the control threshold potential (-26 mV) for comparison to threshold observed in 4-AP. The action potential repolarization was also slightly slower in 4-AP (inset). B: The first interspike interval was also decreased in the presence of 4-AP (same train as A). The decrease in interspike interval was not produced by a change in action potential threshold, the 2nd action potential threshold was similar for control and 4-AP. The change in the interspike appeared to result from a reduction of a hyperpolarizing influence during the interspike interval, and supports the hypothesis that I_A is normally activated at this time. The action potential train was initiated from resting potential (-41 mV) by a +2 nA current stimulus. Analog to digital sample interval = 1 ms (300 ms for inset).

Effect of forskolin on membrane excitability

In the previous chapter, it was shown that forskolin, applied extracellularly at 100 μM, is a powerful modulator of I_A inactivation kinetics, increasing the rate of inactivation. Since this effect is relatively independent of any change in activation kinetics or the underlying conductance, forskolin can be used to evaluate the consequences of I_A inactivation during spike trains. Figure IV-10 shows the increase in excitability observed when forskolin was bath applied at 100 μM. The control record is compared to a record obtained 10 minutes after the application of forskolin. The major effect was a marked reduction in the AHP, action potential threshold and duration were essentially unchanged. The inset shows action potentials recorded in control and forskolin salines, emphasizing the reduction of the AHP. The change in the response under current clamp presumably results from a reduction in the I_A inactivation time constant, and an accompanying decrease in the peak I_A, as was observed in voltage clamp. The lack of change in the action potential threshold or duration suggest that neither the rate of I_A inactivation or the magnitude of the peak I_A are important in the regulation of excitability at this time.

Using a descriptive model, Byrne (1980b) has shown that the rate of I_A inactivation is a major factor controlling the long response times observed in *Aplysia* ink motor neurons. This hypothesis has not been tested experimentally. As described earlier, barnacle neurons also show response times lasting up to several seconds, if the resting potential is deep, or following hyperpolarizing pre-pulses. It was therefore of interest to know if forskolin could reduce the response time by speeding up the rate of I_A inactivation. Forskolin was found to markedly reduce the response time, and the time course of development of this effect was similar to the development of the decrease in the inactivation time constant observed under voltage clamp. In the experiment shown in Figure IV-11 the first action potential in the control saline followed a 2.5 second delay, and this was reduced to 1.3 seconds after 5 minutes in 100 μM forskolin. The voltage at which the ramp depolarization begins (-38 mV in the control) was not altered in forskolin, suggesting that activation of I_A during the depolarization was not changed. Note that in addition to the reduced response time, the AHP following each action potential was also reduced after treatment with forskolin.

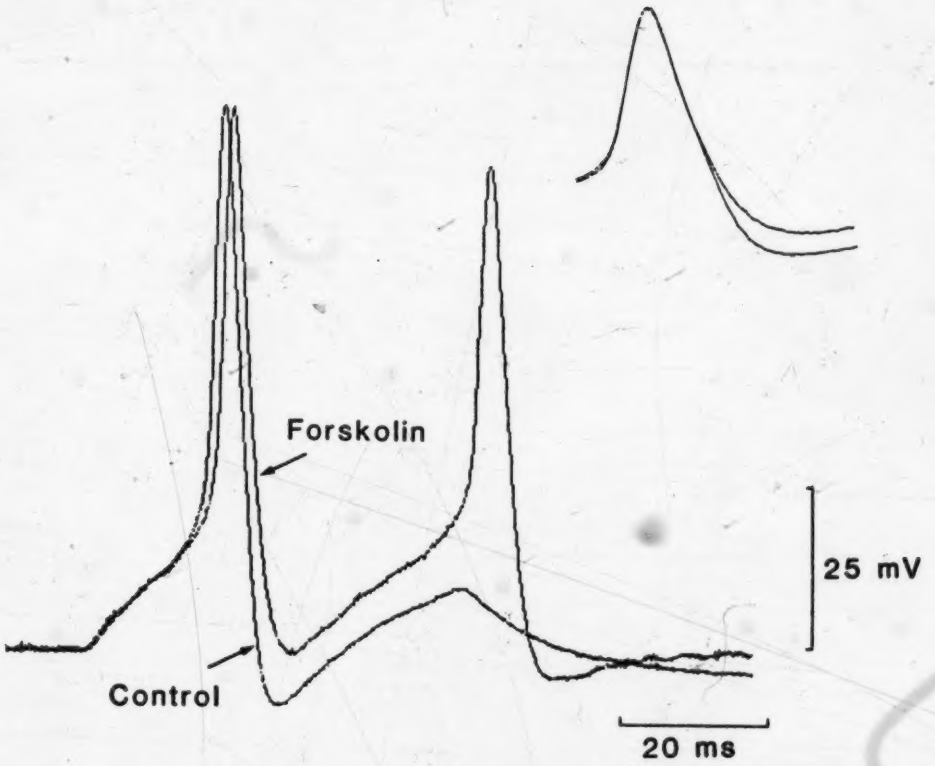

Figure IV-10. Effect of 100 μM forskolin on membrane excitability. The major effect of forskolin was a reduction in the AHP, which decreased the first interspike interval by increasing the rate of rise of membrane voltage during the interspike interval. There was no effect on action potential or duration. The inset shows superimposed control and forskolin records, with the rising phases aligned (forskolin has the reduced AHP). The action potentials were elicited from resting potential (-52 mV) by a +5 nA, 50 ms current pulse. The forskolin record was taken 10 minutes after bath application of forskolin. Analog to digital sample interval = 200 μs.

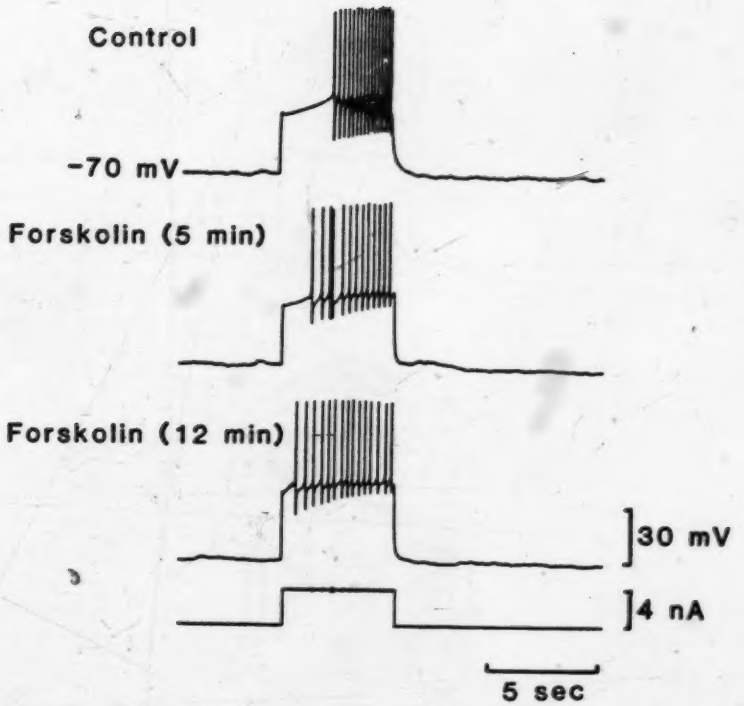

Figure IV-11. Effect of 100 μM forskolin on the neuronal response time. Forskolin was bath applied in order to test its effect on a neuron with a particularly long response time, and presumably a relatively large contribution of I_A. The neuron was hyperpolarized to -70 mV prior to the onset of a +4 nA, 5 sec stimulus. In the control, the response time was 2.5 sec, and forskolin decreased this to 1.3 sec after 5 min and 0.6 sec after 12 min. The effect of forskolin was not limited to a reduction of the response time; the AHP was also reduced, and the input resistance was decreased, which may account for the reduced action potential frequency observed after treatment with forskolin. The action potentials were attenuated by the pen recorder, response DC to 60 Hz.

Exploration of the role of I_A in membrane excitability using a descriptive model

The experimental results presented earlier in this chapter suggest that I_A contributes to action potential repolarization, as well as to regulation of very much slower phenomena, such as the slow ramp responses to depolarization. A numerical simulation can be used to predict whether or not the observed voltage dependence and kinetics of I_A are consistent with these varied roles in excitability. In addition, a descriptive model is useful in the analysis of the effects of Ca^{2+}-free saline and forskolin on excitability.

The mathematical model was based on modified Hodgkin-Huxley equations which were evaluated by a simple Euler integration method. The version used in the following simulations represents the neuron membrane as a five branch, parallel conductance, electrical model. Four ionic currents, I_{Na}, I_K, I_A, and I_L are included, as well as the non-ionic current which flows through the membrane capacitance, I_C. These are the major components of total membrane current, I_M, and those which were of primary interest in the present analysis. I_{Ca} and $I_{K(Ca)}$ were omitted because they have not been analyzed in sufficient detail, and because a model would have to incorporate intracellular Ca^{2+} buffering and distribution to approximate the activation of $I_{K(Ca)}$. Also, voltage-dependent inactivation of I_K was not included because several characteristics of the inactivation process suggest that inactivation is not governed by a single H-H type variable. Possible effects of these omissions will be discussed in detail later.

In order to describe I_{Na}, equations identical to the H-H model were used, except for the addition of the parameter shifts suggested by the analysis in Chapter II. The time- and voltage-dependent behavior of the *m* and *h* parameters assumed to control I_{Na} were calculated using the modified H-H rate constants and steady-state voltage dependences as described in the Appendix. The time- and voltage-dependent behavior of the *n* parameter controlling I_K, as well as *a* and *b* controlling I_A were calculated, using the best fit curves for the time constants and steady-state voltage dependences presented earlier (Chapters II and III). I_L was assumed to be time-independent, and a linear function of membrane voltage. The values for the maximal conductances used in the model were the averages measured in the previous chapters, except for $\bar{g}_{Na}$, which was set to equal the maximum experimental

value observed in order to produce the correct action potential amplitude ($\bar{g}_{Na}$ = 25 μS, $\bar{g}_A$ = 2.5 μS, $\bar{g}_K$ = 3.6 μS, g_L = 0.2 μS). The values used for reversal potentials and shift parameters are given in the Appendix. The version of this model based on the average parameter measurements will be referred to as the 'standard' barnacle model.

The standard barnacle model produced a calculated resting potential of -44 mV, close to the average of -43 mV observed in current clamped neurons. The resting membrane conductance was 0.27 μS, somewhat higher than the experimental average of 0.17 μS, but within the range of experimentally observed values. The resting membrane conductance was primarily determined by g_L and g_A, and small changes in g_L could reproduce the range of resting conductances usually observed. At -44 mV the ionic conductance parameters had the following steady-state values, m = 0.05, h = 0.80, n = 0.05, a = 0.60, b = 0.29.

The minimum stimulus current to produce a single action potential was +1.4 nA, and +1.5 nA produced an 'infinite' train. During most of the simulations shown, a stimulus intensity of +2.0 nA was used to elicit repetitive firing. Figure IV-12A compares an action potential produced by the standard model, and one recorded from a barnacle neuron under current clamp. The experimental record was chosen because of its similarity to the simulation, but nevertheless, makes the point that the reconstruction of a single action potential is quite accurate. Following a +2.0 nA stimulus, the model produced an action potential with a threshold of -30 mV, peak amplitude of +36.6 mV, and duration of about 3 ms measured at one-half amplitude. In each of these characteristics the model compares favorably to values measured experimentally.

The ionic currents calculated to underlie a single membrane action potential are shown in Figure IV-12B. In this figure, the calculated I_A and I_K are plotted at the same gain, illustrating the surprisingly large contribution of I_A to repolarization of the action potential. I_A also activates earlier, at the peak of the action potential, I_{Na} = 44.9 nA, I_A = 32.3 nA, and I_K = 7.6 nA. I_A is clearly important for repolarizing the action potential in spite of the larger current carrying capacity of I_K. This situation arises because of the much faster I_A activation time constant (τ_a), and the fact that there is significant removal

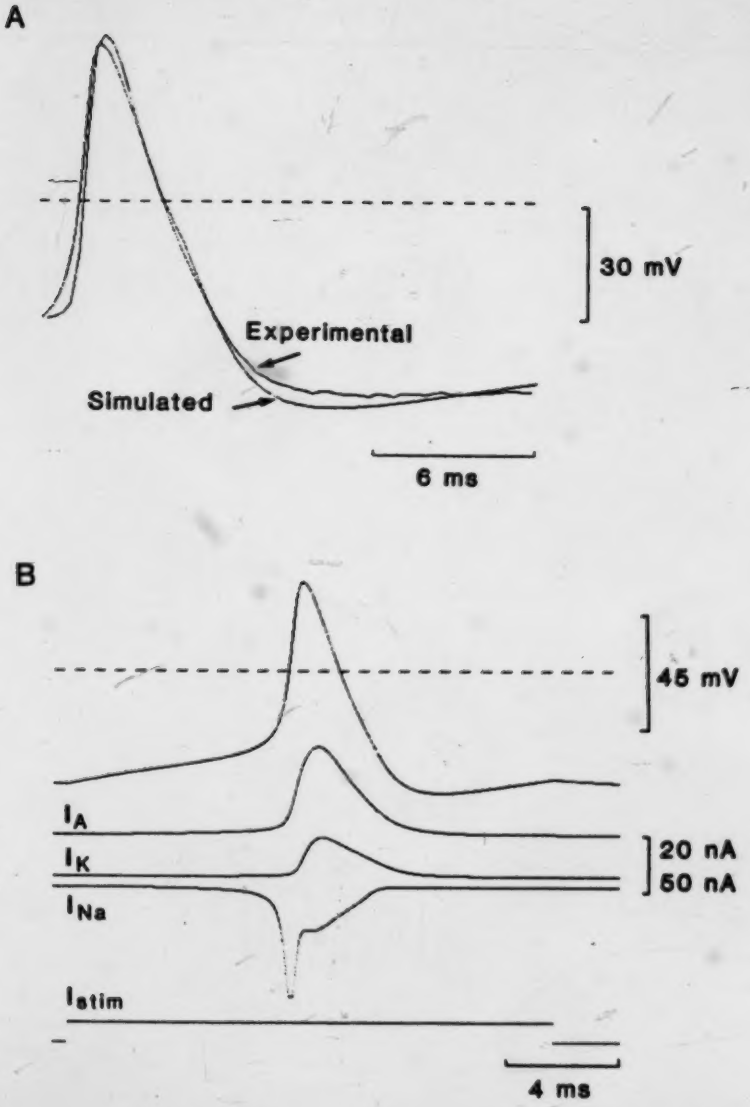

Figure IV-12. Simulation of the membrane action potential. A: The simulated action potential, produced by the standard barnacle model, is compared to an experimental record. Both action potentials were elicited by a +2 nA stimulus from resting membrane potential. The dashed line is 0 mV. The integration interval used to calculate the action potential was 25 μs. The analog to digital sample interval was 250 μs for the experimental action potential. B: Membrane ionic currents underlying the simulated action potential. The upper trace (action potential) is the calculated membrane voltage response to a +2 nA, 30 ms stimulus. The lower traces show the underlying ionic currents which produced the voltage response. Following the slow approach to action potential threshold, I_{Na} rapidly depolarizes the membrane. I_A then activates, followed by a smaller contribution of I_K. Note that I_A and I_K are plotted at higher gain (scale = 20 nA) than I_{Na} (scale = 50 nA). Integration interval = 25 μs.

of I_A inactivation at the -44 mV resting potential. The following results were obtained using the model to predict the role of I_A in action potential repolarization, but are not shown as figures. Setting τ_a to a fixed value which represents the average τ_a at -10 mV (1.7 ms), but with no voltage dependence, markedly reduced the activation of I_A during the action potential. Paradoxically, setting g_A to 0 μS (no I_A) only slightly broadens the action potential, because there is a proportionate increase in I_K. A similar shift of the relative importance of I_A and I_K was noted during long action potential trains, particularly at higher action potential frequencies (as discussed below).

Calculations from the model suggest that the ratio of I_A:I_K during an action potential is dependent on the pre-stimulus voltage, and on the position of the action potential in a train. Figure IV-13 shows the membrane voltage response to a +3 nA stimulus, lasting 1 second, initiated from a pre-stimulus voltage of -53 mV. The initial voltage response at the onset of the current stimulus is similar to the trajectory observed experimentally from pre-stimulus voltages in this range (refer to Figure IV-1). The rapid initial depolarization is followed by a small overshoot and slow depolarizing ramp, leading to a delayed first action potential. The membrane currents underlying the ramp depolarization will be discussed below. This figure shows dramatically the shift from I_A predominating to I_K predominating during the action potential train. This shift is most obvious following a hyperpolarized pre-stimulus, which maximizes I_A, but a qualitatively similar result is also observed for action potential trains initiated from the resting potential. It is interesting that as the train progresses and I_K becomes more important for repolarization, the sum of I_A and I_K remains fairly constant. Early in the train, the AHP's are more negative going, and these become reduced as the train progresses. A similar response was observed experimentally following the slow ramp depolarization. The simulation does differ from the experimental result in that the calculated action potential train does not show the pronounced acceleration associated with the long response times.

I have yet to determine exactly what causes the shift from I_A to I_K during repolarization. As the spike train in Figure IV-13 progressed, the value of b (controlling I_A inactivation, 1 = inactivation removed) fell from 0.15 after the first action potential to 0.07

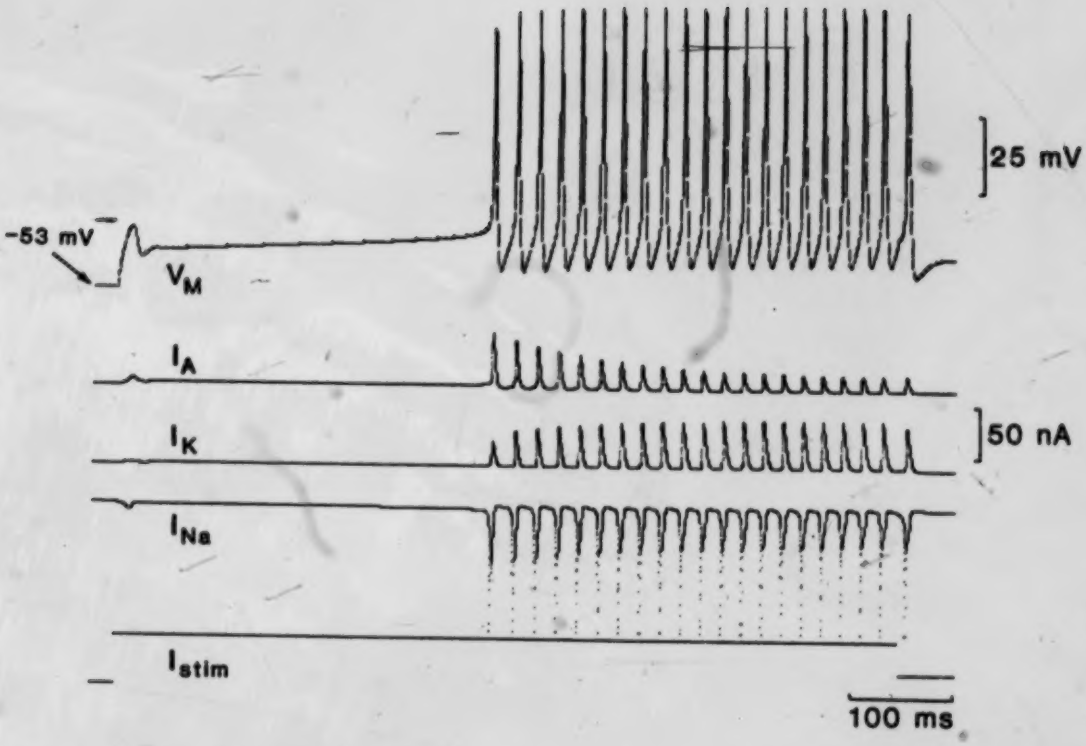

Figure IV-13. Simulation of a repetitive action potential train following membrane pre-hyperpolarization. In this simulation a +3 nA depolarizing stimulus, lasting 1 sec, was initiated from a pre-stimulus membrane voltage of -53 mV. The onset of the stimulus was followed by a slow ramp depolarization lasting 370 ms, prior to the initiation of the first action potential. I_A is most important in repolarizing the first action potential. As the train progresses the relative contribution of I_A and I_K shifts, so that late in the train I_K is most important for action potential repolarization. Integration interval = 100 μs.

after the 8th. The values for other conductance parameters were relatively constant after each action potential. Therefore, it appears that steady-state I_A inactivation which is removed by the pre-pulse builds up during the spike train because of the net increase in depolarization associated with the action potential train, reducing the fraction of I_A available to repolarize the action potential. At lower spike frequencies, b declines more slowly during the train, because there is more removal of inactivation during the AHP (see below).

The pre-stimulus voltage alters the duration of the action potential in the model, as was observed experimentally. Figure IV-14 compares the first action potential of a train which followed a 200 ms pre-pulse to either -40 or -60 mV. The action potential duration was reduced, and the AHP increased following the -60 mV pre-pulse. The model does not include removal of inactivation from I_K, and therefore indicates that the change in duration is a result of removal of inactivation of I_A. The similarity of this calculation to the experimental result (Figure IV-5) supports the experimental conclusion that I_A does repolarize the action potential in these neurons.

When depolarizations are initiated from hyperpolarized membrane voltages the model predicts long response times, and the associated slow ramp depolarization, (shown in Figure IV-13). The simulated membrane currents which underlie this response are shown in Figure IV-15. The slow depolarization leading to action potential threshold appears to result from the co-activation of I_A and I_{Na}. The rapid increase in I_A to a very slowly decaying plateau, counteracts the depolarizing stimulus, while simultaneously I_{Na} slowly drives the voltage to threshold. However, the simulation also predicts a small, steady increase in the membrane conductance throughout the slow depolarization, from 0.36 μS to 0.58 μS. This disagrees with the experimental result (Figure IV-2) of a decrease in membrane conductance, from 0.33 to 0.14 μS, during the slow ramp depolarization. I have been unable to determine the source of this discrepancy. The experimentally measured +2 to +3 nA outward current during the early part of the ramp depolarization actually agrees quite well with the model, which predicts a net +2.2 nA outward current at this time. The outward current measured in the switched current-voltage clamp experiment (Figure IV-3) declined slowly, but this could have resulted from a simultaneously activating inward current, as the model predicts.

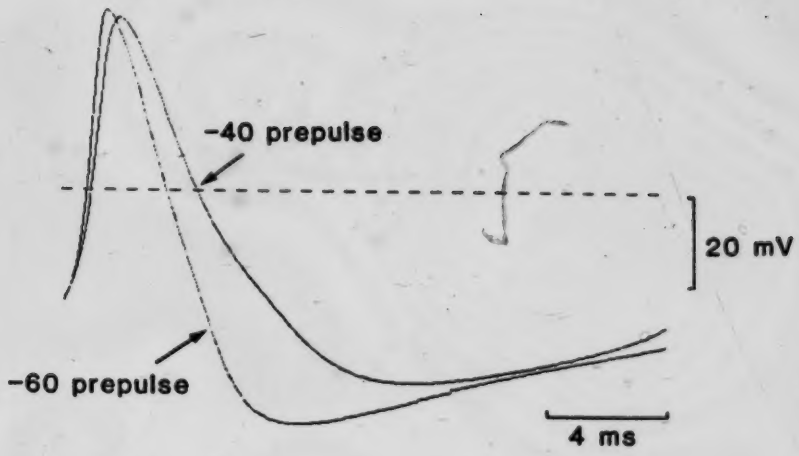

Figure IV-14. Simulation of the effect of pre-stimulus voltage on action potential repolarization. The action potentials are the first in a train following a 200 ms pre-pulse to yield pre-stimulus voltages of -40 or -60 mV. A +4 nA stimulus was used to elicit the action potentials. The action potential repolarizes more rapidly following the -60 mV pre-pulse and the AHP is increased in magnitude. Integration interval = 25 s.

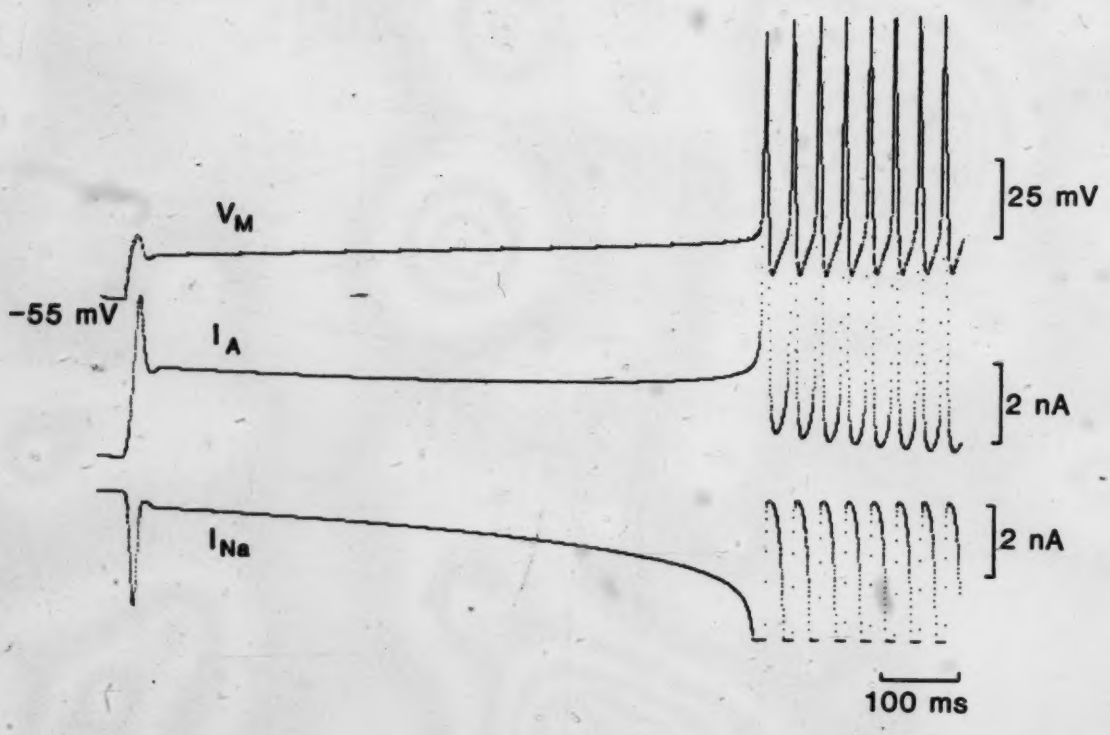

Figure IV-15. Simulation of the membrane currents underlying the slow ramp depolarization. This figure shows the calculated response to a +2.5 nA depolarizing stimulus, initiated from a pre-stimulus voltage of -55 mV. The predicted behavior of I_A and I_{Na} are shown along with the membrane voltage. I_K has been omitted, since it played no role in the generation of the slow ramp depolarization. At -55 mV I_A is small (0.1 nA) as is I_{Na} (0.0 nA). At the onset of the stimulus both rise transiently during the initial voltage overshoot. After this I_A reaches a plateau at 2.5 nA, and declines slowly to a minimum of 2.3 nA. Throughout the duration of the ramp depolarization, I_{Na} is slowly increasing, until the first action potential is produced. Thus, the model predicts that the transient behavior of I_{Na} contributes to the slow development of excitation. Integration interval = 100 μs.

Thus, the voltage clamp data appear to be consistent with the predictions of the model; whereas the conductance test under current clamp suggests that the mechanism by which the model generates long response times may be different. Also, in current clamp experiments the slow ramp depolarization is followed by an accelerating action potential train (Figure IV-1), but the model predicts a train with only slight acceleration (Figure IV-15).

The model predicts that events qualitatively similar to those occurring during the ramp depolarization also occur during the interspike interval. Figure IV-16 shows a simulation of a low frequency (3.7 Hz) action potential train. The duration of the interspike interval appears to be controlled mainly by the interaction of I_A and I_{Na}. The events during the interspike interval are described in the legend to Figure IV-16. The predicted voltage response is quite typical of barnacle neurons whose resting potential is less negative than the action potential AHP. The response time is short, but the first interspike interval is much longer, presumably because more I_A inactivation is removed during the AHP than was removed at rest. If g_A is set to 0, and the same stimulus applied to the model, the first interspike interval is only slightly longer than the response time. This simulation of low frequency repetitive firing differs from Connor and Stevens' model (1971c) in that I_A keeps increasing during the interspike interval. In their model, it is the rise, then fall of I_A which allows the membrane to slowly depolarize. Here, the slow increase in I_{Na} is very important in determining the voltage trajectory during the interspike interval.

It was of interest to determine whether the model could mimic the changes in excitability observed in Ca^{2+}-free (Mn^{2+}) saline and in forskolin, using the alterations in I_A obtained under voltage clamp. The effects of both treatments were assumed to only change I_A parameters. The effect of Ca^{2+}-free saline was simulated by applying the parameter changes measured experimentally in Co^{2+} replaced saline. Steady-state inactivation was shifted by +8 mV, τ_a was shifted by +20 mV, τ_b was increased by 50% at all voltages, and g_A was reduced by 40%. These alterations approximate the effect of Ca^{2+}-free (Co^{2+}) saline on I_A (refer to Chapter III). The results for simulated control saline (standard model) and Ca^{2+}-free (Co^{2+}) are shown in Figure IV-17. The action potential broadening observed

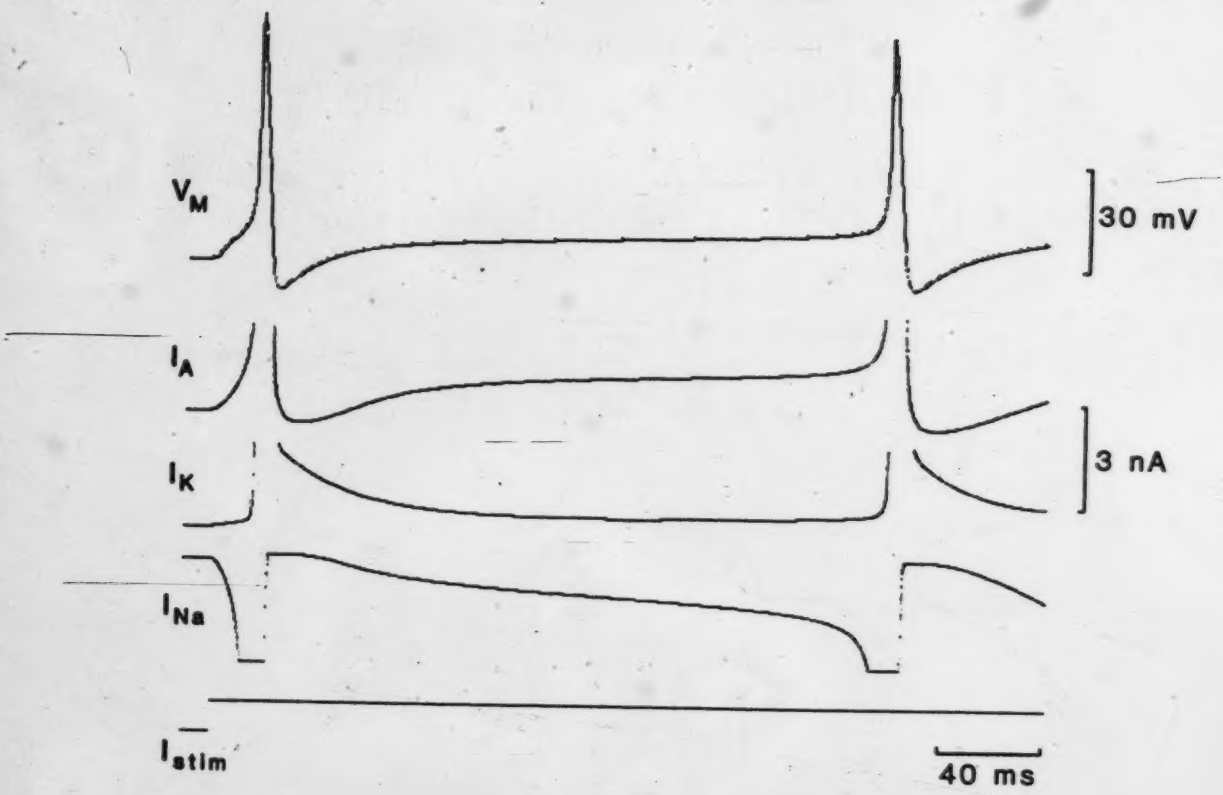

Figure IV-16. Simulation of the membrane currents underlying slow repetitive firing. The membrane voltage and ionic currents during a +1.6 nA stimulus from resting potential are shown. The first action potential occurs with little delay, followed by a long first interspike interval of 270 ms (= 3.7 Hz). The underlying I_A, I_K and I_{Na} are shown below, all at the same gain. At the onset of the stimulus the membrane voltage rises rapidly to threshold, controlled primarily by I_{Na}, I_A and the membrane capacitative current (not shown). I_K is relatively unimportant until later in the action potential. I_{Na} falls to near zero just following the action potential peak, and shortly after, I_A declines to a value which is less than that at rest. More slowly, I_K declines, controlling the later part of the AHP. As the membrane voltage rises I_A is re-activated following removal of inactivation during the AHP, and slowly increases throughout the interspike interval. The increase in conductance reduces the effect of the depolarizing stimulus. I_{Na} also slowly increases during the interspike interval, adding to the membrane depolarization; eventually a voltage is reached where I_{Na} breaks away, producing a second action potential. Integration interval = 50 μs.

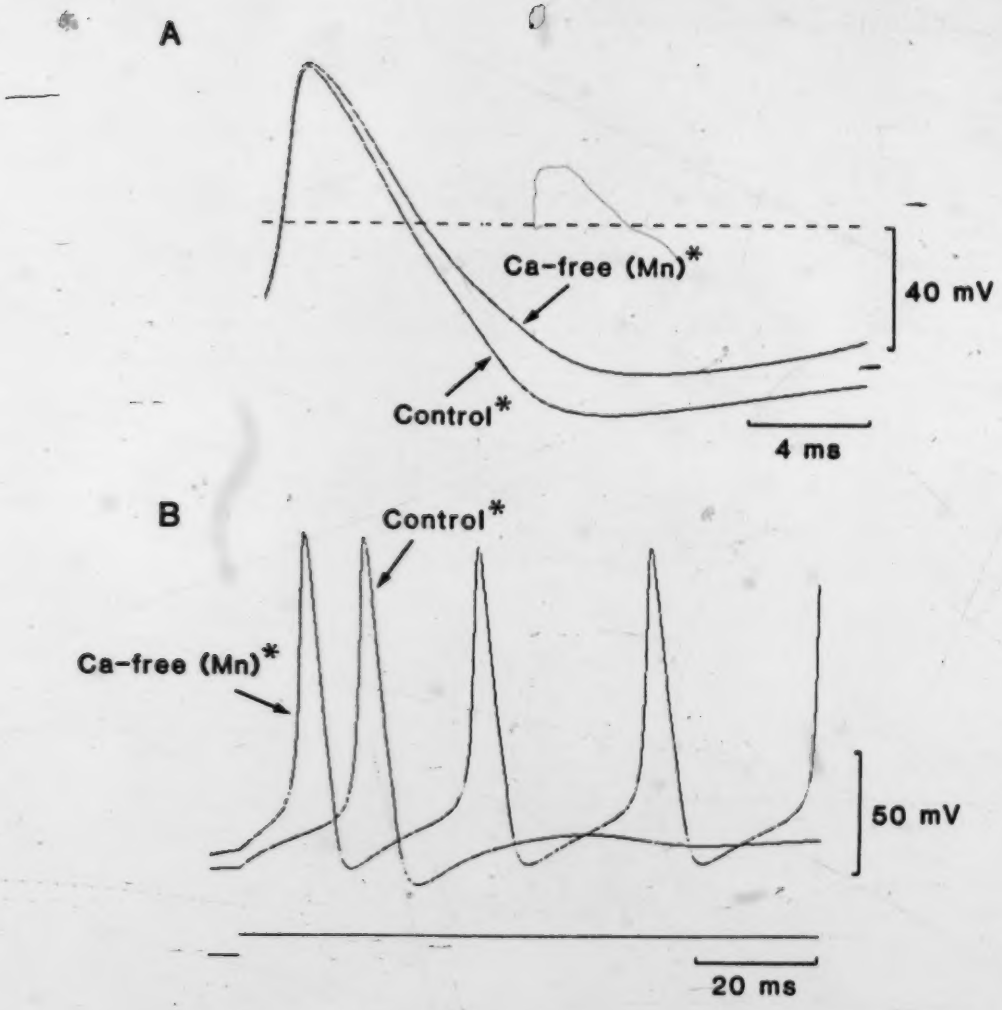

Figure IV-17. Simulation of the effect of Ca^{2+}-free (Co^{2+}) saline on membrane excitability. The effect of Ca^{2+}-free (Co^{2+}) saline was simulated by reducing g_A by 40%, in addition to the shifts in voltage dependence described in the text. A: The simulation predicts a broadening of the action potential, and a reduction of the AHP in simulated Ca^{2+}-free (Co^{2+}) saline. B: The repetitive firing frequency is increased, and the resting potential depolarized in simulated Ca^{2+}-free (Co^{2+}) saline. The response time is also reduced, primarily as a function of the change in resting potential. The asterisks in this and following figures denote simulated responses. Integration interval = 25 μs.

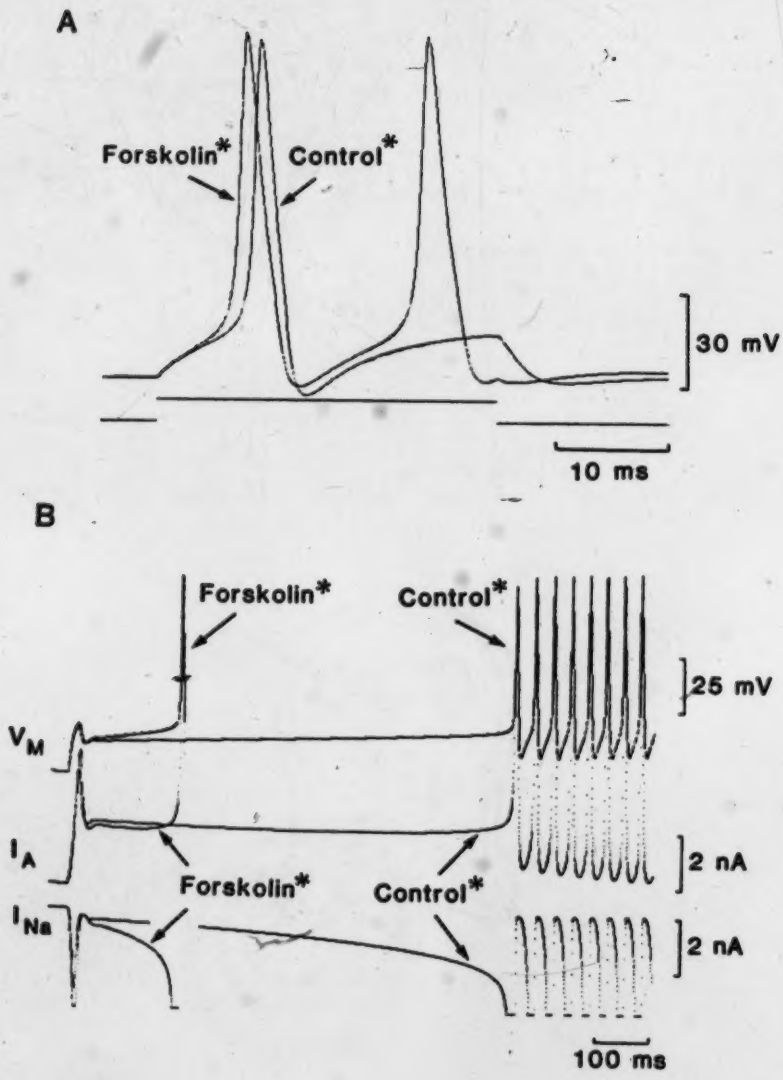

Figure IV-18. Simulation of the effect of forskolin on membrane excitability. The effect of forskolin was modelled as a 40% reduction in the I_A inactivation time constant. A: The simulation predicts a reduction of the AHP, with no change in action potential duration. The control produced one action potential, and for the simulated forskolin two action potentials during the +2.2 nA, 30 ms stimulus. Integration interval = 25 μs. B: The simulation indicates that forskolin blocks the slow ramp depolarization by decreasing the magnitude of I_A. The simulated forskolin response shows that a reduction of only 0.2 nA in I_A allows the voltage to be driven to action potential threshold much earlier. Integration interval = 100 μs.

experimentally (Figure IV-7, Mn^{2+} replaced saline) is qualitatively reproduced, although the increase in duration was more pronounced in the experimental data. The increase in action potential frequency observed experimentally could also be mimicked by the above alterations to I_A (Figure IV-17B). These results from the simulations support the experimental results in that they indicate that changes in I_A alone could account for the increased excitability observed in Ca^{2+}-free saline.

The effect of forskolin on membrane excitability was approximated in the simulation by assuming that a voltage independent, 40% reduction in τ_b was the only effect on I_A. This is probably an oversimplification of the effects of forskolin. Nevertheless, the kinds of changes observed under current clamp were reproduced fairly well using this simulation of the forskolin effect (Figure IV-18). The AHP following an action potential was reduced, with no change in threshold or action potential duration, and this agrees quite well with the experimental result for 100 μM forskolin (Figure IV-10). Although the model seems to be inaccurate in its portrayal of the long response times following membrane hyperpolarization, as pointed out above, the decrease in response time produced by forskolin is reproduced. Figure IV-18B shows that a 40% reduction in τ_b decreases the response time by about 75%. However, the effect is not through an increased rate of decline of the I_A plateau, as might be expected. Rather, I_A is reduced immediately after the initial depolarization, and this allows the membrane voltage to rise to threshold much more rapidly. It appears that the major changes in excitability observed experimentally following forskolin application can be simulated by assuming a 40% reduction of τ_b. Therefore, the model indicates that the increase in excitability observed experimentally in forskolin containing saline could arise by speeding the rate of inactivation of I_A.

DISCUSSION

The experimental results presented show that I_A plays a major role in the regulation of excitability in barnacle neurons. The results from the mathematical simulation are in agreement with many of the experimental results and indicate those aspects of excitability for which I_A may be most important. The possible role of I_A in regulation of the response

time, action potential threshold, action potential repolarization, and early interspike intervals are discussed below.

Response time

Regulation of the neuronal response time is probably a major role of I_A in these neurons. This is particularly true for the long response times observed following membrane hyperpolarization, or in those neurons with normally deep resting potentials. Under these conditions a slowly depolarizing ramp trajectory leads to the first action potential following a depolarizing stimulus. During the ramp depolarization the membrane conductance initially increases, then falls to a reduced value prior to the first action potential. A small outward current (2 to 3 nA), measured under voltage clamp, decays slowly during the ramp depolarization. This current is most likely to be I_A because I_A is the only outward membrane current activated in the voltage range where the ramp trajectory is observed (-45 to -40 mV). Supporting this idea, the response time is increased in a voltage-dependent manner by prior membrane hyperpolarization, and the voltage dependence overlaps the removal of inactivation from I_A.

The magnitude of g_A activated, and the inactivation time constant, τ_b, are probably the major factors determining the response time (in addition, to the characteristics of the depolarizing I_{Na}). The importance of the inactivation time constant was demonstrated experimentally by the application of 100 μm forskolin, which reduces τ_b, and also markedly reduces the response time. Initially, the results from Ca^{2+} replacement experiments seem to be at odds with the results of the forskolin experiments. Ca^{2+}-free (Co^{2+}) saline has little effect on the response time, although similar treatment under voltage clamp reduced the peak I_A by 40 to 75%. I interpret this result as follows. Although the magnitude of peak I_A is reduced in Ca^{2+}-free (Co^{2+}) saline, the time constants are increased over the voltage range where the slow ramp depolarizations are prominent. Because of this, even though less I_A is activated, the current would decay more slowly. Therefore, this result is not inconsistent with the hypothesis that the I_A inactivation time constant governs the duration of the response time.

The standard model, as described in the Results and Appendix sections, indicates that only I_A and I_{Na} are substantially activated during the slow ramp depolarizations. With regard to the voltage trajectory and time course of the slow ramp depolarization, the model agrees reasonably with the experimental results. The model predicts that spike trains initiated from -40 mV have short response times (about 20 ms) while those initiated from more negative pre-stimulus voltages (*i.e.* -50 to -60 mV.) have longer response times which increase in a voltage-dependent manner. In addition, the model correctly predicts the reduced response time observed in forskolin experiments, based on the assumption that forskolin reduces τ_b by 40%. However, the simulated responses to long current steps from hyperpolarized pre-stimulus voltages differ in one very important aspect from the experimental results. Small 'conductance testing' current pulses show that membrane conductance is maximal at the start of the slow ramp, and that this declines as the voltage trajectory rises toward spike threshold. On the other hand, the model indicates a small conductance increase throughout the duration of the slow ramp leading to threshold. This occurs because, although I_A is declining slightly over this period, I_{Na} is increasing at a greater rate. Thus, the model predicts that an interaction of I_A and I_{Na} gives rise to the ramp trajectory, while the experimental data suggest that a decrease in I_A alone leads to an increased stimulus efficacy.

The standard model predicts the voltage wave form for a single action potential quite well (*i.e.* threshold potential, amplitude and duration). However, it is possible that the standard model is not accurate at subthreshold voltages. The values for the I_{Na} parameters around spike threshold are difficult to measure accurately under voltage clamp. At these voltages, I_{Na} increases rapidly, even for small voltage changes. I_{Na} can increase from being negligible, to several hundred nA over a 10 to 20 mV range. In addition, any small voltage discrepancy due to lack of space clamp at the I_{Na} generating regions will tend to amplify this problem. A second problem which would contribute to inaccuracy in the subthreshold region is the description of I_L used in the model. The leakage conductance is both difficult to define, and difficult to measure, the model assumes a time and voltage-independent ohmic conductance with a reversal potential of -40 mV. None of these characteristics are

likely to be strictly true. The measured leakage conductance is, in part, of ionic origin and therefore leakage channels must have time constants and voltage-dependence associated with channel opening and closing. Also, the magnitude of the measured leakage conductance probably represents the sum of the 'real' membrane ionic leakage and leakage due to impalement damage. Nevertheless, I believe that the model presented here summarizes the available data accurately, and captures the major features of the ionic currents in these neurons.

Action potential threshold

Action potential threshold was not greatly altered by treatments which change the activation or kinetics of I_A. Intuitively, it seems likely that the interaction of I_A and I_{Na} should be of major importance in the regulation of action potential threshold in these neurons. I_A and I_{Na} kinetics are more rapid, while I_K activates slowly at threshold voltages. Hyperpolarizing pre-pulses to remove inactivation from I_A did not change action potential threshold; nor did replacement of the external Ca^{2+} with Mn^{2+} or Co^{2+} shift threshold in a manner consistent with regulation by I_A. A reduction in g_A, and a slowing of activation kinetics (as are observed in Ca^{2+} replaced saline under voltage clamp), would be expected to shift action potential threshold towards more negative voltages. This would occur because of a reduction in the stabilizing affect of I_A on I_{Na}. Nevertheless, experiments in Co^{2+} or Mn^{2+} saline show that threshold is either unaffected, or shifted slightly to more positive voltages. A positive shift is more consistent with a surface charge effect on I_{Na} than with a reduction of I_{Na}. The possibility exists that any negative shift in threshold was masked by a positive shift in I_{Na}, although it seems unlikely that these two effects would be of matching amplitude. Forskolin, which reduces peak g_A by increasing the rate of inactivation also had no strong effect on threshold, supporting the conclusion that I_A is relatively unimportant in the regulation of action potential threshold in these neurons.

The negative shift in action potential threshold observed in 4-AP is likely to be a specific effect of this drug and not characteristic of a reduction of I_A. I believe this to be true because the effect was only observed in 4-AP, and not during the other treatments

which either increased or decreased I_A. This point is arguable however, as 4-AP does reduce I_A more completely than do Ca^{2+}-free solutions or forskolin. The observation that 4-AP usually altered only the threshold for the first action potential of a train is interesting, and may relate to the use-dependent aspect of 4-AP block of I_A observed by Thompson (1982) in molluscan neurons.

Simulations using the standard model indicate that action potential threshold is controlled primarily by the interaction of I_{Na} and I_A. The properties of the I_{Na} system are much more important in determining threshold however. For example, a +5 mV shift in the I_{Na} parameters shifts threshold by +4 mV, while a +5 mV shift of I_A parameters shifts threshold by less than 1 mV. Simulations in which g_{Na}, g_A and g_K were altered also indicate that the threshold potential is determined predominantly by the characteristics of the I_{Na} system.

Action potential repolarization

There is little question that I_A is important during action potential repolarization in these neurons. Action potential repolarization is faster following short hyperpolarizing pre-pulses which remove inactivation from I_A, and slower following prior depolarization. Similarly, perfusion with Ca^{2+}-free (Mn^{2+}) saline to reduce I_A, increased action potential duration and reduced the AHP. Ca^{2+}-free (Mn^{2+}) saline slowed the repolarization primarily later in the action potential, at voltages of less than about 0 mV. This was also the voltage range where the I_A activation time constant was most increased by Co^{2+} and Mn^{2+}. Forskolin, which affects primarily I_A inactivation did not alter the rate of repolarization, but reduced the following AHP. This result suggests that I_A is activating during the falling phase of the action potential and inactivating during the AHP. 4-AP slowed action potential repolarization, and the effect began early during the repolarizing phase, broadening the action potential even at the peak. This could suggest that I_A is important in governing action potential amplitude; however, as mentioned previously, it is difficult to rule out non-specific effects of 4-AP on other membrane current components as being causal to this result.

Predictions from the model indicate that I_A, by virtue of its rapid, voltage-dependent activation kinetics, is likely to be activated substantially even when action potentials are initiated from resting membrane potentials. Early in a spike train, I_A predominates, but at high action potential frequencies, and at later times in the train, I_K is more important for action potential repolarization. This finding though, is particularly biased by the values of g_A and g_K used in the simulation. Reducing I_A by one-half (to 1.3 μS) and increasing g_K two-fold (to 7.2 μS) yields predicted action potential trains in which I_K predominates throughout. It should be noted that this large change in parameter values is still within the range of values observed experimentally for g_A and g_K. Thus, while the model predicts the behavior of the 'average' barnacle neuron, this may not truly represent the characteristics of any individual neuron. It is unlikely that a given neuron will possess the mean of each of the measured parameters, and because of this, the calculated responses could differ from those obtained experimentally.

Repetitive firing

In this discussion I refer primarily to the instantaneous firing rate during the first interspike interval to avoid complications associated with membrane conductances that regulate firing rate later in a train (primarily $I_{K(Ca)}$ see below). Action potential trains initiated by depolarizing stimuli in neurons with relatively deep resting potentials accelerate while the stimulus is maintained. The experimental results are consistent with the hypothesis that membrane hyperpolarization removes inactivation from I_A, and that this effect declines with maintained depolarization. Presumably, I_A lowers the early spike frequency by adding a hyperpolarizing bias to offset the stimulus induced depolarization. The observation that the first few AHP's in an accelerating train reach more negative voltages supports the hypothesis of an increased K^+ conductance at this time.

Barnacle neurons can repetitively fire at quite low frequencies, although about 2 Hz is usually the minimum observed. In Ca^{2+}-free (Mn^{2+} or Co^{2+}) saline this minimum frequency is increased to 7 to 10 Hz. Usually Ca^{2+} replacement decreases the input resistance and/or shifts spike threshold to more depolarized voltages. Both of these effects

would tend to reduce the minimum firing frequency, exactly the opposite of the experimental result. The effect of Ca^{2+}-free (Mn^{2+} or Co^{2+}) saline was studied over a wide range of stimulus intensities and correspondingly, spike frequencies. Only in the lower range of repetitive firing frequencies (less than about 20 Hz) was the increase in excitability prominent. Therefore, it appears that the membrane current affected by perfusion with Ca^{2+}-free (Mn^{2+} or Co^{2+}) saline is important only during lower frequency repetitive firing. The previous chapter (III) provided evidence that a reduction in amplitude and slowing of I_A kinetics are major effects of this treatment. It therefore seems likely I_A is important for the regulation of low frequency repetitive firing in these neurons.

A possible problem with this interpretation is that it is difficult to rule out a contribution of the slower Ca^{2+}-dependent outward current, $I_{K(Ca)}$, even during the first interspike interval. Almost certainly, the broadening of action potentials observed in Ca^{2+}-free (Mn^{2+} or Co^{2+}) saline is due to alteration of I_A activation, because $I_{K(Ca)}$ is kinetically too slow to contribute to action potential repolarization. But later events during the interspike interval could be influenced by $I_{K(Ca)}$, even with its slower kinetics. Both the Connor and Stevens model, and the one presented here, omit $I_{K(Ca)}$ because of difficulties associated with modelling intracellular Ca^{2+} distribution and buffering. Therefore it is not possible to estimate the contribution of $I_{K(Ca)}$ through modelling. The results obtained by simulation of the effects of Ca^{2+}-free saline on I_A indicate that the changes in repetitive firing observed experimentally could result from alterations in I_A. Pharmacological elimination of $I_{K(Ca)}$ was not attempted, but may provide an experimental means of clarifying this problem.

The increased firing rate observed in 100 μM forskolin, was primarily caused by a reduction in the magnitude of the AHP. Using the model, results obtained in forskolin were simulated by assuming a 40% reduction of τ_b to be the only effect of forskolin. The calculated increase in excitability was in good agreement with the experimental result, and predicted a reduced AHP and increased spike frequency. Since I_A is activating during the action potential, and is inactivating during the AHP, increasing τ_b probably causes I_A to turn off more rapidly, at a time when it would normally add to membrane

hyperpolarization.

Comparison with the previous literature

Spike train acceleration, sometimes called "warming up" was first described in crustacean axons, by Hodgkin (1948) and later by Chapman (1966). Both studies showed, using extracellular recording, that following an anodal current pulse the spike train accelerated after an initial delay. Connor and Stevens (1971c) observed a similar phenomenon in nudibranch neurons, and proposed a mechanism by which this might occur. They suggested that removal of I_A inactivation by hyperpolarizing pre-pulses is followed by activation, then inactivation of I_A when the membrane is depolarized. The model of Connor *et. al.* (1977) based on crab axon conductances also indicates that the inactivation time constant of I_A is an important factor controlling the response time, and following acceleration of action potentials. Of these modelling studies, Byrne (1980b) has analyzed the currents which underlie the slow depolarization in most detail. His simulations show that I_A activates, and then inactivates completely during the slow rise to action potential threshold. The rate of inactivation of I_A was found to directly control the duration of the slow depolarization. The model presented here differs in that I_A reaches a plateau, so that a gradual increase in I_{Na} activation is also important in controlling the duration of the slow depolarization. The finding that forskolin decreases the response time in barnacle provides for the first time, strong experimental evidence that I_A inactivation does control the response time. In addition, the experimental data presented here show that the response time is voltage-dependent, and that this voltage dependence is probably derived from the voltage-dependent removal of I_A inactivation.

Few studies have investigated the role of I_A in the regulation of action potential threshold or in action potential repolarization. The modelling studies of Connor and Stevens (1971c), Connor et al. (1977) and Byrne (1980b) do not discuss these aspects of excitability. Segal *et. al.* (1984), have shown that in hippocampal neurons, external application of 4-AP (5 mM) blocks I_A in voltage clamp, and increases membrane excitability recorded in current clamp. Their major finding was that in the presence of 4-AP action

potential threshold was shifted to more negative potentials. However, the figure they use to illustrate this result (their Figure 3B) clearly shows that only the first action potential threshold of the single train shown is reduced, following action potentials appear to have a higher threshold than the control. Segal *et. al.* do not discuss this point. I have observed similar 'complex' effects of 4-AP on action potential trains, and attribute these to use- and voltage-dependent aspects of the 4-AP blockade of I_A channels (see Thompson, 1982). The complex interactions of 4-AP with I_A channels (and other channels) probably precludes its usefulness in current clamp studies.

MacDermott and Weight (1982) initially suggested that a Ca^{2+}-sensitive I_A contributes to action potential repolarization in bullfrog sympathetic ganglia neurons. In those neurons I_A peaks rapidly, at less than 5 ms at -10 mV, and is reduced by application of Mn^{2+}, Co^{2+}, or Cd^{2+}. The same treatment in current clamp increased action potential duration, with no obvious effect on the threshold potential. The results presented here agree with both these findings. In another study, on rat sympathetic neurons, pre-hyperpolarization removes inactivation from I_A recorded in voltage clamp, and decreases action potential duration in current clamp, providing evidence that I_A repolarizes the action potential (Belluzi *et. al.*, 1985). The experimental results using barnacle neurons, and those of the neuron simulation, also show that I_A is important during action potential repolarization. Thus it appears that in both vertebrate and invertebrate neurons I_A contributes to action potential repolarization.

Connor and Stevens (1971c) initially forwarded the hypothesis that I_A regulates low frequency repetitive firing by opposing the applied stimulus current during the interspike interval. Their empirical model showed that removal of inactivation of I_A during the spike AHP could increase I_A activation during the later part of the interspike interval. This scenario is thought to hold only for low frequency repetitive firing, because at higher frequencies the AHP does not reach such a negative voltage, and therefore does not remove inactivation from I_A. I am not aware of any experimental tests of this model. The work of Connor (1975) and Connor *et. al.* (1977) supports the earlier Connor and Stevens model indirectly by showing that the presence of I_A is correlated with the ability of crab axons to

produce action potentials at low repetitive frequencies. Axons lacking I_A had a minimum firing frequency much greater than those in which I_A was present.

The model presented here also produces low frequency repetitive firing (down to about 3 Hz), if a branch describing the behavior of I_A is included in the simulation. This agrees qualitatively with the results of the earlier I_A simulations (Connor and Stevens, 1971c; Connor *et. al.*, 1977; Byrne, 1980b). The I_A observed in barnacle neurons differs mainly in the steep bell-shaped voltage dependences of activation and inactivation, and this was included in the model. Partly as a function of this, the quantitative aspects of the behavior of the ionic currents during slow repetitive firing are different. The barnacle model emphasizes the interaction of I_A and I_{Na} during the interspike interval, rather than the decline of I_A that was reported in the earlier simulations. I am currently examining the effects of systematically shifting the parameters controlling I_A (g_A, a_∞, b_∞, τ_a, τ_b) in order to further evaluate the effect of each parameter on the interspike interval. This type of theoretical analysis may provide a basis for better understanding the varied roles of I_A in the regulation of membrane excitability.

DESCRIPTION OF THE MATHEMATICAL MODEL

For the simulations shown in the results section, the behavior of the membrane voltage as a function of time, $V_M(dt)$ was calculated from the relation,

$$dV_M/dt = (I_{stim} - I_{Na} - I_A - I_K - I_L)/C_M$$

where I_{stim} was the current used to drive the voltage response, and the membrane current components were calculated as described below. The value of C_M used was the average measured cell capacitance (1.4 nF) and dt was the integration interval used for calculations. The integration interval was pre-set at the start of a simulation to a value between 25 and 100 μs. Usually single action potentials were calculated using a 25 μs interval and long trains using a 100 μs interval. The integration was carried out using the 'simple' Euler method.

Sodium current, I_{Na}

The value of I_{Na} during the simulation, was calculated as,

$$I_{Na} = \bar{g}_{Na} m^3 h (V_M - E_{Na})$$

where $\bar{g}_{Na}$ = 25.0 μS, E_{Na} = +45 mV, and the values of m and h were calculated from the Hodgkin-Huxley squid axon values for the voltage-dependent rate constants. The initial value of m at the start of the simulation was calculated using the steady-state activation curve,

$$m_\infty = \alpha_m/(\alpha_m+\beta_m)$$

where the Hodgkin-Huxley rate constants were,

$$\alpha_m = (-0.1*(V+35+MSHFT)/(EXP(-(V+35+MSHFT)/10)-1))*NAFAC*TEMP$$

$$\beta_m = (4*EXP(-(V+60+MSHFT)/18))*NAFAC*TEMP$$

The value of the voltage shift parameter, MSHFT was +17 mV as determined by fitting to the I_{Na} activation data of Chapter II. The scaling factor NAFAC was determined to be 0.36 from the curve fit to the barnacle τ_h data. The temperature scaling factor, TEMP was set to 1.87, in order to alter the 6 °C squid axon rate constants to 12 °C. The voltage-dependent change in m with time was calculated from,

$$dm/dt = \alpha_m(1-m) - \beta_m m$$

The value of h was obtained in a manner analagous to that used for m, using the following equations,

$$h_\infty = \alpha_h/(\alpha_h+\beta_h)$$

$$\alpha_h = (0.07*EXP(-(V+60+HSHFT)/20))*NAFAC*TEMP$$

$$\beta_h = (1/(EXP(-(V+30+HSHFT)/10)+1))*NAFAC*TEMP$$

$$dh/dt = \alpha_h(1-h) - \beta_h h$$

where the value of HSHFT is +22 mV, and NAFAC and TEMP have the same values as above.

Transient potassium current, I_A

The value of I_A was calculated from the equation,

$$I_A = \bar{g}_A a^4 b (V_M - E_A)$$

where $\bar{g}_A$ = 2.5 μS, E_A = -65 mV, and the values of a and b were calculated from the steady-state activation and inactivation curves, and curves describing the time constant voltage dependences measured for I_A in chapter III. The equations used were,

$$a_\infty = (1/(1+EXP((-19-(V+ASHFT))*2.0*.041))^{1/6}$$

$$\tau_a = 2.63*(0.94/(1+EXP((-45(V+TASHFT))/12))*(1+EXP(((V+TASHFT)+37)/12))+0.06)*TAFAC$$

$$da/dt = (a_\infty - a)/\tau_a$$

$$b_\infty = (1/(1+EXP(((V+BSHFT)+53)/9))$$

$$\tau_b = 2.5*(0.96/(1+EXP((-35-(V+TBSHFT))/30))*(1+EXP(((V+TBSHFT)+32)/5.7))+0.04)*TBFAC$$

$$db/dt = (b_\infty - b)/\tau_b$$

where, in the standard model, the voltage shift parameters were set to have no effect (ASHFT = 0, BSHFT = 0, TASHFT = 0, TBSHFT = 0). The time constant scaling factors were also set to have no effect (TAFAC = 1, TBFAC = 1).

Delayed potassium current, I_K

The value of I_K was calculated from the relation,

$$I_K = \bar{g}_K n^2(V_M - E_K)$$

where $\bar{g}_K$ = 3.6 μS, E_K = -60 mV, and the value of n was calculated in a manner analagous to that used for the a. The following equations were derived from the curve fits to the I_K data presented in Chapter II,

$$n_\infty = (1/(1+EXP((6-(V+NSHFT))*2.0*0.041)))^{1/2}$$

$$\tau_n = 75*(0.98/(1+EXP((-20-(V+NSHFT))/8))*(1+EXP(((V+NSHFT)-4)/10))+0.02)*TNFAC$$

$$dn/dt = (n_\infty - n)/\tau_n$$

where, in the standard model, the voltage shift parameter NSHFT = 0, and the time constant scaling factor TNFAC = 1.

Linear leakage current, I_L

The linear leakage current was calculated from the relation,

$$I_L = g_L(V_M - E_L)$$

where g_L = 0.2 μS, and E_L = -40 mV.

V. VOLTAGE AND CALCIUM DEPENDENCE OF THE SLOW MEMBRANE CURRENT RESPONSIBLE FOR SPIKE FREQUENCY ADAPTATION

INTRODUCTION

Spike frequency adaptation, a decrease in action potential frequency in the presence of a maintained supra-threshold stimulus, is a property of many excitable cells. Generally, the spike frequency declines with a time course of a few to many seconds, to a steady-state value dependent on the stimulus intensity. It is commonly believed that adaptation during the initial part of a train, termed early adaptation, differs mechanistically from late adaptation which may take many seconds to reach steady-state (Jack *et. al.*, 1983). This study investigates primarily the mechanisms which contribute to the slow, later phase of adaptation. This slower phase of adaptation is prominent in the adaptation of barnacle neurons, although an early adapting component is also present.

Following periods of repetitive activity many neurons become hyperpolarized from their normal resting potential at the termination of the stimulus. The development of this post-stimulation hyperpolarization (PSH) is often temporally correlated with the onset of adaptation (Meech, 1974a) and is thought to reflect a slow decay of the process giving rise to adaptation. Although a variety of mechanisms have been proposed to produce slow adaptation (see Jack *et. al.*, 1983), two slowly developing membrane processes are considered to be most important in both adaptation and the generation of the following PSH. One is the activation of an electrogenic pump which produces a net hyperpolarization, the other is activation of a slowly developing K^+ conductance. The relative importance of each mechanism varies from species to species, and within neurons of the same ganglion (Jansen and Nicholls, 1973). The strongest evidence for the role of an electrogenic pump in adaptation was obtained by Sokolove and Cooke (1971) for slowly adapting stretch receptors in crayfish. They found that treatments which interfered with the activity of the Na^+-K^+ exchange pump (strophanthidin or cyanide application, perfusion with Na^+-free saline, and cooling to low temperatures) also eliminated adaptation; similar results have been obtained variety of other neurons (*e.g.* Richie and Straub, 1957; Nakajima and Takahashi, 1966;

Koketsu, 1971; Jansen and Nichols 1974). However, the PSH in molluscan neurons is thought not to be generated by an electrogenic pump, and to result instead from an increased conductance primarily to K^+ (Brodwick and Junge 1972; Partridge and Stevens, 1976; Colding-Jorgenson, 1977). The K^+ conductance has been reported to be Ca^{2+}-independent in some cases (Brodwick and Junge, 1973; Partridge and Stevens, 1976; Partridge, 1980a) and Ca^{2+}-dependent in others (Meech, 1974a; Minota, 1974; Lewis and Wilson, 1982). Of these studies, only Lewis and Wilson (1982) directly investigated the Ca^{2+}-dependence of the slow outward current and its relation to adaptation. That study provides strong evidence, using the intracellular Ca^{2+} monitor, arsenazo III, that Ca^{2+} influx activates a K^+ current responsible for adaptation in giant neurons of *Aplysia*.

Although adaptation occurs in almost all neurons the mechanisms are still not fully understood, and relatively few studies have looked at the underlying membrane current changes. It was also of interest to determine whether adaptation in crustacean ganglionic neurons is based on the activation of an electrogenic pump, as in crustacean stretch receptors, or whether the mechanism is more similar to that proposed for molluscan central neurons. This study examines the Ca^{2+}-dependence of the later slow phase of adaptation and the following PSH in barnacle neurons. The results that will be presented support the hypothesis that the development of a slow Ca^{2+}-dependent current is causal to adaptation and PSH. The Ca^{2+}- and voltage-dependence of the slow membrane current is then analyzed using the voltage clamp technique, in combination with intracellular Ca^{2+} iontophoresis.

METHODS

The methods used for extracellular perfusion, and two-electrode voltage clamp were as described previously (Chapter II). Some experiments were carried out using a third intracellular microelectrode for the iontophoretic injection of Ca^{2+}, K^+, Na^+, Cl^-, or EGTA (ethylene glycol-bis(B-aminoethyl ether)-N, N-tetraacetic acid). For Ca^{2+} iontophoresis electrodes were filled with 0.4 M $CaCl_2$, and Ca^{2+} was ejected using +10 to +50 nA current pulses. Ca^{2+} was always iontophoretically injected while cells were voltage clamped, thus avoiding any net depolarizing current flow across the membrane. A transport number of 0.3

was used to calculate the amount of Ca^{2+} iontophoretically injected. This value has been measured for glass microelectrodes filled with 0.5 mM $CaCl_2$ by Gorman and Thomas (1980). Other ions were injected in a similar manner to Ca^{2+}, after filling the injection electrode with 0.4 M KCl or NaCl. For EGTA iontophoresis, electrodes were filled with 0.5 M EGTA in distilled water, adjusted to pH 7.4 using KOH. Cells were loaded with EGTA by passing -2 to -5 nA DC current for 10 to 20 minutes. The effects of EGTA injection appeared to be irreversible, at least on the short time scale used in these experiments (20 to 40 min). When using three electrodes, there were initially capacitative coupling problems which made the voltage clamp system less stable than normal. These were overcome by shielding the voltage clamp electrodes with aluminum foil, and placing a heavy copper plate between the clamping electrodes and iontophoretic electrode. The results presented are from experiments on 29 ventral ganglionic neurons.

RESULTS

Spike frequency adaptation and post-burst hyperpolarization

All barnacle neurons tested showed spike frequency adaptation in the presence of a maintained, supra-threshold constant-current stimulus. However, the time course of the frequency decline, and the steady-state frequency attained were quite variable from cell to cell. The relative degree of adaptation was correlated with the magnitude of the PSH. Those cells that showed strong adaptation usually had the largest (most negative going) PSH. I also observed that, in general, neurons with a large soma diameter showed the most prominent adaptation and largest PSH. Although the reason for this is not clear, it was fortuitous, because these neurons were most amenable to the three microelectrode experiments described below.

As shown in Figure V-1, a depolarizing constant current stimulus given in control saline elicited an action potential train with an initially high frequency, which adapted to a lower value while the stimulus was maintained. At the termination of the stimulus the cell stopped firing and the membrane potential fell rapidly to a value several millivolts

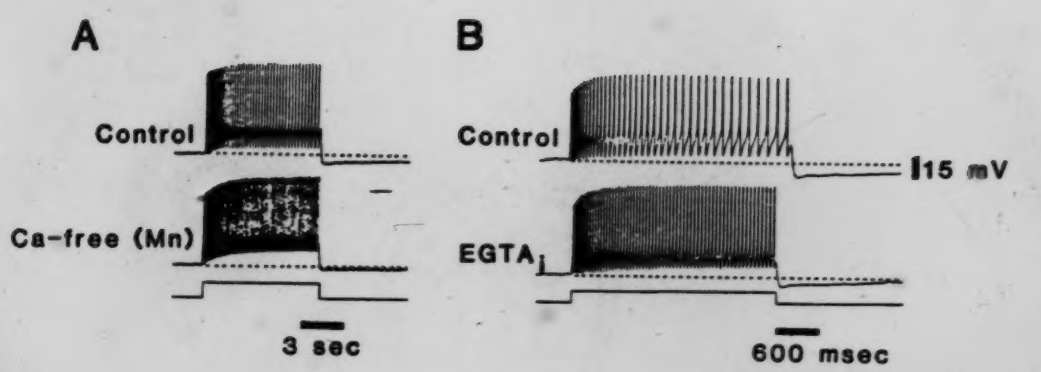

Figure V-1. Effect of Ca^{2+}-free (Mn^{2+}) saline and EGTA injection on spike frequency adaptation and PSH. A: The control spike train (upper record) initiated by a +6 nA, 8 sec stimulus, shows a characteristic decrease in spike frequency in the presence of a maintained stimulus. The adaptation is reduced after perfusion with Ca^{2+}-free (Mn^{2+}) saline for 15 minutes. The post-stimulus hyperpolarization (PSH) which followed the adapting control train was reduced from 7 mV to 1 mV in Ca^{2+}-free (Mn^{2+}) saline. The dashed line shows the resting membrane potential prior to the stimulus. B: Adaptation and the following PSH are also reduced by intracellular injection of the Ca^{2+} chelator EGTA. The PSH was reduced from 12 to 7 mV following EGTA injection. EGTA was injected iontophoretically by a -5 nA DC current pulse for 10 minutes. The action potentials were attenuated by the pen recorder (frequency response, DC to 60 Hz).

hyperpolarized to the pre-stimulus resting potential. Adapting action potential trains were always followed by a slowly declining PSH (except in the situation described below). The PSH measured in standard barnacle saline normally reached a maximum hyperpolarization of 3 to 15 mV negative to the resting membrane potential in various cells; in absolute terms this represented membrane voltages of -55 to -60 mV. In a few cells with unusually deep resting potentials (about -60 mV) the PSH was of reduced amplitude, and was smaller than the values quoted above. The characteristics of the spike frequency decrease during a maintained stimulus were not analyzed in detail because it was quite variable from cell to cell. Measured approximately the 'time constant' for the frequency decrease ranged from about 0.3 to 2 seconds. However, the frequency decline was not well fitted by a single exponential in any of the neurons studied.

Extracellular perfusion with Ca^{2+}-free (Mn^{2+}) saline, to eliminate Ca^{2+} influx from the external medium, reduced the amount of adaptation and PSH (Figure IV-1A), and both phenomena were blocked with approximately the same time course. After 3 to 5 minutes of perfusion adaptation became less pronounced, and the PSH was reduced slightly in amplitude. When the changes in spike frequency adaptation stabilized after 10 to 15 minutes of perfusion, the PSH amplitude was also stabilized. For the cell shown, the initial frequency of the control spike train was 11 Hz (averaged over the first second) and this declined to 4 Hz after 8 seconds. The adapted frequency was 36% of the initial frequency. After perfusion with Ca^{2+}-free (Mn^{2+}) saline for 15 minutes, the initial average frequency was unchanged (11 Hz), but the frequency at 8 seconds (8 Hz) was higher than in control saline. The frequency decrease due to adaptation was reduced, so that the frequency at the end of the train was 73% of the initial frequency. Therefore, about 58% of the adaptation was eliminated by perfusion with Ca^{2+}-free (Mn^{2+}) saline. Usually PSH was reduced to a very small value in Ca^{2+}-free (Mn^{2+}) saline. For the cell shown PSH was reduced from 7 mV in the control to 1 mV in Ca^{2+}-free (Mn^{2+}) saline, or about an 85% reduction.

Intracellular iontophoresis of the Ca^{2+} chelator EGTA also reduced the degree of adaptation and PSH (Figure V-1B). As was observed for perfusion with Ca^{2+}-free (Mn^{2+}) saline, both phenomena are partially eliminated with similar time courses and sensitivity.

Iontophoresis of EGTA was not as effective in eliminating adaptation and PSH as was perfusion with Ca^{2+}-free saline. However, this could result from problems associated with the iontophoretic technique, *i.e.* inability to inject sufficient EGTA to stabilize intracellular Ca^{2+}, rather than a true difference in sensitivity to the two methods of limiting the depolarization induced rise in intracellular Ca^{2+}. For the cell shown (Figure IV-1B), the control frequency at 2 seconds was 25% of the initial frequency. After injection of EGTA (-5 nA, 10 minutes) the frequency at 2 seconds was 58% that of the initial frequency. EGTA was only injected successfully in two experiments, in another cell in which EGTA was injected at -10 nA for 20 minutes, the adaptation was eliminated more completely than for the cell shown in Figure V-1B.

Perfusion with Ca^{2+}-free (Mn^{2+}) saline and iontophoresis of EGTA decrease the rate of adaptation by eliminating a hyperpolarizing influence which is active during the interspike interval and PSH. In Figure 1, it can be seen that a marked reduction of the spike after hyperpolarization (AHP) is associated with both treatments that block adaptation. Other experiments not illustrated have confirmed that adaptation and the PSH results from a 10 to 25% increase in the membrane conductance above that measured prior to the depolarizing stimulus. The PSH is inverted in polarity, *i.e.* appears as a slow post-depolarization, in 10x normal K^+ (80 mM) saline, and the PSH following a burst of action potentials reverses polarity if the membrane potential is hyperpolarized below about -65 mV. The conductance increase normally associated with PSH is reduced in Ca^{2+}-free (Mn^{2+}) saline. Therefore, it seems likely that adaptation and PSH result from a Ca^{2+}-dependent, increased conductance to K^+, as has been suggested in *Aplysia* neurons (Lewis and Wilson, 1982).

The adaptation and following PSH observed in current clamp are associated with the development of a slow outward current in voltage clamp. Figure V-2 shows the results from an experiment in which the same neuron was studied in current and voltage clamp. The short duration action potential train (500 ms) was followed by a small rapidly decaying PSH, while the long current stimulation (5 sec) produced a larger, more slowly decaying PSH. In voltage clamp the voltage command to -26 mV (the approximate mean voltage during the spike train) was associated with a slowly developing outward current. At the

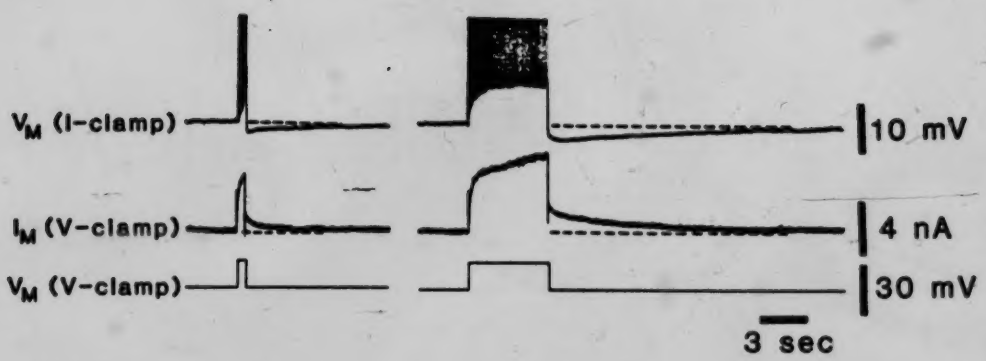

Figure V-2. Membrane current associated with spike frequency adaptation and PSH. A +10 nA stimulus in current clamp was used to elicit either a 500 ms or 5 sec spike train from the resting potential (-40 mV). The longer spike train adapted to a lower final frequency (not shown) and was followed by a large, more slowly decaying PSH. The same cell was then voltage clamped (at -40 mV) following application of 1 μM TTX. The cell was voltage clamped to -26 mV, which was approximately the mean voltage during the spike trains generated in current clamp. During the depolarizing voltage clamp step, an outward current developed slowly. At the termination of the step the membrane current decayed with a time course similar to the decay of PSH following spike trains. The outward tail current appears to result from a slow relaxation of the membrane current activated during the voltage clamp step. The decrease in the tail current parallels the return to resting membrane voltage observed in current clamp.

termination of the voltage clamp step, a slow tail current decayed with a time course similar to the decay of PSH. The magnitude and duration of the slow outward current tail was positively correlated to the duration of the depolarizing clamp step, as was the magnitude of PSH correlated to the duration of the spike train. The development and decay of the slow outward current is kinetically similar to the time course observed for adaptation and PSH.

The reversal potential for the slow outward current tail was measured in order to establish the ionic species which carries the current. However, it was difficult to measure the reversal potential accurately for the slow outward current using a standard two pulse protocol because its amplitude was quite small. Therefore the reversal potential was measured using a 'fast *I-V*' procedure which was more accurate for measuring small, slow current changes. This procedure is illustrated in Figure V-3. One *I-V* curve was run prior to a long depolarizing voltage clamp step to activate the outward current. Two hundred ms after termination of the depolarizing step, during the decay of the slow tail, another *I-V* curve ("experimental") was run. Subtraction of the two curves yielded the reversal potential for current present in the second *I-V* curve but not the first. For the two cells shown in Figure V-3 the reversal potentials for the current activated during the slow tail were -60 and -62 mV. In four cells the reversal for the slow outward current averaged -63 mV. In one cell, a 10 minute, -10 nA iontophoretic injection of Cl^- had no effect on the reversal potential of the slow tail, suggesting that the tail is not carried by Cl^-. These results provide evidence that the slow outward current, like PSH, is carried by K^+, although experiments in which the external K^+ concentration was varied were not attempted. The slow outward current and the following tail were also found to be very sensitive to external application of the K^+ channel blocker TEA, and could be eliminated by 2.5 mM TEA, which has a smaller effect on I_K in these cells. The I_A described previously is insensitive to TEA, therefore the slow outward current appears to be distinct from the other K^+ currents in these neurons.

The slow K^+ current, and associated tail current are Ca^{2+}-dependent. The Ca^{2+}-dependence of the slow K^+ current activated by long pulses, and by brief, +40 mV depolarizations is shown in Figure V-4. In control saline, long duration clamp steps (8 sec) to voltages just depolarized to action potential threshold activate the slowly developing

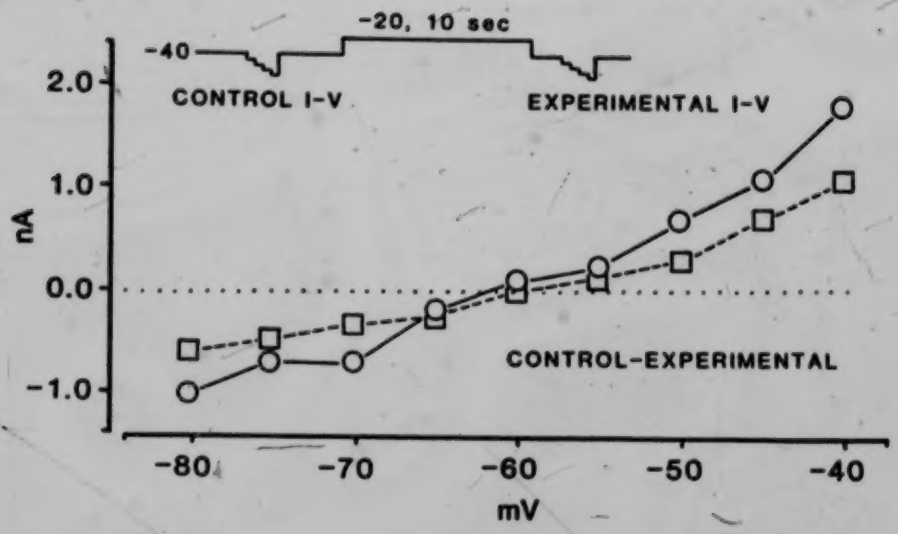

Figure V-3. Reversal potential for the slow outward current. The reversal potential for the slow outward current was measured by subtraction of *I-V* curves taken before (control) and during the slow outward current tail (experimental) generated following a 10 sec voltage clamp step to -20 mV. Fast *I-V* curves were measured by 10 ms duration voltage steps between -80 mV and -40 mV. At each test voltage the membrane current before the depolarizing voltage step was subtracted from that recorded after, during the slow tail current. The subtraction measured in this way yields an accurate measure of the current which is activated during the slow tail current. The points shown are the results of the subtraction, the circles are one cell, the squares are a different cell. In these cells the slow outward current reversed at -60 and -62 mV (intersection with the zero current line). The positive slope indicates that the conductance active during the experimental *I-V* was increasing over this voltage range. The subtraction procedure is only valid for measuring the reversal potential for currents whose relaxation time constants are much greater than 10 ms. The inset shows the voltage protocol used.

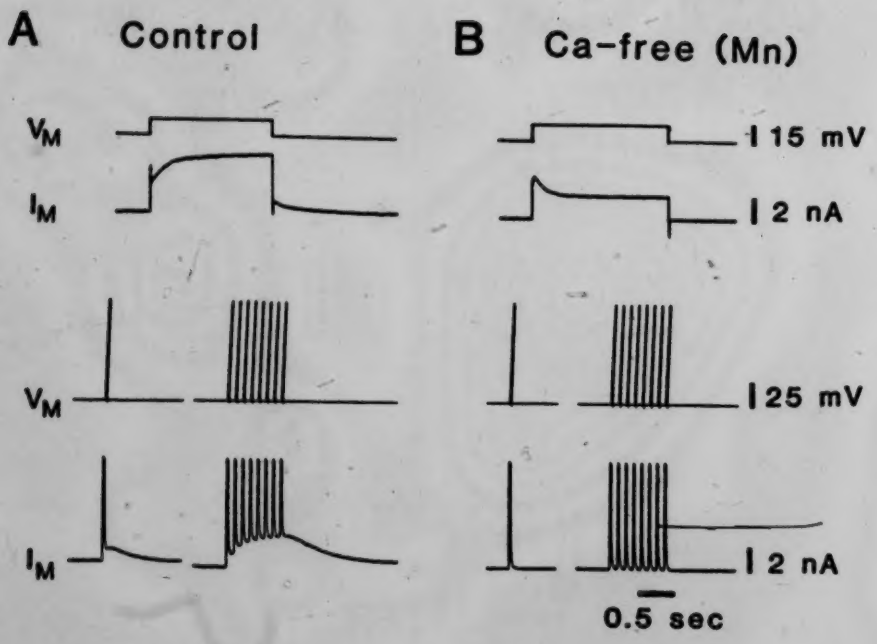

Figure V-4. Effect of Ca^{2+}-free (Mn^{2+}) saline on the slow outward current. A: The outward current activated slowly during a 1.7 sec voltage clamp step to -15 mV (top), and could also be activated by brief (10 ms) pulses to +40 mV. For the voltage pulses to +40 mV only the tail currents following the depolarizing voltage step are shown, recorded at -40 mV. When given as a 10 Hz train, the brief depolarizing pulses yielded slow tail currents which summated into a plateau. For the train of 8 pulses shown, the outward tail current summated to a maximum of +2.5 nA. The repetition frequency determined the magnitude of the outward plateau, for lower frequencies the outward current stabilized at a lower steady plateau (not shown). B: Both the slow current activated during the voltage clamp step, and the slow tail currents were abolished after perfusion with Ca^{2+}-free (Mn^{2+}) saline for 15 minutes. The outward current remaining during the long step to -15 mV is mostly linear leakage current, except for the early peak which may be I_A. The external saline contained 1 μM TTX.

current, which showed no inactivation while the clamp step was maintained. Ca^{2+}-free (Mn^{2+}) saline completely eliminated the slowly developing current, and the associated slow tail current. Brief (10 ms) voltage clamp steps to +40 mV also activated the slow outward current in this cell. The peak current was off scale, and only the slow tail current relaxations at the holding potential (-40 mV) are shown. These slow tail currents following brief depolarization took about 500 ms to decay, and because of this could summate when depolarizing clamp steps were given as a train. A train of 10 ms pulses given at 10 Hz is shown (Figure V-4, bottom), during which. the slow tail currents summated to a net plateau of about +2.5 nA. The slow tail currents, and therefore the outward summation, were eliminated by perfusion with Ca^{2+}-free (Mn^{2+}) saline.

These experiments suggest that the slow, Ca^{2+}-dependent K^+ current is responsible for the adaptation observed in current clamp. The outward current generated by depolarizing voltage pulses activates slowly, with a time course similar to the onset of adaptation. The deactivation kinetics of the outward tail current resemble the decay of PSH produced by a train of action potentials. The reversal potential for the the slow outward current (mean = -63 mV) is similar to that for PSH (about -65 mV). The slow K^+ current is activated by brief (10 ms) pulses which are similar in form to action potentials. Even though the decay of the current can take several seconds at the resting membrane potential, activation at more depolarized voltages is rapid. As a result of this, the slow current can summate to a steady plateau, which then takes many seconds to decay. This is reminiscent of the events occurring during adaptation, where after a number of action potentials, a steady frequency is maintained, and the PSH develops following stimulus removal. Finally, the slow current, adaptation and PSH are all reduced in Ca^{2+}-free (Mn^{2+}) saline, with a similar time course. These results strongly support the hypothesis that the slow outward current observed during voltage clamp is responsible for action potential frequency adaptation and PSH observed during current clamp.

The slow outward current appears to be similar to the slow Ca^{2+}-dependent K^+ current initially described in molluscan neurons by Meech and Standen (1975), and I follow their designation of the current as $I_{K(Ca)}$. I have not carried out experiments to see if the

reversal potential for the slow outward current is altered by the external K^+ level in a way consistent with its being carried predominantly by K^+. However, the reversal potential (-63 mV), sensitivity to TEA, and voltage dependence (see below) suggest that the current is carried mainly by K^+.

In the remaining part of this chapter I examine the voltage- and Ca^{2+}-dependence of the slow outward current, $I_{K(Ca)}$, which appears to underlie spike frequency adaptation in these neurons.

Activation of $I_{K(Ca)}$ by depolarizing voltage pulses

$I_{K(Ca)}$ is dependent on both Ca^{2+}- and voltage for activation. During depolarizing voltage pulses, the $I_{K(Ca)}$ activated results from the summed effect of both the Ca^{2+} and intrinsic voltage dependences. This is because in normal saline depolarizing voltage steps above about -30 mV are associated with voltage dependent activation of transmembrane Ca^{2+} flux via I_{Ca}. The measured voltage dependence of $I_{K(Ca)}$ reflects both of these controlling factors. Nevertheless, measurement of $I_{K(Ca)}$ voltage dependence by voltage pulses can be useful because it demonstrates the 'effective' voltage dependence of $I_{K(Ca)}$. $I_{K(Ca)}$ begins to be significantly activated by depolarizing voltage steps at about -30 mV, and increases in a steeply voltage dependent manner as the depolarization is increased. At minimal voltages for activation (-30 to -20 mV) $I_{K(Ca)}$ develops very slowly and the current waveform is not well described as a single exponential process. In fact, the activation time course is almost linear in some cells, and sigmoidal in others. I believe that the complex time course reflects the dynamics of submembrane Ca^{2+} distribution (Gorman and Thomas, 1980; Barish and Thompson, 1983) and thus does not represent the actual time constant associated with $I_{K(Ca)}$ gating. This point is discussed in more detail below.

Figure V-5 shows $I_{K(Ca)}$ activated by small depolarizing voltage clamp steps, within a voltage range close to action potential threshold. In this cell, $I_{K(Ca)}$ developed almost linearly with time, and showed no sign of reaching an asymptote over the 5 sec duration of the clamp steps. The decay of the deactivation tails was clearly much slower than the current onset during the depolarization, and the time to 1/2 decay was 2.5 to 3 sec at the

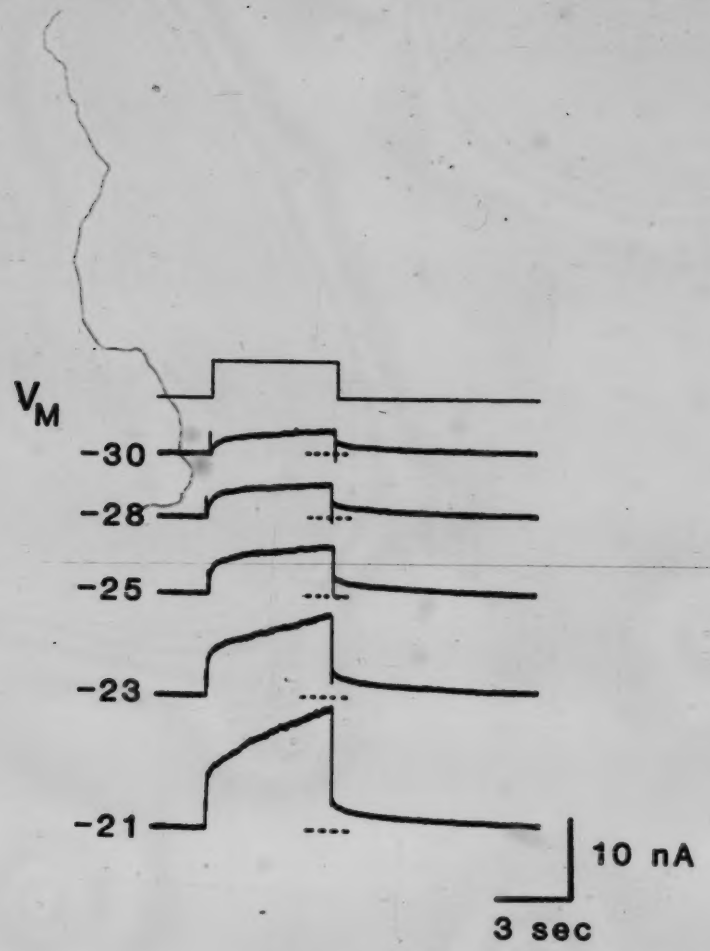

Figure V-5. Voltage dependence of $I_{K(Ca)}$ activated by long depolarizing steps. $I_{K(Ca)}$ was activated by 5 sec depolarizing steps to the membrane voltage values shown next to each record. The holding potential was -40 mV. Over this voltage range, and in the absence of a hyperpolarizing pre-pulse, there was essentially no contribution of I_K or I_A to the outward current measured. The activation of the current was slow over this voltage range, and showed no sign of having reached a asymptote for any of the voltage steps. The maintained rapid outward current deflection at the onset of the more depolarized steps probably resulted from current flowing through the membrane leakage, as it was linearly related to the magnitude of the voltage step. On the other hand, the $I_{K(Ca)}$ generated by the end of each pulse is quite voltage dependent. The increase in $g_{K(Ca)}$ over this voltage range was calculated to be *e*-fold for a 9 mV depolarization. The dashed line in each record is 0 nA. The external saline contained 1 μM TTX.

holding potential (-40 mV). The conductance developed during the depolarization increased exponentially, at a rate of approximately *e*-fold for a 9 mV depolarization. For four cells measured over the voltage range where $g_{K(Ca)}$ was most steeply voltage-dependent (-30 to 0 mV) $g_{K(Ca)}$ increased on average, *e*-fold for a 7.3 mV depolarization.

To measure the effective voltage dependence of $I_{K(Ca)}$ over a wider voltage range, one of two methods can be used. At membrane voltages above about -10 mV I_K begins to be activated significantly and this makes it difficult to measure the smaller, slower $I_{K(Ca)}$. To measure $I_{K(Ca)}$ during the voltage clamp step, depolarizing clamps in control and Ca^{2+}-free saline can be subtracted to measure the voltage dependence of $I_{K(Ca)}$. An example of this method of isolating $I_{K(Ca)}$ was shown in Figure II-13 (chapter 2). This type of analysis is time consuming and can be complicated by the surface potential effects discussed in Chapter III. In addition, the subtraction records are contaminated by I_{Ca}, which is also eliminated in Ca^{2+}-free saline and shows up in the subtraction record. To avoid these problems, I have investigated the voltage dependence of $I_{K(Ca)}$ using analysis of the slow tail currents. The decay time constants for $I_{K(Ca)}$ current tails at -40 mV range from approximately 0.4 to 1.3 sec and are therefore 50 to 200x slower than I_K or I_A tails. (I_{Ca} and I_{Na} tails are a least an order of magnitude faster than I_K or I_A). Therefore, measurements of the outward $I_{K(Ca)}$ tails taken at 100 ms after the depolarizing pulse should be free from contamination by other membrane current components. Figure V-6 shows the slow $I_{K(Ca)}$ tail currents which follow 500 ms depolarizing commands. In this and the following figures, $I_{K(Ca)}$ tail currents were measured at the holding potential of -40 mV. In control saline $I_{K(Ca)}$ tail currents increased with voltage steps up to about 0 mV, above this the peak tail current amplitude began decrease. Generally no $I_{K(Ca)}$ tails could be measured for depolarizations above +60 mV. In the cell shown, the tail current amplitude was maximal for the 0 mV command. Figure V-6 also emphasizes an important aspect of this type of analysis: the slow $I_{K(Ca)}$ tails were eliminated in Ca^{2+}-free (Mn^{2+}) saline. Therefore, the tail current measurements were not contaminated by other slow Ca^{2+}-independent processes.

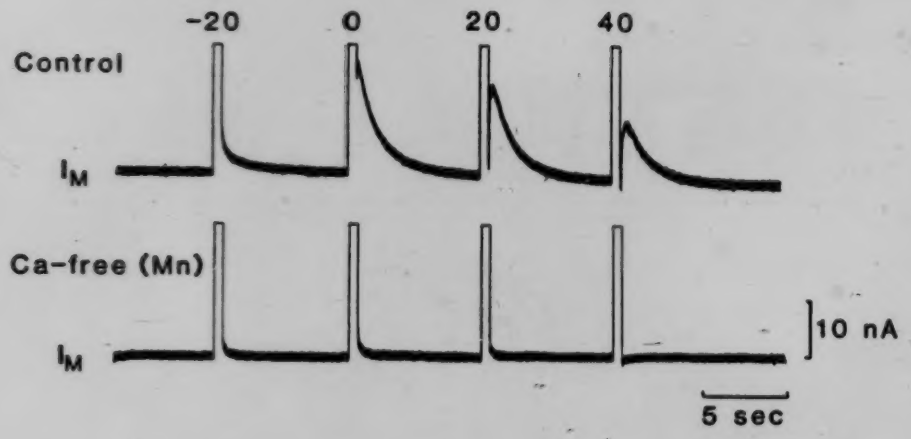

Figure V-6. Voltage and Ca^{2+} dependence of $I_{K(Ca)}$ decay tails. The outward $I_{K(Ca)}$ decay tails were measured at -40 mV following 500 ms depolarizing voltage clamp steps to -20, 0, +20, and +40 mV (top trace). The tail current amplitude was maximal following the step to 0 mV (19.5 nA), and was reduced by further depolarization. The slow $I_{K(Ca)}$ tails are abolished in Ca^{2+}-free (Mn^{2+}) saline (lower trace). For the voltage steps up to +20 mV in Ca^{2+}-free (Mn^{2+}) saline a small rapid tail current remained, which probably represents I_K de-activation. The tail current following the 500 ms step to +40 mV was slightly inward, and could reflect a shift in perineuronal K^+ concentration during long depolarizations. That is, outward movement of K^+ may raise the perineuronal concentration of K^+ enough to shift the I_K reversal potential to a value depolarized to -40 mV. The external saline contained 1 μM TTX.

The time course of the de-activation tail currents was quite variable from cell to cell. In some cells the $I_{K(Ca)}$ tails were fitted quite well as a single exponential decay, however there was often a much smaller, more slowly decaying component which decreased very slowly. This small component was not analyzed in detail because its amplitude was beyond the minimum resolution of the current monitoring system. For the cell shown in Figure V-6, the early decay of the tail currents was well fitted as a single exponential over the voltage range studied ($r^2 > 0.98$ when fitted as a single exponential decay). The time constant increased from 0.72 sec at -20 mV to 1.21 sec at +40 mV. This trend was consistent amongst the cells which were analyzed, the decay time constant increased with depolarization ($n = 4$).

Most of the effective voltage dependence of $I_{K(Ca)}$ is derived from the voltage dependence of transmembrane Ca^{2+} flux through I_{Ca} channels. Figure V-7 shows the voltage dependence of $I_{K(Ca)}$, measured from tail currents (circles) and the voltage dependence of I_{Ca} measured in the same cell (squares). The overlap of the two curves indicates that the effective voltage dependence of $I_{K(Ca)}$ is regulated by the voltage dependence of I_{Ca}. The similarity of the two curves also suggests that there is a linear relationship between I_{Ca} and the activation of $I_{K(Ca)}$. Since the tail currents were measured at -40 mV, and the $I_{K(Ca)}$ reversal potential was -64 mV in this cell, the maximal $g_{K(Ca)}$ was 396 nS assuming an ohmic conductance. In three cells the peak $g_{K(Ca)}$ (usually at +10 mV) activated by 500 ms voltage steps ranged 205 to 780 nS. The conductance values measured do not represent the maximal $g_{K(Ca)}$ obtainable, because longer voltage clamp steps appeared to increase the intracellular Ca^{2+} concentration further. In some cells, $g_{K(Ca)}$ was still increasing after 20 sec clamp steps to +10 mV, suggesting that there was still Ca^{2+} influx. Even for these long clamp steps, $I_{K(Ca)}$ tails were not observed to decline in amplitude and therefore $I_{K(Ca)}$ appears to show little, if any, inactivation.

Activation of $I_{K(Ca)}$ by Ca^{2+} iontophoresis

The preceding experiments have shown that with depolarizing voltage clamp steps, much of the voltage dependence of $I_{K(Ca)}$ is correlated with depolarization induced Ca^{2+}

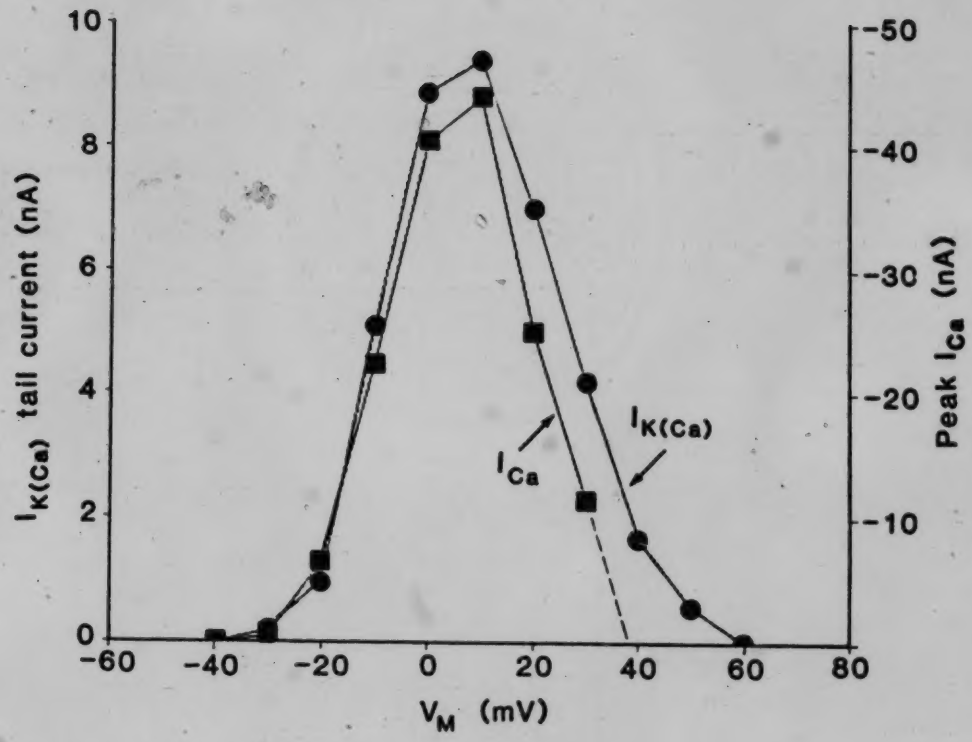

Figure V-7. Voltage dependence of $I_{K(Ca)}$ tail current and peak I_{Ca}. The circles show the bell-shaped dependence of $I_{K(Ca)}$ tail currents on membrane voltage. The tail currents were measured as the peak amplitude following 1 sec depolarizing voltage clamp steps to the values of V_M shown. After measuring the tail currents the cell was perfused with external saline containing 1μM TTX, 100 mM TEA and 1 mM 4-AP, to abolish inward I_{Na} and as much of the outward current as possible. Under these conditions, the membrane current recorded is mostly I_{Ca}, except for a small degree of contamination by residual outward currents. The voltage dependence of I_{Ca} measured under these conditions is shown as the squares. I_{Ca} is plotted so that inward current is upward for comparison with the $I_{K(Ca)}$ data. Up to 0 mV the similarity of the two curves is striking, and indicates that I_{Ca} is a major determinant of the $I_{K(Ca)}$ voltage dependence. For the more depolarized voltages, the I_{Ca} curve deviates from symmetry with $I_{K(Ca)}$, presumably because of contamination of the I_{Ca} records by residual unblocked outward currents.

influx. The following experiments were undertaken to further evaluate the activation of $I_{K(Ca)}$ under conditions of controlled Ca^{2+} influx.

Iontophoretic injection of Ca^{2+} at the holding voltage of -40 mV activated an outward current which developed slowly over several seconds to a transient peak and then declined (insets to Figure V-8). Iontophoretic injection of similar amounts of Na^+, K^+, or Cl^- had no effect on the membrane current. At -40 mV, the current was activated with a time constant of approximately 2 to 3 seconds, and decayed after a transient peak with time constants of 4 to 6 seconds. As was observed for $I_{K(Ca)}$ tail currents, there was a smaller, very slowly decaying phase which was not analyzed in detail.

The peak outward current activated was a function of the intensity and duration of the iontophoretic Ca^{2+} injection. Figure V-8A shows the results of Ca^{2+} injection at the holding voltage (-40 mV). The amount of Ca^{2+} injected was linearly related to the peak $g_{K(Ca)}$ activated. Different amounts of Ca^{2+} were injected either by varying the intensity of the injection for a fixed time period (squares) or by varying the duration of Ca^{2+} injection at a fixed intensity (circles). For the range of Ca^{2+} injections shown there was reasonably good linearity for either method of increasing the internal Ca^{2+} concentration. The slope of the line describing the data in which intensity was varied is 8.7 nS/nC, and for variable duration is 6.9 nS/nC. Neither line passes through the origin, indicating that a small amount of Ca^{2+} must be injected to prime the conductance. This offset may measure the amount of injected Ca^{2+} which is sequestered before reaching the inner membrane surface where binding to the channel occurs. Larger Ca^{2+} injections eventually produced a saturation of $g_{K(Ca)}$, so the true form of the function is probably sigmoidal, and the linear relation over this Ca^{2+} injection range could be fortuitous. For seven cells tested at -40 mV, the average sensitivity to Ca^{2+} injections in the linear range was 4.4 nS/nC of charge injected (assuming the average measured reversal for $I_{K(Ca)}$ elicited by Ca^{2+} injection is -66 mV, see below). Equivalently, 170 nA of $I_{K(Ca)}$ was activated per μC of charge. The insets show partial raw data equivalent to each of the data sets.

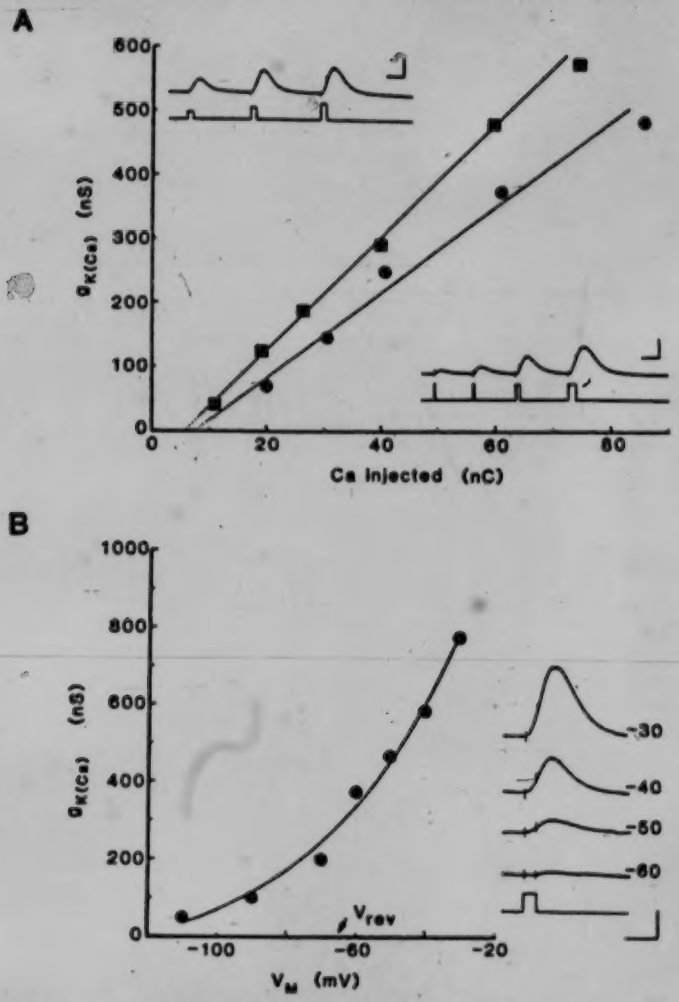

Figure V-8. Sensitivity of $g_{K(Ca)}$ to injected Ca^{2+}, and intrinsic voltage dependence of $g_{K(Ca)}$. A: The outward current activated by iontophoretic injection is linearly related to the intensity of Ca^{2+} injected. The x-axis is the total charge passed during iontophoresis, in nC. The squares show the peak $g_{K(Ca)}$ activated by increasing the intensity of the injection current (from 5 nA to 34 nA) maintaining a fixed duration (2.5 sec). The sensitivity of $g_{K(Ca)}$ to Ca^{2+} injection was less if similar amounts of Ca^{2+} were injected by increasing the duration of the injection (circles). The insets show part of the corresponding raw data, upper inset is the data for increasing intensity, the lower is the data for increasing the duration of the injection. The scale bars in the insets are 7.5 sec, 5 nA (I_M), and 35 nA (iontophoretic current). The values of $g_{K(Ca)}$ were calculated using the observed reversal potential of -64 mV. B: The $g_{K(Ca)}$ activated by injection of a Ca^{2+} at a fixed intensity is intrinsically voltage dependent. A 125 nC injection intensity was used to activate $g_{K(Ca)}$ at membrane holding potentials between -110 mV and -10 mV. Over this voltage range $g_{K(Ca)}$ increased e-fold for a 28.0 mV depolarization. The values for $g_{K(Ca)}$ were calculated using the measured eversal potential of -65 mV. The inset shows partial raw data at holding potentials from -60 mV to -30 mV. The scale bars in the inset are 7.5 ms, 10 nA (I_M), and 75 nA (iontophoretic current). The data shown in A and B are from different cells, both of which were bathed in Ca^{2+}-free (Mn^{2+}), 1 μM TTX saline.

The amount of Ca^{2+} iontophoretically injected (M) was estimated from the relation

$$M = nit/zF \qquad \text{(V-1)}$$

where n is the transport number for Ca^{2+} ($\simeq 0.3$, for glass microelectrodes, refer to Gorman and Hermann, 1979), i is the injection current, t is the duration of the injection, z is the valence (2 for Ca^{2+}), and F is the Faraday constant. This estimation assumes that the intracellular Ca^{2+} concentration is infinitely small compared to that of the electrode. Calculated in this way, the amount of Ca^{2+} injected for the data shown in Figure V-8A ranged from 15 fM (10 nC) to 120 fM (80 nC), and the equivalent slope sensitivities would be 5.8 nS/fM and 4.6 nS/fM respectively.

The peak $g_{K(Ca)}$ was also intrinsically dependent on membrane voltage, when measured at various holding voltages with a fixed amount of Ca^{2+} injected (Figure 8B). In this experiment, a 38 nC injection was given at holding voltages between -110 mV and -10 mV (cell bathed in Ca^{2+}-free (Mn^{2+}) saline). The same Ca^{2+} injection activated $g_{K(Ca)}$ more at depolarized membrane voltages. The best fit single exponential curve describing the voltage dependence had a slope of an e-fold increase in $g_{K(Ca)}$ per 28.0 mV depolarization. The inset shows the raw data for 4 of the test voltages, and illustrates the strictly voltage-dependent portion of the activation of $I_{K(Ca)}$. For four cells the mean slope was an e-fold increase in $g_{K(Ca)}$ per 23.7 mV depolarization. Note that a number of the Ca^{2+} injections were made at voltages negative to the reversal potential (-64 mV), therefore $I_{K(Ca)}$ was inward at these voltages. For four cells the average reversal potential for $I_{K(Ca)}$ elicited by Ca^{2+} injection was -66 mV.

The average voltage-dependent increase in $g_{K(Ca)}$ activated by depolarizing voltage clamp steps was an e-fold increase in $g_{K(Ca)}$ for a 7.3 mV depolarization, while that for fixed charge Ca^{2+} injections was 23.7 mV. Therefore, voltage-dependent Ca^{2+} influx via I_{Ca} channels accounts for about 70% of the effective voltage-dependence of $g_{K(Ca)}$. Because of this, the amount of $I_{K(Ca)}$ activated in a given cell during will be strongly influenced by the magnitude of I_{Ca}, even if the density of $I_{K(Ca)}$ channels was similar in different cells.

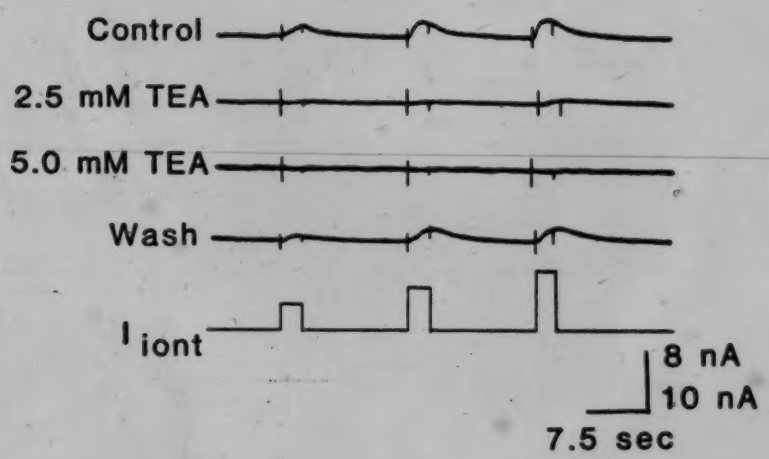

Figure V-9. Effect of external TEA on $I_{K(Ca)}$ activated by Ca^{2+} injection. In this cell the TEA sensitivity of $I_{K(Ca)}$ was investigated using iontophoretic injection of Ca^{2+} at -40 mV. The records were taken in control saline, and in 2.5 mM TEA (after 5 minutes), 5.0 mM TEA (5 minutes), and after a 5 minute wash in control saline. $I_{K(Ca)}$ was decreased rapidly even in 2.5 mM TEA, and most of the outward current was blocked after 5 minutes. 5 mM TEA completely abolished the Ca^{2+}-activated outward current. The effect was partially reversible after a 5 minute wash, and a longer wash may have allowed for a more complete reversal. Cell bathed in normal barnacle saline.

The $I_{K(Ca)}$ activated by Ca^{2+} iontophoresis was extremely sensitive to externally applied TEA (Figure V-9). 2.5 mM TEA blocked over 90% of the outward current activated at -40 mV by Ca^{2+} iontophoresis. Increasing the TEA concentration to 5 mM completely abolished the outward current. The blocking effect was removed by a 5 minute wash in normal saline, suggesting that TEA blocks $I_{K(Ca)}$ by binding at a site accessible from the outer surface of the membrane. This result was obtained from a single trial and the concentration effects quoted could vary with a larger sample size. Data from a single trial are included on the justification that the success rate for healthy three microelectrode impalements with these small cells was quite low.

The previous figures (V-8 and V-9) have shown that $I_{K(Ca)}$ is activated transiently by short Ca^{2+} injections. It was of interest to know whether the transient nature of this response represents a true inactivation of $I_{K(Ca)}$, or whether it is a reflection of the rise and fall of the submembrane Ca^{2+} concentration. I attempted to evaluate this by using very long, high intensity Ca^{2+} injections which could be expected to produce relatively high, stable intracellular Ca^{2+} concentrations. The results from one such experiment are shown in Figure V-10. Initially, a short, high intensity injection was used activate I_{Ca} near maximally at the -40 mV holding potential. This was followed by a long injection pulse at the same intensity. One might expect this protocol to generate a much longer lasting $I_{K(Ca)}$. However, the Ca^{2+}-activated current was still transient, even for very long injections, and the current decayed only slightly more slowly than was observed for the short duration injection. As shown in Figure V-10, a following second short duration injection elicited a similar $I_{K(Ca)}$ wave form, suggesting that the long injection did not produce any long term alteration of Ca^{2+} sensitivity. It appears that the time-course of the $I_{K(Ca)}$ generated is independent of the duration of the Ca^{2+}-injection. Unfortunately, in these experiments, it is still not possible to determine whether the relatively fixed $I_{K(Ca)}$ decay results from a constant time course for intracellular Ca^{2+} sequestration or whether $I_{K(Ca)}$ shows true inactivation in the presence of high Ca^{2+} concentrations. Other studies have reported that $I_{K(Ca)}$ was reduced or completely inhibited following long duration Ca^{2+} injections (Hermann and Hartung, 1982), but I saw no evidence of this, and in several cells $I_{K(Ca)}$ appeared to be slightly

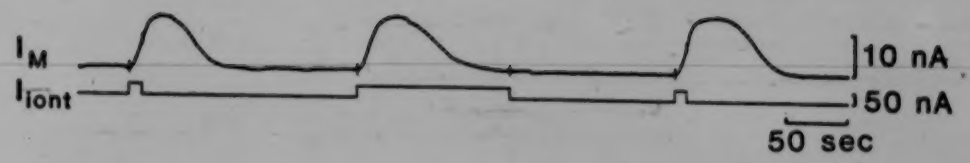

Figure V-10. Effect of prolonged high intensity Ca^{2+} injection on $I_{K(Ca)}$. In this experiment, a short, high intensity Ca^{2+} injection (10 sec, 50 nA) was given while the cell was voltage clamped at -40 mV. The $I_{K(Ca)}$ generated was compared to that produced during a long, high intensity injection (120 sec, 50 nA). The $I_{K(Ca)}$ reached the same amplitude and decayed with a similar time course during the maintained injection. Another short test pulse given after the long pulse showed that the sensitivity to Ca^{2+} injection was unaltered. Cell bathed in Ca^{2+}-free (Mn^{2+}), 1 μM TTX saline.

facilitated after long injections.

Effect of Ca^{2+} injection on adapting spike trains

The results presented previously suggest that spike frequency adaptation in these neurons is produced by the development of a slow voltage- and Ca^{2+}-activated membrane current, $I_{K(Ca)}$, during the spike train. Part of the evidence for these conclusions is indirect, and involves extrapolation of voltage clamp results to the current clamp situation. The following experiments support the above hypothesis more directly by showing that injection of femto molar quantities of Ca^{2+} during action potential trains greatly augments the degree of adaptation in these neurons.

Experiments to evaluate the effects of Ca^{2+} injection during current clamp were carried out using a three-electrode technique. Cells were penetrated with one 3 M KCl electrode to monitor cell voltage, and two current-passing electrodes. One current electrode was filled with 0.4 M $CaCl_2$, the other with 0.4 M KCl and each was connected to a separate current clamp amplifier with the output current matched to ± 0.1 nA. A manually operated switch allowed either electrode to be selected for current passing. In this manner, the depolarizing current used to elicit spike trains was associated with either increased K^+ influx (KCl electrode) or increased Ca^{2+} influx ($CaCl_2$ electrode). Control (K^+ influx) and augmented Ca^{2+} spike trains could then be compared directly in the same neuron. Control and augmented Ca^{2+} stimulations were alternated to correct for the possibility of intracellular Ca^{2+} buildup.

The results for two current clamp Ca^{2+} injection experiments are shown in Figure V-11. Spike trains generated by depolarizing current pulses carried by K^+ (KCl electrode) were compared to those carried by Ca^{2+} ($CaCl_2$ electrode) and which have augmented Ca^{2+} influx. For both cells shown the initial frequency at the start of the train did not differ for the KCl and $CaCl_2$ electrodes, but the decline in spike frequency was much more pronounced when the train was accompanied by an augmented increase in intracellular Ca^{2+}. The amount of Ca^{2+} necessary to produce this effect was very small; for the cell in A approximately 15 fM of Ca^{2+} was injected and 38 fM for the cell in B. It should be noted

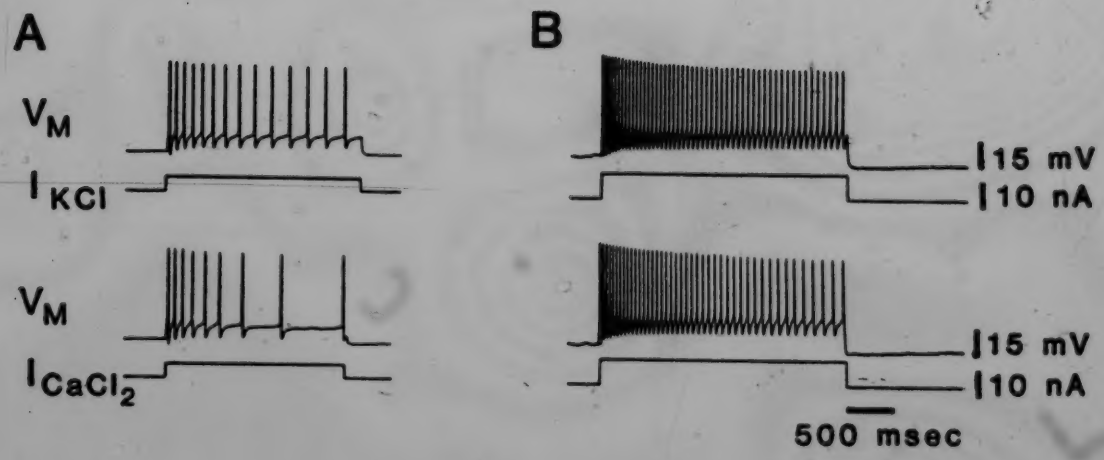

Figure V-11. Effect of Ca^{2+} injection on frequency adaptation in current clamped spike trains. In this experiment, spike trains elicited by KCl and $CaCl_2$ electrodes were compared using the three electrode technique described in the text. The results shown are from two different cells (A and B). In both cases the spike train driven with the $CaCl_2$ electrode showed substantially more adaptation. The same result was observed for all trials on these cells, and at a variety of stimulation currents (more than 20 trials for each cell). The records shown were obtained using a +5 nA, 2 sec stimulus in A and a +10 nA, 2.5 sec stimulus in B, and show that augmented Ca^{2+} influx increased for both low frequency and higher frequency adaptation. The initial frequency at the onset of the stimulus did not differ between electrodes.

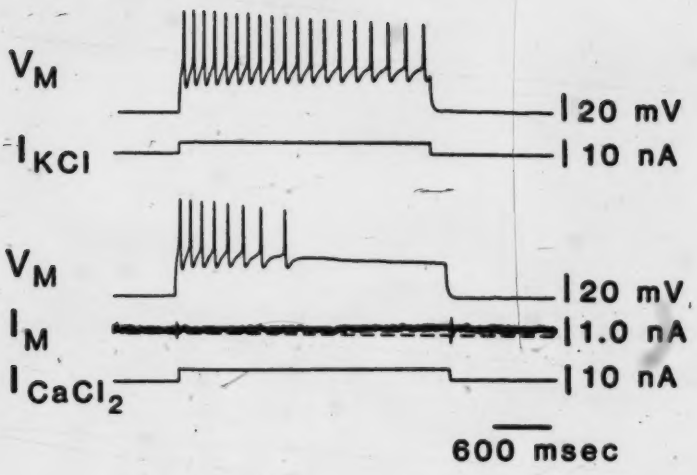

Figure V-12. Measurement of $I_{K(Ca)}$ activated by Ca^{2+} injection during an action potential train. The upper V_M trace shows the voltage response elicited by a +4 nA stimulus using a KCl electrode. The lower V_M trace shows the same stimulus with increased Ca^{2+} influx produced by passing current with a $CaCl_2$ electrode. In this cell repetitive firing was inhibited by this intensity of Ca^{2+} injection. The trace marked I_M shows the membrane current elicited by the same Ca^{2+} injection in voltage clamp at a holding voltage of -35 mV, which was approximately the value of V_M during the interspike interval. The amount of $I_{K(Ca)}$ activated by the Ca^{2+} injection was about 0.3 to 0.4 nA, although this may be an underestimate, for the reasons discussed in the text.

that there was already some adaptation present in both cells, in the absence of Ca^{2+} injection, so this measure reflects the amount of Ca^{2+} which produced the increase in adaptation. Assuming that the neuron volume can be approximated as a sphere of the same diameter as the soma (about 50 μM in these cells), and that none of the injected Ca^{2+} is sequestered, the internal Ca^{2+} concentration would have reached approximately 0.22 mM for the cell in A, and 0.55 mM for the cell in B. This value initially seems very high; however, Ca^{2+} is almost certainly sequestered during the injection, and the real submembrane Ca^{2+} concentration increase at the inner side of the membrane would be much lower than this. These values represent the absolute maximum Ca^{2+} concentration that would be associated with the injections. Qualitatively similar effects were obtained in seven cells using this technique. The major difference between cells studied was in the amount of Ca^{2+} needed to produce a change in adaptation. Cells with less pronounced adaptation in the control needed larger Ca^{2+} injections to obtain the same degree of adaptation. These results suggest that $I_{K(Ca)}$ is not activated maximally by Ca^{2+} influx via I_{Ca} during normal spike trains.

An advantage of the three-electrode technique is that the magnitude of outward current generated by Ca^{2+} injection during the spike trains produced with the Ca^{2+} electrode could be measured. The electronic feedback was switched to voltage clamp mode between the two KCl electrodes, and the same Ca^{2+} injection (intensity and duration) repeated. In these experiments, the voltage was clamped to a value which approximated the average membrane potential during the interspike interval in current clamp. This was generally about -35 to -40 mV. Figure V-12 shows the result for an experiment in which the Ca^{2+} injection augmented adaptation to such a degree that repetitive firing was inhibited. This represents a major alteration of the action potential output of this cell. The $I_{K(Ca)}$ activated by the Ca^{2+} injection was only 0.3 to 0.4 nA. The $I_{K(Ca)}$ activated during the injection was measured at a holding potential of -35 mV, and may slightly underestimate the $I_{K(Ca)}$ activated by the same injection while in current clamp, because of the voltage increase during the action potentials. However, it is remarkable that this small amount of outward current is capable of producing a large change in the neuronal output. For the cells shown in Figure V-11, the augmented adaptation in A was produced by approximately 0.3

nA of $I_{K(Ca)}$, and that in B by 0.6 nA of $I_{K(Ca)}$. Clearly, small Ca^{2+}-activated membrane currents can have pronounced effects on membrane excitability during the interspike interval.

DISCUSSION

I have examined the Ca^{2+} dependence of spike frequency adaptation observed in barnacle neurons. Both adaptation and the following post-stimulus hyperpolarization (PSH) are reduced under conditions which limit the rise in intracellular Ca^{2+} during a spike train (replacement of external Ca^{2+} with Mn^{2+}, or injection with EGTA). Adaptation is also reduced by similar treatments in *Aplysia* giant neurons (Lewis and Wilson, 1982) and crayfish stretch receptors (Ottoson and Swerup, 1982). The PSH following a burst of action potentials has been shown to be Ca^{2+}-dependent in a variety of neurons in which adaptation was not specifically studied (*e.g.* North, 1973; Meech, 1974a; Minota, 1974; Brown and Griffith, 1983; Hirst *et. al.*, 1985). Therefore, Ca^{2+}-dependent spike frequency adaptation is probably a widespread phenomenon. However, French (1986) reports that adaptation in a cockroach mechanoreceptor is unaffected by the external application of Co^{2+} or Cd^{2+}, although the hyperpolarization following impulses is eliminated under similar conditions (French, 1985). Thus, there does appear to be several independent mechanisms involved in the adaptation process in different types of neurons. The possibility of a relatively smaller contribution by an electrogenic pump still needs to be analyzed. In barnacle neurons, Ca^{2+}-free Mn^{2+} saline blocks most, but not all, of the adaptation and this suggests that another Ca^{2+}-independent process may also be involved in adaptation.

The slow outward current observed in voltage clamp is likely to produce the frequency decline observed in current clamp. The time course of development of the slow outward current is reminiscent of the time course of the onset of adaptation, although this is difficult to show directly because voltage clamp measures only development of the slow current in the steady-state. Repetitive, brief (10 ms) depolarizations to +40 mV activate the outward current significantly, suggesting that it could be activated during action potential trains. The decay of the slow outward current tail at the end of a depolarizing voltage clamp step is similar to the decay of the PSH. The slow outward current and PSH both

appear to be carried mainly by K^+. Finally, conditions which block Ca^{2+} influx reduce both the slow outward current and PSH. Augmented Ca^{2+} influx by Ca^{2+} iontophoresis increases the slow outward current and increases the degree of adaptation during spike trains. Therefore, I conclude that the slow Ca^{2+}-dependent outward current progressively develops and adds a hyperpolarizing bias during the interspike interval, producing the spike frequency adaptation observed in current clamp.

Relatively few studies have investigated the characteristics of membrane currents underlying adaptation. Partridge and Stevens (1976) have shown that in molluscan neurons a K^+ current develops with a slow, exponential time course (τ = 0.5 to 2.0 sec) and produces a decline in spike frequency. However, this current was reported to be Ca^{2+}-insensitive and therefore differs from the one I have described. My results are probably most similar to those reported by Lewis and Wilson (1982) in *Aplysia* giant neurons, where both adaptation and the development of a "hyperpolarizing post-stimulus current" are Ca^{2+}-dependent. In both barnacle neurons and *Aplysia* neurons the Ca^{2+}-dependent membrane current appears to be carried mainly by K^+.

Most of the evidence suggests that the slow Ca^{2+}-dependent outward current which I have described in barnacle neurons is analagous to the membrane current originally called $I_{K(Ca)}$ (Meech and Standen, 1975) or I_C (Thompson, 1977) in molluscan neurons. I prefer the $I_{K(Ca)}$ nomenclature because it is traditional to use I_C instead to designate the non-ionic current flowing through the membrane capacitance. In this discussion of the characteristics of $I_{K(Ca)}$ I refer primarily to those studies in which $I_{K(Ca)}$ was specifically activated by intracellular Ca^{2+} injection, because there is a high degree of ambiguity in studies which activate $I_{K(Ca)}$ indirectly via I_{Ca}.

In barnacle neurons there appeared to be a linear relationship between the $I_{K(Ca)}$ activated and the amount of Ca^{2+} injected. Expressed as current activated per unit of charge iontophoresed, the average sensitivity was 170 nA/μC at -40 mV. A similar linear relationship has been reported for other neurons, although the sensitivity varies between species (*Aplysia*, 8 nA/μC, Gorman and Hermann, 1979; *Helix*, 38 nA/μC, Hermann 1982;

Periplaneta (cockroach), 170 nA/μC, Thomas, 1984). The range of sensitivity appears to reflect cell volume differences; the *Aplysia* neurons studied were the largest (400 μm diameter) and the cockroach neurons were the smallest (50 μm diameter). The cause of the apparently linear relationship between Ca^{2+} injected and $g_{K(Ca)}$ activated has been the subject of some controversy. Gorman and Thomas (1980) initially suggested that this relation provides evidence that there is 1:1 binding of Ca^{2+} to $I_{K(Ca)}$ channels during activation. However, as pointed out by Thomas (1984) it is probably not correct to imply too much about stoicheiometry from these findings. Most single channel studies of $I_{K(Ca)}$ find a second order relationship between Ca^{2+} concentration and channel open time (Barrett *et. al.*, 1981; Auerbach and Sachs, 1984).

The Ca^{2+}-activated conductance, $g_{K(Ca)}$ is also intrinsically voltage-dependent when activated by a fixed Ca^{2+} injection at different holding voltages. The average for four cells was an *e*-fold increase in $g_{K(Ca)}$ for a 23.7 mV depolarization. This is very similar to the voltage dependence reported for molluscan neurons, where there is an *e*-fold increase in 25 to 31 mV (Gorman and Thomas, 1980; Hermann and Hartung, 1982). Thomas (1984) also found voltage dependences of an *e*-fold increase in $g_{K(Ca)}$ in 28 and 38 mV for two cells in the cockroach metathoracic ganglion. Thus the results seem fairly consistent amongst the data reported for invertebrate neurons. In one report of Ca^{2+} injections under voltage clamp in vertebrate neurons (bullfrog sympathetic neurons, Adams et al. 1982b) the sensitivity appears to be much higher, with $g_{K(Ca)}$ increasing *e*-fold in 11 mV. However, the calculations of Adams *et. al.* use an approximate measure of E_K, rather than measuring the actual reversal potential for $I_{K(Ca)}$, to calculate $g_{K(Ca)}$. The results from several studies have confirmed that the reversal of $I_{K(Ca)}$ is slightly depolarized to the thermodynamic E_K, probably because the channel is not totally K^+ selective (*e.g.* Gorman and Herman, 1979). Thus the slope of the voltage dependence calculated by Adams *et. al.* may be too steep, and might not represent a true deviation from the results obtained for the invertebrate species.

As mentioned above, the average voltage dependence of $g_{K(Ca)}$ activated by Ca^{2+} injections in barnacle neurons is an *e*-fold increase for a 23.7 mV depolarization. However, the 'effective' voltage dependence of $g_{K(Ca)}$ activated by depolarizing voltage steps in the

presence of an inward Ca^{2+} current is an *e*-fold increase for a 7.3 mV depolarization (over the -30 to 0 mV range). Therefore, most of the effective voltage dependence of $g_{K(Ca)}$ is obtained indirectly by voltage-dependent Ca^{2+} influx via I_{Ca} channels, or possibly by voltage-dependent release from intracellular stores. The fact that the voltage dependence of $I_{K(Ca)}$ tail current is very similar to the voltage dependence of peak I_{Ca} supports the idea that influx via I_{Ca} is more important.

Two aspects of the activation of $I_{K(Ca)}$ by I_{Ca} were not investigated in the present study, but could be very important. First, it would be useful to know how rapidly Ca^{2+} influx activates $I_{K(Ca)}$. Presumably there must be a short lag as Ca^{2+} diffuses to $I_{K(Ca)}$ channels, unless I_{Ca} channels are in close association with $I_{K(Ca)}$ channels. In barnacle neurons even large positive voltage steps (to +10 mV) appear to activate $I_{K(Ca)}$ with a distinct delay period of several to tens of milliseconds (personal observation) suggesting that Ca^{2+} diffuses fairly slowly through the submembrane area to activate $I_{K(Ca)}$. In most molluscan neurons activation is also quite slow (Adams *et. al.*, 1980). A recent study of $I_{K(Ca)}$ in guinea-pig myenteric neurons (Hirst *et. al.*, 1985) provides evidence that $I_{K(Ca)}$ activates with a delay of about 60 ms. This type of delay mechanism could be expected to alter the functional role of $I_{K(Ca)}$ because the current would be activated only during slower types of membrane phenomena. However, Adams *et. al.* (1982b) have reported that in bullfrog sympathetic neurons, $I_{K(Ca)}$ is activated more rapidly than I_K ($\tau < 20$ ms at 0 mV) and could therefore be very important for action potential repolarization. Thus, there appears to be a range of kinetic profiles for $I_{K(Ca)}$ and this must presumably be reflected in its functional role.

It has been shown previously that intracellular Ca^{2+} injection causes a decrease in excitability in cat spinal neurons (Krnjevic and Lisiewicz, 1972) and *Aplysia* neurons (Meech, 1974b). In both cases this appeared to result from an increase in a K^+ conductance following Ca^{2+} injection. The results presented for barnacle neurons agree with these findings, and extend them by measuring the outward current associated with injections that augment adaptation. Very small outward currents (less than 1 nA) appear to be capable of producing quite major changes in the action potential frequency. These experiments also

provide strong evidence in support of the hypothesis that a Ca^{2+}-dependent outward current is responsible for spike frequency adaptation.

The data presented are consistent with the conclusion that in barnacle neurons, $I_{K(Ca)}$ is slowly activated during adapting spike trains by the increase in intracellular Ca^{2+} that accompanies depolarization. $I_{K(Ca)}$ has no obvious threshold for activation in the presence of sufficient Ca^{2+}, and can even be activated as an inward current by Ca^{2+} injections. Therefore it is likely that $I_{K(Ca)}$ is very important in controlling membrane excitability in the voltage range between -50 and -30 mV where there is less activation of other membrane current components. The other major component of membrane current which is active over part of this voltage range is I_A. As was shown in the previous chapter (IV) a fraction of I_A is also dependent on Ca^{2+} for activation. Based on several observations, I rule out the possibility of a major contribution of I_A during adaptation. First, adaptation is markedly reduced in Ca^{2+}-free saline, but this treatment does eliminate the long ramp depolarizations which follow hyperpolarizing pre-pulses (Chapter IV, Figure IV-8). A similar result was observed for EGTA injection during this study. Second, the kinetics of decay of the PSH (and slow tail currents) observed are not consistent with a major contribution of I_A which would have substantially faster kinetics at these voltages. Third, adaptation is observed even for strong depolarizing stimuli in which the spike AHP does not fall below -40 mV, under these conditions there would be little removal of inactivation, and I_A would be expected to decline as the train progresses. It seems likely, based on the kinetic parameters and voltage dependences of these two outward currents, that the Ca^{2+}-dependent fraction of I_A contributes mostly to spike frequency regulation during the early part of a train, and as the train progresses $I_{K(Ca)}$ becomes more important.

VI. GENERAL DISCUSSION

The two major aims of this thesis were; 1) to describe the membrane ionic currents present in the soma of ventral ganglionic neurons of the giant barnacle *Balanus nubilus*, and 2) to analyze the roles of the transient K^+ current and slow Ca^{2+}-dependent K^+ current in the regulation of membrane excitability. Since the experimental results have already been treated in some detail, the purpose of this final discussion will be to integrate some of the main points brought up in the earlier chapters, and to put them in a broader perspective. For this reason I will only summarize the data in a qualitative fashion.

Representative crustacean neurons?

Are the neurons I have studied typical crustacean neurons, and are the membrane properties described representative of neurons from this class of animals? Even if one considers just the variety of properties reported for crustacean motor neurons alone, the heterogeneity of structural and electrical characteristics is quite remarkable. There is enough variability that it would be of little practical value to consider any set of characteristics as being 'typical' of crustacean motor neurons. In spite of this, it seems useful to try to place the data obtained for this sample of barnacle neurons into the spectrum of characteristics observed in other preparations. Evoy (1977) stated in his review of the properties of crustacean motor neurons that "...the cell bodies are devoid of synaptic contacts. No fibres are seen in the region of the cell bodies, and intracellular recordings generally reveal attenuated spikes, usually not more than 5-10 mV in amplitude...". Clearly this situation differs from that seen in the barnacle neurons which I have studied. Dendritic processes are seen to emerge either directly off the soma, or at a point close to where the soma tapers into the axon, suggesting that there is synaptic input to these regions. The action potentials in most of the neurons examined overshoot 0 mV, and often the action potential peak was about +40 mV. Therefore, it seems likely that the soma of these neurons would be considered extremely 'active' in comparison with the reported characteristics of other crustacean neurons which are often considered to be 'passive'. The neurons used preferentially in this study were usually the largest in the ganglion, and other neurons which have characteristics more like those described by Evoy are also present, but were not

analyzed in detail.

I suspect that the membrane phenomena that I have investigated in these barnacle somata apply to many crustacean neurons; but that in more 'typical' neurons these properties are only expressed in the neuropilar spike initiation zone and thus are not amenable to study. Unfortunately there is no real evidence to either support or reject this idea.

Voltage-dependent membrane currents

The properties of the strictly voltage-dependent membrane ionic currents described for barnacle neurons closely resemble those which have been reported for other neuronal cell bodies. In fact, the similarities are much more obvious than the differences and demonstrate the rather conservative nature of neuronal evolution.

The inward I_{Na} and I_{Ca} are somewhat reduced in relative magnitudes, but their voltage dependences and kinetics appear to be quite typical when compared to other cell types (see Adams *et. al.*, 1980; Aldrich and Thompson, 1980; Hille, 1984). When applied externally, TTX blocks the more rapidly activating I_{Na}, and the slower I_{Ca} is most effectively blocked by replacement of Ca^{2+} with other divalent cations. I_{Ca} is only weakly blocked by the organic Ca^{2+} antagonist, verapamil, even at moderately high external concentrations which do block K^+ currents (see below). This suggests that the inner end of the barnacle Ca^{2+} channel (where verapamil probably enters the channel) is structurally different from Ca^{2+} channels in vertebrate cardiac muscle, smooth muscle, and neurons where verapamil is reported to be an effective Ca^{2+} channel antagonist (Hagiwara and Byerly, 1981).

The delayed outward (or delayed rectifier) current, I_K of barnacle neurons is also quite similar to the analagous membrane current seen in other neurons. The voltage dependence of activation is shifted to slightly more depolarized values, and because of this little I_K is activated at membrane voltages under -10 to 0 mV. There is also some evidence that the I_K described may not represent a single population of identical I_K channels, but

rather may represent several subpopulations with slightly different kinetics. For this reason, the activation of I_K was not well fitted by a Hodgkin-Huxley n^3 formulation. A similar multiple component I_K has been observed previously for molluscan neuronal somata (Connor and Stevens, 1971a; Strong and Kaczmarek, 1986). Sensitivity to external TEA seems to be characteristic of I_K in most neuronal somata and many axons. It is worth noting that the squid axon is unusual in that internal application TEA is needed to block I_K; external TEA up to 250 mM has no effect on I_K (Hille, 1984).

I_K in barnacle neurons inactivates almost completely during long depolarizing voltage clamp steps which are maintained for several seconds. This type of inactivation of I_K has been observed in axons (Ehrenstien and Gilbert, 1966) and molluscan neurons (Aldrich *et. al.*, 1979a; Thompson and Aldrich, 1980), but the mechanism and possible physiological roles are not well understood. Decline of I_K has been suggested to produce frequency-dependent broadening of soma spikes in molluscan neurons (Aldrich *et. al.*, 1979b; Reuben and Thompson, 1984). It is not known how widespread this role might be. I have observed that verapamil accelerates the rate of inactivation of I_K in a manner quite similar to its effect on I_A, although this was not specifically discussed in this thesis. This is an interesting finding, because it suggests that a similar process governs inactivation of both I_K and I_A, even though the rate of inactivation is 10 to 100x slower for I_K. This is a topic which I plan to pursue in future experiments because it may provide clues which would lead to a better understanding of the gating process which inactivates K^+ channels.

The fast, transient K^+ current, I_A, activates rapidly following depolarization, and then inactivates with a slow exponential decay. The kinetics are steeply voltage-dependent, and as a result of this I_A has a more varied role in the regulation of excitability than in other neurons where it has been studied. The current is tonically activated at potentials where it would stabilize the resting membrane potential, and yet is also activated rapidly during the action potential, contributing significantly to repolarization. I_A also appears to be very important in controlling the neuronal response time following depolarizing stimuli. This is especially true when stimuli are initiated from hyperpolarized pre-stimulus membrane potentials, which remove steady-state inactivation of I_A and produce a slow ramp

depolarization prior to the onset of an accelerating action potential train. In some cells the normal resting potential is deep enough to produce this response without the need for pre-hyperpolarization, suggesting that the properties of I_A would determine the response time of these neurons to synaptic input *in vivo*.

An important finding is the observation that a fraction of I_A appears to be dependent on Ca^{2+} influx via I_{Ca} channels for activation. A reduction of I_A under conditions which block I_{Ca} has been previously reported in several muscle and nerve cells (see references in Chapter III). However, it is difficult to determine whether or not surface potential effects account for these results because in most studies no attempt was made to evaluate possible shifts in voltage dependence. The results which I presented examined the possibility that a surface potential shift was causal to the reduction in I_A observed and concluded that no simple, uniform potential shift could account for the reduction in I_A. The data supported the conclusion that Ca^{2+} itself, and not other divalent cations, must be present for maximal I_A activation.

Ca^{2+}-dependent membrane currents

In these neurons a large percentage (up to about 50%) of the total outward current is dependent on Ca^{2+} for normal activation. This is surprising in light of the fact that the inward Ca^{2+} currents are usually relatively small. Often, the outward Ca^{2+}-dependent membrane current generated by depolarizing voltage steps is 5 to 10 times the magnitude of the inward I_{Ca} for the same voltage step. Therefore, the stabilizing (hyperpolarizing) effects of Ca^{2+} influx on membrane voltage tend to be more important than the de-stabilizing (depolarizing) effects. The inward Ca^{2+} and outward K^+ current carrying systems function in concert as a negative feedback loop and hence control cell voltage through what appears to be a fairly high-gain feedback system. The Ca^{2+}/K^+ feedback system present in barnacle neurons has two quite different time constants governing its operation.

Rapid feedback, which can limit the duration of a single action potential, is produced by the Ca^{2+}-dependent fraction of I_A, which appears to activate in a few milliseconds, following Ca^{2+} influx during the action potential. This type of ligand-gated K^+ current with rapid kinetics can therefore fulfill a function normally associated with strictly voltage-gated processes (*i.e.* I_K) in other neuronal systems. It does seem curious that nature has not exploited this phenomenon and developed rapidly activating, Na^+-dependent K^+ currents for repolarization of action potentials. Although two recent reports, one on crayfish neurons (Hartung, 1985) and one on chick spinal neurons (Bader, 1986) do provide evidence that a small fraction of the K^+ current in those neurons is Na^+-dependent, this is not considered to be a general principle. It is possible that the internal Na^+ concentration is not regulated tightly enough to make this type of feedback practical. Certainly the internal Ca^{2+} concentration is regulated to a lower basal value, and is governed by a sequestration system with many more opportunities for fine tuning of the submembrane Ca^{2+} level.

A longer time constant Ca^{2+}/K^+ feedback system is produced by the interaction of I_{Ca} and $I_{K(Ca)}$. This system is not likely to respond rapidly enough to be effective during repolarization of individual action potentials. Rather, the long time constant provides a mechanism for 'clamping' the average membrane potential to a value near rest during periods of sustained action potential activity. During spike frequency adaptation for example, this feedback system appears to reduce the action potential frequency by adding a hyperpolarizing bias as the spike train progresses. A major function of this feedback system may also be to limit Ca^{2+} influx by hyperpolarizing the membrane, and de-activating I_{Ca}. Bouts of action potentials are associated with a rise in the intracellular Ca^{2+} concentration (*e.g.* Stinnakre and Tauc, 1973; Lewis and Wilson, 1982) and activation of $I_{K(Ca)}$ may help to keep the concentration from rising too much. It seems plausible that the $I_{Ca}/I_{K(Ca)}$ feedback system could also be important in regulating the membrane potential when neurons are at rest. $I_{K(Ca)}$ has no clear voltage threshold, and therefore could be activated at (or even below) resting membrane potentials. This system would also be self-regulating since depolarizations above about -30 mV initiate Ca^{2+} influx, which would tend to activate $I_{K(Ca)}$ and hyperpolarize the cell, thus maintaining the membrane potential below this value. If the

membrane potential fell to a hyperpolarized value, the combination of reduced Ca^{2+} influx and proximity to E_K would reduce $I_{K(Ca)}$ lessening its hyperpolarizing effect.

Experiments in which the characteristics of $I_{K(Ca)}$ were analyzed by intracellular Ca^{2+} iontophoresis have shown that $I_{K(Ca)}$ is activated by an increase in the internal Ca^{2+} concentration, and that there is a Ca^{2+} range over which this relationship is fairly linear. $I_{K(Ca)}$ has a weak intrinsic voltage dependence, but most of the 'effective' voltage dependence is derived from the voltage-dependent influx of Ca^{2+} carried by I_{Ca}. The properties of $I_{K(Ca)}$ activated in this way are almost identical to those reported for molluscan neurons under similar experimental conditions (*e.g.* Gorman and Hermann, 1979). The sensitivity to Ca^{2+} injections is much greater for barnacle neurons, but this probably a reflection of the smaller surface to volume ratio of barnacle neurons.

An important aspect of the function of Ca^{2+}-dependent K^+ currents is that they are likely to be regulated by hormones, neurotransmitters, and neuromodulators. Many of these have specific effects on I_{Ca} (*e.g.* Gershenfeld *et. al.*, 1986) and would therefore influence the K^+ systems indirectly. However, evidence is mounting which also suggests that Ca^{2+}-dependent K^+ channels are the specific targets of some modulatory substances (*e.g.* Adams *et. al.*, 1986). Neurons which have a large contribution of these currents would then tend to be more 'plastic' in their excitability profile and therefore be able to fulfill a wider variety of functions than otherwise possible.

Repetitive action potential trains

It is important to remember that crustacean motor neurons are not merely relay units, but are capable of integrating inputs from sensory and interneuronal systems. Thus, the characteristic action potential discharge pattern of each neuron reflects the properties of both the synaptic input, and the membrane characteristics of that individual neuron. In this thesis I have studied only action potential trains produced by current pulses injected at the soma, and although these responses will obviously differ from those initiated by synaptic input, the mechanisms underlying the encoding process should be similar in both cases.

The barnacle neurons examined in this study generated repetitive action potential trains in the presence of a maintained supra-threshold current stimulus. The frequency increased smoothly with stimulus intensity, and most neurons could fire repetitively over a frequency range of approximately 2 to 50 Hz. Therefore, these neurons appear to be of the 'encoder' type which can accurately transduce stimulus intensity to action potential frequency (Connor and Stevens, 1971c). It should be stressed that while all of the neurons used in experiments had this capability, many other ventral ganglionic neurons had quite different firing patterns, or could not be driven to spike at all. Although a spectrum of properties is present, I have examined only the encoder types in detail and therefore the results presented should be considered in this context.

During low frequency repetitive firing the voltage trajectory throughout the interspike interval appears to be strongly influenced by I_A. This was demonstrated in experiments where I_A was reduced by blocking Ca^{2+} influx (replacing the Ca^{2+} with Co^{2+} or Mn^{2+}). This treatment also reduced the linearity, and increased the slope of the *f-I* relationship at low frequencies. The results presented for experiments where I_A was reduced by other pharmacological agents (4-AP and forskolin) are also consistent with the hypothesis that I_A regulates low frequency repetitive firing in barnacle neurons.

The major voltage-dependent ionic currents present in these neurons were described by a set of Hodgkin-Huxley type equations, and these were used to simulate the events occurring during repetitive action potential trains. The simulation indicates that I_A is important during the interspike interval, providing a hyperpolarizing bias, which slows the rate of voltage rise to threshold. However, the simulation also predicts that the opposing effects of I_A and I_{Na} on membrane voltage are important in producing the interspike voltage trajectory, rather that this being a function of I_A alone.

Concluding remarks

The variability in membrane currents observed from cell to cell was not dealt with specifically in this thesis, but is a striking feature of the neurons studied. Cells vary not so

much in the type of membrane currents expressed, but rather in the relative contributions of each current. Cells were observed in which I_A was the most predominant membrane current at most voltages, while others had little I_A and large contributions of I_K or $I_{K(Ca)}$. Certain membrane current profiles are correlated with a particular type of repetitive firing pattern. This type of variability, and its correlation to neuronal excitability may prove a profitable direction for further research. The marked variability in kinetics of one membrane current component when compared between cells is also intriguing. For example, there is a large range in the measured values for the I_A inactivation time constant, and I_K activation time constants could vary as much as five-fold. However, I have observed that identifiable, homologous cells do have similar membrane current profiles when studied in different preparations. Therefore, it seems likely that a portion of the variability is genetically controlled, with the ensemble of membrane currents being specified in such a way as to give each neuron a particular set of electrical characteristics.

The major objective of this thesis has been to quantitatively relate membrane ionic currents to observed action potential train characteristics in central neurons of barnacles. Although the repetitive firing of action potentials has been fairly intensively studied, the underlying mechanisms in neuronal somata are still not well understood. In barnacle neurons several complexities make the analysis particularly interesting. In addition to the familiar 'Hodgkin-Huxley' type membrane currents, an inward Ca^{2+} current, transient K^+ current and two different Ca^{2+}-dependent K^+ currents interact to regulate neuronal excitability. The contribution of each component of membrane current during an action potential train is a complex function of, among other factors: cell type, internal Ca^{2+} level, instantaneus voltage, voltage pre-history and stimulus magnitude and duration. This complex ensemble of ionic currents, and hence voltage responses is undoubtedly important in determining the integrative properties of central neurons.

VII. REFERENCES

Adams, D.J., Smith, S.J. & Thompson, S.H. 1980. Ionic currents in molluscan soma. Ann. Rev. Neurosci. 3, 141-167.

Adams, P.R., Brown, D.A. & Constanti, A. 1982a. M-currents and other potassium currents in bullfrog sympathetic neurones. J. Physiol. 330, 537-572.

Adams, P.R., Constanti, A., Brown, D.A. & Clark, R.B. 1982b. Intracellular Ca^{2+} activates a fast voltage-sensitive K^+ current in vertebrate sympathetic neurones. Nature 269, 746-749.

Adams, P.R., Jones, S.W., Pennefather, P., Brown, D.A., Koch, C. & Lancaster, B. 1986. Slow synaptic transmission in frog sympathetic ganglia. J. exp. Biol. 124, 259-285.

Akaike, N., Lee, K.S. & Brown, A.M. 1978. The calcium current of *Helix* neurons. J. Gen. Physiol. 71, 509-531.

Aldrich, R.W., Getting, P.A. & Thompson, S.H. 1979a. Inactivation of delayed outward current in molluscan neurone somata. J. Physiol. 291, 507-530.

Aldrich, R.W., Getting, P.A. & Thompson, S.H. 1979b. Mechanism of frequency-dependent broadening of molluscan neurone soma spikes. J. Physiol. 291, 531-544.

Arhem, P. 1980. Effects of some heavy metal ions on the ionic currents of myelinated fibres from *Xenopus laevis*. J. Physiol. 306, 219-231.

Armstrong, C.M. & Matteson, D.R. 1986. The role of calcium ions in the closing of K

channels. J. Gen. Physiol. 87, 817-832.

Atwood, H.L. 1982. Membrane physiology of crustacean neurons. In, *Membrane physiology of invertebrates.* (Ed: Podesta, R.B). Marcel Dekker Inc. New York. pp.342-393.

Auerbach, A. & Sachs, F. 1984. Patch clamp studies of single ionic channels. Ann. Rev. Biophys. Bioeng. 13, 269-302.

Bader, C.R., Bernhiem, L. & Bertrand, D. 1985. Sodium-activated poteassium current in cultured avian neurones. Nature 317, 540-542.

Barish, M.E. & Thompson, S.H. 1983. Calcium buffering and slow recovery kinetics of calcium-dependent outward current in molluscan neurones. J. Physiol. 337, 201-219.

Beeler, G. W. & Reuter, H. 1977. Reconstruction of the action potential of ventricular myocardial fibers. J. Physiol 268, 177-210.

Benson, J.A. & Cooke, I.M. 1984. Driver potentials and the organization of rhythmic bursting in crustacean ganglia. Trends. Neurosci. 3, 83-91.

Blaustein, M.P. & Goldman, D.E. 1968. The action of certain polyvalent cations on the voltage-clamped lobster axon. J. Gen. Physiol. 51, 279-291.

Belluzzi, O., Sacchi, O. & Wanke, E. 1985. A fast transient outward current in the rat sympathetic neurone studied under voltage-clamp conditions. J. Physiol. 358, 91-108.

Brehm, P. & Eckert, R. 1978. Calcium entry leads to inactivation of calcium channel in

Paramecium. Science 202, 1203-1206.

Brismar, T. 1980. The effect of divalent and trivalent cations on the sodium permeability of myelinated nerve fibres of *Xenopus laevis*. Acta Physiol. Scand. 108, 23-29.

Brodwick, M. & Junge, D. 1972. Post-stimulus hyperpolarisation and slow potassium conductance increase in *Aplysia* giant neurone. J. Physiol. 223, 549-570.

Brown, A.M., Morimoto, K., Tsuda, Y. & Wilson, D.L. 1981. Calcium and voltage-dependent inactivation of calcium channels in *Helix aspersa*. J. Physiol. 320, 193-218.

Brown, D.A. & Griffith, W.H. 1983. Calcium-activated outward current in voltage clamped hippocampal neurones of the guinea pig. J. Physiol. 337, 287-301.

Brown, H.M., Hagiwara, S., Koike, H. & Meech, R.W. 1971. Electrical characteristics of a barnacle photoreceptor. Fed. Proc. 30, 69-78.

Brown, H.M., Meech, R.W., Koike, H. & Hagiwara, S. 1969. Current-voltage relations during illumination: Photoreceptor membrane of a barnacle. Science 166, 240-243.

Bruner, J., Czternasty, G., Shimahara, T. & Stinnakre, J. 1986. Arsenazo III transients and calcium current in a normally non-spiking neuronal soma of crayfish. J. Physiol. 374, 571-583.

Byrne, J.H. 1980a. Analysis of ionic conductance mechanisms in motor cells mediating inking behavior in *Aplysia californica*. J. Neurophysiol. 43, 630-650.

Byrne, J.H. 1980b. Quantitative aspects of ionic conductance mechanisms contributing to

firing pattern of motor cells mediating inking behavior in *Aplysia californica*. J. Neurophysiol. 43, 651-668.

Chaplain, R.A. 1975. Evidence for Ca^{2+} control of the tranducer mechanism in crayfish stretch receptor. J. Membr. Biol. 21, 335-351.

Chapman, R.A. 1966. The repetitive responses of isolated axons from the crab, *Carcinus menaes*. J. Exp. Biol. 45, 475-488.

Colding-Jorgenson, M. 1976. A description of adaption in excitable membranes. J. Theor. Biol. 63, 61-87.

Colding-Jorgensen, M. 1977. Impulse dependent adaption in *Helix pomatia* neurones: Demonstration of the adaptation conductance. Acta Physiol. Scand. 101, 382-393.

Connor, J.A. 1975. Neural repetitive firing: A comparative study of membrane properties of crustacean walking leg axons. J. Neurophysiol. 38, 922-932.

Connor, J.A. & Stevens, C.F. 1971a. Inward and delayed outward membrane currents in isolated neural somata under voltage clamp. J. Physiol. 213, 1-19.

Connor, J.A. & Stevens, C.F. 1971b. Voltage clamp studies of a transient outward membrane current in gastropod neural somata. J. Physiol. 213, 21-30.

Connor, J.A. & Stevens, C.F. 1971c. Prediction of repetitive firing behavior from voltage clamp data on an isolated neurone soma. J. Physiol. 213, 31-53.

Connor, J.A., Walter, D. & McKown, R. 1977. Neural repetitive firing, modification of the Hodgkin-Huxley axon suggested by experimental results from crustacean

axons. Biophys. J. 18, 81-102.

Coraboeuf, E. & Carmeliet, E. 1982. Existence of two transient outward currents in sheep cardiac Purkinje fibres. Pflugers Arch. 392, 352-359.

Cooper, E. & Shrier, A. 1985. Single-channel analysis of fast transient potassium currents from rat nodose neurones. J. Physiol. 369, 199-208.

Dionne, V.E. & Stevens, C.F. 1975. Voltage dependence of agonist effectiveness at the frog neuromuscular junction: resolution of a paradox. J. Physiol. 251, 245-270.

Dodge, F.A. 1961. Ionic permeability changes underlying nerve excitation. In *Biophysics of Physiological and Pharmacological Actions*, A.A.A.S., Washington, D.C. 119-143.

Dubois, J.M. 1981. Evidence for the existence of three types of potassium channels in the frog Ranvier node membrane. J. Physiol. 318, 297-316.

Eckert, R. & Tillotson, D.L. 1981. Calcium-mediated inactivation of the calcium conductance in caesium-loaded giant neurones of *Aplysia californica*. J. Physiol. 314, 265-280.

Edwards, D.H. & Mulloney, B. 1984. Compartmental analysis of electrotonic structure and synaptic integration in an identified neurone. J. Physiol. 348, 89-113.

Ehrenstein, G., Blumenthal, R., Latorre, R. & Lecar, H. 1974. Kinetics of the opening and closing of individual excitability-inducing material channels in a lipid bilayer. J. Gen. Physiol. 63, 707-721.

Ehrenstein, G. & Gilbert, D.L. 1966. Slow changes of potassium permeability in the squid giant axon. Biophys. J. 6, 553-566.

Evoy, W.H. 1977. Crustacean motor neurons. In, *Identified Neurons and Behavior of Arthropods* (ed. G. Hoyle), pp. 67-86. New York, Plenum.

Fox, A.P. 1981. Voltage-dependent inactivation of a calcium channel. Proc. Natl. Acad. Sci. USA 78, 953-956.

Frankenhaeuser, B. 1963. A quantitative description of potassium currents in myelinated nerve fibres of *Xenopus laevis*. J. Physiol. 169, 424-430.

Frankenhaeuser, B. & Huxley, A.F. 1964. The action potential in the myelinated nerve fibre of *Xenopus laevis* as computed on the basis of voltage clamp data. J. Physiol. 171, 302-315.

Frankenhaeuser, B. & Hodgkin, A.L. 1957. The action of calcium on the electrical properties of squid axons. J. Physiol. 137, 218-244.

French. A.S. 1985. After-hyperpolarization and receptor potential attenuation following bursts of action potentials in an insect mechanoreceptor. Can. J. Physiol. Pharmacol. 63, 18-22.

French, A.S. 1986. The role of calcium in rapid adaptation of an insect mechanoreceptor. J. Neurosi 6, 2322-2326.

Galvan, M. 1982. A transient outward current in rat sympathetic neurones. Neuroscience Letters 31, 295-300.

Geduldig, D. and Gruener, R. 1970. Voltage clamp of the *Aplysia* giant neurone, early sodium and calcium currents. J. Physiol. 211, 217-244.

Geduldig, D. & Junge D. 1968. Sodium & calcium components of action potentials in the

Aplysia giant neurone. J. Physiol. 199, 347-365.

Gershenfeld, H.M., Hammond, C. & Paupardin-Tritsch, D. 1986. Modulation of the Ca^{2+} current in molluscan neurons by neurotransmitters. J. exp. Biol. 124, 73-91.

Gestrelius, W., Grampp, W. & Sjolin, L. 1981. Subthreshold and near-threshold membrane currents in lobster stretch receptor neurones. J. Physiol. 310, 191-203.

Gilbert, D. L. & Ehrenstein, G. 1969. Effect of divalent cations on potassium conductance of squid axons: Determination of surface charge. Biophys. J. 9, 447-463.

Gilly, W.F. & Armstrong, C.M. 1982a. Slowing of sodium channel opening kinetics in squid axon by extracellular zinc. J. Gen. Physiol. 79, 935-964.

Gilly, W.F. & Armstrong, C.M. 1982b. Divalent cations and the activation kinetics of potassium channels in squid giant axons. J. Gen. Physiol. 79, 965-996.

Goldman, L. & Schauf, C.L. 1972. Inactivation of the sodium current in *Myxicola* giant axons. Evidence for coupling to the activation process. J. Gen. Physiol. 59, 659-675.

Goldman, L. & Schauf, C.L. 1973. Quantitative description of sodium and potassium currents and computed action potentials in *Myxicola* giant axons. J. Gen. Physiol. 61, 361-384.

Gorman, A.L.F. & Thomas, M.V. 1978. Changes in the intracellular concentration of free calcium ions in a pace-maker neurone, measured with the metallochromic indicator dye arsenazo III. J. Physiol. 275, 357-376.

Gorman, A.L.F. & Hermann, A. 1979. Internal effects of divalent cations on potassium

permeability in molluscan neurons. J. Physiol. 296, 393-410.

Gorman, A.L.F. & Thomas, M.V. 1980. Intracellular calcium accumulation during depolarization in a molluscan neurone. J. Physiol. 308, 259-285.

Gustafsson, B., Galvan, M., Grafe, P. & Wigstrom, H. 1982. A transient outward current in a mammalian central neurone blocked by 4-aminopyridine. Nature 299, 252-254.

Gwilliam, G.F. 1976. Mechanism of the shadow reflex in cirripedia III. Rhythmical patterned activity in central neurons and its modulation by shadows. Biol. Bull. 151, 141-160.

Hagiwara, S. 1961. Nervous activities of the heart of crustacea. Ergeb. Biol. 24, 287-311.

Hagiwara, S. 1973. Ca spike. Av. Biophys. 4, 71-102.

Hagiwara, S. & Byerly. L. 1981. Calcium channel. Ann. Rev. Neurosci. 4, 69-125.

Hagiwara, S., Kusano, K. & Saito, N. 1961. Membrane changes of *Onchidium* nerve cell in potassium-rich media. J. Physiol. 155, 470-489.

Hagiwara, S. & Saito, N. 1959. Voltage-current relations of the *Onchidium* nerve cell in potassium-rich media. J. Physiol. 148, 161-179.

Hartung, K. 1985. Potentiation of a transient outward current by Na influx in crayfish neurons. Pfugers. Arch. 404, 41-44.

Hermann, A. & Gorman, A.L.F. 1981. Effects of 4-aminopyridine on potassium currents on a molluscan neurone. J. Gen Phys. 78, 63-86.

Hermann, A. & Hartung, K. 1982. Properties of a Ca^{2+} activated K^+ conductance in *Helix* neurones investigated by intracellular Ca^{2+} ionophoresis, Pfluegers Arch. 393, 248-253.

Hill, A.V. 1932. *Chemical Wave Transmission in Nerve.* Cambridge University Press, Cambridge.

Hille, B. 1968. Charges and potentials at the nerve surface: Divalent ions and pH. J. Gen. Physiol. 51, 221-236.

Hille, B. 1984. *Ionic channels of excitable membranes.* Sinauer Associates Inc., Sunderland, Mass.

Hille, B., Woodhull, A.M. & Shapiro, B.I. 1975. Negative surface charge near sodium channels of nerve: Divalent ions, monovalent ions, and pH. Phil. Trans. R. Soc. Lond. Ser. B 270, 301-318.

Hirst, G.D.S., Johnson, S.M. & van Helden, D.F. 1985. The slow calcium-dependent potassium current in a myenteric neurone of the guinea-pig ileum. J. Physiol. 316, 315-337.

Hirst, G.D.S. & Spence, I. 1973. Calcium action potentials in mammalian peripheral neurones. Nature, New Biology 243, 54-56.

Hodgkin, A.L. 1948. The local electrical changes associated with repetitive action in a nonmedullated axon. J. Physiol. 107, 165-181.

Hodgkin, A.L. & Huxley, A.F. 1952a. Currents carried by sodium and potassium ions through the membrane of the giant axon of *Loligo.* J. Physiol. 116, 449-472.

Hodgkin, A.L. & Huxley, A.F. 1952b. The components of membrane conductance in the giant axon of *Loligo*. J. Physiol. 116, 473-496.

Hodgkin, A.L. & Huxley, A.F. 1952c. The dual effect of membrane potential on sodium conductance in the giant axon of *Loligo*. J. Physiol. 116, 497-506.

Hodgkin, A.L. & Huxley, A.F. 1952d. A quantitative description of membrane current and its application to conduction and excitation in nerve. J. Physiol. 117, 500-544.

Hudspeth, A.J., Mu Ming Poo & Stuart, A.E. 1979. Passive signal propagation and membrane properties in median photoreceptors of the giant barnacle. J. Physiol. 272, 25-43.

Jack, J.J.B., Noble, D. & Tsien, R.W. 1983. *Electric Current Flow in Excitable Cells*. Oxford University Press, London, 518 pp.

Jansen, S.K.S. & Nicholls, J.G. 1973. Conductance changes, an electrogenic pump and the hyperpolarisation of leech neurones following impulses. J. Physiol. 229, 635-655.

Julian, F. J., Moore, J.W. & Goldman, D.E. 1962. Current-voltage relations in the lobster giant axon membrane under voltage clamp conditions. J. Gen. Physiol. 45, 1217-1238.

Junge, D. 1967. Multi-ionic action potentials in molluscan giant neurones. Nature 215, 546-548.

Junge, D. 1985. Calcium dependence of the A-currents in perfused *Aplysia* neurons. Br. Res. 346, 294-300.

Katz, G.M. & Schwartz, T.L. 1974. Temporal control of voltage-clamped membranes: an

examination of principles. J. Memb. Biol. 17, 275-291.

Kasai, H., Kameyama, M., Yamaguchi, K. & Fukuda, J. 1986. Single transient K channels in mammalian sensory neurons. Biophys. J. 49, 1243-1247.

Kazmarek, L.K. & Strumwasser, F. 1984. A voltage clamp analysis of currents underlying cAMP-induced membrane modulation in isolated peptidergic neurons of *Aplysia*. J. Neurophysiol. 52, 340-349.

Kernell, D., & Sjoholm, H. 1973. Repetitive impulse firing: comparisons between neurone models based on voltage clamp equations of spinal motoneurones. Acta Physiol. Scand. 87, 40-56.

Klie, J. W. & Wellhoner, H.H. 1973. Voltage clamp studies on the stretch response in the neuron of the slowly adapting crayfish stretch receptor. Pfluegers Arch. 342, 93-104.

Koketsu, K., Cerf, J.A. & Nishi, S. 1959. Further observations on the activity of frog spinal neurons in sodium-free solutions. J. Neurophysiol. 22, 693-703.

Kostyuk, P.G., Krishtal, O.A. & Doroshenko, P.A. 1975. Outward currents in isolated snail neurones. I. Inactivation kinetics. Comp. Biochem. Physiol. 51C, 259-263.

Kostyuk, P.G. Krishtal, O.A. & Doreshenko, P.A. 1976. Outward currents in the nerve cell membrane. Bioelec. and Bioeng. 3, 319-327.

Kristal, O.A., Pidoplichko, V.I. & Shakhovalov, Y.A. 1981. Conductance of the calcium channel in the membrane of snail neurones. J. Physiol. 310, 423-434.

Krnjevic, K. & Lisiewicz, A. 1972. Injections of calcium ions into spinal motoneurones. J. Physiol. 225, 363-390.

Lancaster, D. 1975. *Active filter cookbook*. H.W. Sams Co. Inc. Indianapolis, Indiana. 240 pp.

Lewis, D.V. & Wilson, W.A. 1982. Calcium influx and poststimulus current during early adaption in *Aplysia* neurons. J. Neurophysiol. 48, 202-216.

MacDermott, A.B. & Weight, F.F. 1982. Action potential repolarization may involve a transient Ca^{2+}-sensitive outward current in a vertebrate neurone. Nature 300, 185-188.

Magleby, K.L. & Pallotta, B.S. 1983. Calcium dependence of open and shut interval distributions from calcium-activated potassium channels in cultured rat muscle. J. Physiol. 344, 585-604.

McAllister, R.E., Noble, D. & Tsien, R.W. 1975. Reconstruction of the electrical activity of cardiac Purkinje fibres. J. Physiol. 251, 1-59.

Meech, R.W. 1974a. Calcium influx induces a post-tetanic hyperpolarization in *Aplysia* neurones. Comp. Biochem. and Physiol. 48A, 387-395.

Meech, R.W. 1974b. The sensitivity of *Helix aspersa* neurones to injected calcium ions. J. Physiol. 237, 259-277.

Meech, R.W. 1978. Calcium-dependent potassium activation in nervous tissues. Ann. Rev. Biophys. Bioeng. 7, 1-18.

Meech, R.W. & Standen, N.B. 1975. Potassium activation in *Helix aspersa* neurones under

voltage clamp: a component mediated by calcium influx. J. Physiol. 249, 211-239.

Minota, S. 1974. Calcium ions and the post-tetanic hyperpolarization of bullfrog sympathetic ganglion cells. Jap. J. Physiol. 24, 501-512.

Mirolli, M. 1981. Fast inward and outward current channels in a non-spiking neurone. Nature 292, 251-253.

Mirolli, M. 1983. Inward and outward currents in isolated dendrites of crustacean coxal receptors. Cell. Molec. Neurobiol. 3, 355-370.

Moore, J.W. & Cole, K.S. 1963. Voltage clamp techniques. In: *Physical Techniques in Biological Research.* W.L. Nastuk, editor. Academic Press, Inc., New York. 6, 263-321.

Mounier, Y. & Vassort, G. 1975. Evidence for a transient potassium membrane current dependent on calcium influx in crab muscle fibre. J. Physiol. 251, 609-625.

Mozhayeva, G.N. & Naumov, A.P. 1970. Effect of surface charge on the steady-state potassium conductance of nodal membrane. Nature 228, 164-165.

Mozhayeva, G.N. & Naumov, A.P. 1972. Influence of the surface charge on the steady potassium conductivity of the membrane of a node of Ranvier. II. Effect of bivalent cations. Biofizika 17, 801-808.

Nakajima, S. 1966. Analysis of K inactivation and TEA action in the supra-medullary cells of puffer. J. gen. Physiol. 49, 629-640.

Nakajima, S. & Takahashi, K. 1966. Post-tetanic hyperpolarization & electrogenic Na pump

in stretch receptor neurone of crayfish. J. Physiol. 187, 105-127.

Narahashi, T., Moore, J.W. & Scott, W.R. 1964. Tetrodotoxin blockage of sodium conductance increase in lobster giant axons. J. Gen. Physiol. 47, 965-974.

Neher, E. 1971. Two fast transient current components during voltage clamp of snail neurons. J. Gen. Physiol. 58, 36-53.

Neher, E. & Lux, H.D. 1972. Properties of somatic membrane patches of snail neurons under voltage clamp. Pflugers Arch. 322, 35-38.

Noble, D. 1960. Cardiac action and pacemaker potentials based on Hodgkin-Huxley equations. Nature 188, 495-497.

Ottoson, D. & Swerup, C. 1982. Studies on the role of calcium in adaptation of the crustacean stretch receptor. Effects of intracellular injection of calcium, EGTA and TEA. Brain Res. 244, 337-341.

Pallotta, B.S., Magleby, K.L. & Barrett, J.N. 1981. Single channel recordings of Ca^{2+}-activated K^+ currents in rat muscle cell culture. Nature 293, 471-474.

Palti, Y. 1969. Measurement of membrane conductances and capacity by means of a varying potential clamp. J. Memb. Biol. 1, 431-458.

Partridge, L.D. 1980a. Calcium independence of slow currents underlying spike frequency adaption. J. Neurobiol. 11, 613-622.

Partridge, L.D. 1980b. A mechanism for the control of low-frequency repetitive firing. Cell. and Molec. Neurobiol. 2, 33-45.

Partridge, L.D. & Stevens, C.F. 1975. A mechanism for spike frequency adaption. J. Physiol. 256, 315-332.

Pelhate, M. & Pichon, Y. 1974. Selective inhibition of potassium currents in the giant axon of the cockroach. J. Physiol. 242, 90P. (Abstr.)

Pitman, R.M. 1979. Intracellular citrate or externally applied tetraethylammonium ions produce calcium-dependent action potentials in an insect motoneurone cell body. J. Physiol. 291, 327-337.

Plant, R.E. & Kim, M. 1976. Mathematical description of a bursting pacemaker neuron by a modification of the Hodgkin-Huxley equations. Biophys. J. 16, 227-244.

Premack, B.A., Ruben, P. & Thompson, S.H. 1984. Calcium-sensitive transient potassium current influences rhythmic motor output in barnacle neurons. Soc. Neurosci. Abstr. 44.1.

Quinta-Ferreira, M.E., Rojas, E. & Arispe, N. 1982. Potassium currents in the giant axon of the crab *Carcinus menaes*. J. Memb. Biol. 66, 171-181.

Rall, W. 1969. Time constants and electrotonic length of membrane cylinders and neurons. Biophys. J. 9, 1483-1508.

Ritchie, J. M. & Straub, R.W. 1957. The hyperpolarization which follows activity in mammalian non-medullated fibres. J. Physiol. 136, 80-97.

Rogowski, M.A. 1985. The A-current: How ubiquitous a feature of excitable cells is it? Trends. Neurosci. 8, 214-219.

Ross, W.N., Stockbridge, L.L. & Stockbridge, N.L. 1986. Regional properties of calcium

entry in barnacle neurons determined with arzenazo III and a photodiode array. J. Neurosci. 6, 1148-1159.

Ruben, P. & Thompson, S.H. 1984. Rapid recovery from K current inactivation on membrane hyperpolarization in molluscan neurons. J. Gen. Physiol. 84, 861-875.

Salkoff, L. 1983. Drosophila mutants reveal two components of fast outward current. Nature 302, 249-251.

Sandeman, P.R. 1969. The site of synaptic activity and impulse initiation in an identified motoneurons in the crab brain. J. Exp. Biol. 50, 100-114.

Schwarz, W. & Passow, H. 1983. Ca^{2+}-activated K^+ channels in erythrocytes and excitable cells. Ann. Rev. Physiol. 45, 359-374.

Seamon, K.B., Padgett, W. & Daly, W.J. 1981. Forskolin: Unique diterpene activator of adenylate cyclase in membranes and in intact cells. Proc. Natl. Acad. Sci. U.S.A. 78, 3363-3367.

Segal, M. 1983. Rat hippocampal neurons in culture: Potassium conductances. J. Neurophysiol. 51, 1409-1433.

Segal, M., Rogowski, M.A. & Barker, J.L. 1984. A transient potassium conductance regulates the excitability of cultured hippocampal and spinal neurons. J. Neurosci. 4, 604-609.

Shimahara, T., Czternasty, G., Stinnakre, J. & Bruner, J. 1985. Calcium action potential induction in an 'inexcitable' motor neuron cell body: a study with Arsenazo III. In: *Neural mechanisms of conditioning*, ed. Alkon, D., & Woody, C., pp.

283-289. Plenum Publ.

Siegelbaum, S.A. and Tsien, R.W. 1980. Calcium-activated transient outward current in calf cardiac Purkinje fibres. J. Physiol. 299, 485-506.

Simpson, W.G. 1985. The calcium channel blocker verapamil and cancer chemotherapy. Cell Calcium 6, 449-467.

Smith, T.G., Barker, J.L., Smith, B.M. & Colburn, T.R. 1980. Voltage clamping with microelectrodes. J. Neurosci. Meth. 3, 105-128.

Sokolove, P.G. & Cooke, I.M. 1971. Inhibition of impulse activity in a sensory neuron by an electrogenic pump. J. Gen. Physiol. 57, 125-163.

Stanfield, P.R. 1973. Tetraethylammonium ions and the potassium permeability of excitable cells. Rev. Physiol. Biochem. Pharmacol. 97, 1-67.

Stinnakre, J. & Tauc, L. 1973. Calcium influx in active *Aplysia* neurones detected by injected aequorin. Nature New Biology 242, 113-115.

Strong, J.A. 1984. Modulation of potassium current kinetics in bag cell neurons of Aplysia by an activator of adenylate cyclase. J. Neurosci. 4, 2772-2783.

Strong, J.A. & Kaczmarek, L.K. 1986. Multiple components of delayed potassium current in peptidergic neurons of *Aplysia*: Modulation by an activator of adenylate cyclase. J. Neurosci. 6, 814-822.

Takata, M., Pickard, W.F., Lettvin, J.Y. & Moore, J.W. 1966. Ionic conductance changes in lobster axon membrane when lanthanum is substituted for calcium. J. Gen. Physiol. 50, 461-471.

Takeda, K. & Kennedy, D. 1964. Soma potentials and modes of activation of crayfish montoneurons. J. Cell. Comp. Physiol. 64, 165-182.

Tazaki, K. & Cooke, I.M. 1983. Separation of neuronal sites of driver potential and impulse generation by ligaturing in the cardiac ganglion of the lobster, Homarus americanus. J. Comp. Physiol. 151, 329-346.

Tazaki, K. & Cooke, I.M. 1984. In, *Neural control of rhythmic movements (Society for Experimental Biology, Symposium No. 37).* Roberts, B.L. & Roberts, A. (Eds.) Cambridge University Press, Cambridge.

Thomas, M.V. 1984. Voltage clamp analysis of a calcium-mediated potassium conductance in cockroach central neurons. J. Physiol. 350, 159-178.

Thompson, S.H. 1977. Three pharmacologically distinct potassium channels in molluscan neurones. J. Physiol. 265, 465-488.

Thompson, S.H. 1982. Aminopyridine block of transient potassium current. J. Gen. Physiol. 80, 1-18.

Thompson, S.H. & Aldrich, R.W. 1980. Membrane potassium channels. In: *The Cell Surface and Neuronal Function,* eds. C. W. Cotman, G. Poste & G. L. Nicolson, 49-85. Elsevier/North-Holland Biomedical Press, Amsterdam.

Tillotson, D. 1979. Inactivation of Ca conductance dependent on entry of Ca ions in molluscan neurons. Proc. Natl. Acad. Sci. USA 76, 1497-1500.

Tsien, R.W. 1983. Calcium channels in excitable cell membranes. Ann. Rev. Physiol. 45, 341-358.

Zar, Z.H. 1974. *Biostatistical analysis.* Prentice-Hall Inc. Englewood Cliffs, N. Jersey.

Zbicz, K.L. & Weight, F.F. 1985. Transient voltage and calcium-dependent outward currents in hippocampal CA3 pyramidal neurons. J. Neurophysiol. 53, 1038-1058.